Doctoral Dissertation

OPTIMIZATION OF THREE-LAYER CORRUGATED METAL GASKET BASED ON CONTACT WIDTH AND CONTACT STRESS

(積層型メタルガスケットの最適形状に関する研究)

September 2017

I MADE GATOT KAROHIKA

Graduate School of Science and Engineering
Yamaguchi University
Japan

CONTENTS

CHAPTER IV ANALYSIS STUDY OF CONTACT WIDTH AND CONTACT STRESS OF THREE-LAYER CORRUGATED METAL GASKET

CHAPTER V THE LEAKAGE PERFORMANCE OF THREE-LAYER CORRUGATED METAL GASKET

CHAPTER VI OPTIMIZATION OF THREE-LAYER METAL GASKET USING TAGUCHI

CHAPTER VII CONCLUSION

REFERENCES

LIST OF FIGURE

LIST OF TABLES

ACKNOWLEDGEMENT

It would have been impossible to make this thesis without the help and support of several persons:

First of all, I would like to express my deepest appreciation and thanks to my supervisor, Professor Ken KAMINISHI and Professor Shigeyuki HARUYAMA, for his excellent guidance throughout this work. Thank you for your patience, time for discussions, and critical review of my work. I receive generous scientific and practical knowledge as well as for letting me become a PhD student in such interesting field.

Mr. Akinori SATO and Mr. Yuji IDA as teamwork of new metal gasket project have given great contributions and inputs to my work, I really appreciate for those. Dear friends and members of Strength of Material laboratory Yamaguchi University Japan, thank you for contributing to a very pleasant working environment. I also would like to thank all lecturers in Mechanical Engineering Department for a nice education atmosphere. Appreciation to Mr. OKAJIMA, Mr. KADOTA and Ms. ASANO for good administration helps.

I am grateful to all my friends in Ube city for our friendships. Thanks to all Indonesian students during living in Japan for our togetherness and all member of PPI Yamaguchi. Appreciation is also addressed to Indonesian Embassy for great helps. Gratitude is given to my colleagues in Udayana University for their great encouragement and support during my study in Japan. I am very gratefully to Director General of Higher Education, Ministry of National Education Republic of Indonesia for giving chance to pursuing study in Japan with scholarship financial support since 2014 until 2017.

Finally, I would like to especially thank my dear wife, Luh Dewi Susanti and my children's, Ni Putu Shantigita Nareswari, I Made Satwika Daneswara, Ni Nyoman Berliana Pradnya Kayana, for great understanding during difficult times and a fare away love.

I Made Gatot KAROHIKA
Ube city, September 2017

ABSTRACT

Metal gaskets are used extensively as static seal in many industries due to resistance to heat and chemicals, capability to withstand pressure, recyclable, and reliability in critical situations. However, the high axial force is required to deform the solid metal gasket and the loss of tightness of the bolted flange due to the effect of the relaxation of joint. Nurhadiyanto et al. optimized the corrugated metal gasket SUS304 based on an elastic contact stress (0-MPa mode) and plastic contact stress (400-MPa mode) considering forming effect. The research found that gasket 400-MPa mode design better than gasket 0-MPa mode. Haruyama et al. clarified that flange surface roughness effect the sealing performance of the corrugated metal gasket. The main problem in this regard is the fact that a metal gasket SUS304 performance decrease when contact with flange having high surface roughness. This is because when gasket SUS304 in contact with a flange that has high surface roughness, contact width containing plastic contact stress condition is reduce so that the sealing performance of the gasket also decreased. Based on this reason, improvement of metal gasket performance continues researched to increase contact width having high plastic contact stress therefore not leakage when contact with flange having high surface roughness. In this research, we laminate the soft metal as surface layer at the top and bottom of the SUS304 gasket therefore when contact with the flange having high surface roughness the soft metal will be deformed plastically and fill the gap of the imperfect flange surface. Thereby increase the contact width in plastic condition and reduced the axial force for tightening. However, the relationship of the parameters affecting the sealing performance of the three-layer metal gasket is not yet well understood.

This paper clarifies the optimum shape for the three layer metal gasket utilizing the spring effect from parameters and surface roughness which influence leakage prevention. The summary is as follows. We investigated the performance and scope of various gaskets and presented the problems in previous research and clarified the outline of the research in this paper (Chapter 1). Influence of contact condition on leakage performance of SUS304, 25A-size Single Layer Metal Gasket, the numerical analysis and analysis using a leak test revealed that the larger the plastic deformation area at the contact portion, the higher the sealing performance (Chapter 2). From the study by numerical analysis, the influence of change in yield stress on contact stress and contact area was clarified as material properties

of surface layer member of three-layer metal gasket (Chapter 3). From the study by numerical analysis with fixed model, clarify using the material with low modulus of elasticity showed a decrease in contact stress as contact width is increased, and it was shown that the average contact stress decreased as the contact width increased, when the thickness ratio was further increased (Chapter 4). The value analysis of the non-fixed model as the boundary condition between the laminated members in the three-layer metal gasket revealed the influence of flange surface roughness on contact stress and contact area. Furthermore, from the evaluation by the leakage test, it was revealed that the three-layer metal gasket, which is surface layer mainly the plastic region, is less affected by the surface roughness of the flange than the single layer metal gasket and has high sealing performance (Chapter 5). Numerical analysis of the optimum shape under non-fixed model and fixed model condition by contact stress condition revealed has higher contact width in plastic contact stress condition and high stress ratio, based on this we can state that optimum design three-layer gasket has better sealing performance than gasket single layer (Chapter 6). We summarized the obtained results and clarified the optimum shape of three-layer metal gasket, which is hardly affected by surface roughness of flange in leakage performance. Further consideration is needed, such as creep characteristics under high temperature environment and consideration of the influence of gasket surface treatment etc., future issues and prospects were mentioned (Chapter 7).

CHAPTER I
INTRODUCTION

1.1 Background

In the piping system, the gasket plays an important role to prevent leakage. The gasket insert between two flanges that have surface imperfections so that very effective in prevent the leakage. Gasket material commonly used is asbestos because it is resistant to chemicals and have a wide temperature range. However, after asbestos was known contain chemicals that are dangerous and can cause serious illness, its usage was prohibited. In Japan, production and usage of asbestos has been banned since 2008 [1], so it is necessary to find alternative materials for asbestos gasket replacement.

Researchers have a challenge to find alternative materials as a substitute for asbestos. The new material is expected to have the same performance as asbestos. Some researchers have attempted to investigate new materials and some other researchers developed a new sealing system by optimize multiple design parameters to improve sealing performance. There is no ideal product that can replace asbestos gaskets so that different materials needed to be developed to suit the various applications.

Various kinds of materials investigated as a gasket material in order to obtain a good sealing performance. Glass Fiber Reinforced Plastic (GFRP) materials are used because their resistance to corrosion [2] and [3]. However, this material is expensive and low in operating pressure compare than carbon steel. Exfoliated graphite material used as the filler for metal based designs such as a Spiral wound Gasket (SWG), is appropriate for use in high-pressure and high-temperature conditions [2] and [4]. However, this material has problems associated with fragility, purity, and storage. Polytetrafluoroethylene (PTFE) exhibits extreme chemical resistance, but it lacks creep resistance [2] and [5]. In fact, the performance of the replacement of asbestos gasket material is lower than that achieved by asbestos and also has a short period of use.

Persson et al. [6] and [7] studied the contact stress distribution. They compared the contact stress distribution result obtained using an analytical model with the (exact)

numerical result obtained for contact between a cylinder and a nominal flat substrate with surface roughness having many different length scales and found good agreement between the two. Specially, the theory predicted that the area of contact in most cases varies linearly with the load and that it depends on the magnification; both predictions showed excellent agreement with the (exact) numerical results.

Persson et al. [8] developed contact mechanics theory to calculate the leak-rate of static seals. They assumed that purely elastic deformation occurs in the solid, which is the case for rubber seals. For metal seals, strong plastic deformation often occurs in the contact region. They presented a theory of the leak-seals, which is based on the percolation theory to predict the apparent contact area as a function of the magnification. It shows some interfacial surface is observed, the increasing of magnification effect on decreasing contact area. In the next study, Lorenz et al. [9] calculated the volume-flow per unit time of leak-rate (Q) on rubber gasket. The calculated leak-rate is in good agreement with experiment.

In above study they assumed that only elastic deformation occurs. However, the theory can be generalized to the case that plastic deformation occurs simply by replacing the boundary condition, which describes that plastic deformation occurs in the contact area when the local stress has reached σ_Y [10].

The use of metal gaskets might appropriate. It is preferred because of certain advantages such as chemical resistance, capability in wide temperature range, capability to withstand pressure, recyclability, low cost and most importantly its reliability in critical situations. The comparison of heat resistance, pressure resistance, and minimum axial force work condition between metal and other gasket materials shown in Table 1.1 [11]. However, disadvantage of metal gasket are the axial forces need to be high to deform the solid metal gasket and the loss of tightness of bolted flange due to the relaxation of the joint. Gasket and bolt are the joint members that give the largest bolt load relaxation ratio over time. In general, bolted joints relax extensively during the first few hours of service due to the excessive short term creep of the gasket. However, in the long term, the contribution of the bolt creep becomes significant especially at high temperature [12].

Table 1.1 Comparison of temperature and pressure work condition

Seal Material	Heat Resistance [°c]	Pressure resistance [MPa]	Minimum axial force [MPa]
Asbestos	～1000	14.7	11
Metal	～520	14.0	200
Graphite	-240～400	2.0	20
Resin	-50～150	1.0	20
Gum	-60～120	0.5	1.4

To decrease the axial forces for solid metal gasket and the loss of tightness of bolted flange due to the relaxation of the joint, the researcher using corrugated metal gasket. Saeed et al. [13] proposed super seal gasket, a new 25A size metal gasket that incorporates strategically placed circumferential annular lips. These lips, owing to the spring effect of the metal, form seal line with flanges. The circumferential annular lips are provided on upper and lower of gasket. When the flange is tighten by bolts, it can be generated high local contact stress on convex section of gasket to obtain a low loading metal gasket as shown in the Fig. 1.1. Also, the elastic regions on the flat sections (denoted by blue line) produce the spring effect of metal gasket, and it can be reduce the effect of the occurring of loosening of bolts.
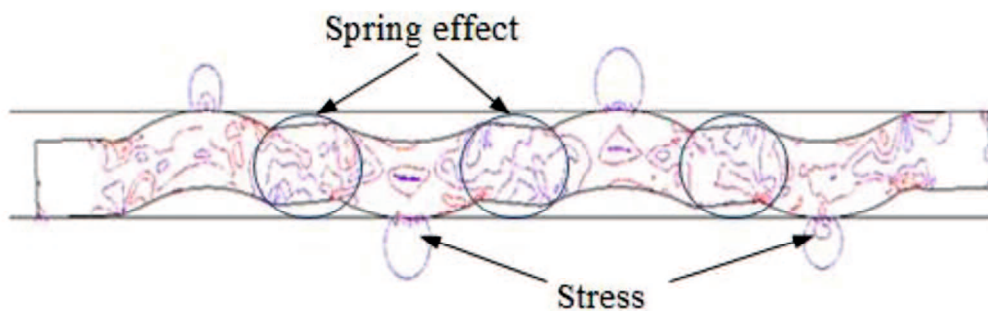
Fig. 1.1 High local contact stress on corrugated metal gasket

The contact stress and contact width were consider important design parameters for

optimizing the gasket performance. However, the value of the contact width as design has not yet been defined. Haruyama et al. investigated the allowable limits of the contact width [14]. A contact width for which no leakage occurs in the newly developed gasket was determined by comparing the evaluation results of the relationship between the axial force of the flange and the contact width as obtained using finite element method (FEM) analysis with the experimental results of the axial force and the leakage. These results were used to obtain the optimum contact width. The contact width shows a relationship with helium leakage; increasing the contact width results in a decrease the leakage. Choiron et al. [15] studied a method for validating the contact width measurement by using a simulation-based analysis. They compared the simulation result with experimental one obtained using pressure-sensitive paper and found good agreement between the two. In the increasing of axial force value, the helium leak quantity is decreasing and the contact width is increasing. Based on this circumstance, it can be concluded that the contact width has relationship with the helium leakage quantity. This fact is very useful if used in the evaluation of gasket performance. The result of the present study shows that the contact width can be employed to evaluate the sealing performance.

All 25A size metal gasket model on the previous study use the assumption an elastic contact stress. In fact, plastic deformation occurs in the contact area when the local stress has been reached. The use of simulation is beneficial in the design of metal forming operations because it is more cost effective than trial and error. The development of hardware and software support the metal forming simulation to define an elastic and plastic contact stress. It is also predict the forces and stresses necessary to execute the forming operation [16]. All 25A size metal gasket model on the previous study use the assumption exclude forming effect. It was known that the forming process produced residual forming data such as characterizing geometric imperfections and residual stresses [17]. The use of simulation is beneficial in the design of metal forming operations because it is more cost effective than trial and error. The development of hardware and software support the metal forming simulation to define the shape and initial material. It is also predict the forces and stresses necessary to execute the forming operation [18]. Press forming is performed to

4

produce gasket shape by a punch forces the initial material to slide into a die. Therefore, the forming effect is considered for gasket design modeling assessment. By using forming effect, the limit of contact width on the previous model which excluded forming effect for no leakage will be evaluated.

An important characteristic to consider in the development of a new metal gasket is a function to prevent leakage depending on the surface roughness standard used. Leakage is a function of surface roughness for molded rubber sealing [19] —it increases with the surface roughness. Person et al. [8] and Lorenz et al. [9] studied theory leak-rate of seals, which is the case for rubber seals. They have presented a theory of the leak-rate of seal, which based on percolation theory and developed contact mechanics theory. They have presented numerical results for the leak-rate $\dot{Q}$, and for surface roughness lateral size λ_c and the height u_c of the critical construction. They have presented result for how leak-rate depended on lateral size and the height surface roughness and on the pressure with which the rubber is squeezed against the rough counter-surface.

Nurhadiyanto et al. [20] studied a gasket design optimization based on an elastic and plastic contact stress analysis considering forming effect using FEM. The gasket design based on elastic called 0-MPa mode and the gasket design based on plastic contact stress called 400-MPa mode. The helium leak test shows that a gasket based on the plastic contact stress design better than a gasket based on elastic stress design. However, both types of gasket can be used as a seal, because it did not leak in the helium leak test. Haruyama et al. [21], [22] studied a gasket model include a flange surface roughness effect. A finite element method was employed to develop simulation solution. A uniform quadratic mesh used for meshing the gasket material and a gradually quadrilateral mesh used for meshing the flange. The gasket model was simulated by using two simulation stages which is forming and tightening simulation. A simulation result shows that a smoother of surface roughness has higher slope for force per unit length. This mean a squeezed against between flange and gasket will be strong. The slope of force per unit length for gasket 400-MPa mode was higher than the gasket 0-MPa mode. Finally, the helium leakage quantity was determined to evaluate the leakage performance. The experimental result shows that the gasket in 400-

MPa mode shows better sealing performance than the gasket in 0-MPa mode. For a low axial force, changes in the surface roughness caused significant changes in the leakage; the same was not observed for a high axial force. Haruyama et al. [23] and Nurhadiyanto et al. [24] conducted the surface roughness evaluation of 25A-size metal gasket before and after use. The results denote the real contact width after contact with flange having different surface roughness. The real contact width for the flange having smoother surface roughness is wider than the rougher one.

The main problem in this regard is the fact that a metal gasket SUS304 performance decrease when contact with flange having high surface roughness. This is because when gasket SUS304 contact with a flange that has high surface roughness, contact width containing plastic contact stress condition is also reduced so that the sealing performance of the gasket also decreased. Based on this reason, improvement of metal gasket performance continues researched therefore not leakage when contact with flange having high surface roughness.

In this research we inserted the soft metal as surface layer at the top and bottom of the SUS304 gasket therefore when contact with the flange having high surface roughness the soft metal will be deformed plastically and fill the gap of the imperfect flange surface. Thereby increase the contact width and reduced the axial force for tightening. However, the relationship of the parameters affecting the sealing performance of the three-layer gaskets is not yet well understood.

For that reason, the aims of these studies are (1) To obtain the influence of soft metal as surface layer by varies tangent modulus on contact width and contact stress. (2) To obtain the influence of thickness ratio and modulus elasticity ratio of three-layer corrugated metal gasket on contact width and contact stress. (3) To obtain the influence of surface roughness of flange in correlation with contact width and contact stress of the three-layer corrugated metal gasket. Comparison contact width in simulation and experiment result. (4) To obtain the optimum design of three-layer corrugated metal gasket by using Taguchi method.

1.1 Research Purposes

Based on explanation above, we developed the three-layer corrugated metal gasket. The real contact area and contact stress are affected by the load. The quantity of leakage paths are reduced under increasing compression. This assumption is connected with previous study that contact area and contact stress as main parameter affected the leakage. In this study, metal gasket evaluation method is investigated based assumption different surface roughness due to the leakage mechanism theory on metal gasket has not been provided yet. The surface roughness is set to fulfill the JIS standard. Therefore, the leakage test is used to obtain performance evaluation method on new metal gasket. It is not possible to decide whether there was a leakage or no leakage from the helium leakage test.

Saeed et al. [13] results justify the selection of contact area as reasonable performance evaluation criteria, but the limits size of contact area for no leak as design parameter was not defined yet. The leakage can be reduced with increasing the contact width. Choiron et al. [15] justify that the contact width validation is provided by using Finite Element Analysis (FEA) and the result is compared to experimental using pressure sensitive paper. The quantitative evaluation of helium leakage rate and the contact width of the gasket which has no leakage by the water pressure test are carried out as design concept.

Choiron et al. [16] justify that the optimum design on new metal gasket considering plastic contact stress is realized by using Taguchi method. They studied, that the optimum design use seven parameter and it is chosen due to assumption that the better sealing performances are desirable because the large contact stress creates sealing lines on contact width. Based on plastic contact stress consideration on contact width, the optimized gasket is determined by deleting contact width with contact stress below of 400MPa. The optimum design of new 25A-size metal gasket has been obtained. By using forming effect, the limit of contact width on the previous model which excluded forming effect for no leakage was evaluated. Initial blank thickness is varied by adding 0% ($t_{0\%}$), 5% ($t_{5\%}$) and 10% ($t_{10\%}$) of the final thickness of the gasket. The result shows that the final design shapes produced the defect occurred on the radius shape of convex contact. The lack of die fill defect is

decreased with increasing initial blank thickness. The $t_{0\%}$ forming model provide contact width trend as similar with the non-forming model. The forming models show a higher contact stress than it's the non-forming models due to residual stress of forming effect. The increasing initial blank thickness will need extra force to forming process. This treatment will change the characteristic of material gasket. We need another treatment to decreasing lack of die fill defect.

Widder [19] studied the surface finish effect in static sealing. Leakage is a function of surface roughness —it increases with the surface roughness. Person et al. [8] and Lorenz et al. [9] studied theory leak-rate of seals, which is the case for rubber seals. They have presented numerical results for the leak-rate and for surface roughness. They have presented result for how leak-rate depended on lateral size and the height surface roughness and on the pressure with which the rubber is squeezed against the rough counter-surface.

Nurhadiyanto et al. [20] studied a gasket design optimization based on an elastic and plastic contact stress analysis considering forming effect using FEM. The gasket design based on elastic called 0-MPa mode and the gasket design based on plastic contact stress called 400-MPa mode. The helium leak test shows that a gasket based on the plastic contact stress design better than a gasket based on elastic stress design. However, both types of gasket can be used as a seal, because it did not leak in the helium leak test. Haruyama et al. [21], [22] studied a gasket model include a flange surface roughness effect. A finite element method was employed to develop simulation solution. A uniform quadratic mesh used for meshing the gasket material and a gradually quadrilateral mesh used for meshing the flange. The gasket model was simulated by using two simulation stages which is forming and tightening simulation. A simulation result shows that a smoother of surface roughness has higher slope for force per unit length. This mean a squeezed against between flange and gasket will be strong. The slope of force per unit length for gasket 400-MPa mode was higher than the gasket 0-MPa mode. Finally, the helium leakage quantity was determined to evaluate the leakage performance. The experimental result shows that the gasket in 400-MPa mode shows better sealing performance than the gasket in 0-MPa mode. For a low axial force, changes in the surface roughness caused significant changes in the leakage; the

same was not observed for a high axial force. Haruyama et al. [23] and Nurhadiyanto et al. [24] conducted the surface roughness evaluation of 25A-size metal gasket before and after use. The results denote the real contact width after contact with flange having different surface roughness. The real contact width for the flange having smoother surface roughness is wider than the rougher one.

Based on explanation above, the aims of this study are:

1. What are the influences of soft material as the surface layer and tangent modulus on three-layer metal gasket based on contact width and contact stress considering forming effect? What is the influence of modulus elasticity ratio and thickness ratio on three layer metal gasket based on contact width and contact stress considering forming effect?

2. What is the influence of flange surface roughness and thickness of surface layer on three- layer metal gasket to leakage test and the correlation with contact width and contact stress? How to measure a contact width in simulation and experiment result?

3. What is the optimum design of three-layer corrugated metal gasket based on contact width considering forming and contact stress effect?

Contact stress and contact area are important parameter for leakage		In the past, leak or no leak judgment by Water pressures test
Evaluation of axial force and tightening procedure	-Gasket tightening simulation analysis -Gasket trial manufacture	Leak rate test by Helium leak Test
Evaluation of lack of die fill defect	The optimum 25A-size metal gasket design by using Taguchi method	The influence of surface roughness to the real contact width and contact
The influence of surface roughness to the leakage		
Evaluation of different material surface layer	Three-layer Gasket: - Simulation analysis - Trial manufacture	The influence of surface roughness to the leakage
Evaluation of different surface layer thickness		

First Stage — The influence of tangent modulus, modulus elasticity ratio and thickness ratio on three layer metal gasket based on contact width and contact stress by simulation method.

Second Stage — The influence of flange's surface roughness on three-layer metal gasket with a different thickness of surface layer based on contact width and contact stress by simulation and helium leak test.

Third Stage — The optimum three-layer corrugated metal gasket by using Taguchi method

Fig. 1.2 The layout of research stages

The layout of research step is shown in Fig.1.2. The work is divided based on three stages as follows:

1. **First Stage:** A development of three-layer metal gasket which design based on previous research. The material used as surface layer are soft material with varies tangent modulus. There are 2 type gaskets, which are 0-MPa mode and 400-MPa mode. In this stage, the influence of thickness ratio and modulus of elasticity ratio on three layer-metal gasket based on contact width considering forming and contact stress effect is studied. Gasket models based on optimal design from previous research, which are 400-MPa mode and 0-MPa.

2. **Second Stage:** Previous stages did not include the flange surface roughness effect. In this stage the surface roughness influence is determined through different thickness layer and the result comparison between simulation and experiment. An experiment analysis by measuring leakage and a simulation analysis result based on contact stress and contact width.

3. **Third Stage:** Based on increasing contact width with considering contact stress, the optimum shape of three-layer metal gasket is developed by Taguchi method.

1.3 Outline

The dissertation outline is described below. This dissertation contains seven chapters. The first chapter describes the introduction, which consist of motivation and background of this research. We investigate the performance and application range of various gaskets and show the problems in the previous research and clarify the outline of the research in this paper. The basic theory that used as a base for this project is given in the Chapter 2. The asbestos history, forces acting on a gasket joint, FEA, Taguchi Method, contact mechanics theory, leakage theory, and contact between two surfaces roughness model were describes completely in this chapter. A new approach of leak test method was used to evaluate the leakage of metal gasket using helium leak and water pressure tests continuously. FEM analysis was used to analyze the contact width and it is validated using pressure sensitive paper. By using the results of the FEM analysis and the leak measurement results, the

design concept of the 25A-size metal gasket was realized; the design was developed by using the relationship between the contact width and leakage. The flange surface roughness effect the sealing performance of the corrugated metal gasket. A metal gasket SUS304 performance decrease when contact with flange having high surface roughness because contact width containing plastic contact stress condition is reduced. It shows that gasket 400-MPa mode better sealing performance than 0-MPa mode because has larger contact width in plastic contact stress condition

In the Chapter 3, a three-layer metal gasket is developed to improve gasket performance from previous research by finite element method. The design used on optimal design from single layer SUS304 for 0-MPa and 400-MPa mode. This research proposed three-layer metal gasket with surface layer properties softer than the base metal. The three layer material with SUS304 as base metal and soft material as the surface layer was chosen so that when contact with flanges it will form the micro seal to cover roughness of the flange. The better design based on the increasing contact width in plastic contact stress condition with considering forming and contact stress effect. Gasket with surface layer mat1 has highest contact width than the others. Gasket with surface layer mat3 has highest contact stress than the others. Surface material with high tangent modulus will give high contact stress. Chapter 4 is investigated the effect of modulus elasticity ratio and thickness ratio with previous design for fix model on contact width and contact stress was also clarified. By using the material with lower modulus elasticity ratio, will increase contact width in contact stress plastic condition. In addition increase thickness ratio produces increase contact width in plastic contact stress condition. For gasket 0-MPa mode, thickness ratio [Ts/Tg] = 0.1/1.2; 0.2/1.2; 0.3/1.2 shown significant contact width improvement, higher than that ratio, contact width tend to constant. For gasket 400-MPa mode, thickness ratio [Ts/Tg] = 0.1/1.5, 0.2/1.5 and 0.3/1.5 shown significant contact width improvement, higher than that ratio contact width result tend to constant. Chapter 5, the influences of flange surface roughness on contact stress and contact width for gasket three-layer with no-fix model by numerical and experiment was clarified. Gasket three-layer 400MPa mode with C1020 as surface layer and SUS304 as base material, thinner surface layer show better

sealing performance than single layer SUS304 in contact with high surface roughness of flange because has large contact width in plastic contact stress condition at low axial force. Chapter 6, the optimum design was clarified by numerical analysis for no-fix model metal gasket three-layer under each factor and level design. The optimum design has larger contact width in plastic contact stress condition than single layer. Based on this we can assume our optimum gasket design will give better sealing performance than single layer SUS304. Summarize the result, we clarified the three-layer metal gasket has good sealing performance in high surface roughness of flange because produce larger contact width in plastic contact stress condition. However, it is necessary to consider the influence of creep characteristics and surface treatment in high temperature environment for future issues and challenge are presented in Chapter 7.

CHAPTER II

LITERATURE STUDY

2.1. Asbestos History

Asbestos is the name given to a group of six different fibrous minerals (amosite, chrysotile, crocidolite, and the fibrous varieties of tremolite, actinolite, and anthophyllite) that occur naturally in the environment. One of these, namely chrysotile, belongs to the serpentine family of minerals, while all of the others belong to the amphibole family. All forms of asbestos are hazardous, and all can cause cancer, but amphibole forms of asbestos are considered to be somewhat more hazardous to health than chrysotile. The serpentine group includes the chrysotile (white asbestos) and the amphibole group includes the crocidolite (blue asbestos) and the amosite (brown asbestos) (see Fig. 2.1).
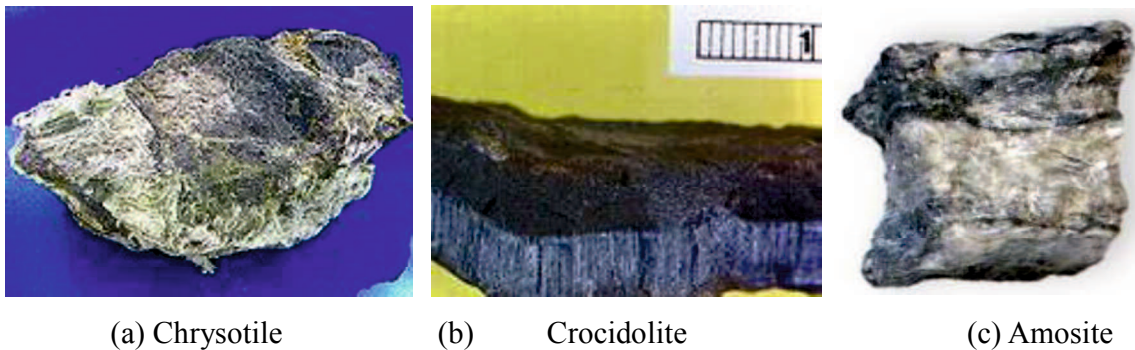
(a) Chrysotile   (b)   Crocidolite   (c) Amosite

Fig. 2.1 Types of asbestos

Asbestos fibers do not evaporate into air or dissolve in water. However, pieces of fibers can enter the air and water from the weathering of natural deposits and the wearing down of manufactured asbestos products. Small diameter fibers and fiber-containing particles may remain suspended in the air for a long time and be carried long distances by wind or water currents before settling. Larger diameter fibers and particles tend to settle more quickly. Asbestos fibers are not able to move through soil. They are generally not broken down to other compounds in the environment and will remain virtually unchanged

over long periods. However, the most common form of asbestos, chrysotile, may have some minor mineral loss in acidic environments. Asbestos fibers may break into shorter pieces or separate into a larger number of individual fibers as a result of physical processes. When asbestos fibers are breathed in, they may get trapped in the lungs. Levels of fibers in lung tissue build up over time, but some fibers, particularly chrysotile fibers, can be removed from or degraded in the lung with time.

If we breathe asbestos fibers into our lungs, some of the fibers will be deposited in the air passages and on the cells that make up our lungs. Most fibers are removed from our lungs by being carried away or coughed up in a layer of mucus to the throat, where they are swallowed into the stomach. This usually takes place within a few hours. Fibers that are deposited in the deepest parts of the lung are removed more slowly. In fact, some fibers may move through our lungs and can remain in place for many years and may never be removed from your body. If we swallow asbestos fibers (either those present in water or those that are moved to our throat from your lungs), nearly all of the fibers pass along our intestines within a few days and are excreted in the feces. A small number of fibers may penetrate into cells that line our stomach or intestines, and a few penetrate all the way through and get into our blood. Some of these become trapped in other tissues, and some are removed in our urine. If we get asbestos fibers on our skin, very few of these fibers, if any, pass through the skin into our body.

Asbestos workers have increased chances of getting two principal types of cancer: cancer of the lung tissue itself and mesothelioma, a cancer of the thin membrane that surrounds the lung and other internal organs. These diseases do not develop immediately following exposure to asbestos, but appear only after a number of years. There is also some evidence from studies of workers that breathing asbestos can increase the chances of getting cancer in other locations (for example, the stomach, intestines, esophagus, pancreas, and kidneys), but this is less certain. Members of the public who are exposed to lower levels of asbestos may also have increased chances of getting cancer, but the risks are usually small and are difficult to measure directly. Lung cancer is usually fatal, while mesothelioma is almost always fatal, often within a few months of diagnosis. Some

scientists believe that early identification and intervention of mesothelioma may increase survival [25].

Coming to the forms of asbestos, they are basically three in number, which are divided into two groups called serpentine group and amphibole group. In 2005, 2.2 million tons of asbestos were mined worldwide. Russia was the largest producer with about 40% world share followed by China and Kazakhstan.
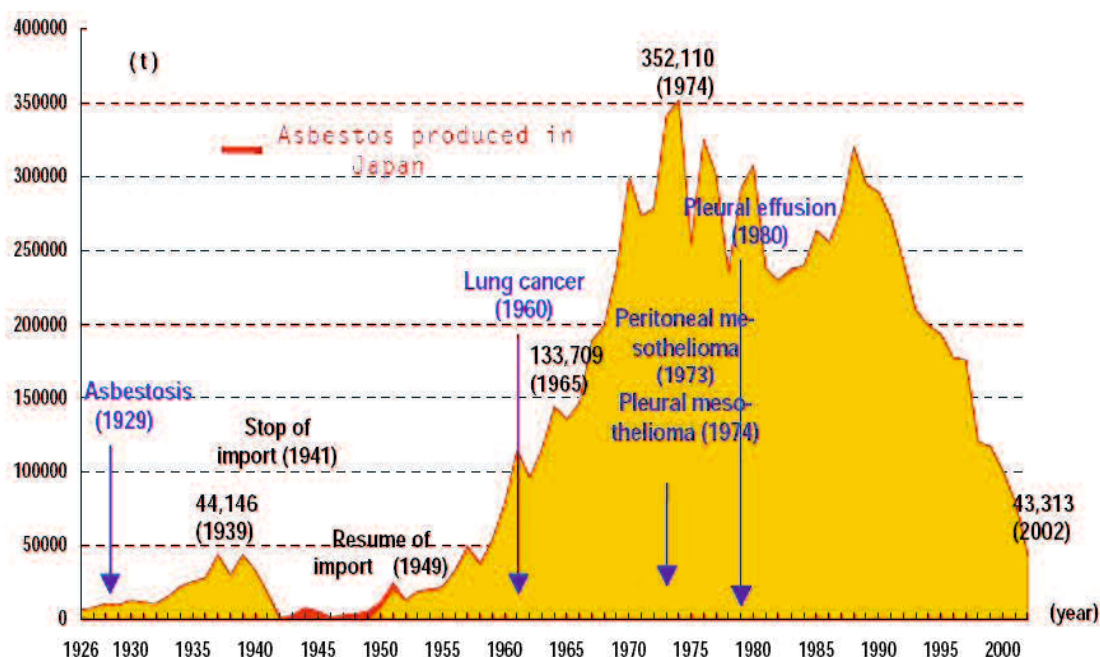
Fig. 2.2 Annual asbestos import to Japan and asbestos-related diseases in Japan

Japan is one of the biggest consumer/importer countries of asbestos in the world, particularly after World War II. Asbestos was used in the manufacture of ammonium sulfate for purposes of rice production, sprayed upon the ceilings, iron skeletons, and walls of railroad cars and buildings (during the 1960s), and used for energy efficiency reasons as well [26]. Asbestos imports increased during the period of Japan industrial growth in the 1960s and 1970s. In 1974, annual imports reached a peak at 352,110 tons (Fig. 2.2). Thus the figure for 1988 represents the second peak in the use of asbestos in Japan. But

following a global trend, Japanese asbestos industry stopped importing crocidolite (blue asbestos) since 1988 and amosite (brown asbestos) since 1993. Thereafter only chrysotile (white) asbestos has been used in Japan.

Asbestos is known to have toxicity. The inhalation of toxic asbestos fibers can cause serious illnesses, including malignant mesothelioma, lung cancer, and asbestosis. Since the mid of 1980s, many uses of asbestos have been banned in several countries. In Japan, the first asbestosis case was reported in 1929, lung cancer due to asbestos exposure in 1960 and mesothelioma in 1973. The Minister of Health, Labor and Welfare announced in 2002 that Japanese Government was thinking about the ban of chrysotile. In 2005, Japanese Minister Hidehisa Otsuji announces a total asbestos ban in Japan within 3 years.

2.2. Forces Acting on a Gasket Joint

Gasket are used to create a static seal between two stationary members of a mechanical assembly and to maintain that seal under operating conditions which may vary dependent upon changes in pressures and temperatures. If it were possible to have perfectly mated flanges and it were possible to maintain an intimate contact of these perfectly mated flanges throughout the extremes of operating conditions, a gasket would not be required.

There are three principal forces acting on any gasket joint, which are:

1. Bolt load and/or other means of applying the initial compressive load that it flow the gasket material into surface imperfections to form a seal.

2. The hydrostatic end force, that tends to separate flanges when the system is pressurized.

3. Internal pressure acting on the portion of the gasket exposed to internal pressure, tending to blow the gasket out of the joint and/or to bypass the gasket under operating conditions.

Figure 2.3 indicates the three primary forces acting upon a gasket joint. The initial compression force applied to a joint must serve several purposes.

- It must be sufficient to initially seat the gasket and flow the gasket into the imperfections on the gasket seating surfaces regardless of operating conditions.

- Initial compression force must be great enough to compensate for the total hydrostatic

end force that would be present during operating conditions.

- It must be sufficient to maintain a residual load on the gasket/flange interface.
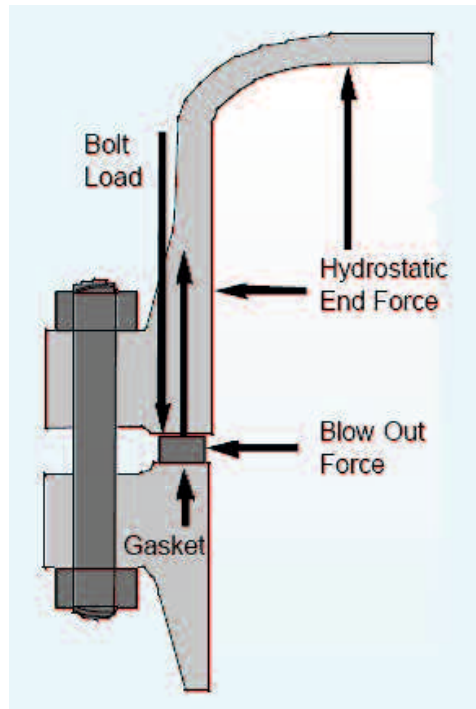
Fig. 2.3 Forces acting on a gasket joint

From a practical standpoint, residual gasket load must be "X" times internal pressure if a tight joint is to be maintained. This unknown quantity "X" is what is known as the "m" factor in the ASME boiler and pressure vessel code [27] and will vary depending upon the type of gasket being used as shown in the Table 2.1. Actually the "m" value is the ratio of residual unit stress (bolt load minus hydrostatic end force) on gasket (psi) to internal pressure of the system. The larger the number used for "m," the more conservative the flange design would be, and the more assurance the designer has of obtaining a tight joint. The initial bolt load required to seat a gasket sufficiently is defined as:

$$W_{m2} = \pi b G y \qquad (2\text{-}1)$$

The required operating bolt load must be at least sufficient, under the most severe operating conditions, to contain the hydrostatic end force and, in addition, to maintain a residual compression load on the gasket that is sufficient to assure a tight joint. ASME defines this bolt load as:

$$W_{m1} = \frac{\pi}{4}G^2P + 2b\pi GmP \qquad\qquad (2\text{-}2)$$

After W_{m1} and W_{m2} are calculated, then the minimum required bolt area A_m is determined:

$$A_{m1} = \frac{W_{m1}}{S_b}$$

$$A_{m2} = \frac{W_{m2}}{S_a}$$

$$A_m = A_{m1} \text{ if } A_{m1} \geq A_{m2} \quad \text{or} \quad A_m = A_{m2} \text{ if } A_{m2} \geq A_{m1} \qquad\qquad (2\text{-}3)$$

Bolts are then selected so that the actual bolt area A_b is equal to or greater than A_m

A_b = (Number of Bolts) x (Minimum Cross-Sectional area of bolts in inches^2)

$$A_b \geq A_m \qquad\qquad (2\text{-}4)$$

The maximum unit load $Sg_{(max)}$ on the gasket bearing surface is equal to the total maximum bolt load in pounds divided by the actual sealing area of the gasket in inches^2.

$$Sg_{(max)} = \frac{A_b S_a}{\pi/4\left[(OD-0.125)^2 - (ID)^2\right]} \Bigg\} \quad \text{Spiral wound gasket}$$

$$Sg_{(max)} = \frac{A_b S_a}{\pi/4\left[(OD)^2 - (ID)^2\right]} \Bigg\} \quad \text{All other types of gasket} \quad (2\text{-}5)$$

Except as noted, the symbols and definitions below are:

A_b = actual total cross-sectional area of bolts at root of thread or section of least diameter under stress (inches^2).

A_m = total required cross-sectional area of bolts, taken as the greater of A_{m1} or $A_{m2'}$ (inches^2).

A_{m1} = total cross-sectional area of bolts at root of thread or section of least diameter under stress, required for the operating conditions.

A_{m2} = total cross-sectional area of bolts at root of thread or section of least diameter under stress, required for gasket seating.

b = effective gasket or joint-contact-surface seating width (inches) in Table 2.2

b_o = basic gasket seating width (inches) as shown in Table 2.2

G = diameter at location of gasket load reaction as shown in Table 2.2

When bo ≤ 1/4 in., G = mean diameter of gasket contact face (inches).

When bo > 1/4 in., G = outside diameter of gasket contact faceless 2b (inches).

m = gasket factor as shown in the Table 2.1.

N = width, in inches, used to determine the basic gasket seating width bo, based upon the possible contact width of the gasket (Table 2.2)

P = design pressure (lbf/inch^2).

Sa = allowable bolt stress at ambient temperature (lbf/inch^2).

Sb = allowable bolt stress at operating temperature (lbf/inch^2).

Sg = Actual unit load at the gasket bearing surface (lbf/inch^2).

W_{m1} = required bolt load for operating conditions (lbf).

W_{m2} = minimum required bolt load for gasket seating ((lbf)

y = gasket or joint-contact-surface unit seating load, minimum design seating stress, PSI (Table 2.1).

Table 2.1 Gasket materials and contact facing

Gasket factors (m) for Operating Conditions and Minimum Design Seating Stress (Y)

Gasket Material		Gasket Factor (m)	Minimum Design Seating Stress (Y) (psi)	Sketches and Notes	Seating Width (See Table)	
					Gasket Group	Column
Self-Energizing Types O-rings, metallic, elastomer, and other gasket types considered as self-sealing		0	0			

Elastomers without fabric
    Below 75A Shore Durometer
    75A or higher Shore Durometer
		0.50
		1.00
			0
			200
					(1a), (1b)
					(1c), (1d),
					(4), (5)	

Elastomers with cotton fabric insertion		1.25	400			
Vegetable fiber		1.75	1100			
Flexicarb based products	MRG Flexpro NR SR ST	2.00 2.00 2.00 2.00 2.00	2,500 2,500 2,500 2,500 2,500			
Spiral wound metal, with filler		3.00	10,000		(1a), (1b)	
Spiral wound Style LS, Flexicarb Filled/PTFE filledThermiculite filled		3.00	5,000			
Corrugated metal with filler or Corrugated metal jacketed with filler	Soft aluminum Soft copper or brass Iron or soft steel Monel or 4%-6% chrome Stainless steels & Nickel based alloys	2.50 2.75 3.00 3.25 3.50	2900 3700 4500 5500 6500		(1a), (1b)	II
Corrugated metal	Soft aluminum Soft copper or brass Iron or soft steel Monel or 4%-6% chrome Stainless steels & Nickel based alloys	2.75 3.00 3.25 3.50 3.75	3700 4500 5500 6500 7600		(1a), (1b), (1c), (1d)	
Flat metal jacketed, with filler	Soft aluminum Soft copper or brass Iron or soft steel Monel 4%-6% chrome Stainless steels & Nickel based alloys	3.25 3.50 3.75 3.50 3.75 3.75	5500 6500 7600 8000 9000 9000		(1a)$_2$, (1b)$_2$, (1c), (1d), (2)	
Grooved metal	Soft aluminum Soft copper or brass Iron or soft steel Monel or 4%-6% chrome Stainless steels & Nickel based alloys	3.25 3.50 3.75 3.75 4.25	5500 6500 7600 9000 10100		(1a), (1b), (1c), (1d), (2), (3)	
Solid flat metal	Soft aluminum Soft copper or brass Iron or soft steel Monel or 4%-6% chrome Stainless steels & Nickel based alloys	4.00 4.75 5.50 6.00 6.50	8800 13000 18000 21800 26000		(1a), (1b), (1c), (1d), (2), (3), (4), (5)	I
Ring Joint	Iron or soft steel Monel or 4%-6% chrome Stainless steels & Nickel based alloys	5.50 6.00 6.50	18000 21800 26000		(6)	

Notes:
This table gives a list of many commonly used gasket materials and contact facings with suggested design values of m and y that have generally proved satisfactory in actual service when using effective gasket seating width b given in the table on the next page. The design values and other details given in this table are suggested only and are not mandatory.

Table 2.2 Effective Gasket Width

Facing Sketch Exaggerated		Basic Gasket Seating Width, b_o	
		Column I	Column II
(1a)		$\dfrac{N}{2}$	$\dfrac{N}{2}$
(1b) See Note (2)			
(1c) $w \leq N$		$\dfrac{W+T}{2} \; ; \; \left(\dfrac{W+N}{4} \text{ max.}\right)$	$\dfrac{W+T}{2} \; ; \; \left(\dfrac{W+N}{4} \text{ max.}\right)$
(1d) See Note (2) $w \leq N$			
(2) $w \leq N/2$		$\dfrac{W+N}{4}$	$\dfrac{W+3N}{8}$
(3) $w \leq N/2$		$\dfrac{N}{4}$	$\dfrac{3N}{8}$
(4) See Note (2)		$\dfrac{3N}{8}$	$\dfrac{7N}{16}$
(5) See Note (2)		$\dfrac{N}{4}$	$\dfrac{3N}{8}$
(6)		$\dfrac{W}{8}$	

Effective Gasket Seating Width, b

$b = b_o$, when $b_o \leq 1/4"$; $b = 0.5\sqrt{b_o}$, when $b_o > 1/4"$

Location of Gasket Load Reaction

22
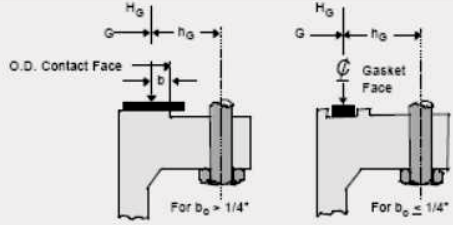
2.3. Finite Element Analysis

The basic idea in the finite element method as one of numerical technique is to get the solution of a complex problem by replacing it by a simpler one [28]. Since the actual problem is replaced by a simpler one in finding the solution, it will be able to find only an approximate solution rather than the exact solution. The existing mathematical tools will not be sufficient to find the exact solution of most of the practical problems. The name *finite element* was coined by Clough. Since its inception, many technical papers and books have appeared on the development and application of Finite Element Analysis (FEA). The books by Desai and Abel (1971), Oden (1972), Gallagher (1975), Huebner (1975), Bathe and Wilson (1976), Ziekiewicz (1977), Cook (1981), and Bathe (1996) have influenced the current state of FEA. In the finite element method, it will often be possible to improve or refine the approximate solution by spending more computational effort. In the finite element method, the solution region is considered as built up of many small, interconnected sub regions called finite elements. In each piece or element, a convenient approximate solution is assumed and the conditions of overall equilibrium of the structure are derived. The satisfaction of these conditions will yield an approximate solution for the displacements and stresses.

Fig. 2.4 shows the categories schematic of finite element analysis in engineering fields. The digital computer provided a rapid means of performing the many calculations involved in the finite element analysis and made the method practically viable. Along with the development of high-speed digital computers, the application of the finite element method also progressed at a very impressive rate. With all the progress, today the finite element method is considered one of the well-established and convenient analysis tools by engineers and applied scientists.
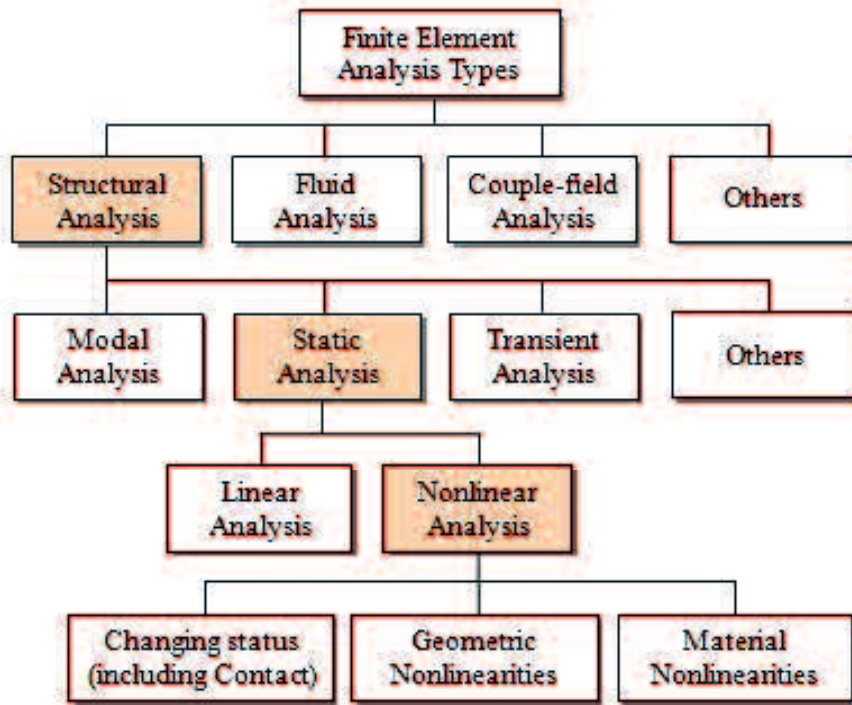
Fig. 2.4 Categories of FEA in engineering field

In the finite element method, the actual continuum or body of matter, such as a solid, liquid, or gas, is represented as an assemblage of subdivisions called finite elements. The type of element can be shown in the Fig. 2.5 [28]. These elements are considered to be interconnected at specified joints called nodes or nodal points. The nodes usually lie on the element boundaries where adjacent elements are considered to be connected. Since the actual variation of the field variable (e.g., displacement, stress, temperature, pressure, or velocity) inside the continuum is not known, we assume that the variation of the field variable inside a finite element can be approximated by a simple function. These approximating functions (also called interpolation models) are defined in terms of the values of the field variables at the nodes. When field equations (like equilibrium equations) for the whole continuum are written, the new unknowns will be the nodal values of the field variable. By solving the field equations, which are generally in the form of matrix equations,

the nodal values of the field variable will be known. Once these are known, the approximating functions define the field variable throughout the assemblage of elements. The solution of a general continuum problem by the finite element method always follows an orderly step-by-step process.
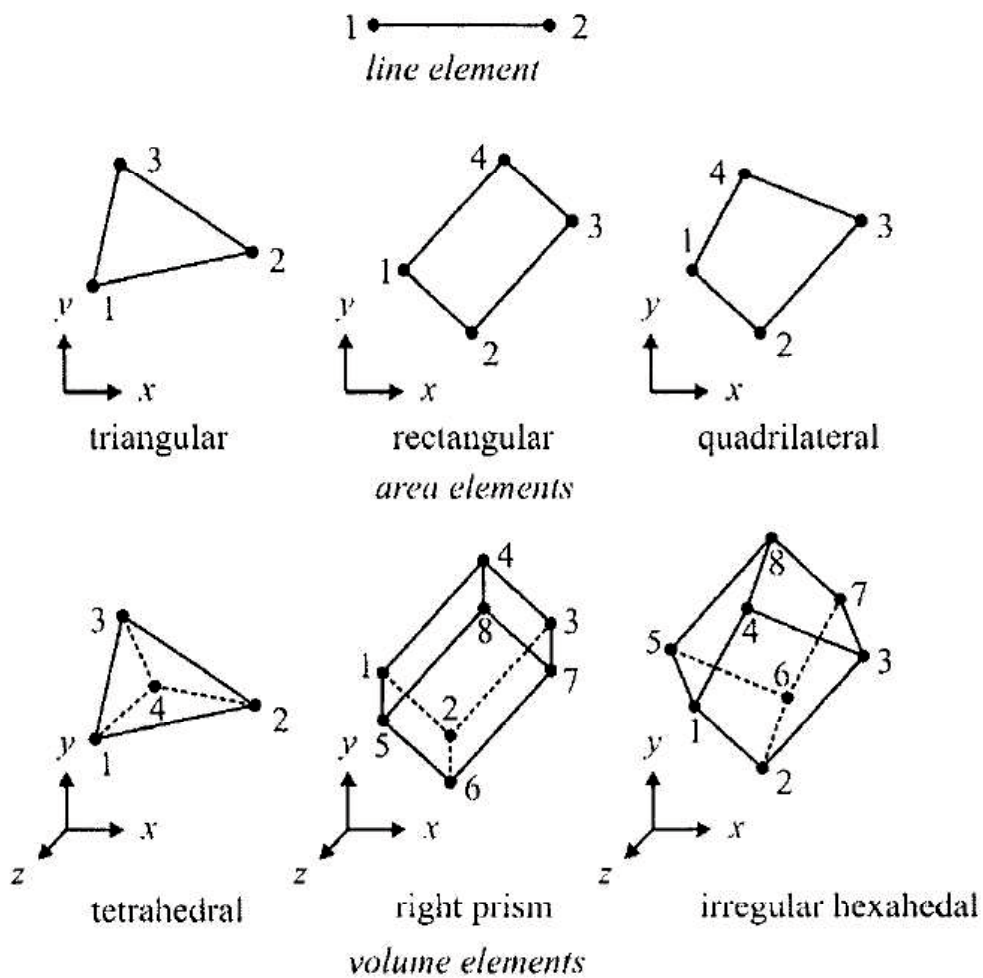
Fig. 2.5 The type of element

The finite element analysis method requires the following major steps:

1. Discretization of the domain into a finite number of sub domains (elements).

2. Selection of interpolation functions.

3. Development of the element matrix for the sub domain (element).

4. Assembly of the element matrices for each sub domain to obtain the global matrix for the entire domain,

5. Imposition of the boundary conditions.

6. Solution of equations.

7. Additional computations (if desired).

There are three main approaches to constructing an approximate solution based on the concept of FEA [29]:

1. Direct Approach

    This approach is used for relatively simple problems, and it usually serves as a means to explain the concept of FEA and its important steps.

2. Weighted Residuals

    This is a versatile method, allowing the application of FEA to problems which functional cannot be constructed. This approach directly utilizes the governing differential equations, such as those of heat transfer and fluid mechanics.

3. Variation Approach

    This approach relies on the calculus of variations, which involves extremizing a functional. This functional corresponds to the potential energy in structural mechanics

In solid mechanics, this is known as the principle of minimum potential energy, which states that among all compatible displacement fields satisfying the boundary conditions, the correct displacement field satisfying the equilibrium equations is the one that renders the potential energy an absolute minimum. A solution satisfying both equilibrium equations and boundary conditions is, of course, "exact"; however, such solutions are difficult, if not impossible, to construct for complex problems. Therefore, approximate solutions are obtained by assuming admissible displacement fields with unknown coefficients. The values of these coefficients are determined in such a way that the total potential energy of the system is a minimum. The principle of virtual work is applicable for any material behavior, whereas the principle of minimum potential energy is

applicable only for elastic materials. However, both principles yield the same element equations for elastic materials. The total potential energy of the structural system shown in Fig. 2.6 is defined as:

$$\pi_p = W + Q \tag{2-6}$$

where W = the strain energy

Q = the potential energy arising from the presence of body forces, surface tractions, and the initial residual stresses.

Strain energy is the capacity of the internal forces (or stresses) to do work through strains in the structure. For a linear elastic material, the strain energy of the deformed structure is given by

$$W = \frac{1}{2} \int_V (\varepsilon - \varepsilon^*)^T \sigma dV \tag{2-7}$$
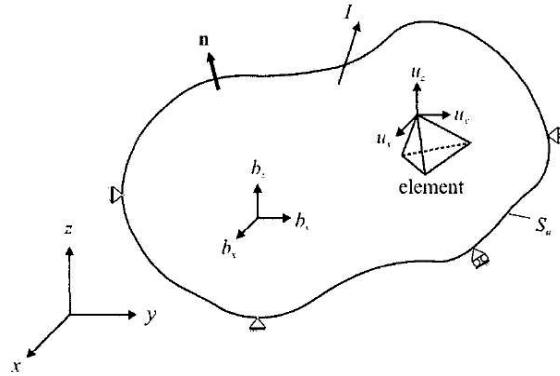
Fig. 2.6 A 3D body with displacement constraints, body and concentrated forces and surface traction.

where σ is the vector of stress components arising from the difference between the total strains, ε, and initial strains, ε*. It can be expressed as

$$\sigma = D\,(\varepsilon - \varepsilon^*) \tag{2-8}$$

in which

$$\sigma^T = \{\sigma_{xx} \quad \sigma_{yy} \quad \sigma_{zz} \quad \sigma_{xy} \quad \sigma_{yz} \quad \sigma_{zx}\}$$

$$\varepsilon^T = \{\varepsilon_{xx} \quad \varepsilon_{yy} \quad \varepsilon_{zz} \quad \gamma_{xy} \quad \gamma_{yz} \quad \gamma_{zx}\}$$

And the material property matrix

$$D = \frac{E}{(1+v)(1-2v)} \cdot \begin{bmatrix} 1-v & v & v & 0 & 0 & 0 \\ v & 1-v & v & 0 & 0 & 0 \\ v & v & 1-v & 0 & 0 & 0 \\ 0 & 0 & 0 & \frac{(1-2v)}{2} & 0 & 0 \\ 0 & 0 & 0 & 0 & \frac{(1-2v)}{2} & 0 \\ 0 & 0 & 0 & 0 & 0 & \frac{(1-2v)}{2} \end{bmatrix} \tag{2-9}$$

where σ_{ij} and ε_{ij} represent the stress and strain components, with $i,j = x,y,z$ being the Cartesian coordinates. The elastic modulus and Poisson's ratio are denoted by E and v, respectively.

The potential energy arising from the presence of body forces, b, surface tractions, T, and the initial residual stresses, σ*, is given by

$$\pi_p = -\int_V u^T b\,dv - \int_{S_V} u^T T\,dS - \int_V \varepsilon^T \sigma *dV \tag{2-10}$$

$$b^T = \{b_x \quad b_y \quad b_z\}$$

$$T^T = \{T_x \quad T_y \quad T_z\}$$

$$u^T = \{u_x \quad u_y \quad u_z\}$$

in which b_x, b_y, and b_z are the components of body force (in units of force per unit volume), and T_x, T_y, and T_z represent the components of the applied traction vector (in units of force per unit area) over the surface defined by S_σ. The entire surface of the body having a volume of V is defined by S, with segments S_u and S_σ subjected to displacement and

traction conditions, respectively. The displacement components are given by u_x, u_y, and u_z in the x-, y- , and z-directions, respectively. Also, included in the expression for the total potential is the initial residual stresses denoted by σ^*. The initial stresses could be measured, but their prediction without full knowledge of the material's history is impossible. After partitioning the entire domain occupied by volume V into E number of elements with volume V^e, the total potential energy of the system can be rewritten as

$$\pi_p(u_x, u_y, u_z) = \sum_{e=1}^{E} \pi_p^{(e)}(u_x, u_y, u_z)$$

in which

$$\pi_p^{(e)} = \frac{1}{2}\int_{V^{(e)}} \varepsilon^T D\varepsilon\, dV - \int_{V^{(e)}} \varepsilon^T D\varepsilon^*\, dV + \frac{1}{2}\int_{V^{(e)}} \varepsilon^{*T} D\varepsilon^*\, dV - \int_{V^{(e)}} u^T b\, dV - \int_{S_\sigma^{(e)}} u^T T\, dS + \int_{V^{(e)}} \varepsilon^T \sigma^*\, dV \tag{2-11}$$

where the superscript e denotes a specific element. Based on kinematical considerations, the components of the total strain vector ε, in terms of the displacement components are expressed as:

$$\begin{Bmatrix} \varepsilon_{xx} \\ \varepsilon_{yy} \\ \varepsilon_{zz} \\ \gamma_{xy} \\ \gamma_{yz} \\ \gamma_{zx} \end{Bmatrix} = \begin{bmatrix} \dfrac{\partial}{\partial x} & 0 & 0 \\ 0 & \dfrac{\partial}{\partial y} & 0 \\ 0 & 0 & \dfrac{\partial}{\partial z} \\ \dfrac{\partial}{\partial y} & \dfrac{\partial}{\partial x} & 0 \\ 0 & \dfrac{\partial}{\partial z} & \dfrac{\partial}{\partial y} \\ \dfrac{\partial}{\partial z} & 0 & \dfrac{\partial}{\partial x} \end{bmatrix} \cdot \begin{Bmatrix} u_x \\ u_y \\ u_z \end{Bmatrix} \quad , \text{ or } \quad \varepsilon = L \cdot u \tag{2-12}$$

in which L is the differential operator matrix.

The finite element process seeks a minimum in the potential energy based on the approximate form of the dependent variables (displacement components) within each element. The greater the number of degrees of freedom associated with the element (usually

means increasing the number of nodes), the more closely the solution will approximate the true equilibrium position. Within each element, the approximation to the displacement components can be expressed as

$$u_x^{(e)} \approx \widetilde{u}_x^{(e)} = \sum_{r=1}^{n} N_r^{(e)} u_{x_r}^{(e)} \qquad u_y^{(e)} \approx \widetilde{u}_y^{(e)} = \sum_{r=1}^{n} N_r^{(e)} u_{y_r}^{(e)} \qquad u_z^{(e)} \approx \widetilde{u}_z^{(e)} = \sum_{r=1}^{n} N_r^{(e)} u_{z_r}^{(e)}$$

with n representing the number of nodes associated with element e. The nodal unknowns and shape functions are denoted by $u_{x_r}^{(e)}, u_{y_r}^{(e)}, u_{z_r}^{(e)}$ and $N_r^{(e)}$, respectively. In matrix form, the approximate displacement components can be expressed as

$$\widetilde{u}^{(e)} = N^{(e)T} U^{(e)} \tag{2-13}$$

In which

$$\widetilde{u}_x^{(e)T} = \left\{ \widetilde{u}_x^{(e)} \quad \widetilde{u}_y^{(e)} \quad \widetilde{u}_z^{(e)} \right\}$$

$$N^{(e)T} = \begin{bmatrix} N_1 & 0 & 0 & N_2 & 0 & 0 & . & . & . & N_n & 0 & 0 \\ 0 & N_1 & 0 & 0 & N_2 & 0 & . & . & . & 0 & N_n & 0 \\ 0 & 0 & N_1 & 0 & 0 & N_2 & . & . & . & 0 & 0 & N_n \end{bmatrix}_{3x3n}$$

$$U^{(e)T} = \left\{ u_{x_1}^{(e)} \quad u_{y_1}^{(e)} \quad u_{z_1}^{(e)} \quad u_{x_2}^{(e)} \quad u_{y_2}^{(e)} \quad u_{z_2}^{(e)} \quad ... \quad u_{x_n}^{(e)} \quad u_{y_n}^{(e)} \quad u_{z_n}^{(e)} \right\}$$

With the approximate form of the displacement components, the strain components within each element can be expressed as

$$\varepsilon \approx B^{(e)} U^{(e)} \tag{2-14}$$

Where

$$B^{(e)} = L \, N^{(e)T} \tag{2-15}$$

leading to the expression for the total potential in terms of element nodal displacements, U

$$\pi_p^{(e)} = \frac{1}{2} U^{(e)T} k^{(e)} U^{(e)} - U^{(e)T} p^{(e)} + \frac{1}{2} \int_{V^{(e)}} \varepsilon *^T D\varepsilon * dV \qquad (2\text{-}16)$$

in which the element stiffness matrix, k, and the element force vector, p, are defined as

$$k^{(e)} = \int_{V^{(e)}} B^{(e)T} DB^{(e)} dV \qquad (2\text{-}17)$$

$$p^{(e)} = p_b^{(e)} + p_T^{(e)} + p_{\varepsilon*}^{(e)} + p_{\sigma*}^{(e)}$$

with $p_b^{(e)}$, $p_T^{(e)}$, $p_{\varepsilon*}^{(e)}$, and $p_{\sigma*}^{(e)}$ representing the element load vectors due to body forces, surface tractions (forces), initial strains, and initial stresses, respectively, defined by

$$p_b^{(e)} = \int_{V^{(e)}} N^{(e)} b \, dV$$

$$p_T^{(e)} = \int_{S_\sigma^{(e)}} N^{(e)} T \, dS$$

$$p_{\varepsilon*}^{(e)} = \int_{V^{(e)}} B^{(e)} D\varepsilon * dV$$

$$p_{\sigma*}^{(e)} = \int_{V^{(e)}} B^{(e)T} \sigma * dV$$

Evaluation of these integrals results in the statically equivalent nodal forces in the elements affected by the body force, the surface tractions, and the initial strains and initial stresses. In the presence of external concentrated forces acting on various nodes, the potential energy is modified as:

$$\pi_p = \frac{1}{2} U^T \left\{ \sum_{e=1}^{E} k^{(e)} \right\} U - U^T \left\{ \sum_{e=1}^{E} \left(p_b^{(e)} + p_T^{(e)} + p_{\varepsilon*}^{(e)} - p_{\sigma*}^{(e)} \right) - p_c \right\} + \frac{1}{2} \sum_{e=1}^{E} \int_{V^{(e)}} \varepsilon *^T D\varepsilon * dV \qquad (2\text{-}18)$$

where P_c is the vector of nodal forces and U represents the vector of nodal displacements

for the entire structure. Note that each component of the element nodal displacement vector, $U^{(e)}$ appears in the global (system) nodal displacement vector, U. Therefore, the element nodal displacement vector $U^{(e)}$ can be replaced by U with the appropriate enlargement of the element matrices and vectors in the expression for the potential energy by adding the required number of zero elements and rearranging. The summation in the expression for the potential energy implies the expansion of the element matrices to the size of the global (system) matrix while collecting the overlapping terms. Minimization of the total potential energy requires that

$$\left\{ \frac{\partial \pi_p}{\partial U} \right\} = 0 \tag{2-19}$$

Leading to the system (global) equilibrium equations in the form

$$K\,U = P$$

In which K and P is the assembled (global) stiffness matrix and the assembled (global) nodal load vector, respectively, defined by

$$K = \sum_{e=1}^{E} k^{(e)}$$

$$K = \sum_{e=1}^{E} \left(p_b^{(e)} + p_T^{(e)} + p_{\varepsilon*}^{(e)} - p_{\sigma*}^{(e)} \right) - p_c \tag{2-20}$$

This global equilibrium equation cannot be solved unless boundary constraints are imposed to suppress the rigid-body motion. Otherwise, the global stiffness matrix becomes singular. After obtaining the solution to the nodal displacements of the system equilibrium equations, the stresses within the element can be determined from

$$\sigma = D \, B^{(e)} \, U^{(e)} - D \, \varepsilon^* + \sigma^* \tag{2.21}$$

The global stiffness matrix and the load vector require the evaluation of the integrals associated with the element stiffness matrix and the element nodal load vector.

The term "3D solid" is used to mean a three-dimensional solid that is unrestricted as to shape, loading, material properties, and boundary conditions [30]. A consequence of this generality is that all six possible stresses (three normal and three shears) must be taken into account, see Fig. 2.7. Also, the displacement field involves all three possible components, u, v, and w. Typical finite elements for 3D solids are tetrahedral and hexahedra, with three translational degree of freedom (DOF) per node. Fig. 2.7b shows a hexahedral element.
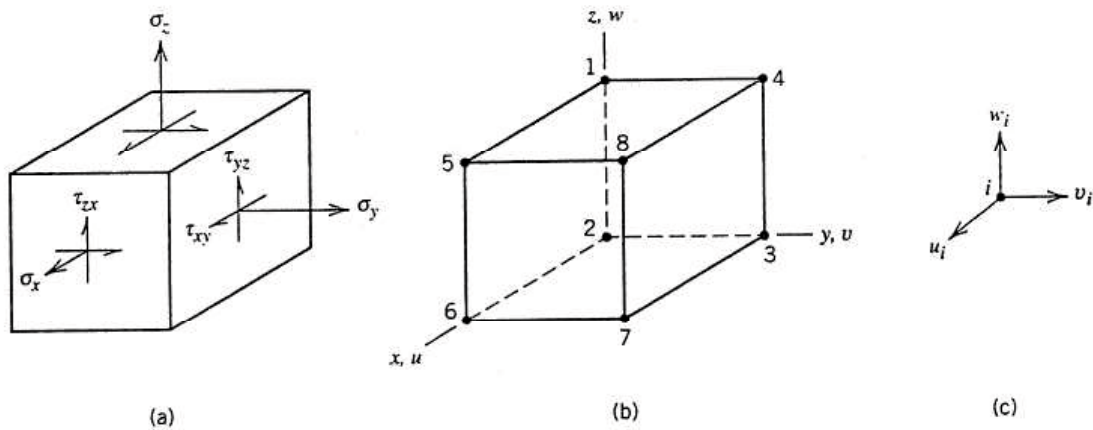
Fig. 2.7 (a) 3D state of stress (b) an eight-node hexahedron FE (c) the DOF at a typical node (i = 1,2,…, 8)

A solid of revolution, also called an axisymmetric solid, is generated by revolving a plane figure about an axis in the plane [30]. Common examples include a hose nozzle and a light bulb, although the light bulb has a very thin wall and would be properly classed as a shell of revolution for stress analysis purposes. Loads and supports may or may not have axial Symmetry. In the case where geometry, elastic properties, loads, and supports are all axisymmetric, consequently, nothing varies with the circumferential coordinate θ, material

points displace only radially and axially, and shear stresses $\tau_{r\theta}$ and $\tau_{\theta z}$ are both zero. Thus the analysis problem is mathematically two-dimensional. Axisymmetric finite elements are often pictured as plane triangles or quadrilateral, but these plane shapes are actually cross sections of annular elements, and what appear to be nodal points are actually nodal circles (Fig. 2.8).
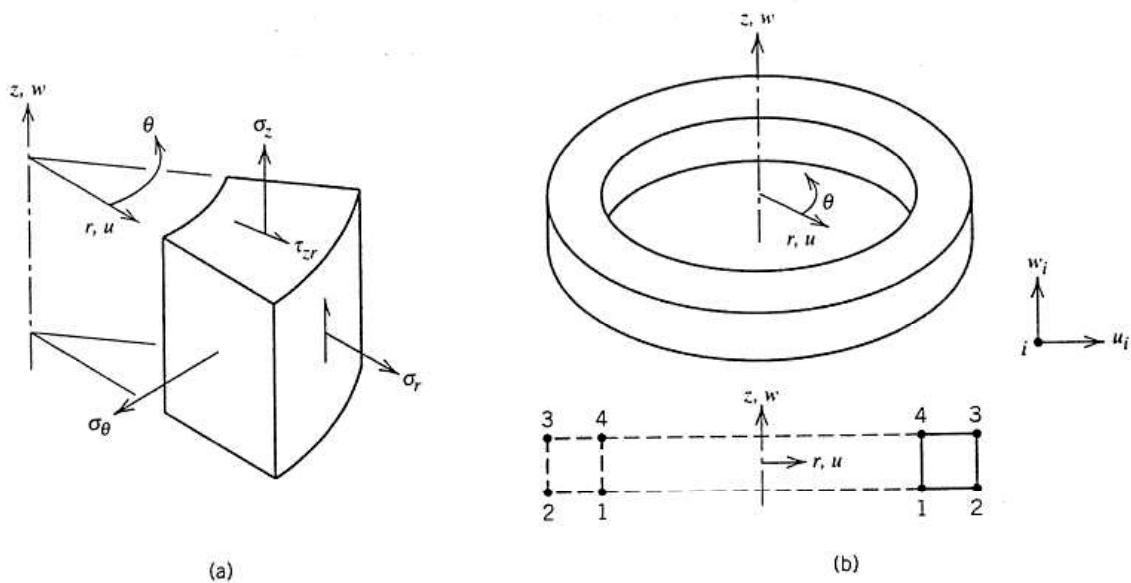
Fig. 2.8 (a) Axisymmetric state of stress (b) A four-node axisymmetric element and DOF at a typical node (i = 1,2,3,4)

2.4. Contact Mechanics Theories

Surface roughness on many different length scales, even a highly polished surface. Surface roughness has an important influence on many important physical phenomena such as contact mechanics, sealing, adhesion, and friction. When two bodies with nominally flat surfaces are brought into contact, real contact will only occur in small randomly distributed area. We can visualize the contact region as small areas where asperities from one solid are squeezed against asperities of the other solid. It depending on the conditions the asperities may deform elastically or plastically [6].

34

2.4.1   Hertz Theory

The area of real contact when two solids are brought into contact is important. The contact area and gab between two solids is very important for seals. Hertz [32] studied the frictionless contact between elastic solids with smooth surface profiles which could be approximated as parabolic close to the contact area. This theory predicts that the contact area A increases non-linearly with the squeezing force F as A ~ $F^{2/3}$. The simplest model of a randomly rough but nominal flat surface consist of a regular array of spherical bumps (asperities) with equal radius of curvature R and equal height, see Fig. 2.9. If such of surface is squeezed against an elastic solid with a flat surface, the Hertz contact theory can be applied to each asperity contact region and one expects that the area of real contact should scale as $F^{2/3}$ with the load or squeezing force F.

Fig. 2.9 Hertz models of rough surface

The Hertz theory describes the contact between two elastic spherical bodies (radius R_1 and R_2, respectively) with perfectly smooth surfaces. Fig 2.10 shows the Hertz theory. Assume that the spheres are squeezed together by force F and a circular contact area (radius r_0) is formed. The deformation field in the solids can be determined by minimizing the elastic deformation energy. The radius r_0 of the circular contact region is given by

$$r_0 = \left(\frac{R_1 R_2}{R_1 + R_2}\right)^{1/3} \left(\frac{3F(1-v^2)}{4E}\right)^{1/3} \tag{2.25}$$

where

$$\frac{1-v^2}{E} = \frac{1-v_1^2}{E_1} + \frac{1-v_2^2}{E_2} \tag{2.26}$$

where E_1 and E_2 are the modulus elasticity of solids and v_1 and v_2 the corresponding Poisson ratios. The distance S the two solids approach each other is given by

$$s = \left(\frac{R_1 + R_2}{R_1 R_2}\right)^{1/3} \left(\frac{3F(1-v^2)}{4E}\right)^{2/3} \qquad (2.27)$$
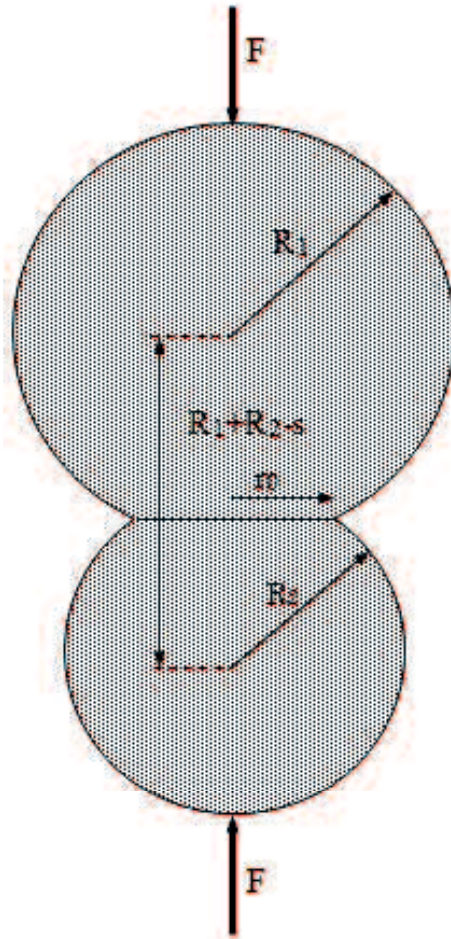
Fig. 2.10 Contact between two elastic spherical object.

For the special case of a sphere (radius *R*) in contact with a flat surface we get from (2.26) and (2.27) the area of contact

$$\pi r_0^2 = \pi R s \qquad (2.28)$$

and the squeezing force

$$F = \frac{4E}{3(1-v^2)} s^{3/2} R^{1/2}$$

(2.29)

The pressure distribution in the contact area depends only on the distance r from the center of the circular contact area:

$$\sigma(r) = \sigma_0 \left[1 - \left(\frac{r}{r_0} \right)^2 \right]^{1/2}$$

where $\sigma_0 = F/\pi r_0^2$ is average pressure.

2.4.2   Persson Theory for Elastic Contact Mechanics

When a surface roughness is studied at low magnification (ζ) it looks as if complete contact occurs between the solid at many *macroaspirity* contact region explained by Persson theory [6]. The contact between two solids at increasing magnification ζ is shown in Fig. 2.13. When the magnification is increased and smaller length scale roughness is detected, it can be observed that only partial contact occurs at the asperities. In fact, it there was no short distance cut-off the true contact area would eventually vanish. In reality, a short distance cut-off always exists, e.g., the interatomic distance. In many cases the local pressure in the contact regions at the asperities may become so high that the material yields plastically before reaching the atomic dimension. In these cases the size of the real contact area will be determined mainly by the yield stress of the solid.
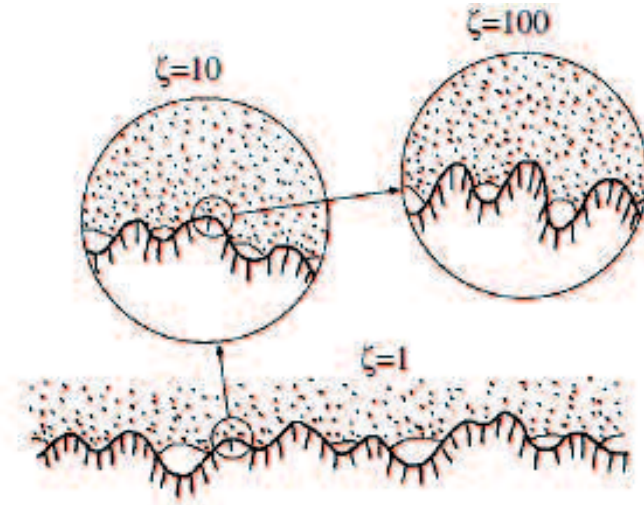
Fig. 2.11 A rubber block (dotted area) in adhesive contact with a hard rough substrate (dashed area)

The magnification ζ refers to some (arbitrary) chosen reference length scale. This could be, e.g., the lateral size L of the nominal contact area in which case $\zeta = \frac{L}{\lambda} = q/q_L$, where λ is the shortest wavelength roughness which can be resolved at magnification ζ.

Let us define the stress distribution at the magnification ζ

$$P(\sigma,\zeta) = \langle \delta(\sigma - \sigma(x,\zeta)) \rangle \qquad (2.30)$$

Here $\sigma(x,\zeta)$ is the stress at the interface calculated when only the surface roughness components with wave vector $q < \zeta q_L$ is included. The angular bracket $\langle ... \rangle$ in (2.30) stands for ensemble average or, what is in most case equivalent, average over the surface area

$$P(\sigma,\zeta) = \frac{1}{A_0} \int_A d^2x \delta(\sigma - \sigma(x,\zeta)) \qquad (2.31)$$

where A is the area of contact. If the integral in (2.31) would be over the whole surface area

A_0 then $P(\sigma, \zeta)$ would have a delta function $[(A_0 - A)/A_0]\delta(\sigma)$ but this term is excluded with the definition we use. The area of real contact, projected on the xy-plane, can be obtained directly from the stress distribution since from (2.31) it follows that

$$\frac{A(\zeta)}{A_0} = \int d\sigma P(\sigma, \zeta) \qquad\qquad (2.32)$$

where $\dfrac{A(\zeta)}{A_0} = P(\zeta)$

The basic idea behind the new contact theory is that it is very important not to exclude a priori any roughness length scale from the analysis. Thus, if $A(\lambda)$ is the (apparent) area of contact on the length scale λ (see figure 2.12), then we study the function $P(\zeta) = A(\lambda)/A(L)$ which is the relative fraction of the surface area where contact occurs on the length scale $\lambda = L/\zeta$ (where $\zeta \geq 1$), with $P(1) = 1$. Here $A(L) = A_0$ denotes the macroscopic contact area (L is the diameter of macroscopic contact area, so $A_0 \approx L^2$).
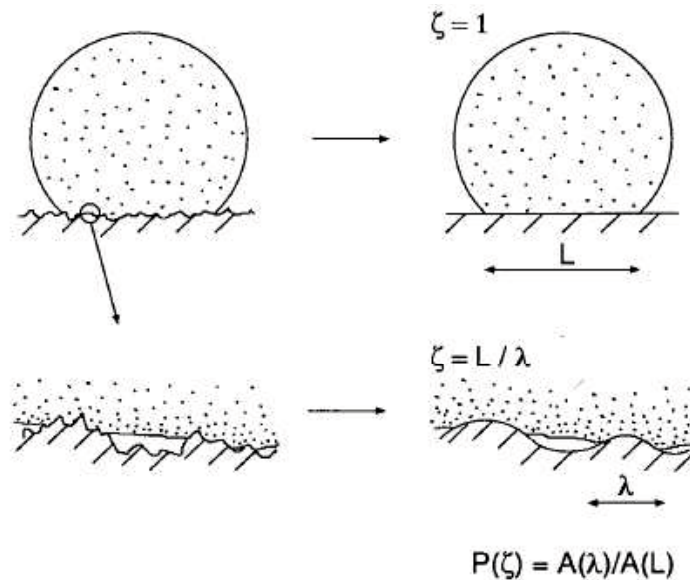
Fig. 2.12 An elastic ball squeezed against a hard, rough, substrate

Consider the system at the length scale $\lambda = L/\zeta$, where L is the diameter of nominal contact area. We define $q_L = 2\pi/L$ and write $q = q_L\zeta$. Let $P(\sigma, \zeta)$ denote the stress distribution in the contact areas under the magnification ζ. The function $P(\sigma, \zeta)$ satisfies the differential equation

$$\frac{\partial P}{\partial \zeta} = f(\zeta)\frac{\partial^2 P}{\partial \sigma^2} \tag{2.33}$$

Where $f(\zeta) = G^`(\zeta)\sigma_0^2$, σ_0 being the average pressure in the nominal contact area, and

$$G(\zeta) = \frac{\pi}{4}\left(\frac{E^*}{\sigma}\right)^2 \int_{q_L}^{\zeta q_L} dq\, q^3 C(q) \tag{2.34}$$

with $E^* = E/(1-v^2)$

where the surface roughness power spectrum

$$C(q) = \frac{1}{(2\pi)^2}\int d^2x\langle h(x)h(0)\rangle e^{-iq.x},$$

where $\langle ... \rangle$ stands for ensemble average. Here E and v are the Young's elastic modulus and the Poisson ratio of the rubber. The height profile $h(x)$ of the rough surface can be measured routinely today on all relevant length scales using optical and stylus experiments.

Equation (2.33) is a diffusion type of equation, where time is replaced by the magnification ζ, and the spatial coordinate with the stress σ (and where the "diffusion constant" depend on ζ). Hence, when we study $P(\sigma, \zeta)$ on shorter and length scales (corresponding to increasing ζ), the $P(\sigma, \zeta)$ function will become broader and broader in σ space. We can take into amount the fact that detachment actually will occur when the local stress reaches $\sigma = 0$ (we assume no adhesion) via the boundary condition

$$P(0, \zeta) = 0$$

In order to solve equation (2.33) we also need an 'initial' condition. This is determined by the pressure distribution at the lowest magnification $\zeta = 1$. If we assume a constant pressure σ_0 in the nominal contact area, then $P_0(\sigma) = \delta(\sigma - \sigma_0)$.

We assume first that only elastic deformation occurs (i.e., the yield stress $\sigma_Y \rightarrow \infty$. In this case

$$P(\zeta) = \int_0^\infty d\sigma\, P(\sigma, \zeta)$$

It is straightforward to solve (2.31) with boundary condition $P(0, \zeta) = 0$ and $P(\infty, \zeta) = 0$ to get

$$P(\zeta) = \frac{2}{\pi} \int_0^\infty dx\, \frac{\sin x}{x} e^{-x^2 G(\zeta)} = \mathrm{erf}\left(\frac{1}{2\sqrt{G}}\right) \tag{2.35}$$

Note that for small load σ_0, $G \gg 1$ and in this case (2.35) reduces to $P(\zeta) \approx P_1(\zeta)$ where

$$P_1(\zeta) = [\pi G(\zeta)]^{-1/2} \tag{2.36}$$

Since $G \sim 1/\sigma_0^2$ it follows that the area of real contact is proportional to the load for small load. Using (2.35) and (2.36) we can write in a general case

$$P(\zeta) = \mathrm{erf}\left(\frac{\sqrt{\pi}}{2} P_1(\zeta)\right) \tag{2.37}$$

The physical meaning of the diffusion-like equation (2.33) is as follows. When the system is studied at the lowest magnification $\zeta = 1$ no surface roughness can be observed and the block makes (apparent) contact with the substrate everywhere in the nominal contact area. In this case, if we neglect friction at the interface, the stress at the interface will everywhere

equal the applied stress σ_0—see Fig. 2.13(a) —so the distribution will initially be delta function like, $P(\sigma, 1) = \delta(\sigma - \sigma_0)$. Increasing the magnification, we include surface roughness with wavelength down to $\lambda = L/\zeta$, and here one may observe some non-contact regions as shown in Fig. 2.13(b). Since the stress must go continuously to zero at the edges of the boundary between the contact and non-contact regions, it follows that the stress distribution $P(\sigma, \zeta)$ will have a tail extending the whole way down to zero stress as indicated in Fig. 2.13(b) (right). There will also be a tail toward larger stresses $\sigma > \sigma_0$ because the average stress must be equal to σ_0. This distribution broadens as in a diffusion problem. With increasing magnification, the stress distribution will broaden further and without limit as indicated in Fig. 2.13(c) (right).
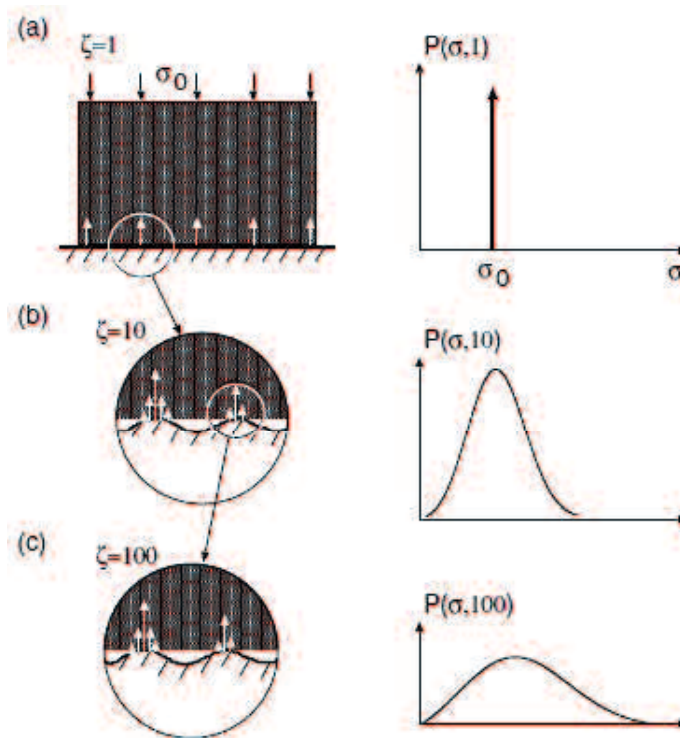
Fig. 2.13 The stress distribution in the contact region between a rigid and an elastic substrate at increasing magnification

2.4.3 Persson Theory for Elastoplastic Contact Mechanics

In the study above we assumed that only elastic deformation occurs. However, the theory can be generalized to the case in where also plastic deformation occurs simply by replacing the boundary condition $P(0, \zeta) = 0$ with $P(\sigma_Y, \zeta) = 0$, which describes that plastic deformation occurs in the contact area when the local stress has reached σ_Y. Increasing magnification the contact area diffuses over the $\sigma = 0$ boundary into non-contact, and over the $\sigma = \sigma_Y$ boundary into plastic contact. Let us to introduce the function $P_{non}(\zeta)$ and $P_{pl}(\zeta)$ which describe the fraction of the original (for $\zeta = 1$) macro-contact area where, under the magnification ζ, non-contact, and contact with plastic yield has occurred, respectively. Thus we have

$$P_{el}(\zeta) + P_{non}(\zeta) + P_{pl}(\zeta) = 1 \tag{2.38}$$

where $P_{el}(\zeta) = P(\zeta)$ describes the fraction of the macro-contact area where elastic contact occurs on the length scale L/ζ. At this point we note that the present theory is strictly valid only as long as $|\nabla h(x)| \ll 1$, which is satisfied in most engineering applications. If this conditions not satisfied, the tangent area can be larger than the projected [on the (x,y) plane] area, and the "conservation law" (2.38) is broken.

Integrating (2.33) from $\sigma = 0$ to σ_Y gives [33]

$$\frac{\partial}{\partial \zeta} \int_0^{\sigma_Y} d\sigma P(\sigma, \zeta) = \int_0^{\sigma_Y} d\sigma f(\zeta) \frac{\partial^2 P}{\partial \sigma^2} = -f(\zeta) \frac{\partial P}{\partial \sigma}(0, \zeta) + f(\zeta) \frac{\partial P}{\partial \sigma}(\sigma_Y, \zeta) \tag{2.39}$$

Since

$$\int_0^{\sigma_Y} d\sigma P(\sigma, \zeta) = P(\zeta) = \frac{A_{el}(\zeta)}{A_0}$$

Where A_{el} is the "elastic contact area", we can write (2.37) as

$$\dot{A}_{el}(\zeta) = -A_0 f(\zeta) \frac{\partial P}{\partial \sigma}(0, \zeta) + A_0 f(\zeta) \frac{\partial P}{\partial \sigma}(\sigma_Y, \zeta) = -\dot{A}_{non}(\zeta) - \dot{A}_{pl}(\zeta) \tag{2.40}$$

Where we have

$$A_{pl}^{\grave{}}(\zeta) = -A_0 f(\zeta) \frac{\partial P}{\partial \sigma}(\sigma_Y, \zeta) \qquad (2.41)$$

is the contact area where plastic deformation has occurred. Thus, (2.38) is just a statement about conservation of area (projected on xy-plane):

$$A_{el}^{\grave{}}(\zeta) + A_{pl}^{\grave{}}(\zeta) + A_{non}^{\grave{}}(\zeta) = 0$$

Or after integration

$$A_{el} + A_{pl} + A_{non} = A_0$$

Next, let us multiply (2.33) with σ and integrate over σ:

$$\frac{\partial}{\partial \zeta}\int_0^{\sigma_Y} d\sigma\, \sigma\, P(\sigma, \zeta) = \int_0^{\sigma_Y} d\sigma\, f(\zeta)\sigma\, \frac{\partial^2 P}{\partial \sigma^2} = f(\zeta)\sigma_Y \frac{\partial P}{\partial \sigma}(\sigma_Y, \zeta) - f(\zeta)\int_0^{\sigma_Y} d\sigma\, \frac{\partial P}{\partial \sigma}(\sigma, \zeta)$$

$$\frac{\partial}{\partial \zeta}\int_0^{\sigma_Y} d\sigma\, \sigma\, P(\sigma, \zeta) = f(\zeta)\left[\sigma_Y \frac{\partial P}{\partial \sigma}(\sigma_Y, \zeta) - P(\sigma_Y, \zeta)\right] \qquad (2.42)$$

Since $F_{el}(\zeta) = A_0 \int_0^{\sigma_Y} d\sigma\, \sigma\, P(\sigma, \zeta)$ is the normal force carried by the elastically deformed contact area, (2.40) gives

$$F_{el}^{\grave{}}(\zeta) = A_0 f(\zeta)\sigma_Y \frac{\partial P}{\partial \sigma}(\sigma_Y, \zeta) - A_0 f(\zeta)P(\sigma_Y, \zeta)$$

Using (2.39) this gives

$$F_{el}^{\grave{}}(\zeta) = -\sigma_Y A_{pl}^{\grave{}} - A_0 f(\zeta)P(\sigma_Y, \zeta) \qquad (2.43)$$

Since the normal stress in the contact region where plastic yield has occurred is equal to σ_Y it follows that the plastically yielded contact regions will carry the load $F_{pl} = \sigma_Y A_{pl}$. Thus, since σ_Y is assumed independent of ζ we get $F_{pl}^{`} = \sigma_Y A_{pl}^{`}$ and (2.41) can be written as

$$F_{el}^{`}(\zeta) = -F_{pl}^{`}(\zeta) - A_0 f(\zeta) P(\sigma_Y, \zeta) \tag{2.44}$$

But the total load $F = \sigma_0 A_0 = F_{el}(\zeta) + F_{pl}(\zeta)$ must be independent of the magnification so that $F_{el}^{`}(\zeta) + F_{pl}^{`}(\zeta) = 0$. Comparing this with (2.44) gives boundary condition $P(\sigma_Y, \zeta) = 0$.

As illustration Fig. 2.14 shows how (a) the logarithm of the (normalized) elastic contact area and (b) the (normalized) plastic contact area depend on the logarithm of the magnification. The calculation is for the surface roughness "polished steel" with the power spectrum and with the (nominal) squeezing pressure $\sigma_0 = 10\,MPa$. The elastic modulus E $= 10^{11}$ Pa, Poisson ratio $v = 0.3$ and for several yield stresses indicated in the figure. Note that with increasing magnification, the plastically yielded contact area A_{pl}/A_0 increases continuously towards the limiting value σ_0/σ_Y
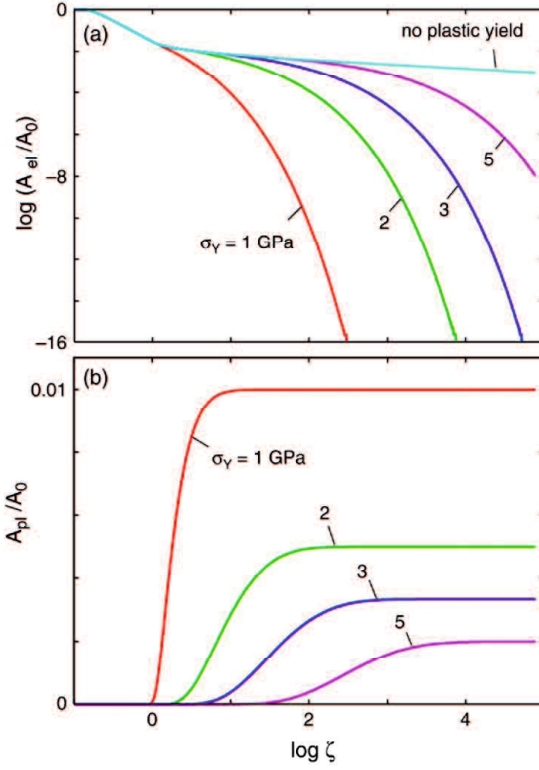
Fig. 2.14 (a) The logarithm of the (normalized) elastic contact area and (b) The (normalized) plastic contact area on the logarithm of magnification

It is straightforward to solve (2.33) with the boundary condition $P(0, \zeta) = 0$ and $P(\sigma_Y, \zeta) = 0$ to get

$$P_{non} = \frac{2}{\pi} \sum_{n=1}^{\infty} \frac{\sin \alpha_n}{n} \{1 - exp[-\alpha_n^2 G(\zeta)]\}, \tag{2.45}$$

$$P_{pl} = -\frac{2}{\pi} \sum_{n=1}^{\infty} (-1)^n \frac{\sin \alpha_n}{n} \{1 - exp[-\alpha_n^2 G(\zeta)]\}, \tag{2.46}$$

where $\alpha_n = n\pi\sigma_0/\sigma_Y$, and where $G(\zeta)$ is given by (2.34). In the elastic limit, $\sigma_Y \rightarrow \infty$, $P_{pl} = 0$, and $P_{el} = 1 - P_{non}$ reduces to Eq. (2.35).
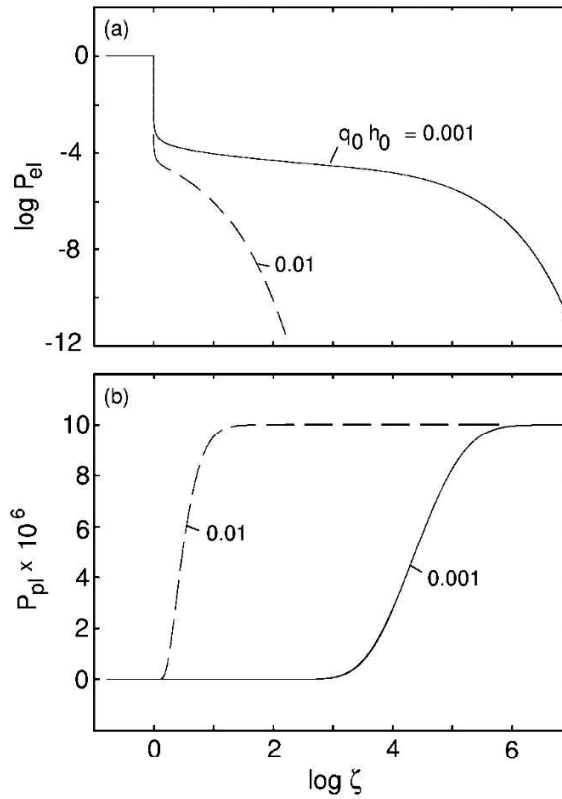
Fig. 2.15 The function (a) P_{el} and (b) P_{pl} describe the fraction of the macroscopic contact area where elastic and plastic contacts occur

In Fig. 2.15 show the dependence of P_{el} and P_{pl} on the magnification ζ [15]. They have used parameters which correspond (roughly) to a cubic steel block ($L = 10$ cm), on steel substrate. They assume $\sigma_0 = 10^4$ Pa, $\sigma_Y = 10^9$ Pa, and $E = 10^{11}$ Pa. The surface roughness of the substrate is assumed to be self-affine fractal with $q_0 h_0 = 0.001$ (solid line) and 0.01 (dashed lines). The theory does not depend on q_0 directly (but only on the product $q_0 h_0$), but if we choose the cutoff wave vector $\lambda_0 = 2\pi/q_0$ of order ≈ 1 mm), then $q_0 h_0 = 0.001$ and 0.01 correspond to the rms roughness $h_0 = 0.1$ and 1μm, respectively. In the calculation they used the fractal exponent $H = 0.8$. Note that for the case $q_0 h_0 = 0.01$ plastic deformation starts already at the cutoff length $\lambda_0 \approx 0.1$ mm all junctions have yielded plastically. However, when $q_0 h_0 = 0.001$ plastic yield starts when ζ is of the order of a few 1000, corresponding to distances of order $\lambda_0/\zeta \approx 0.1\mu$m. On the length $\lambda \approx 20$ Å

47

(corresponding to $\zeta \approx 3 \times 10^5$) all asperities have yielded plastically. However, on this short length scale steel may be much harder than the macroscopically observed yield stress; thus, for "real" steel mainly elastic deformation is likely to prevail when $q_0 h_0 = 0.001$.

2.5.Leakage Theory

Surface roughness is an important factor which influences the rate of leakage through seals. The exact mechanism of roughness induced leakage is not well understood. Practically all macroscopic bodies have surfaces with roughness on many different length scales. When two bodies with nominally flat surfaces are brought into contact, the real (atomic) contact will only occur in small randomly distributed areas and the area of real contact is usually extremely small fraction on nominal contact area.

Most engineering surfaces have a surface roughness that lies in a wide range of length scales and this roughness strongly influences the leakage rate. In other side, accounting for the whole range of surface roughness is impossible using standard numerical methods such as FEM. Fig. 2.9 shows a schematic of how surface roughness leads to imperfect contact between a gasket and a flange. Here, the black and white areas respectively indicate the contacting and non-contacting surfaces. Clearly, the fluid can easily find a path through which to percolate, thus causing leakage to occur.
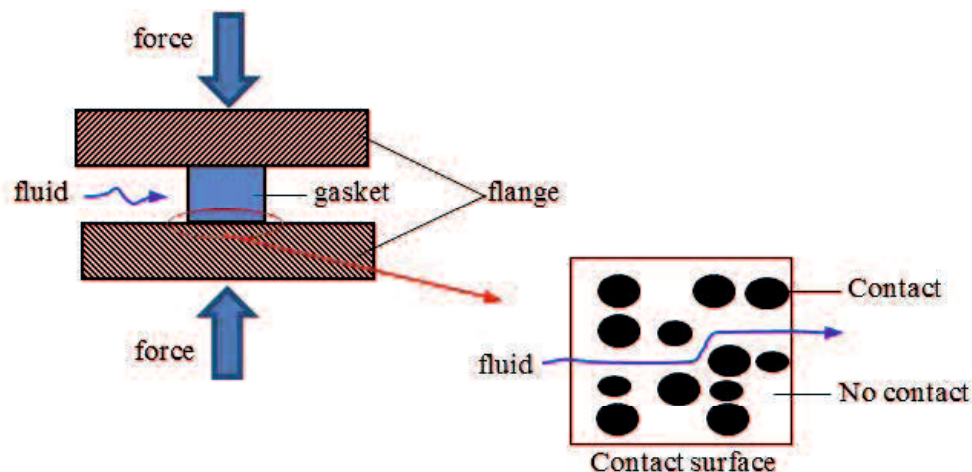
Fig. 2.16 Schematic of leakage occurring in a gasket pressed against a flange by a uniform pressure distribution

A micro scale contact schematic in the Fig. 2.16 can be approximated as square lattice grid as shown in the Fig 2.17.
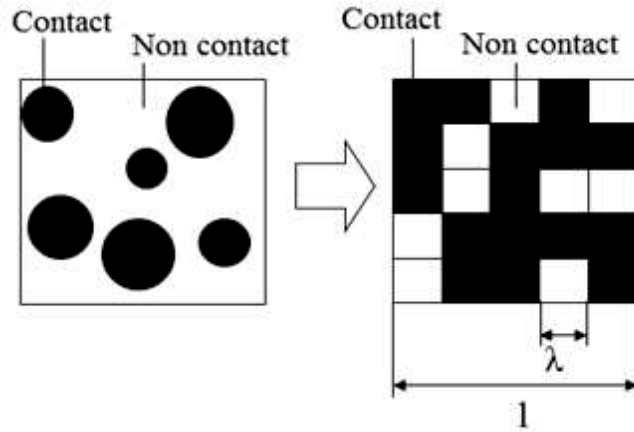
Fig. 2.17 The micro scale contact schematic approximated as square lattice grid

Persson et al. [6] uses percolation theory to predict the apparent contact area as a function of the magnification. The definition on magnification is described in Eq. (2-47). It shows some interfacial surface is observed, the increasing of magnification effect on decreasing contact area.

$$\zeta = \frac{l}{\lambda} \tag{2-47}$$

Where ζ = magnification

λ = length of one side of the square lattice grid

l = length of the apparent contact area

When a contact area is studied at low magnification it appears as if complete contact occurs, but when the magnification is increased it is observed that in actual only partial contact occurs as shown in the Fig. 2.18.
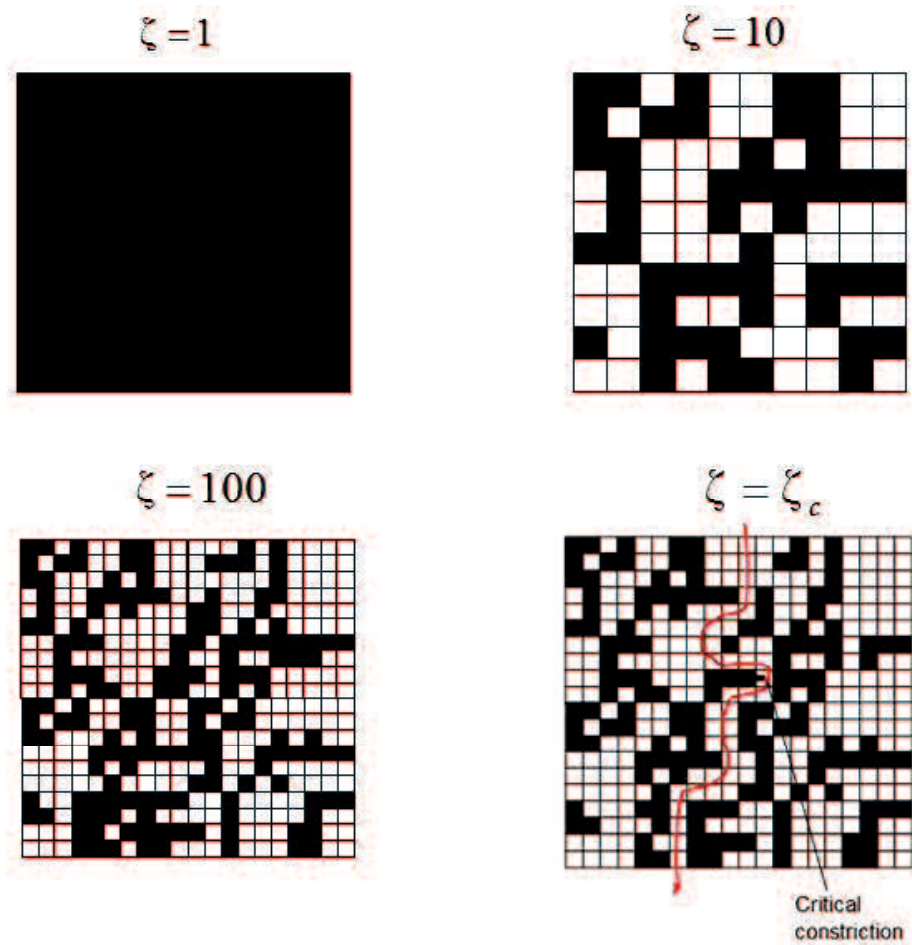
Fig 2.18 The schematic of contact region at different magnifications

When a surface roughness is studied at low magnification, no surface roughness and the block makes contact with the substrate everywhere in the nominal contact area. Increasing the magnification, here one may observe some non-contact regions. At high enough magnification, a percolating path of non-contact area (white square lattice) will eventually be observed at the percolation threshold ($\zeta = \zeta_c$). The non-contact area will percolate as describe by probabilities; $P(\zeta_c)$ in Eq. (2-53) and the leakage will be occurring (red line in the Fig. 2.18) [7] and [9]. If the contact of gasket system produces a higher percolation threshold, it means the low leakage in the system.

$$P(\zeta_c) = 1 - \frac{A(\zeta_c)}{A_0}$$

(2-48)

Where $A(\zeta_c)$ = the noncontact area at the percolation threshold

A_0 = the apparent contact area

Derivation of the expression amount of leakage between parallel plates can explain from Fig. 2.19.
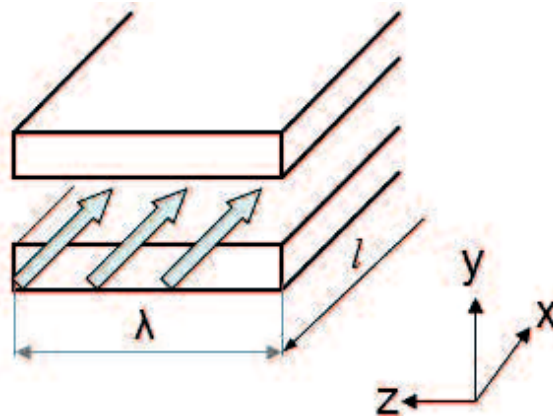
Figure 2.19 Flow between parallel plates

Assuming that only the-x direction of flow

$u \neq 0$ $v = w = 0$

(2-49)

When you assign to this equation of continuity

$\frac{\partial u}{\partial x} + \frac{\partial v}{\partial y} + \frac{\partial w}{\partial z} = 0$ than

$\frac{\partial u}{\partial x} = 0$

(2-50)

And also to assign to the Navier-stokes equations

$\frac{\partial u}{\partial t} + u\frac{\partial u}{\partial x} + v\frac{\partial u}{\partial y} + w\frac{\partial u}{\partial z} = -\frac{1}{\rho}\frac{\partial p}{\partial x} + v\left(\frac{\partial^2 u}{\partial x^2} + \frac{\partial^2 u}{\partial y^2} + \frac{\partial^2 u}{\partial z^2}\right)$ than

$$\frac{\partial u}{\partial t} + u\frac{\partial u}{\partial x} = -\frac{1}{\rho}\frac{\partial p}{\partial x} + v\left(\frac{\partial^2 u}{\partial x^2} + \frac{\partial^2 u}{\partial y^2} + \frac{\partial^2 u}{\partial z^2}\right) \tag{2-51}$$

When you assign equation (2-55) to (2-56)

$$\frac{\partial u}{\partial t} = -\frac{1}{\rho}\frac{\partial p}{\partial x} + v\left(\frac{\partial^2 u}{\partial y^2} + \frac{\partial^2 u}{\partial z^2}\right) \tag{2-52}$$

When a two-dimensional steady flow

$$\frac{\partial u}{\partial t} = 0 \qquad \frac{\partial}{\partial z} = 0$$

Then equation (2-57)

$$0 = -\frac{1}{\rho}\frac{\partial p}{\partial x} + v\frac{\partial^2 u}{\partial y^2}$$

$$\frac{\partial^2 u}{\partial y^2} = \frac{1}{\mu}\frac{\partial p}{\partial x} \tag{2-53}$$

when the integral equation once

$$\frac{\partial u}{\partial y} = \frac{y}{\mu}\frac{\partial p}{\partial x} + C_1$$

integrating one more time

$$u = \frac{y^2}{2\mu}\frac{\partial p}{\partial x} + C_1 y + C_2$$

Boundary   condition

From $u = 0$ at $y = 0,\, y = h$

$$C_2 = 0 \qquad C_1 = -\frac{h}{2\mu}\frac{\partial p}{\partial x}$$

So $u = \frac{y^2 - hy}{2\mu}\frac{\partial p}{\partial x}$ \tag{2-54}

Formula derivation of the amount of leakage

Than Q flow rate this

$$Q = \int_0^h u\lambda dy \qquad\qquad (2\text{-}55)$$

$$Q = \frac{\lambda}{2\mu}\frac{\partial p}{\partial x}\int_0^h (y^2 - hy)dy$$

$$Q = \frac{\lambda}{2\mu}\frac{\partial p}{\partial x}\left[\frac{y^3}{3} - \frac{hy^2}{2}\right]_0^h$$

$$Q = -\frac{\lambda h^3}{12\mu}\frac{\partial p}{\partial x}$$

$$Q = \frac{\lambda h^3}{12\mu}\frac{p_2 - p_1}{\lambda}$$

$$Q = \frac{\lambda h^3}{12\mu}(p_2 - p_1) \qquad\qquad (2\text{-}56)$$

Pressure distribution of magnification can explain using equation (2.57) and Fig. 2.20 [6]. When a surface roughness is studied at low magnification, no surface roughness, the stress at the interface will everywhere equal the applied stress σ_0. Increasing the magnification, there will be a tail toward larger stresses $\sigma > \sigma_0$ because the average stress must be equal to σ_0. The contact stress distribution $P(\sigma, \zeta)$ is investigated [7]. The theory predicts that the area of contact in most cases varies linearly with the load, and that it depends on the magnification.
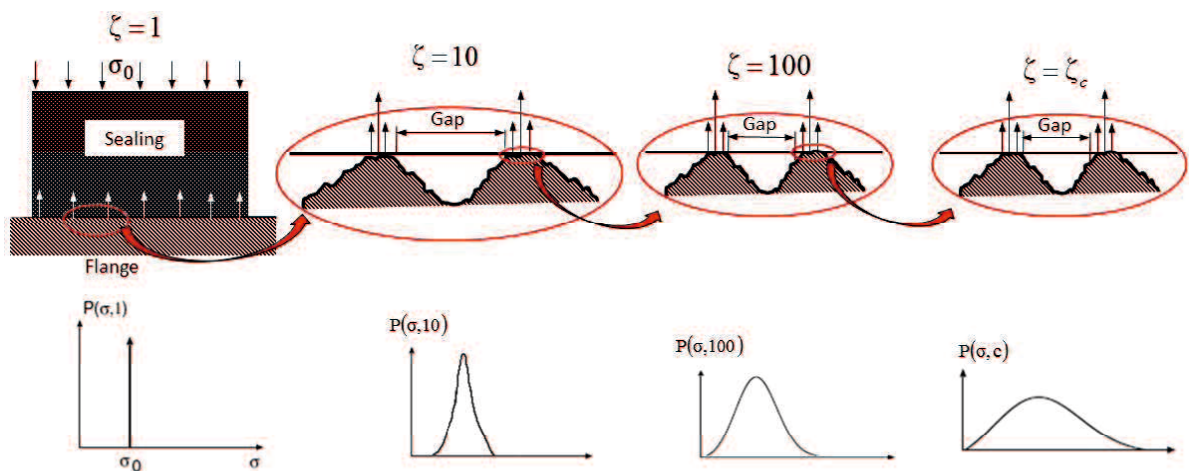
Fig. 2.20 Pressure distribution of magnification

Derivation of the contact area (no elastic deformation bonding), contact area depends on the magnification of the scale to observe ζ also depends on the stress distribution of the contact area $P(\sigma,\zeta)$. Diffusion equation can be represented by

$$\frac{\partial \mathrm{P}}{\partial \zeta} = \mathrm{f}(\zeta)\frac{\partial^2 \mathrm{P}}{\partial \sigma^2}$$ (2.57)

Here the $f(\zeta) = G'(\zeta)\sigma_0^2$ is

Paper "Theory of rubber friction and contact mechanics" derivation is

$$G(\zeta) = \frac{\pi}{4}\left(\frac{E^*}{\sigma}\right)^2 \int_{q_L}^{\zeta q_L} dq q^3 C(q)$$
with $E^* = E/(1-v^2)$.

$$G'(\zeta) = \frac{\pi}{4}E^{*2}q_L q^3 C(q)$$

The effective contact ratio $P(\zeta)$ is
$$P(\zeta) = \int_0^\infty d\sigma P(\sigma, \zeta)$$

$$P(\zeta) = \frac{2}{\pi}\int_0^\infty dx \frac{sinx}{x} e^{-x^2 G(\zeta)} = erf\left(\frac{1}{2\sqrt{G}}\right)$$

With the number of Hurst, derivation of expression of the contact area

$$P(\zeta) = \frac{4\sigma_0\left(1-v^2\right)}{q_0 h_0 E}\left(\frac{1-H}{\pi H}\right)^{1/2} \zeta^{H-1}$$ (2-58)

Which σ_0 = the appearance contact stress

       q_0 = roll-of wavelength

       h_0 = rms roughness

$$P(\zeta) = 1 - \frac{A(\zeta)}{A_0} \tag{2-59}$$

Percolation probability $P(\zeta_c) = 1 - \frac{A(\zeta_c)}{A_0}$

We find that the percolation channel is formed when $\zeta = \zeta_c$, where $\frac{A(\zeta_c)}{A_0} = 0.4$, in accordance with percolation theory [34]

$$\text{so} \qquad 0.6 = \frac{4\sigma_0(1-\upsilon^2)}{q_0 h_0 E} \left(\frac{1-H}{\pi H}\right)^{1/2} \zeta_c^{H-1} \tag{2-60}$$

$$\text{Critical magnification} \quad \zeta_c = \left(\frac{4\sigma_0(1-\upsilon^2)}{0.6 q_0 h_0 E}\right)^{\frac{1}{1-H}} \left(\frac{1-H}{\pi H}\right)^{\frac{1}{2(1-H)}} \tag{2-61}$$

Bottiglione et al. [35] calculated the critical path height (u_c).

$$u_c = \langle h^2 \rangle^{1/2} \frac{1}{\zeta_c^H} \left(\frac{\zeta_m^{2H} - \zeta_c^{2H}}{\zeta_m^{2H} - 1}\right)^{1/2} = q_0^{-2H} \frac{1}{\zeta_c^H} \left(\frac{\zeta_m^{2H} - \zeta_c^{2H}}{\zeta_m^{2H} - 1}\right)^{1/2} \tag{2-62}$$

where $\langle h^2 \rangle = \int d^2 q C(q_1, q_2) = 2\pi \int_0^\infty dq q C(q) \approx q_0^{-2H}$

In the next study, Persson et.al [8] calculated the volume-flow per unit time of leak-rate (Q) on rubber gasket. The calculated leak-rate is in good agreement with experiment.

2.6. Contact between Two Rough Surfaces Model

In practice, all engineering surfaces show some surface roughness. Engineering surfaces often exhibit micro-geometric defect termed roughness and waviness. The actual extent of these defects varies, depending on the machining processes, but they are always present. This fact causes the contact between two engineering surfaces to be located at only a limited number of asperities although the surfaces apparently have a high degree of surface conformity. A variation in the normal load applied through the contact modifies the deformation of the contact asperities and thus changes the number of asperities in contact. The relation between the number of contact asperities and the applied load has raised an exceedingly difficult problem [36].
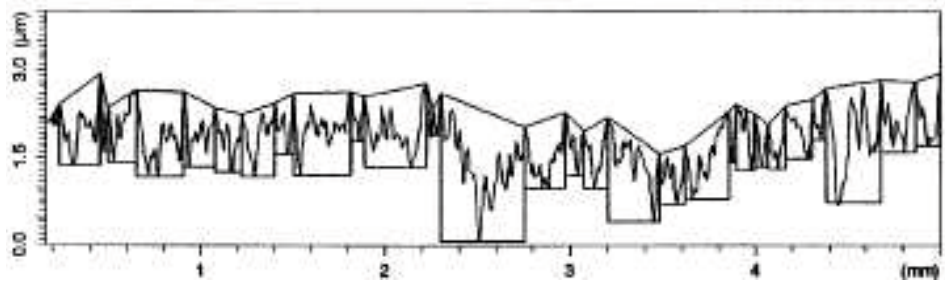
(a)
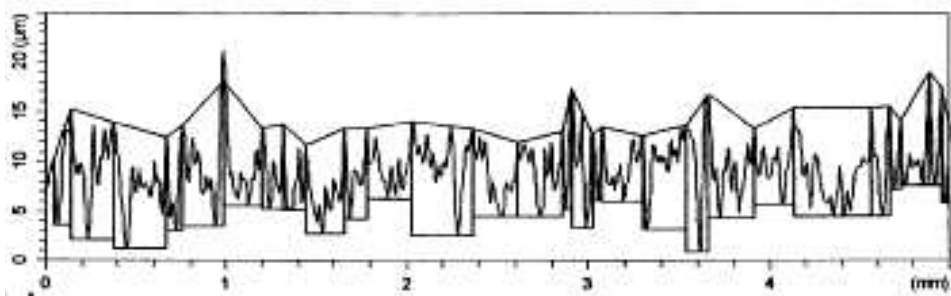
(b)
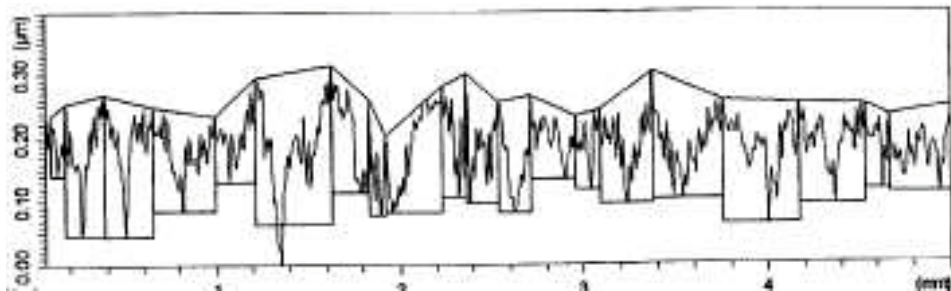
(c)

Fig. 2.21 Roughness motifs obtained on (a) grinding (b) shot-peening and (c) polishing surfaces

The classical standard for roughness and waviness parameter determination uses filtering techniques; these allow the measurement to be decomposed into two profiles called roughness and waviness profiles. Each of these profiles is separately treated to obtain roughness or waviness parameters. The methodology adopted here draws upon the recent ISO standardized method (ISO 12085, 1996). With this method, signal processing is obtained by a graphic technique and uses the called "motif" concept a motif being defined

as that part of the profile which lies between two significant peaks. Because the profiles of engineering surfaces are often very jagged, it is necessary to combine elementary motifs to identify the main asperities and valleys which can describe roughness. The present method defines four conditions for a reproducible determination of the elementary motifs of roughness. They may be identified as follows: the width condition, the envelope condition, the magnification condition and the relationship condition. They, respectively, eliminate low altitude peaks, proximate peaks or valleys and significantly low asperities. After every possible combination has been performed the procedure furnishes the so-called roughness motif of which an example is given in Fig. 2.21 [37].

Roughness parameters can be deduced from the dimensions of the motifs:

- R_m is the mean value of the height R_i of each roughness motif.
- R_{rms} is the root mean square of the R_i values.
- S_m is the mean value of the width S_i of the motif.
- S_{rms} is the root mean square of the S_i values.

Only the first two are used in the micro-geometry model and the notation adopted is, respectively, H_m and Hrms referring to the mean and the root mean square value for amplitude of submit altitudes. Table 2.3 recapitulates the values for roughness and waviness parameters deduced from the motif procedure for the three surfaces described previously.

Table 2.3 Micro-geometrical roughness and waviness parameters of the surface roughness

Surface machining	Roughness				Waviness	
	R_m (µm)	R_{rms} (µm)	S_m (µm)	S_{rms} (µm)	H_m (µm)	H_{rms} (µm)
Shot peening	9.4	2.9	185	105	5.8	1.90
Grinding	1.2	0.43	130	100	0.51	0.24
Polishing	0.19	0.12	150	120	0.30	0.14

The surfaces of most materials are rough and contain irregular geometric features or asperities with sizes ranging over many length scales. Gao et al. [35] analyzed in detail the

behavior of an elastic-perfectly plastic solid with a sinusoidal rough surface that is subjected to contact loading, see Fig. 2.22.
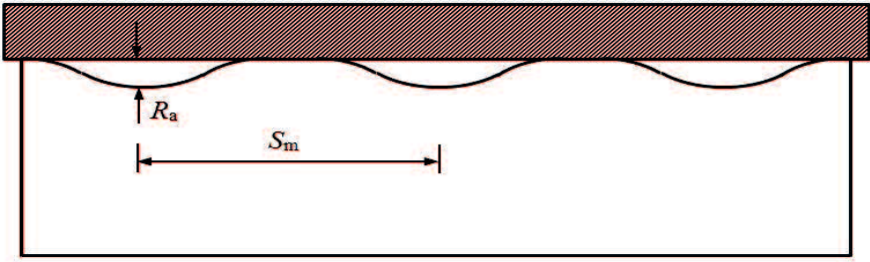
Fig. 2.22 Schematic illustrating indentation of a sinusoidal rough surface

When two nominally flat surfaces are in contact, the actual area of contact is usually only small fraction of the nominal area—only the peaks or asperities on the surface are in contact—and therefore, the real contact stress is higher than the nominal one. When the function of two surfaces is to prevent the leakage of a liquid, this roughness characteristic assumes great importance.
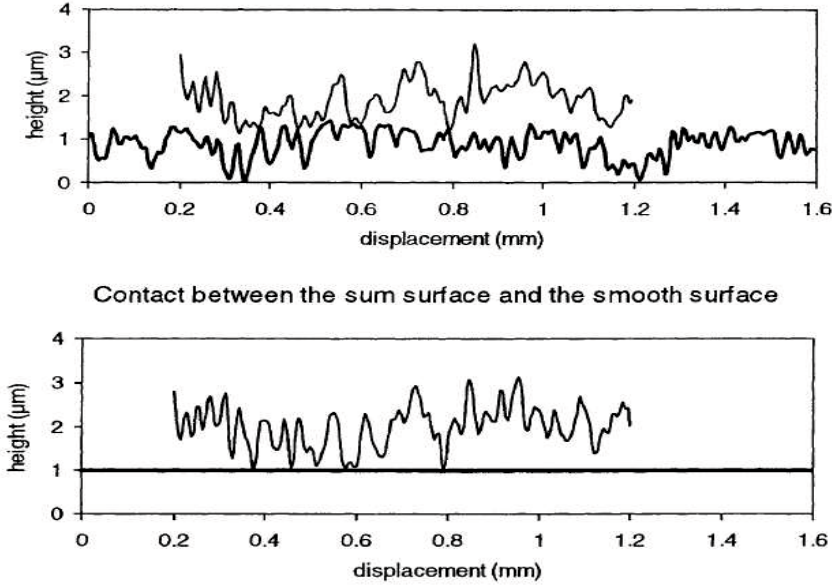
Fig. 2.23 Construction of sum surface

It is difficult to directly analyze the contact between two rough surfaces. Many researchers transform the contact between two rough deformable surfaces into contact between a smooth surface and a rough deformable surface; this is also called as a sum surface [36-39]. The micro-geometric parameters of each surface are combined to obtain the parameters of the sum surface, as shown in Fig. 2.23.

Two contacting rough surfaces are replaced by a single equivalent rough surface in contact with a smooth rigid flat surface. The entire asperity contact state after loading is shown in Fig. 2.24. There are three types of asperities contact states: non-contact asperity, elastic deformed asperity, and plastic deformed asperity. The distribution function of the dimensionless asperity height is described by a dimensionless Gaussian standard probability density function, as shown in Fig. 2.25.
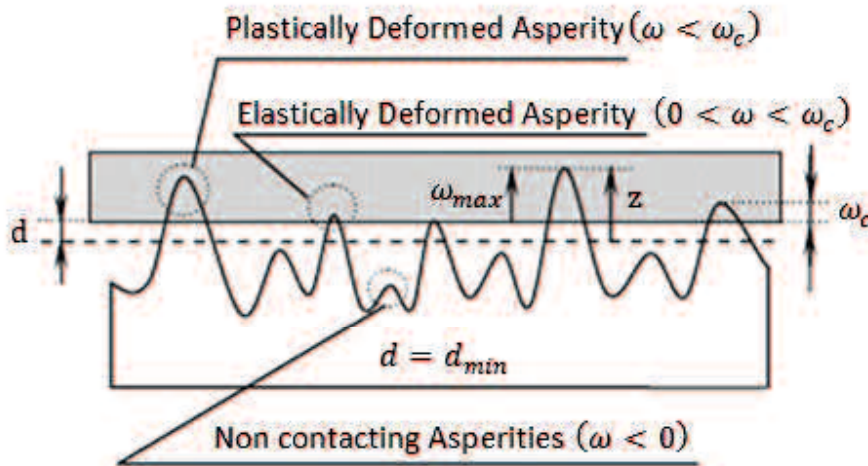
Fig. 2.24 The loading completion
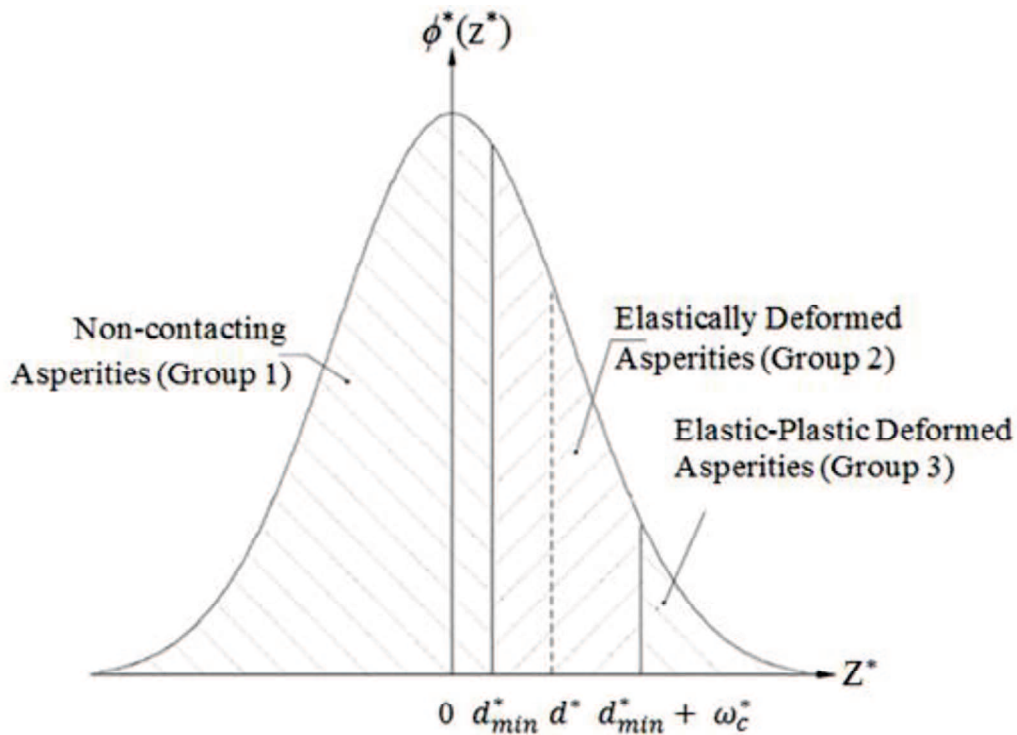
Fig. 2.25 Gaussian distribution of asperity heights

2.7. Taguchi Method

This method is development of the Design of Experiment (DoE) used to improve the quality of products and processes as well as is being able to minimize the cost and resources. This method is extremely helpful in off-line quality control. The target of Taguchi Method is to render the product robust against noise, because it often referred to as robust design.

According to Taguchi's definition of quality is accepted by the public loss since the product was delivered. Genichi Taguchi distinguishes three conditions, namely larger the better as a result of the chemical reaction. Smaller the better as the resultant flue gases by motor vehicles. The target is minimum variation such parts or components of the product.

Taguchi contribution on quality is:

1. Loss function is a function of the losses incurred by the society (producers and consumers) due to the quality produced. For producers, namely the emergence of quality costs, while for consumers is that there is dissatisfaction or disappointment over the products purchased or consumed due to poor quality.

2. Orthogonal array is used to design efficient experiments and to analyze experimental data. Orthogonal array is used to determine the minimum number of experiments that can provide as much information as possible all factors affecting parameter. The most important part of the orthogonal array lies in the selection of a combination of the level of input variables for each experiment.

3. Robustness to minimize the sensitivity of the system to the sources of variation.

These measures are divided into three main phases which include the overall experimental approach. The three phases are (1) the planning phase, (2) the implementation phase, and (3) the analysis phase. Planning phase is the most important phase of the experiment is expected to provide the information. Planning phase is the phase when the factors and levels selected. The second important phase is the implementation phase, the phase when the experimental results have been obtained. If the experiment is planned and executed well, the analysis will be easier and less likely to be able to produce information that is positive about the factors and levels. Analysis phase is when the positive or negative information relating to the factors and levels that have been generated by two previous phases. Analysis phase is the last thing which is important if researchers will be able to produce positive results.

Taguchi method is a robust design approach, which uses many ideas from statistical experimental design for evaluating and implementing improvement in product, processes, and equipment. The fundamental principle of Taguchi method is to improve the quality of a product by minimizing the effect of the causes of variation without eliminating the inevitable causes. The two major tools used in the Taguchi method are Orthogonal Arrays (OA) which are used to study many design parameters simultaneously and Signal-to-Noise Ratio (SNR) which measures quality.

A full factorial experiment conducts all possible combinations of the factor levels and

therefore can reach the overall optimum setting, but it becomes overwhelming in the number of the design's parameters or levels increases. For example, if a new design involves 8 three-level parameters, the experiment needs to conduct 6561 (=3^8) settings. Therefore, the approach is only practical for a limited number of parameters and levels.

An orthogonal array has two major requirements. The first is that the levels of any factor occur with the same frequency. The second is that, for any two factors, each possible combination of levels takes place with the same frequency. If all factor have q levels, an orthogonal arrays is usually expressed as *LM(qm)* where *m* is the number of factors and *M* represents the number of rows in the array (a multiple of *q*2).

In the study of orthogonal arrays, Taguchi [31] explored the entire design space with a few experiments and suggested several standards orthogonal arrays. He classified them into three types: 2-level arrays (*L*4, *L*8, *L*16, *L*32, *L*64), 3-level arrays (*L*9, *L*27, *L*81), and mixed 2-and-3-level arrays (*L*18, *L*36, *L*54). For example, if one has 12 three-level parameters, Taguchi chooses the *L*27 design and so only conducts 27 specified setting. In this way, for design containing many parameters and levels, a fractional factorial approach could determine a feasible parameter setting with much less effort and time because of using the orthogonal array.

The question is can we get similar information with fewer test? Because each setting requires a gasket to product and test, so it means a significant high cost. Therefore option number 2, Taguchi method is chosen as shown in Table 2.4. The motivation is instead of testing all possible combinations of factors, it can test all pairs of combinations in some more efficient way. The key feature is comparing any pairs of factors across all experiments and it can be seen that each combination is represented.

Table 2.4 Array selectors all pairs of combinations

		Number of Levels			
		2	3	4	5
Number of Parameters (P)	2	L4	L9	L'16	L25
	3	L4	L9	L'16	L25
	4	L8	L9	L'16	L25
	5	L8	L18	L'16	L25
	6	L8	L18	L'32	L25
	7	L8	L18	L'32	L50
	8	L12	L18	L'32	L50
	9	L12	L27	L'32	L50
	10	L12	L27	L'32	L50
	11	L12	L27		L50
	12	L16	L27		L50
	13	L16	L27		
	14	L16	L36		
	15	L16	L36		
	16	L32	L36		
	17	L32	L36		
	18	L32	L36		
	19	L32	L36		
	20	L32	L36		
	21	L32	L36		
	22	L32	L36		
	23	L32	L36		
	24	L32			
	25	L32			
	26	L32			
	27	L32			
	27	L32			
	29	L32			
	30	L32			
	31	L32			

The second tool of Taguchi method, the SNR, is used to find which level is suitable for each factor. In communication engineering parlance, the SNR means the measure of signal quality, which corresponds to the solution quality in Taguchi method. While conducting each experiment as per the orthogonal array, the objective function value is computed. A level to a particular factor, which gives the maximum effect in contribution to

the objective function value, is optimal for the concerned factor. As the effect for this level, it is said to have maximum influence or the maximum SNR and so considered as optimal level for the factor. With the conduct of all the experiments as per the orthogonal arrays, the solution obtained with optimal level for each factor, is the optimum solution for the given optimization problem. From the SNR, the optimum conditions of factors are selected. There are several SNR available, depending on the type of characteristic; lower is better (eq. 2-22), nominal is best (Eq. 2-23), or higher is better (Eq. 2-24).

$$\text{SNR} = 10 \log\left(\frac{1}{n}\sum_{i=1}^{n} y_i^2\right) \tag{2-63}$$

$$\text{SNR} = 10 \log\left(\frac{1}{n}\sum_{i=1}^{n} (y_i - S)^2\right) \tag{2-64}$$

$$\text{SNR} = 10 \log\left(\frac{1}{n}\sum_{i=1}^{n} \frac{1}{y_i^2}\right) \tag{2-65}$$

Where y_i = the value each of the better quality characteristic

S = the target value

N = the number of measurements in a trial

2.8. Development of Gasket Asbestos Substitution

Estrada et al [2] developed a detailed strength and leakage three-dimensional and axisymmetric finite element analysis, in which they use a contact formulation to allow loss of contact between the mating flange and the gasket as the internal pressure increases of the joint leakage on GFRP. Also, in the axisymmetric model, they allow fluid penetration into the space where this contact loss occurs; however, this type of loading is not supported in three-dimensional analysis. The analysis was performed on a modified stub flanged joint, see Fig. 2.26. The pipe and hub is filament wound as an integral unit. The metallic backing ring is used to connect the joint to other members. The results shows that over 3/4 of the contact between the gasket and the flange is lost as shown in the Fig. 2.27. However, the pressure on the portion of the gasket that remains in contact is greater than the internal pressure, and the minimum required gasket pressure to keep the joint leak tight.
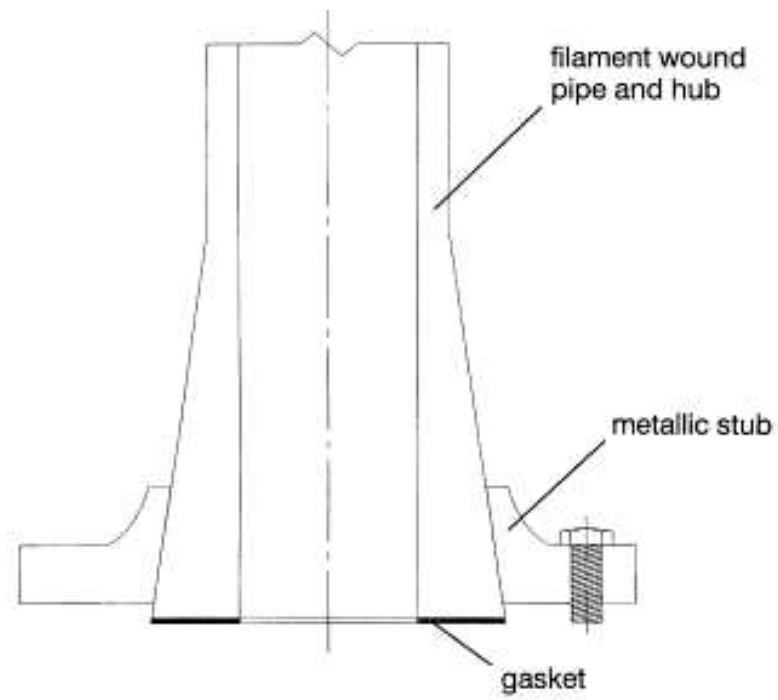
Fig. 2.26 Schematic of the modified stub flange joint
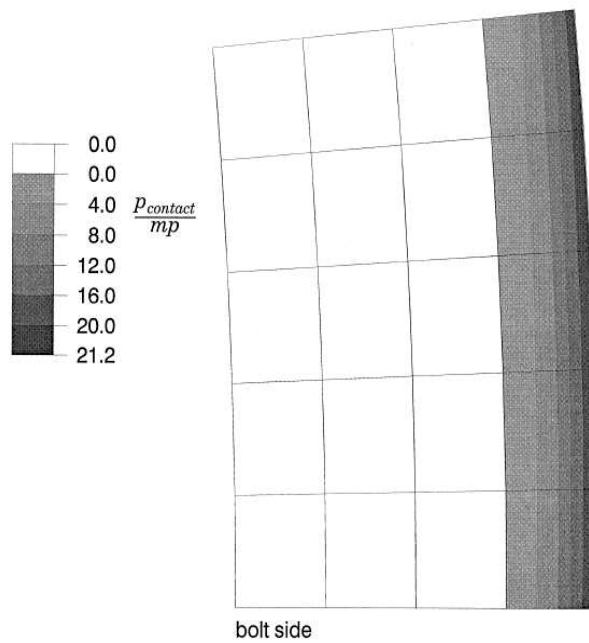
Fig. 2.27 Over 3/4 of the contact between the gasket and the flange is lost

Huang et al [5] investigated critical information on sealing performance and mechanical behavior of a PTFE gasket material through the helium mass leak rate and gasket deflection measurements. The result shows of helium leak rate as a function of gasket stress, see Fig. 2.28. Fig. 2.29 showing the deflection results is a collection of the 15-min incremental measurements during the test.
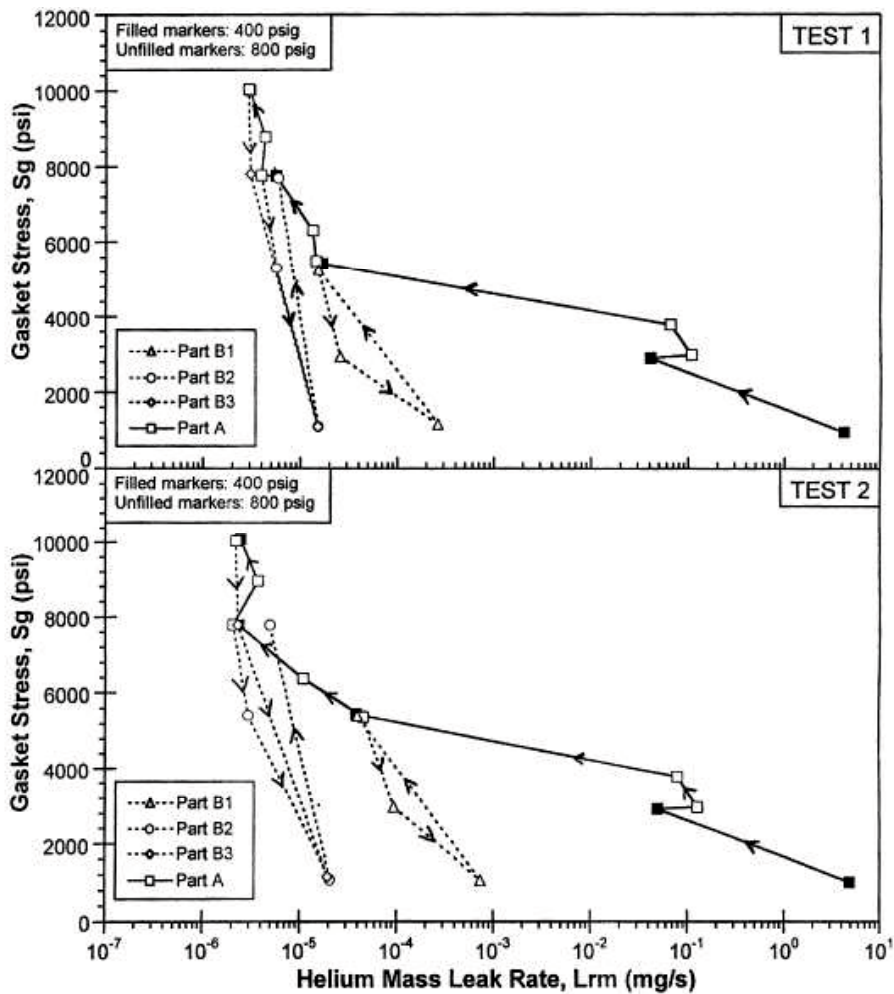
Fig. 2.28 Helium mass leak rate as a function of gasket stress
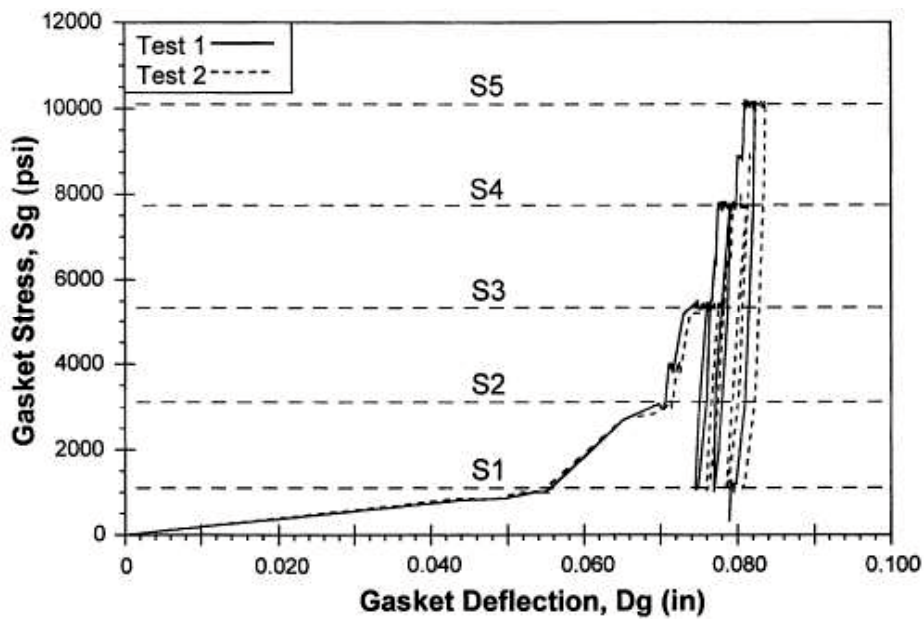
Fig. 2.29 Gasket deflection as a function of gasket stress

Krishna et al [3] studied a 3D FEA of bolted flange joints on spiral wound gasket for finding the contact stresses, see Fig. 2.31. Nonlinearity and hysteresis of the gasket under various loading and operating conditions are taken into account. Three types of gaskets namely asbestos filled (AF), Graphite filled (GF), and PTFE filled (TF). Fig. 2.30 shows the dimensions of the pipe flange and the spiral wound gasket used in the finite element analysis. The results shows that the distribution of contact stress has a more dominant effect on sealing performance than the limit on flange rotation specified by ASME. The variation in contact stress distribution in the radial direction is found to be highest in GF spiral-wound gasket and the least for TF spiral-wound gaskets. The FE method is very useful during the design process for the selection of gasket, pretension of bolts and number of bolts.
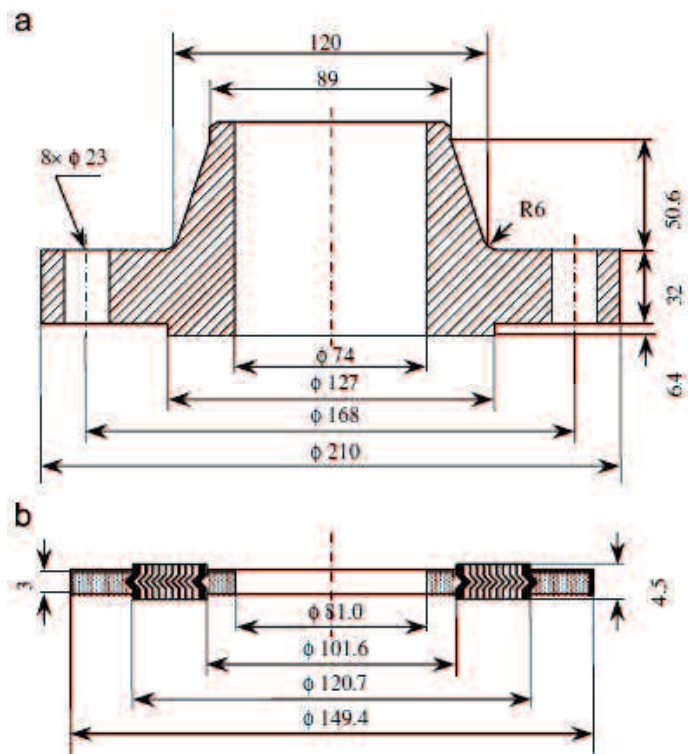
Fig. 3.30 Dimension of the flange and gasket used in the FEA

(a) flange (b) spiral-wound gasket
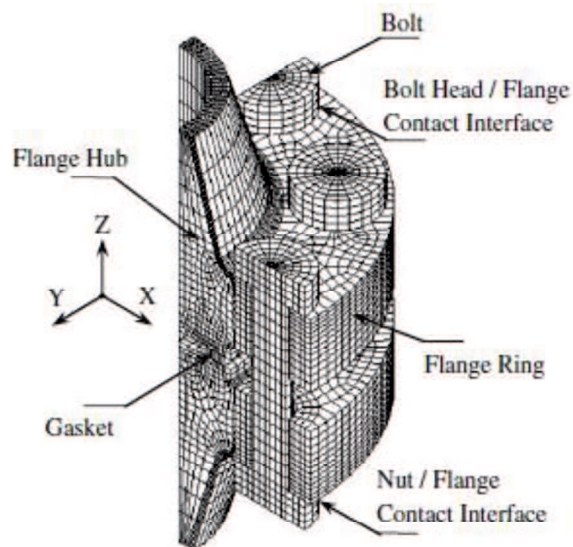
Fig. 2.31 Finite element mesh of bolted flange joint with spiral-wound gasket

Roos et al [4] discuss the gasket characteristic for the design of bolted flange connection of metal-to-metal contact (MMC) type. In this study, flat face flanges and a gasket with a sealing element and distance ring (e.g. graphite SWG with outer distance ring) is used, see Fig. 2.32 and Fig. 2.33. Tightening of the bolts leads to contact between the flanges and the distance ring. Depending on the width of the gasket the required gasket stress for MMC can be too high. The optimum width with respect to adequate MMC stress and tightness is about 10 mm or less. This type of gasket shows excellent tightness or low leakage rate. The leakage rate of graphite filled spiral wound gasket depends on contact stress as shown in the Fig. 2.34.
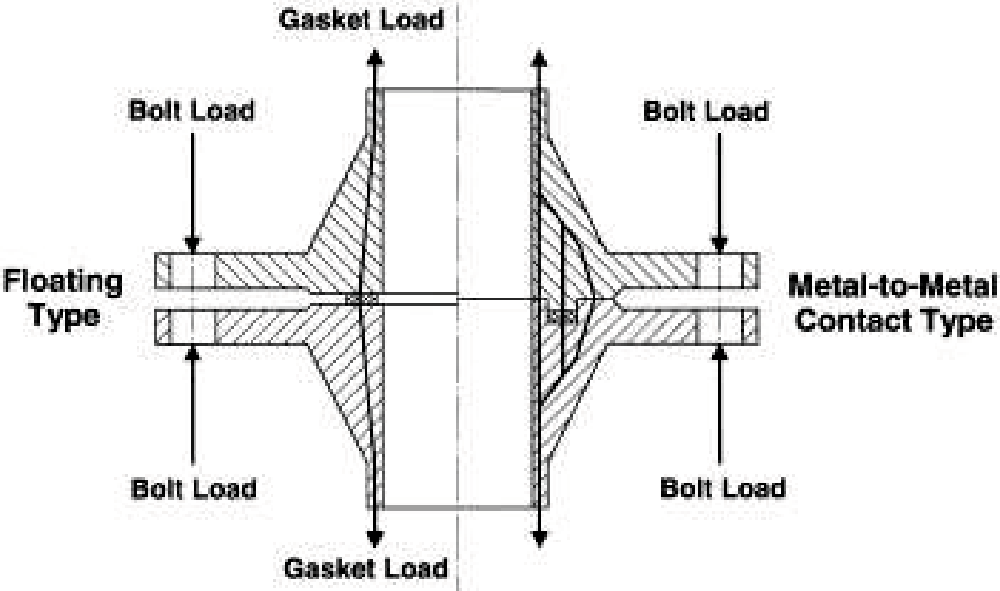
Fig. 2.32 Bolted flange connections (left side) and MMC type (right side) flanged joints
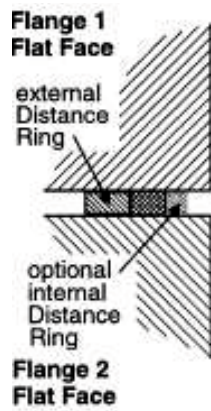
Fig. 2.33 Assembly situation of gaskets in MMC type flanged joints (schematics)
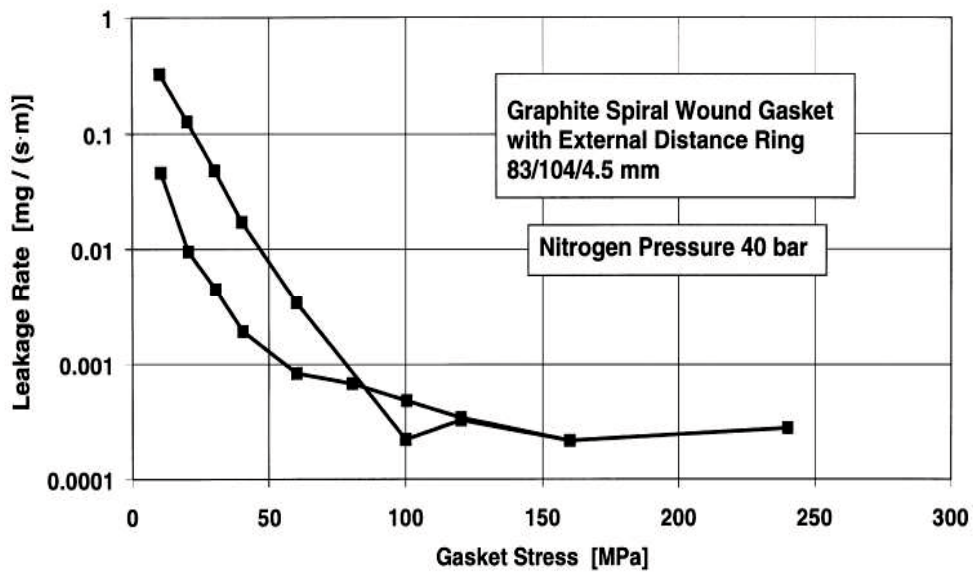
Fig. 2.34 The leakage rate of graphite filled spiral wound gasket depends on contact stress

On flat solid metal gasket, Toshimichi F. [41] presented a 3D FEM for estimating the scatter in bolt preloads and achieving the uniform bolt preloads when tightening each bolt one by one in an arbitrary order. Zou [42] studied on an octagonal metal gasket. Research indicates that the gasket actual contact stress distributes non-uniformly. The leakage rate

decreases with increasing gasket effective contact area and gasket average contact stress as shown in Fig. 2.35.
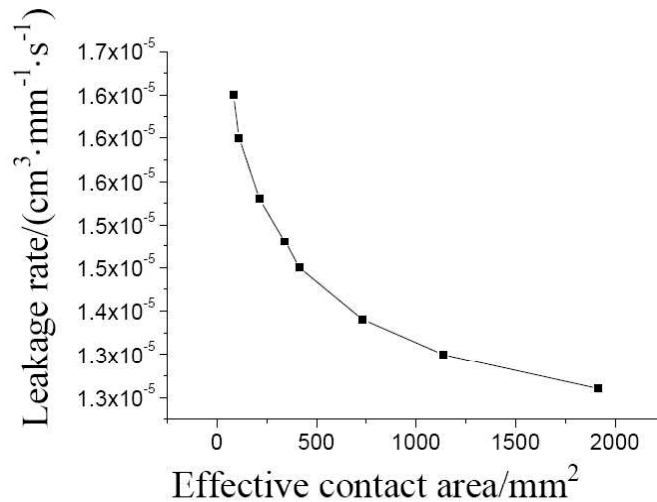
Fig. 2.35 The leakage rate decreases with increasing gasket effective contact area

A 25A size metal gasket, with corrugation has been proposed as show in Fig. 2.36. The gasket has a metal spring effect and produces high local contact stress to create a sealing line with flanges. Saeed, *et al* [13], have indicated that the contact stress and contact width are an important design parameter to control the 25A size metal gasket performance.

Fig. 2.36 The proposed new 25A size metal gasket appearance

The optimum levels for the two evaluation criteria are summarized in Table 2.5. It is obvious that with the exception of material and lip height, both evaluation criteria suggest the same optimum conditions.

Table 2.5 Optimum design levels in Saeed studied

Design factor	Evaluation criterion	
	Contact stress	Contact area
Material	Mat 2	Mat 1
Lip height h [mm]	0.2	0.4
Lip number	2 x 2	2 x 2
Pitch p [mm]	3	3
Overhang OH [mm]	3	3
Thickness t [mm]	1.5	1.5

Performance of the optimum design with 2 x 2 lips based on contact area was verified experimentally using helium leak test. This decision was based on our assumption that a larger contact area is more beneficial than a larger contact stress as it can counter the roughness of the contact surfaces; because it can be argued that provided the contact stress is greater than internal pressure of the contained fluid, there should be no leakage. Higher slope for "Optimized" design shows a higher functionality of leakage performance as shown in the Fig. 2.37. The results justify that parameter factors affect the gasket performance is contact area. However, the limits size of contact width as a design parameter is not yet defined. Other papers have also evaluated contact width in rubber lips seals [43-44] and PTFE lips seals [45], but they have not examined the relationship between the contact width and leakage for the design concept.
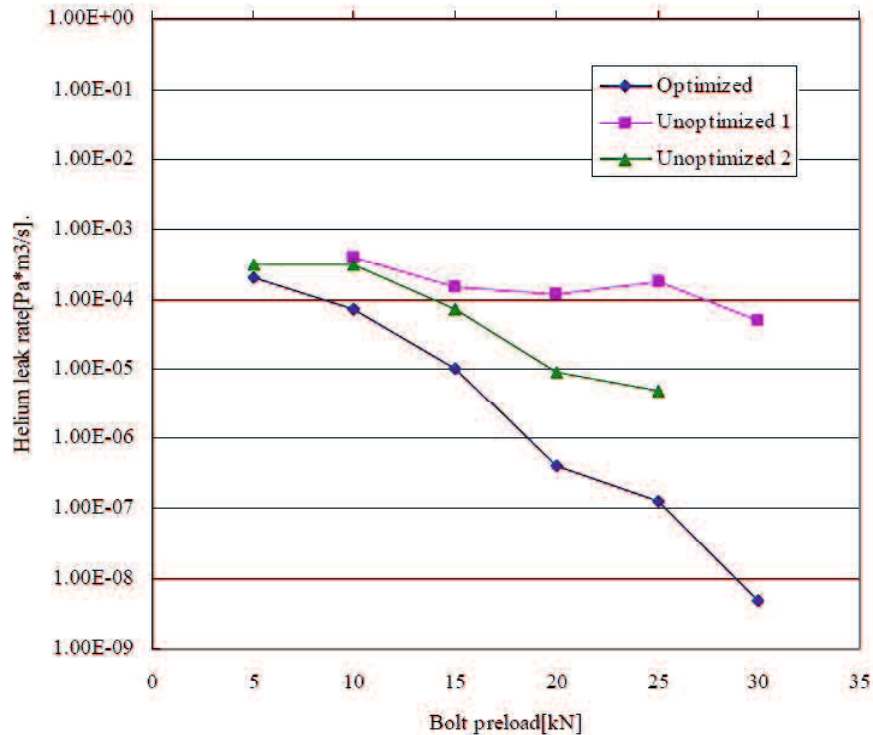
Fig. 2.37 Helium leak result in Saeed studied

In this study, the evaluation method of 25A size metal gasket was determined by using a new approach for leak measurement. Leak measurement was performed continuously to evaluate the 25A size metal gasket performance at the condition of the gasket was tightened to the flanges. The leak evaluation was carried out by using a water pressure test and a helium leak test. FEM analysis was used to analyze the relationship between contact width and axial force and is validated using pressure sensitive paper. By using the results of the FEM analysis and the leak measurement results, the design concept of the 25A size metal gasket was realized; the design was developed by using the relationship between the contact width and leakage. By using this design concept, the limits of contact width for no leakage can be chosen.

Haruyama, *et al* [14] investigated the limits size of contact width as 25A size metal gasket design parameter. In this study, the quantitative evaluation of helium leak rate and contact width of gasket which has no leak by water pressure test had been cleared. From the

above matter, contact width can be used as a main parameter to optimize the gasket design. The leakage can be reduced with increasing the contact width.
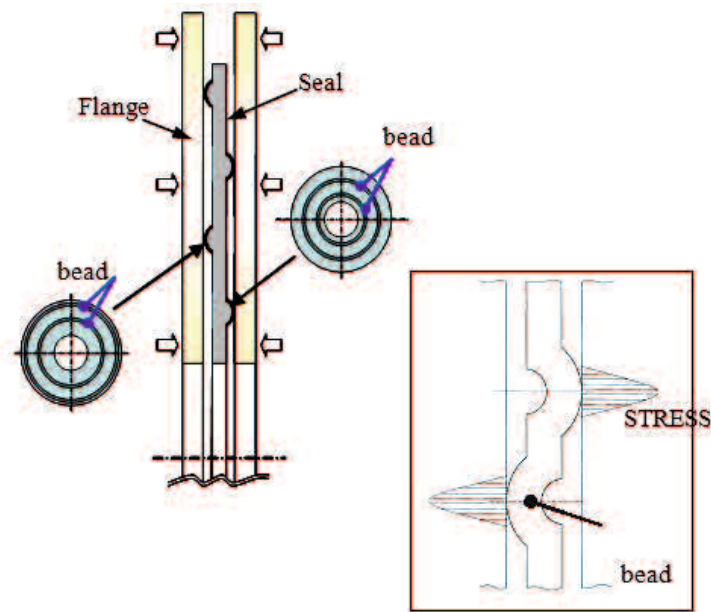
Fig. 2.38 The prevent leakage mechanism of the gasket

The gasket which was used in this research as shown in Fig. 2.38 is in the shape of circumference beads is placed on both front and back sides of a sealing surface alternately. By the tightening of the seal materials to the flange, each bead of both sides surface of gasket contacted the flange and produced high local contact stresses to prevent leakage. Basic dimensions of the gasket that was evaluated is prescribed in JISB2404 and the flange shape is corresponds to 20K pressure and 25A diameter with 1.5 mm thickness. The material selected were SUS304 which could be applied for high-temperature. Nominal stress is $\sigma = 398.83$MPa and modulus of the elasticity is 210GPa. The shape of the gasket is produced by a mold press. Fig. 2.39 shows the basic dimensions of the gasket used in this research.
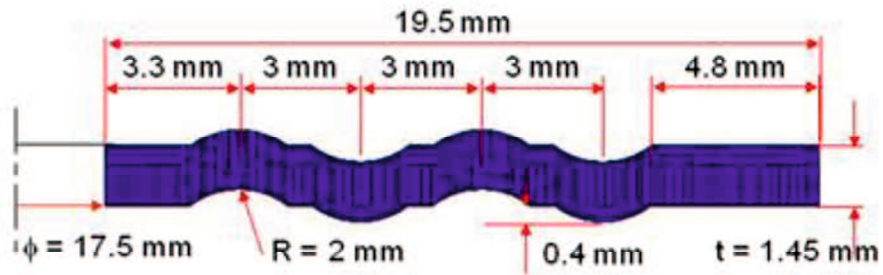
Fig. 2.39 The basic dimensions of the gasket

The condition of the leak occurrence from water pressure test was judged using the quantitative measurement by helium leak test. Therefore, in this research, the method as below is used. In the state that the axial force of the flange is fixed (in this case 20, 25 and 30KN), an experiment of helium leak quantity evaluation was done and helium leak quantity was measured. After that, for every axial force, at the state that the axial force was being loaded, the joint of vacuum piping of helium leak test was exchanged to the water pressure test machine and the water pressure test was performed. Under that circumstance, for 5, 10, 15, 20MPa of water pressure and 600s of maintenance time the leak judgment was done by viewing the presence of leak and the changing of pressure gauge. From this method, it is possible to evaluate axial force of each flange, helium leak quantity and the presence of leak by water test by the same test specimen and axial force.

In the Table 2.6, the experiment results of the helium leak quantity and the presence of leak under the changing of axial force are shown. From the table; in the condition that for SUS304 the helium leak flow is 1.0×10^{-6} Pa.m^3/s at 30 KN axial force, it is observed that the leak by water pressure test did not occurred. Furthermore, it is known that at the helium leak quantity near 1.0×10^{-6} Pa.m^3/s and the internal pressure 20MPa, the leak did not occur. From above matter, for the gasket used in this research, for a quantitative decision criteria to prevent the leak, it is possible to take the condition of helium leak quantity below the 1.0×10^{-6} Pa.m^3/s as a decision criteria for the evaluation of the performance of the gasket design. It also became possible to evaluate the performance of the gasket by quantitative measurement of helium leak quantity and water pressure test

result.

Table 2.6   Comparison of Helium Leak Quantity and Water Pressure Test Result

Axial Force [KN]	Helium leak quantity [Pa・m³/s]	Pressure [MPa]		Result
		0 [s]	600 [s]	
20	5.6×10^{-5}	5	5	No leakage
		10	8.5	Leak
		15	12	Leak
		20	14	Leak
25	9.6×10^{-6}	5	5	No leakage
		10	10	No leakage
		15	15	No leakage
		20	18	Leak
30	1.0×10^{-6}	5	5	No leakage
		10	10	No leakage
		15	15	No leakage
		20	20	No leakage

In previous research, it is clear that contact area and contact stress of the gasket is an important decision criterion for the performance of the gasket, but contact stress and contact area for the presence of leak examination are not sufficient. Therefore, in this study, using the relation of axial force of gasket, leak quantity and the presence of leak gotten from helium leak test and water pressure test, the relation of contact stress and contact area of gasket is examined by FEM analysis.

In this research, from the crush analysis of gasket, the examination of the relation of flange axial force to the contact width of seal material salient part and to the contact stress was done.
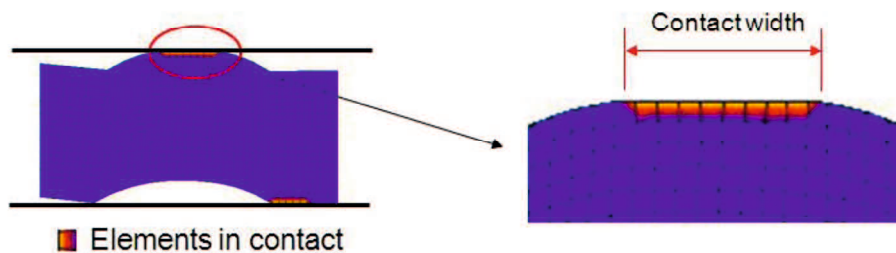
Fig. 2.40 The contact surface of the gasket

For contact area, only at the beads (convex part) of gasket which is effective for avoiding leak is taken as evaluation part. The top surface and bottom surface of contact area increased step by step due to the increment of the axial force to the gasket. From above matter, as shown in Figure 2.40, with the increment of axial force, not only the convex section of gasket surface, but also the edge of external and internal circumference of gasket becomes contacted.

In addition, it is known that the leak quantity has decreased due to the rise of the contact area at the value near 80KN, 100KN and 120KN. Furthermore, Figure 2.41 shows relationship between the contact area and stress in each convex and contact stress. As seen from the figure, contact stress becomes an approximately constant value at the contact part. However, the contact area increased due to the increment of axial force. Moreover, contact stress is in average value at the beads contact part. For the relation of contact area and contact stress from leak quantity, in the state of high contact stress, the contact width became bigger with the axial force. Therefore, as used in this research, for the general-used flange which corresponds to JISB2220 and the gasket, even in the state that the internal pressure exists, for the state that the contact stress occurs because of the internal pressure, it is possible to put an aim for the gasket design condition that if the contact width is above 0.8 mm, the leak by water pressure test will not occur.

In this research, the quantitative evaluation of helium leak quantity and the relation of contact area and contact stress of gasket which has no leak by water test pressure had been cleared. From the above matter, by improving the performance, the optimize designing of gasket become possible.
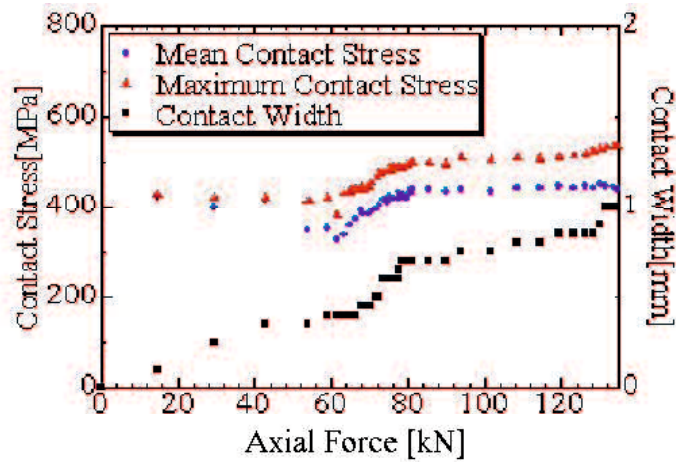
(a) Upper convex section
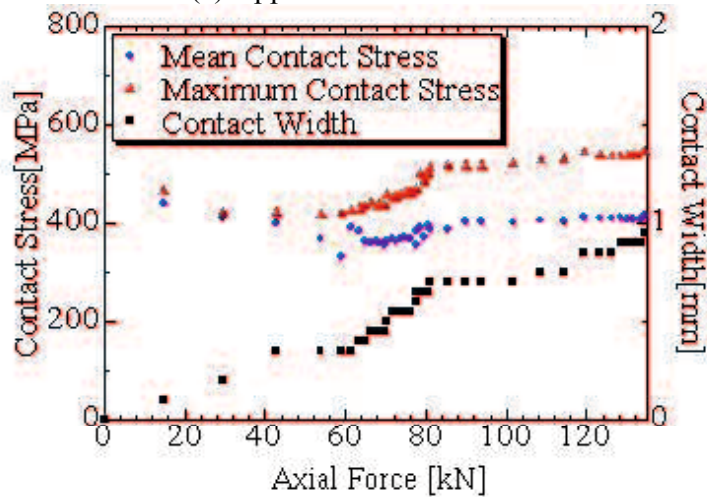
(b) Lower convex section

Fig. 2.41   The relationship between the contact area and contact stress in each axial force

Choiron, et al [15] provided the contact width validation by using simulation analysis and the result is compared to experimental using pressure sensitive paper. The gasket used in this research is circumference beads gasket as illustrated in Fig. 2.42. The shaped of the gasket is produced by a mold press. When the gasket is tightened to the flange, each bead of both surfaces of gasket created elastic effect and produced high local contact stresses to prevent leakage. This circumference made the range of conventional axial force could be possible to use.
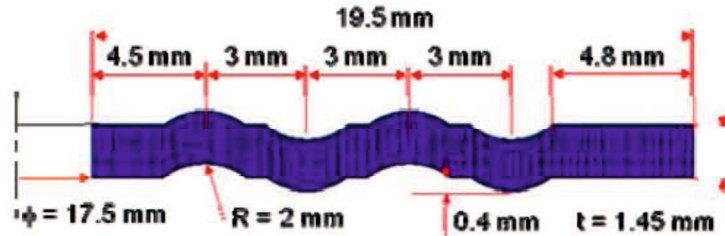
Fig. 2.42 Basic dimensions of the gasket used in this research
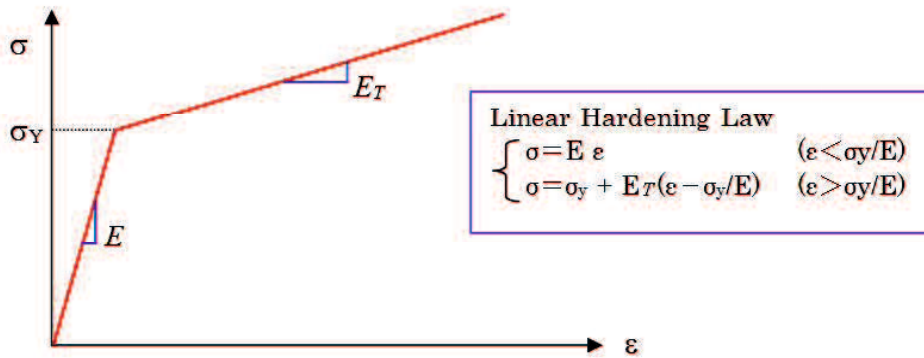
Fig. 2.43 Linear strain hardening model

From the tensile test result, nominal stress (σ_Y) of SUS304 was 398.83MPa, the modulus of the elasticity (E) was 210GPa and the tangent modulus was 1900.53MPa. The material behavior is initially elastic characterized by an elastic modulus E until yielding commences at the uniaxial yield stress σ_Y. Thereafter the material response is elasto-plastic with the local tangent to the curve continually varying and is termed the elasto-plastic tangent modulus E_T (Fig. 2.43). In this study, the model material follows the linear hardening law which divides into two equations for elastic region and plastic region. The flange was assumed as a rigid body on both the sides. Using two-dimensional assumptions, an axisymmetric model was made to implement compression displacement in the axial direction on the gasket in between the top and the bottom of the flange (Fig. 2.44).
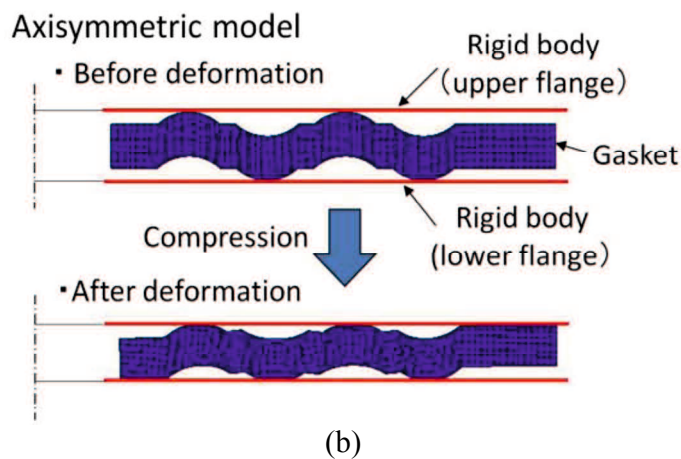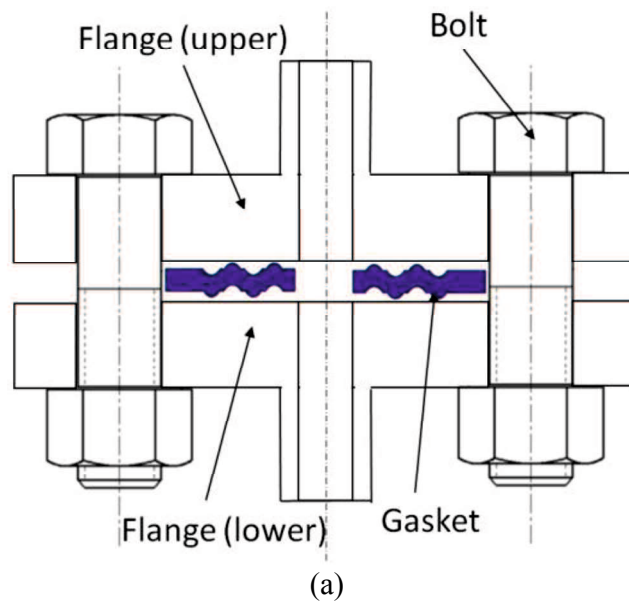
Fig. 2.44 Schematic section of model (a) Physical model, (b) Axisymmetric model

Lee et al. [43] used Fuji pressure sensitive paper to measure the contact width and the pressure profile of the lip seal due to its accuracy, speed, and economic cost. To validate contact width parameter of the proposed new gasket directly, Fuji pressure sensitive paper was used. Due to the ease of application, validation method using pre-scale pressure sensitive paper is one of most popular methods used in contact area and pressure in joint measurement for industrial purpose. Pre-scale pressure sensitive paper is able to produce an accurate and economic permanent high resolution surface topography of contact pressure

distribution [46]. The first procedure of validation method is to form the paper into the designed form. The designed form is furthermore placed in between the joining parts of gasket and flange as shown in Fig. 2.45. The tightening process is carried out based on the axial force. After the load is applied, red patches will be stamped in the paper as illustration of pressure distribution profile that occurred between the two surfaces. A CMOS camera was used to zoom in on the patch. The contact width measurement was performed on eight points located along the contact zone. The measurements using the pressure sensitive paper was compared with the simulation results [15]. The focus of this research is to observe red patches stamped in the paper and measure contact width of the gasket directly. The points of measurement are performed at four point of contact width as depicted in Fig. 2.46.
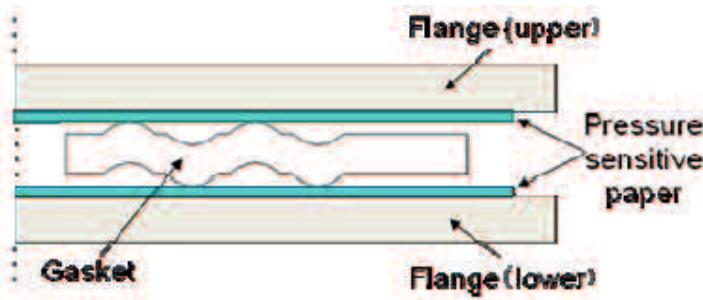
Fig. 2.45 Measurement procedure using pressure sensitive paper
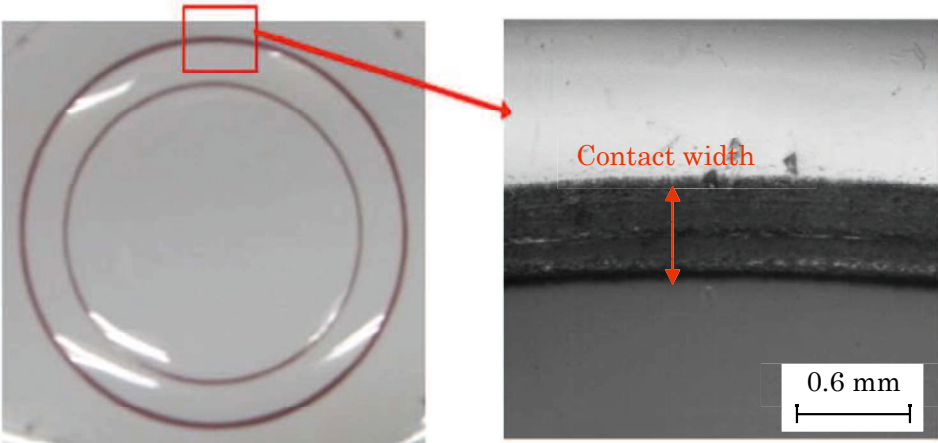
Fig. 2.46 Red patches appeared on pressure sensitive paper after removing load

Contact width modeling was carried out using MSC.Marc, one of finite element method analysis software [47]. The procedure of analysis involves Solidwork, Hypermesh, MSC Marc and MS Excel software as shown in the Fig. 2.47. In this study, a close connection of the information continuity among CAD, Meshing, FEA software's preprocessing and post-processing is developed to fulfill the automatic optimization of process parameters. The virtual gasket model with various designs is generated by using four basic steps. They are the parameterization the models, automatic meshing, computation of preprocessing and post-processing in batch mode and optimization. Firstly, 2-D parameter model is built by utilizing the Solidwork software.
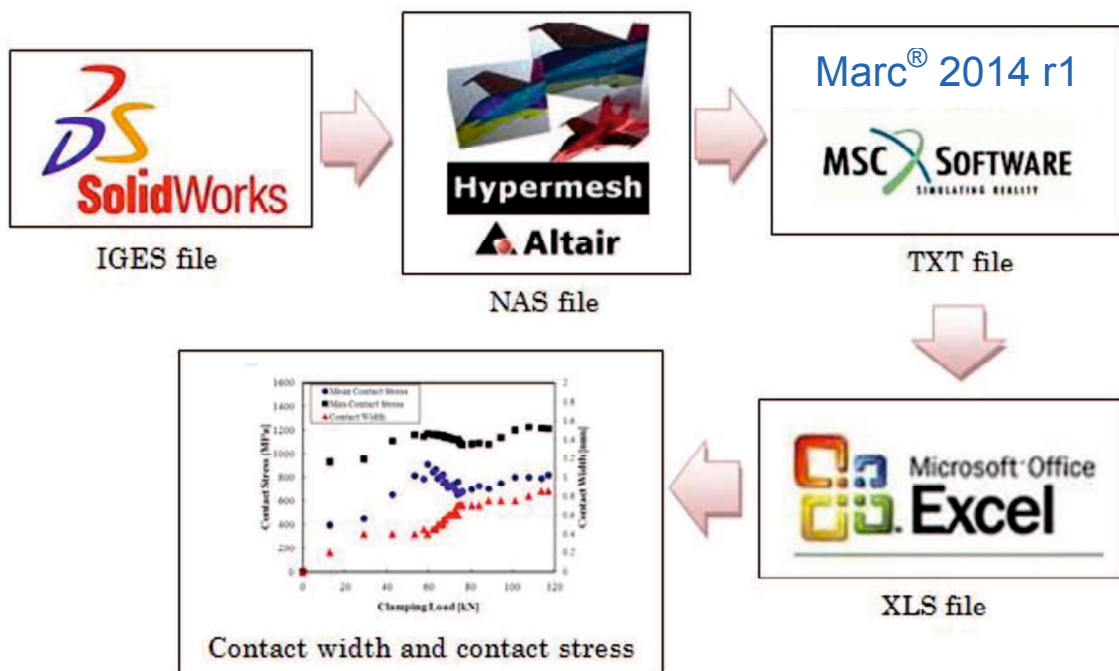
Fig. 2.47 Software used for contact width analysis

To connect drawing data from Solidwork (IGES file) and automatic meshing by using Hypermesh, batch command file is used. The NAS file is produced with that procedure. Then the procedure file is configured to obtain preprocessing and running the model on

MSCMarc software. With this procedure, the graphic user interface (GUI) will not appear and the program just run command in the background. After the FEM analysis is complete, an output file including analysis results could be generated in TXT file. The TXT result file is transformed to Microsoft excel by using MACRO command. The output contains contact status, stress value, body force at each time at every convex position. Calculation of the contact width versus load on convex position number 1 until 4 is produced with several step of MACRO command. Upper and lower contact width is calculated by adding the value of convex position number 1 and 2, 3 and 4 respectively.

The value of contact width could be seen in Fig. 2.48 as a result of measurement using pressure sensitive paper. On the other hand Fig. 2.49 illustrated result produced by MSC.Marc simulation. As shown in both graphs, the axial load affected the contact width significantly. With the more value of axial load, the more the value of contact width. The increase of contact width effect started at axial load value of 60KN. The leak measurement result of the proposed gasket is shown in Fig. 2.50. It is indicated from the figure that the leak quantity decreases with increasing of axial load. In addition, when axial load exceeds 60KN, the inclination of leak quantity decrement is larger. In this study, the qualitative explanation produced by water pressured test is transformed into quantitative value using helium leak test. Therefore, quantitative decision criterion to prevent the leak is determined under the condition of helium leak quantity below the 9.6×10^{-6} Pa m^3/s. It is observed that the leak by water pressure test did not occur at 10MPa condition as shown in Table 2.2. This value is furthermore taken as decision criteria for the evaluation of the performance of the gasket design.
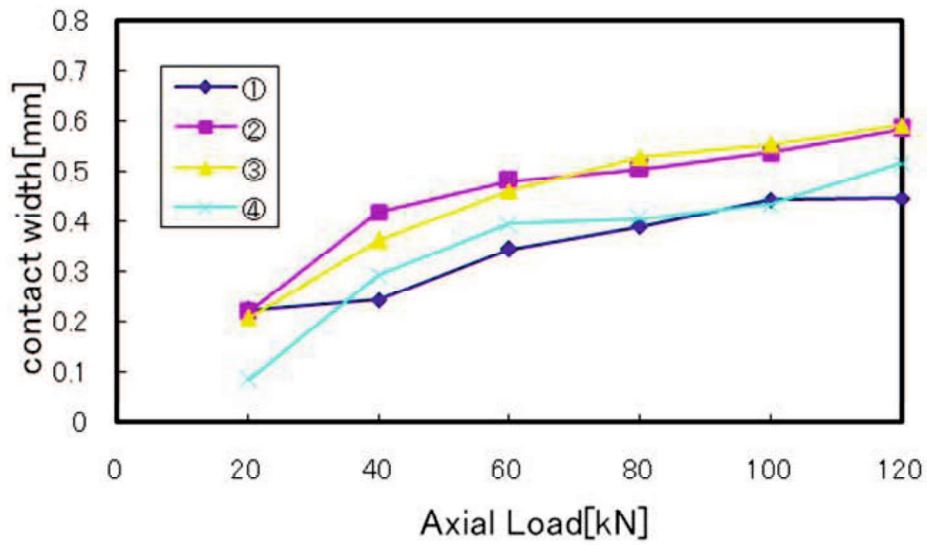
Fig. 2.48 Contact width measurement result produced by pressure sensitive paper
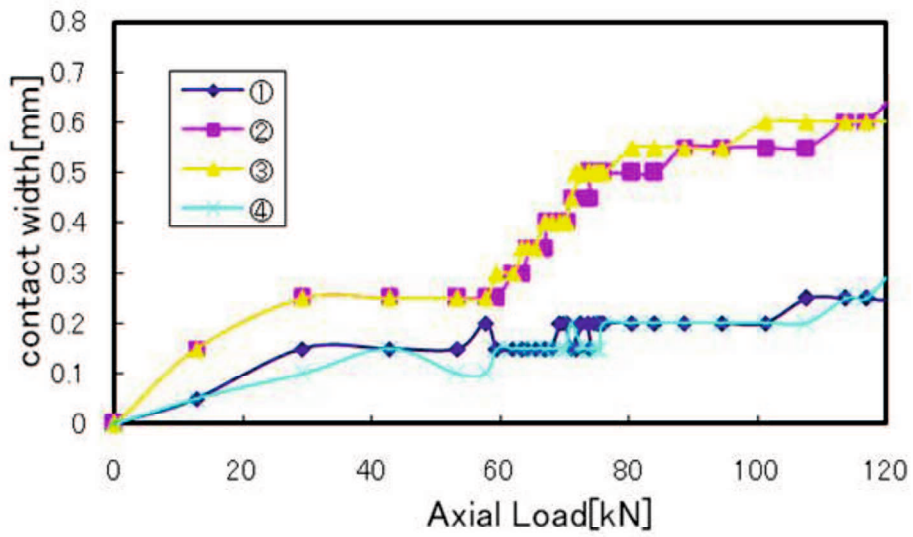
Fig. 2.49 Contact width measurement result produced by MSC.Marc simulation
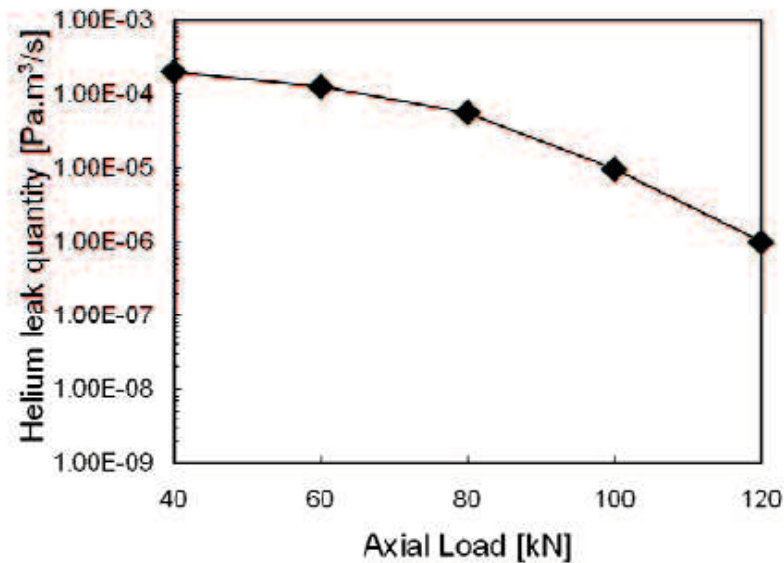
Fig. 2.50 Leak measurement test result

Choiron, et al [16] investigated the optimum 25A-size metal gasket design based on plastic contact stress consideration on contact width. The optimized gasket is determined by deleting contact width with contact stress below of 400MPa. Optimum gasket is chosen by using balancing between contact width and contact stress. The design of experiments (DoE) Taguchi method is used to investigate the factor effect on the contact width and predict the optimal design. The seven factors are overhang (OH), pitch 1 (p_1), pitch 2 (p_2), pitch 3 (p_3), thickness (t), radius (R), and lip height (h). The L18 orthogonal array was built to design experimental matrix for seven factors with three levels.

Gasket used in this study was circumference beads gasket as illustrated in Fig. 2.51. When the gasket is tightened to the flange, each bead of both surfaces of gasket created elastic effect and produced high local contact stress for preventing leakage. This circumstance made the range of conventional axial force could be possible use. Table 2.7 shows the initial basic dimension of the gasket. The gasket material was SUS304 due to its effectiveness in high-temperature and high-pressure environment.
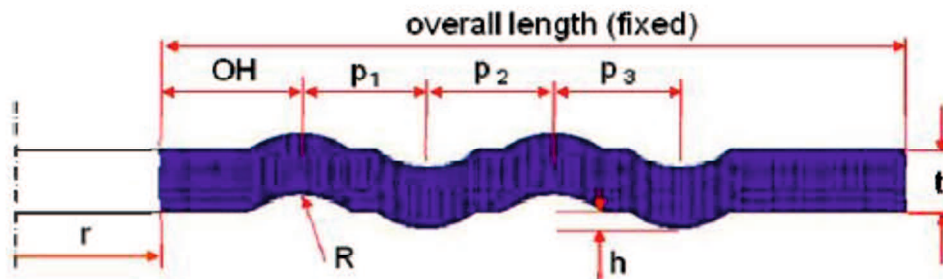
Fig. 2.51 The initial gasket cross section and design parameter

Table 2.7 Initial basic dimensions of the gasket

Design Parameter	Dimension [mm]
1. Inner radius (r)	17.5
2. Overall length (fixed)	19.5
3. Over hang (OH)	4.5
4. Lip height (h)	0.4
5. Thickness (t)	1.45
6. Convex radius (R)	2
7. Pitch ($p_1 = p_2 = p_3$)	3

The contact width modeling was undertaken using FEM analysis software MSC.Marc. The flange was assumed as a rigid body in both sides. Using two dimensional assumptions axisymmetric model was made to adopt compression displacement in axial direction on gasket in between the top and the bottom of the flange. Based on previous study, the plastic contact stress built sealing lines between flange and gasket to avoid leakage, although the value is not yet defined clearly. The optimization design based on the increasing contact width is combined with considering contact stress. The optimum design also determined based on reducing the axial force. It can be denote by using the slope or gradient of the curve of relationship between contact width and axial force. The slope of curve is increased; it will be reduce the axial force. Due to the optimization design based on increasing contact width is combined with considering contact stress. The gasket design

with higher slope is choose as optimum design as shown in Fig. 2.52.
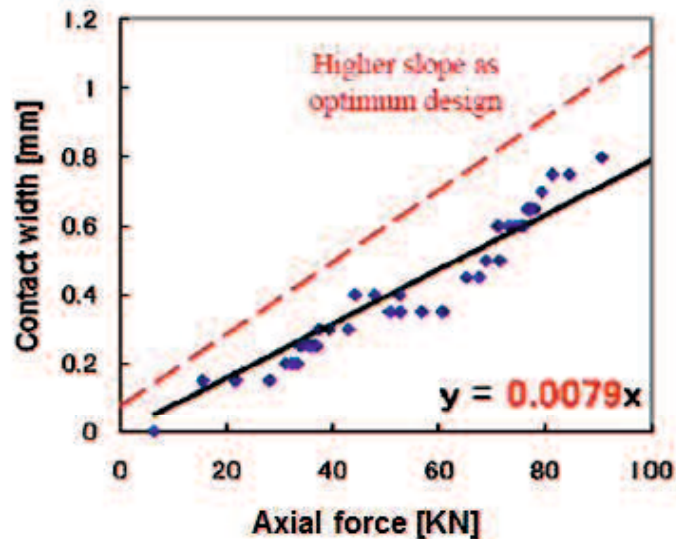
Fig. 2.52 The gasket design with higher slope is choose as optimum design

From MSC Marc result, the contact width is determined based on contact status. Contact status values are 1 and 0 which mean contact and no contact, respectively. This status is done without considering the distribution of the contact stress. This condition is called as gasket design number 1. Moreover, the gasket design number 2 is done by deleting the contact stress value below of 400MPa. It was found from the material properties, the yield stress is 398.83MPa. Therefore, contact width value is more reduced due to contact width with contact stress below of 400MPa is deleted. This procedure is done based on assumption which the large contact stress creates sealing lines on contact width [48].

In this study, the Taguchi DOE method was used to evaluate the effect of each parameter design and predict optimal design of new 25A-size metal gasket. Taguchi method uses a special set of arrays called orthogonal arrays. These standard arrays stipulate the way of conducting the minimal number of experiments, which could give the full information of all factors that affect the performance parameters [49]. The following Table 2.8 shows the Taguchi test matrix for the tests. To design experimental matrix for eight

factors with three levels, the L18 orthogonal array was most applicable.

Table 2.8 Factor and level description

Factor	Factor description	Level 1	Level 2	Level 3
A	Over Hang (OH)	3.0	4.0	-
B	Pitch 1 (p_1)	3.5	4.0	4.5
C	Pitch 1 (p_2)	3.5	4.0	4.5
D	Pitch 1 (p_3)	3.5	4.0	4.5
E	Thickness (t)	1.2	1.5	1.8
F	Radius (R)	1.5	2.5	3.5
G	Lip height (h)	0.30	0.35	0.40
H	Error	1	2	3

The result of relationship between the contact width and axial force, both of optimum design number 1 and initial design are shown in Fig. 2.53. The higher slope of the curve for the optimized design at number 1 provides a marked improvement on the initial design [16]. The level range of load between 80KN and 100KN shows that the optimum design at number 1 can reduce the axial force. The level range of load is improved compared with the initial design which the condition of no leak occurred on 100KN axial force.
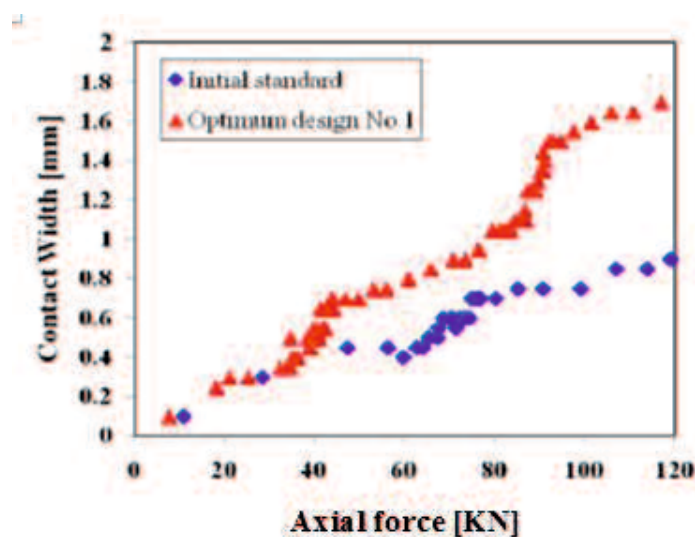
Fig. 2.53 The relationship between contact width and axial force

Fig. 2.54 shows comparison optimum design number 1 and number 2 by condition that contact width with contact stress below of 400MPa is deleted. Based on assumption which the large contact stress creates sealing lines on contact width, slope of the curve for optimized design number 2 is higher than the optimized design number 1.
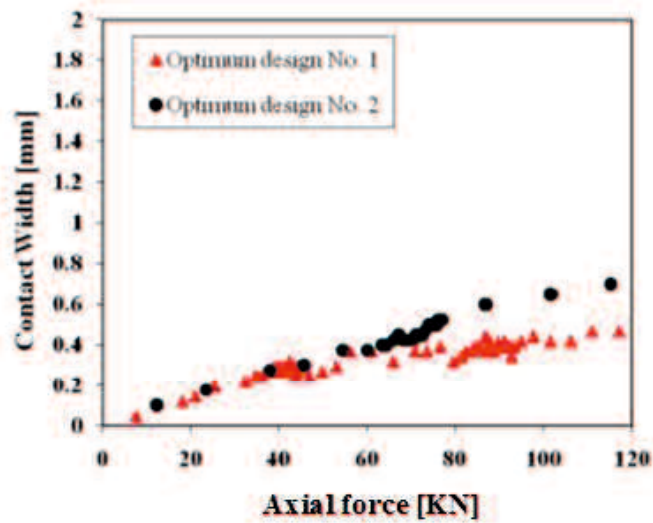
Fig. 2.54 Comparison optimum design number 1 and number 2

In addition, the optimum design of gasket based on results of each of the observed values is illustrated in Table 2.9.

Tables 2.9 Optimum gasket design at number 1 and number 2

Factor	Level Description	
	Optimum design No. 1	Optimum design No. 2
OH	4.0 mm	3.0 mm
p_1	3.5 mm	3.5 mm
p_2	4.0 mm	4.5 mm
p_3	4.0 mm	4.5 mm
t	1.2 mm	1.8 mm
R	3.5 mm	1.5 mm
h	0.4 mm	0.3 mm

Nurhadiyanto et al. [20] investigated the optimum design of 25A-size metal gasket include forming effect according to an elastic and plastic condition respectively derived from FEM analysis. The optimum design of the simulation result was tested using helium leakage test. Here we will be known the gasket performance based on the elastic and plastic design.

SUS304 was used as the gasket material because of its effectiveness in a high-temperature and high-pressure environment. Its material properties were first determined through a tensile test carried out based on JIS Z2241 [51] —the nominal stress, modulus of elasticity (E), and tangent modulus were respectively found to be 398.83MPa, 210GPa, and 1900.53MPa.

The gasket design based on contact status, which is contact and no contact, without considering the distribution of the stress called 0-MPa mode. In the other hand, the gasket design by deleting the contact stress value below of 400MPa called 400-MPa mode. It was found from the material properties, the yield stress is 398.83MPa. In this study, the gasket design based on an elastic condition we call 0-MPa mode while it based on a plastic condition is 400-MPa mode.

In this study, a gasket model is divided into two simulation stage by using two pressing model which is forming and tightening simulation. The design gasket optimized according to an elastic and plastic condition. Both stages were modeled using finite element method analysis software MSC. Marc [47]. In the first stage, the dies were assumed as rigid body in both sides. Using two-dimensional assumptions, the axis symmetric model was adopting a forming process simulation in axial direction on initial gasket material between the top and the bottom of the dies. The second stage is the gasket shape produced by mold press is continuity compressed in axial direction to adopt tightening of the gasket on the flanges.

The optimum design was also determined based on reducing the clamping load. It could be denote by using the slope or gradient of the curve of relationship between contact width and clamping load (Fig. 2.55). The upper and lower contact width was calculated by adding the value of convex contact position number 1 and 2, 3 and 4 respectively. The

slope of curve was increased; it would be reduce the clamping load. The slope of curve was built manually by using trend line command in Microsoft Excel. The process of optimization using L18 Taguchi was illustrated as a circulating loop. Due to the optimization design based on increasing contact width was combined with considering contact stress, and the optimized design was divided as two modes which is 0 MPa and 400 MPa modes. The next circulating loop was generated to fulfill the forming effect by adding forming simulation before the tightening simulation. Finally the optimized design considering forming effect could be achieved.
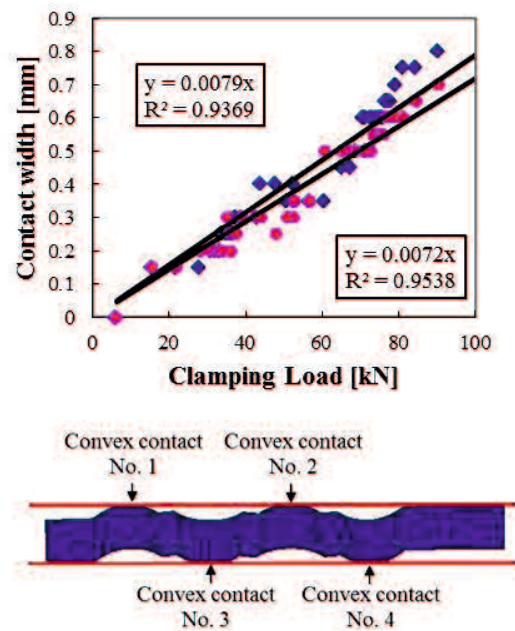
Fig 2.55 The slope of the curve of relationship between contact width and clamping load

Press forming was performed to produce gasket shape by a punch forces the initial material to slide into a die. Therefore, the forming effect was considered for gasket design modeling assessment. From the simulation analysis the lack of die fills defect result. The lack of die fill defect was decreased with increasing the angle of inner radius.

In order to evaluate gasket performance, quantitative measurement of leak flow by

the helium gas was undertaken. In this research, the vacuum method which has the highest detection ability in the helium leak measurement was selected and utilized based on JIS Z2330 [57] and JIS Z2331 standard [58].

Finally, this study suggests the optimum gasket design based on results of each models is shown in Table 2.8.

Table 2.10
Optimum design of gasket 0-MPa mode and 400-MPa mode

Factor	Forming model	
	0 MPa mode	400 MPa mode
OH	3.0 mm	3.0 mm
p_1	4.5 mm	3.5 mm
p_2	4.5 mm	4.5 mm
p_3	4.5 mm	3.5 mm
t	1.2 mm	1.5 mm
R	3.5 mm	2.5 mm
h	0.35 mm	0.3 mm

Fig. 2.56 shows the lack of die fills defect result. The defect is tending occurred on the radius shape of convex contact, both on 0 MPa and 400MPa modes.
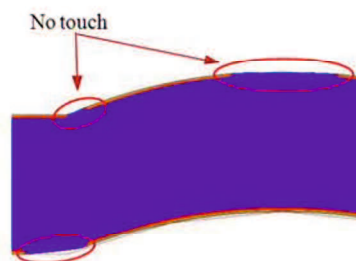
Fig. 2.56 Lack of die fills defect result on one of convex contact

Using MSC Marc Software analysis founded that the lack of die fill defect is decreased with increasing the angle inner radius. The changes in the angle will change the radius and lip height.

Finally, the optimum dimension of dies   to form   a metal gasket is obtained see Fig. 2.57 and Table 2.9.
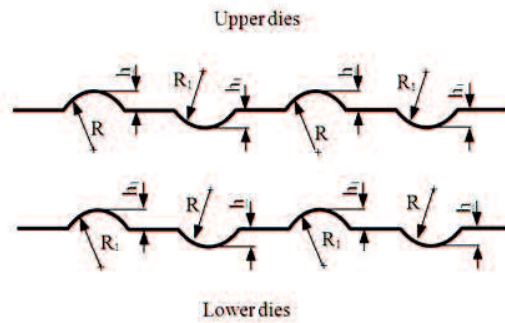
Fig.2.57 Upper and lower dies design

Table 2.11 Optimum dimension of dies for 0 mpa and 400 mpa modes

Gasket	h	R	h_1	R_1
0 MPa Mode	0.35	3.50	0.39	3.20
400 MPa Mode	0.30	2.50	0.33	2.30
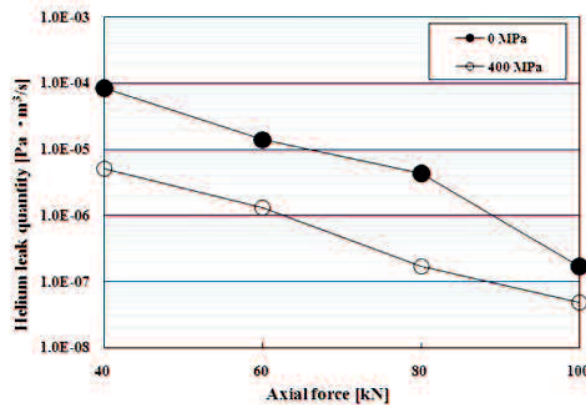
Fig.2.58 Leak measurement test result

The leak measurement result of the proposed gasket is shown in Fig. 2.58. From the figure shows that the gasket 0 MPa mode did not leak on the 100 KN axial load while the gasket 400 MPa mode leak did not occur on the 80 KN axial load. Both types of gaskets shows good performance, because it did not leak at certain axial load. The gasket 400 MPa shows

better sealing performance than gasket 0 MPa mode. Therefore, the gasket design 400 MPa mode is chosen due to the better sealing performances are desirable because the large contact stress.

Haruyama et al. [21, 22] obtain the surface roughness of flange contact to the new 25A-size metal gasket to minimize leakage. It realized by comparing the simulation and experimental analysis. Simulation analysis based on contact stress, contact width, and force per unit length according to surface roughness of flange. Experimental analysis using the helium leak test based on the surface roughness for two kinds of new metal gasket.

This research was used simulation analysis to describe the contact mechanism on a 25A-size metal gasket and rough flange. Using this approach, the relationship between surface roughness parameter to contact stress, contact width, and force per unit length was done. The gasket used in this research was circumference beads gasket. The shape of the gasket was produced by a mold press. When the gasket was tightened to the flange, each bead of both surfaces of gasket created elastic effect. The flange was assumed as rough surface in both sides. The gasket was in the contact condition to the lower and upper side of the flange. The flange pressed a gasket in axial direction. A schematic of gasket tightening on the surface roughness in flange and gasket contact under analysis is shown in Fig. 2.59, where the gasket is shown in corrugated shape and the flange is flat shape.
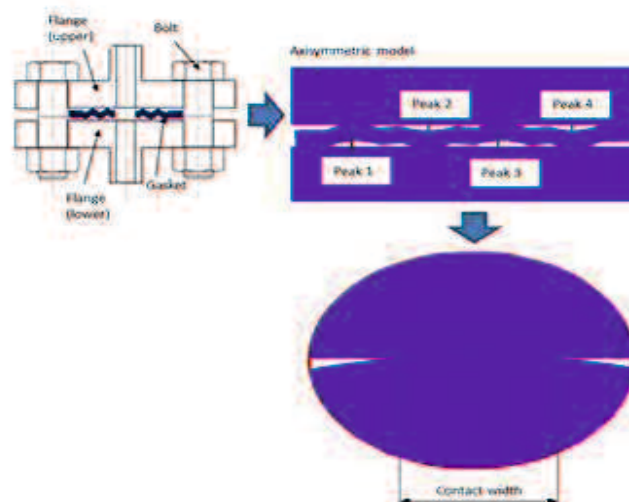

Fig. 2.59 Schematic of gasket tightening of the rough flange

In the research, the flange was divided in three levels surface roughness topography which was Ra 1.5, Ra 2.5, and Ra 3.5. The surface roughness was modeled as a sinusoidal rough surface. Surface roughness of flange measured using handysurf E-35B serial KA8616BE machine. Based on the surface roughness measurements, we obtained average roughness (Ra) and the mean spacing of profile irregularities (RSM). Both Ra and RSM were used to model the surface roughness of the flange. Average roughness describes height asperities and RSM illustrates wavelength of the surface roughness.

The best surface roughness of flange is flange which has minimum leakage. By using this approach, the standard surface roughness of a flange for no leakage can be chosen. It can be denote by using the slope of the curve of relationship between contact width and axial force, contact stress and axial force, or force per unit length and axial force. The force per unit length was obtained by the average contact stress times the contact width. The slope of curve increased, it will be reduce the axial force. Due to the selection of surface roughness based on increasing contact width, contact stress, and force per unit length.

The result of helium leak test for the gasket 400MPa mode is shown in the Fig. 2.60. The gasket which was contact with all roughness levels of flange did not leak on the certain axial force. For the low axial force, there was significantly leakage differences caused surface roughness changes. For the high axial force, the changes of surface roughness did not so influence to leakage.
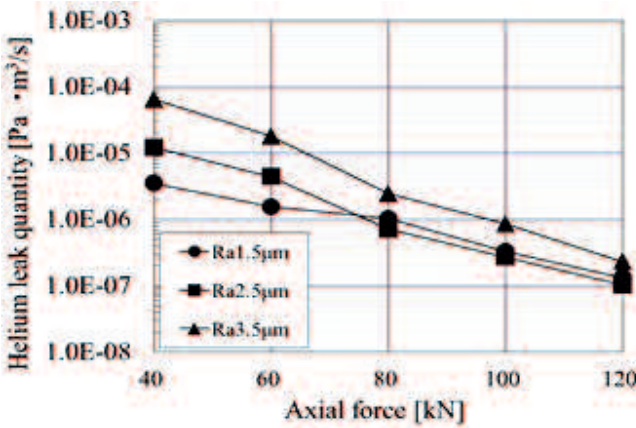

Fig. 2.60 Leak measurement result for 400MPa gasket mode

The result of helium leak test for the gasket 0 MPa mode is shown in the Fig. 2.61. From the figure shows that the gasket contact to flange which has surface roughness Ra 3.5 μm was leak in all of axial force. So, this rough is not good choice for the gasket 0 MPa mode. The gasket contact with flange which has surface roughness Ra 1.5 and Ra 2.5μm did not leak at certain axial force. For the low axial force, there was significantly leakage differences caused surface roughness changes. For the high axial force, the changes of surface roughness did not so influence to leakage.
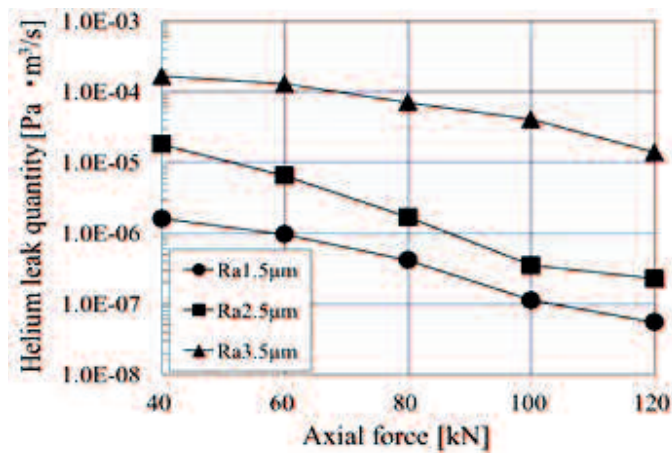
Fig. 2.61 Leak measurement result for 0 MPa gasket mode

Haruyama et al. [23] and Nurhadiyanto et al. [24] determine the real contact width and contact stress when not leakage started on a 25A-size metal gasket. The contact width determined through a comparison between simulation and experimental results. The contact stress determined through a simulation analysis. The experiment involves a helium leakage test using metal gaskets having different surface roughness levels.

The gasket used in this research is circumference beads gasket. The shape of gasket is produced by mold press. When a gasket is tightened to the flange, each bead of both surfaces created elastic effect and produce high local contact stress to prevent leakage. The dimension of gasket used is standar dimension based on JISB2404 [50] with 1.45 mm of gasket thickness. The gasket material was SUS304 due to its effectiveness in

high-temperature and high-pressure environment. The material is SUS304 which has characteristics the nominal stress of SUS304 was 398.83MPa, the tangen modulus was 1900.53MPa and the modulus of the elasticity (E) was 210GPa.

The general-purposed flange based on JISB2220 [56] with 10 K pressure and 25A diameter used in this test. The lower flange and the joint were welded carefully to avoid a distortion, the information of this gasket completely. Types of flange based on the average surface roughness, are 1.5μm, 2.5μm, and 3.5μm. The new 25A-size metal gasket with corrugated shape was used in this test. In this research, gasket and three levels of flange surface roughness were investigated. The types of gasket, based on plastic design, is 400-MPa mode.

Simulation method used to obtained the contact stress and contact width correlation with axial force. We foccused the contact stress and contact width when leakage started on 25A-size metal gasket. Beside that the experimental method to obtained the contact width when the axial force 120 KN. The experimental method as validation for simulation method.

A virtual gasket model with various designs generated through four basic steps as described in Figure 2.62. Forming and tightening analysis were conducted to obtain the contact stress and contact width. First, 2-D parameter models of the flange and the gasket were built using Solid work software. To connect the drawing data obtained from Solid work (IGES file) and the automatic meshing performed using Hypermesh, a batch command file was developed, using which an NAS file generated. We used a quadrilateral mesh for the gasket and flange material because it has a rectangular section. The procedure file was configured to perform the pre-processing and run the model on MARC. The graphic user interface (GUI) does not appear; instead, the program runs commands in the background. After the FEM analysis completed, the output file, including the analysis results can be generated in TXT file that can be converted to a Microsoft Excel file. The output result contains the contact status, contact width, and contact stress force at each time at every peak position. The calculation of the contact width versus the axial force at peak position 1 —4 are performed using a multi-step MACRO command.

The points of measurement are performed at two point of contact width, which are convex number 2 and 3. The digital microscope VH-Z250 series with 500x magnification was used to measure the contact width parameter of the proposed the 25-A size metal gasket. Using the microscope we can Measures the width of grooves which is the real contact width between the flange and the gasket. To evaluate the clamping load and leak quantity, the leakage quantity was measured based on the measurement of that of a helium flow.
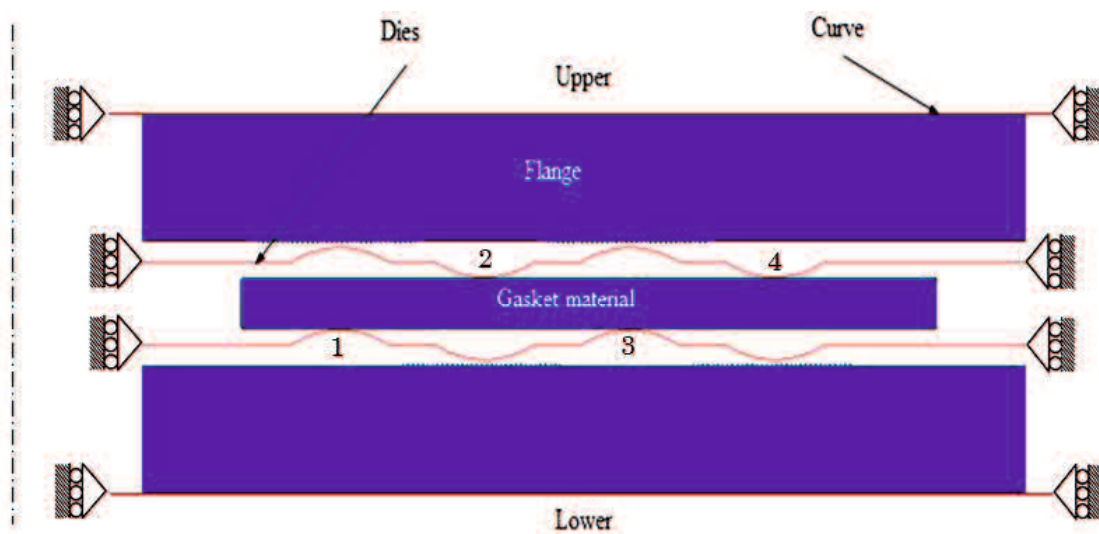

Figure 2.62 Simulation setting up

Figure 2.63 (a) shows the simulation result for contacts of a gasket for the average contact stress. The contact stress for a gasket in contact with flanges having surface roughness values of 1.5, 2.5, and 3.5μm was similar. But, the flange having surface roughness 1.5μm showed the highest propensity than 2.5μm and 3.5μm. This figure shows that the average contact stress increases significantly with the clamping load. The average contact stress for flange having surface roughness 3.5μm was lowest than others. To maintain seal integrity, the effective compressive pressure on the gasket must be greater than the internal pressure by some multiple. Usually, the value of the internal pressure in the piping system is around 10MPa. Figure 2.65 denoted that the contact stress value when the leakage did not occur was around 800MPa; therefore, it is larger enough to reduce the

internal pressure effect, which is 80 times internal pressure. Moreover this gasket had been tested by using water pressure test on 10MPa pressure condition and it is observed that leakage is not occurred. On leak test, the bolt load is adjusted again to ensure the effect of pressure tested can be reduced for next applied of clamping load.

Figure 2.63 (b) shows the simulation result for the contacts of a gasket for the maximum contact stress. The flange having surface roughness 1.5μm showed the highest propensity than 2.5μm and 3.5μm. This figure shows that the maximum contact stress increases significantly with the clamping load.

| (a) | (b) |
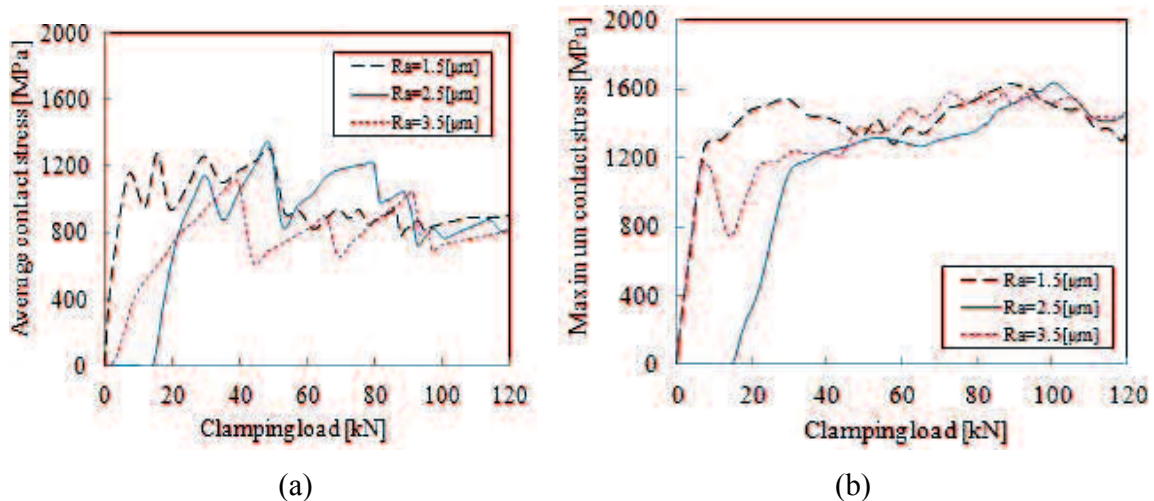
Figure 2.63 Average and maximum contact stress for gasket in 400-MPa mode.

Figure 2.64 shows contact width result both for simulation and experiment result when the clamping load 120kN. There is a good agreement for simulation and experiment result. Contact width for flange having surface roughness 1.5μm is longest than the others. The real contact width is sum of the real contact width after the gasket contact with flange. Because of the number of contact for small surface roughness more than big surface roughness. So contact width for small surface roughness is longer than big surface roughness.

(a) simulation result   (b) experiment result

Figure 2.64 Contact width by simulation and experiment result.

2.9. Product Development Process

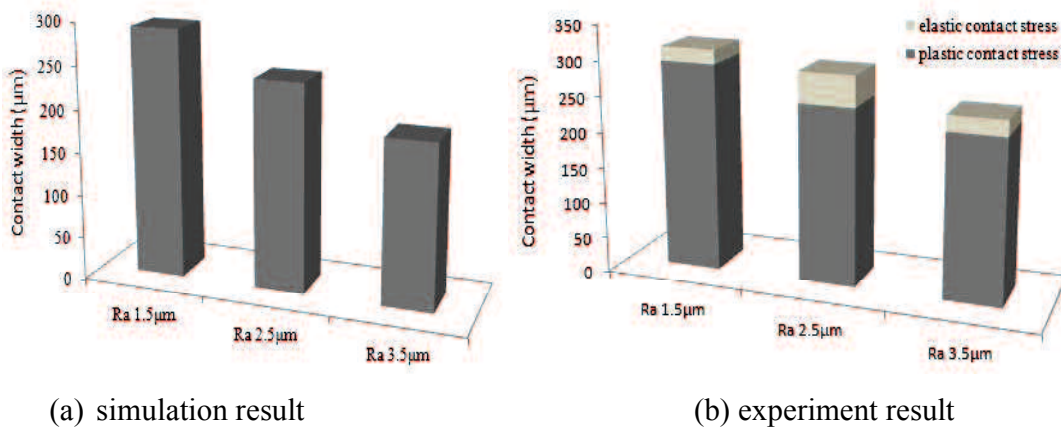The commercial success of new product is strongly influenced by the time to market. Shorter product lead time is of importance for industry in a competitive market. This can be achieved only if the product development process can be realized in small time period. However, the development of metal gasket is usually occurred through the time consuming design and manufacturing test. One of the state-of-the-art efforts in manufacturing process is computer simulation to predict condition requirement using numerical models. These computational models would have great contributing in reducing the number of experiments which traditionally are used for designing stage.

Analysis Led Design (ALD) was used to shorten product development time by getting designs right the first time on conceptual design level [51]. Now when a new size of gasket design is being developed, a series of repetitions are done through simulation until the gasket performance meets the design limits. ALD is a design thought that achieves reduction in development time and cost saving, it uses analysis technology and carries Up Front Engineering of the product quality without exception in an early stage of product development process. Fig. 2.67 shows the relation image of the product development process and the man-hour of Up Front Engineering in ALD.

As shown in figure, there was a peak of the man-hours in a start of production, and much of conventional product development process put product on the market,

improvement in production and defect in market was being corrected. Digital engineering was used changing to perform digital design and digital fabrication, verification of the product after the conceptual design in products development process, but in ALD it carry out the processes from a stage in the conceptual design to a model making - design change and the production start back is a way of idea to minimize a man-hour for design by performing to verification of the safe performance by the robust design.
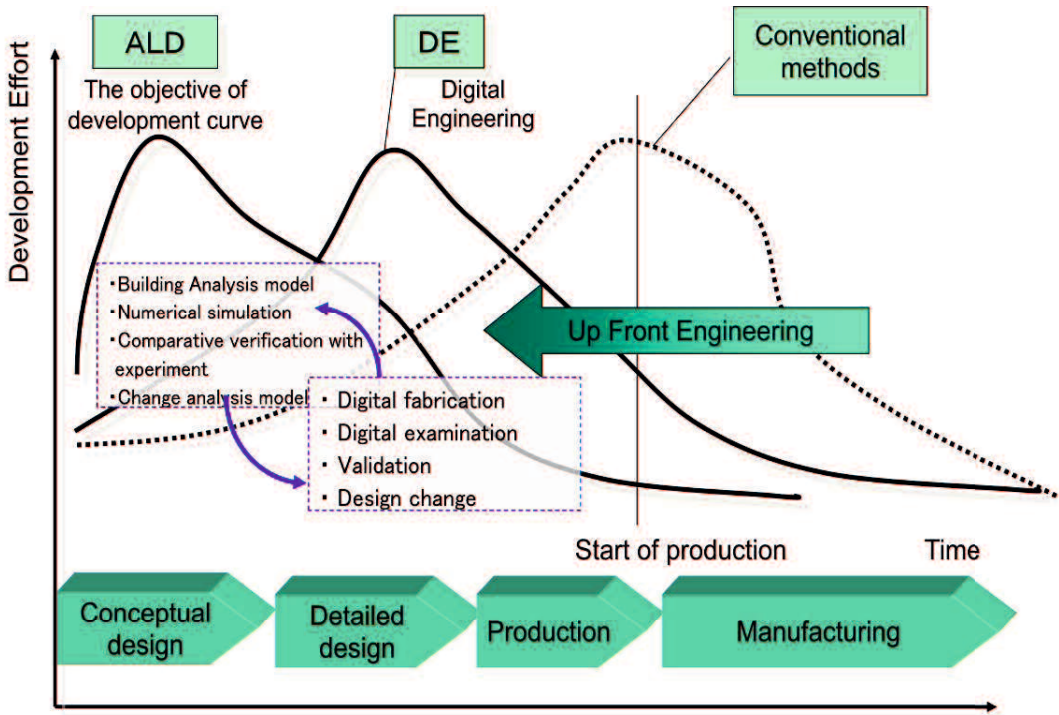
Fig. 2.65 The relationship of the products development process and the man-hour of improving front engineering

In addition, strict prior evaluation, the item corresponding to the development target of the early period of development and the clarification of the standard are important to carry out ALD. In this study, the aim of the performance judgment of the development product in the conceptual design was clarified, and validation of the reliability of the

performance judgment was examined. Here, the aim in the conceptual design stage and the evaluation assumed as way of idea as shown in Fig. 2.68. The characteristic becoming important in next development target of gasket materials is a function to prevent a leak depending on use environment.
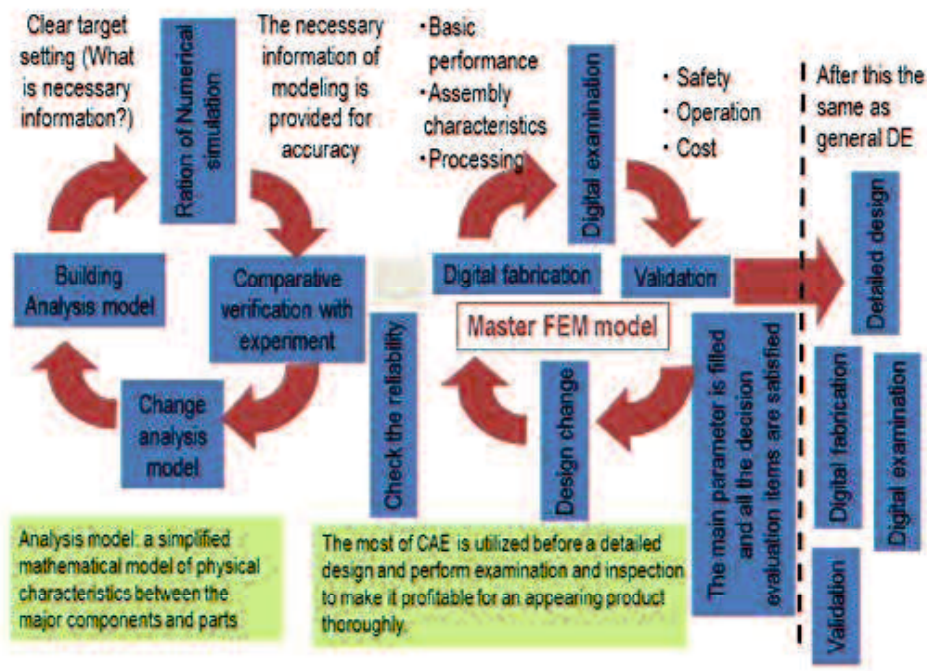
Fig. 2.66 Double loop at conceptual design level

2.10. Contact Analysis Theory

The simulation of many physical problems requires the ability to model the contact phenomena. The analysis of contact behavior is complex because of the requirement to accurately tract the motion of multiple geometric bodies, and the motion due to the interaction of these bodies after contact occurs. This includes representing the friction between surfaces and head transfer between the bodies if required. The numerical objective is to detect the motion of the bodies, apply a constraint to avoid penetration, and apply appropriate boundary conditions to stimulate the frictional behavior and heat transfer [47].

There are two types of contact bodies in Marc —deformable and rigid. Deformable bodies are simply a collection of finite elements as shown in Fig. 2.69. This body has three key aspects to it 1) the elements which make up the body 2) the nodes on the external surfaces which might contact another body or itself 3) the edges (2D) or faces (3D) which describe the outer surface which a node on another body (or the same body) might contact. Rigid bodies are composed of curves (2D) or surface (3D). The most significant aspect of rigid bodies is that they do not deform. Deformable bodies can contact rigid bodies, but contact between rigid bodies is not considered [47].
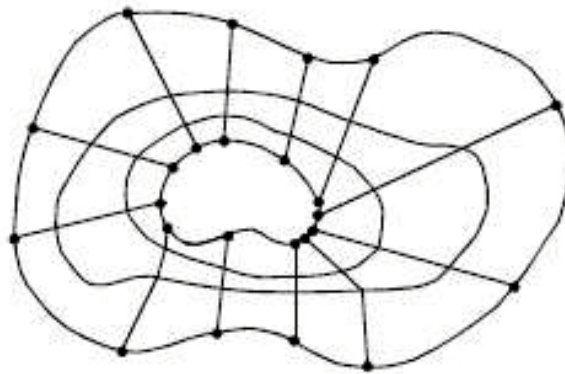

Fig. 2.67 Deformable body

The motion of deformable bodies is prescribed using the conventional method of applying displacements, force or distributed load to the bodies. It is advantageous to not apply displacement or point loads which might come into contact with other rigid bodies. If a prescribed displacement is to be imposed, it is better to introduce another rigid body and apply the motion to the rigid body. There are four ways to prescribe the motion of rigid surfaces, which are velocity, position, load and scaling [47].

During the incremental procedure, each potential contact node is first checked to see whether it is near a contact segment. The contact segments are

either edges of other 2D deformable bodies, faces of 3D deformable bodies or segment from rigid bodies. By default, each node could contact any other segment including segments on the body that belongs to. This allows a body to contact itself. During the iteration process, the motion of the node is checked to see whether it has penetrated a surface by determining whether it has crossed a segment. During the contact process, it is unlikely that a node exactly contacts the surface. For this reason, a contact tolerance (Fig. 2.70) is associated with surface. If a node is within the contact tolerance, it is considered to be in contact with the segment. The default contact tolerance is calculated by the program [47].
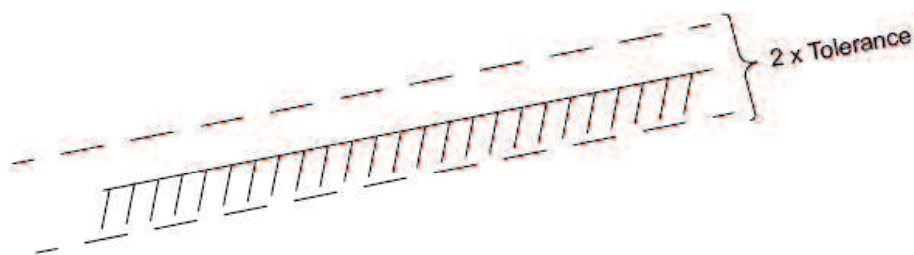

Fig. 2.68 Contact tolerance

During an increment, if node A moves from $A^{(t)}$ to $A^{(t+\Delta)}$, where $A^{(t+\Delta)}$ is beyond the contact tolerance, the node is considered to have penetrated (Fig. 2.71). In such a case, a special procedure is invoked to avoid this penetration.
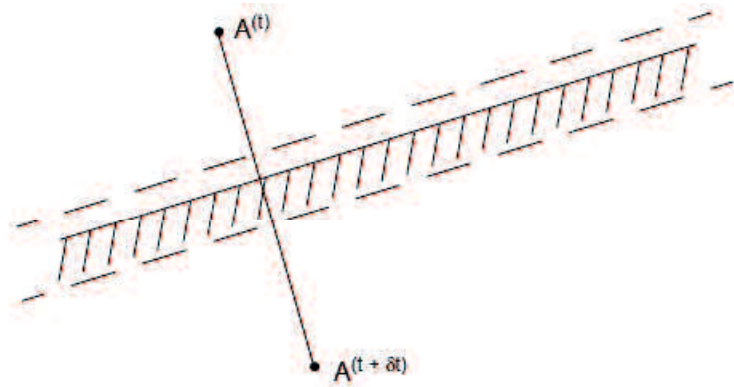
Fig. 2.69 Trial displacement with penetration

Friction is a complex physical phenomenon that involves the characteristic of the surface roughness, temperature, normal stress and relative velocity. An example of this complexity is that quite often in contact problems neutral lines develop. This means that along a contact surface, the material flows in one direction in part of the surface and in the opposite direction in another part of the surface. Such neutral lines are, in general, not known a priori. The most popular friction model is the adhesive friction or coulomb friction model. This model is used for most applications with the exception of bulk forming such as forging. For such applications the shear friction model is more appropriate. The coulomb model can be characterized by:

$$\|\sigma_t\| < \mu\sigma_n \ (stick) \ and \ \sigma_t = -\mu\sigma_n.t \ (slip) \tag{2.66}$$

Where

σ_n is the normal stress

σ_t is the tangential (friction) stress

μ   is the friction coefficient

t is the tangential vector in the direction of the relative velocity

$t = \frac{v_r}{|v_r|}$, in which v_r is the relative sliding velocity

105

Similarly, the Coulomb model can also be written in term of nodal forces instead of stresses:

$$\|f_t\| < \mu f_n \ (stick) \ and \ f_t = -\mu f_n.t \ (slip) \tag{2.67}$$

Where

f_t is the tangential (friction) force

f_n is the normal force

For a given normal stress or normal force, the friction stress or force has a step function behavior based upon the value of the relative sliding velocity v_r or the tangential relative incremental displacement Δu_t, as outlined in Fig. 2.70 for a 2D case, where the relative velocity and incremental displacement are scalar values [47].
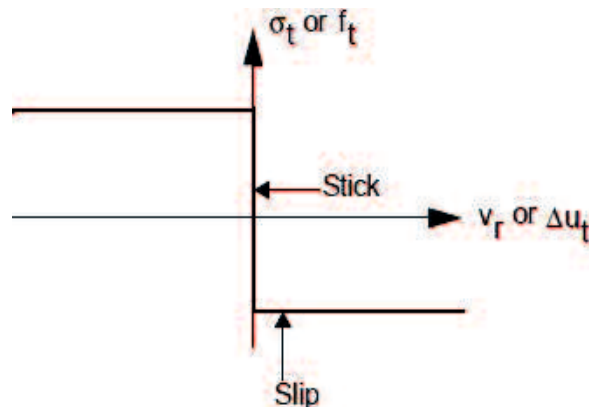

Fig. 2.70 Coulomb friction model

2.11. Boundary Conditions of the Numerical Analysis

Marc is based on the stiffness method and deals primarily with force-displacement relations. In a linear elastic system, force and displacement are related through the constant stiffness of the system; the governing equation of such a system can be expressed as

$$K\,u = F \qquad\qquad\qquad (2.68)$$

Where K is the stiffness matrix and u and F are nodal displacement and nodal force vectors, respectively. Equation (2.68) can be solved either for unknown displacements subjected to prescribed forces or for unknown forces (reactions) subjected to prescribed displacements. In general, the system is subjected to mix (prescribed displacement and force) boundary conditions, and Marc computes both the unknown displacements and reactions. Obviously, at any nodal point, the nodal forces and nodal displacements cannot be simultaneously prescribed as boundary conditions for the same degree of freedom. We must prescribe at least a minimum number of boundary conditions to ensure that rigid body motion does not occur. The prescribed force boundary conditions are often referred to as loads and the prescribed displacement boundary conditions as boundary conditions [47].

For contact between a deformable body and a rigid surface, the constraint associated with no penetration is implemented by transforming the degrees of freedom of the contact node and applying a boundary condition to the normal displacement. This can be considered solving problem [47]:

$$\begin{bmatrix} K_{\hat{a}\hat{a}} & K_{\hat{a}b} \\ K_{b\hat{a}} & K_{bb} \end{bmatrix} \begin{Bmatrix} u_{\hat{a}} \\ u_b \end{Bmatrix} = \begin{Bmatrix} f_{\hat{a}} \\ f_b \end{Bmatrix} \qquad\qquad (2.69)$$

where $\hat{a}$ represent the nodes in contact which have a local transformation, and b represents the nodes not in contact and, hence, not transformed. Of the nodes transformed, the displacement in the normal direction is then constrained such that $\delta u_{\hat{a}n}$ is equal to the incremental normal displacement of the rigid body at the contact point.
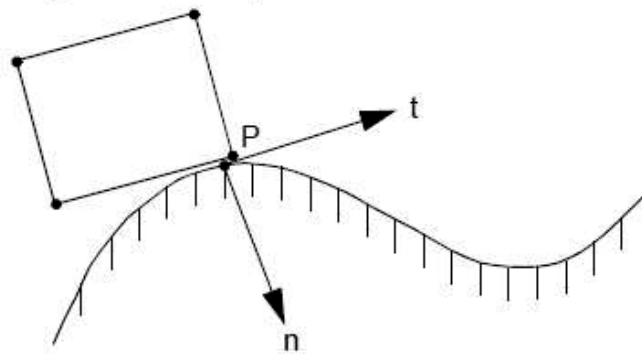
Fig. 2.71 Transformed system (2D)

As a rigid body can be represented as either a piecewise linear or as an analysis surface, two procedures are used. For piecewise linear representations, the normal is constant until node P comes to the corner of two segments as shown in Fig. 2.72. During the iteration process, one of three circumstances occurs. If the angle α is small $(-\alpha_{smooth} < \alpha < \alpha_{smooth})$, the node P slides to the next segment. In such a case, the normal is updated based upon the new segment. If the angle α is large $((\alpha > \alpha_{smooth} \, or \, \alpha < -\alpha_{smooth})$ the node separates from the surface if it is a convex corner, or stick if it is a concave corner. The value of α_{smooth} is important in controlling the computational cost. A larger value α_{smooth} reduces the computational costs, but might lead to inaccuracies. The default values are 8.625^o for 2D [47].

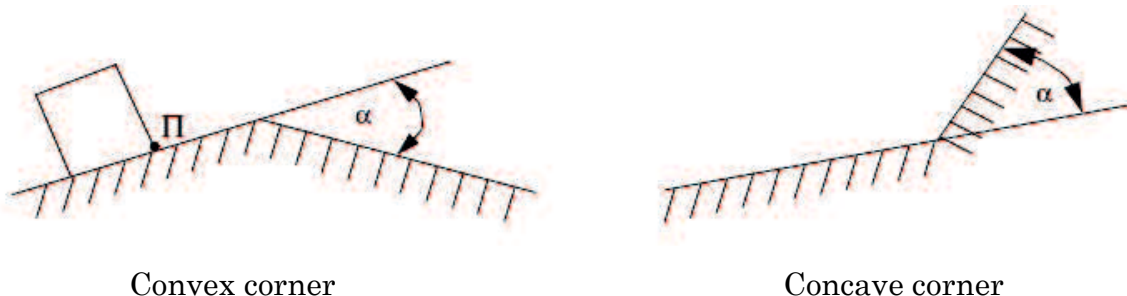Convex corner   Concave corner

Fig. 2.72 Corner conditions (2D)

CHAPTER III

DEVELOPMENT OF 25A-SIZE THREE-LAYER METAL GASKET BY USING FEM SIMULATION

Previous study of 25A-size metal gasket determined using a single material SUS304. The single material gasket can only form a macro seal due to the surface finish of the flanges and because that would reduce the ability of sealing gaskets. From previous study [22], it is also known for 0-MPa mode gasket in contact with flange's surface roughness 3.5 micrometer is still leaking. Further development is needed to improve gasket performance by add surface layer, but the surface layer is softer than base material so that it will cover the flange surface roughness when contact. Based on that, this research proposed three-layer metal gasket with surface layer properties softer than the base metal; therefore, increase seal ability between contacting surfaces. The three-layer material with SUS304 as base metal and soft material as the surface layer was chosen so that when contact with flanges it will form the micro seal to cover roughness of the flange.

The aim of this research is to determine the effect of a different material layer and tangent modulus material layer in three layer metal gasket to minimize leakage. The leakage can be associated with contact width and contact stress. Contact width and contact stress determined by simulation analysis based on an elastic and plastic condition.

3.1 Material and Method

The gasket used in this research is circumference beads gasket. The shape of gasket is produced by mold press. Three layer sheet metals assumed to be fully bonded; consequently, the interface delamination is beyond the scope of this paper. The dimension of gasket based on a previous study [20] with thickness (T) 1.2 mm for elastic mode, 1.5 mm for plastic mode and length (L) 19.5 mm (Fig. 1). In this study, the thickness of the surface layer (T2) was 0.1 mm. The base material (SUS304) has a characteristic modulus of the elasticity (Esus304) was 210 GPa, the nominal stress (σsus304) was 398.83 MPa,

tangent modulus was 1900.53 MPa. Material 1 (mat1) has a characteristic modulus of the elasticity (E1) was 0.35 x Esus304, the nominal stress (σ1) was 0.2 x σsus304, work hardening coefficient (Eh1 = E1/50, E1/100, E1/150). Material 2 (mat2) has a characteristic modulus of the elasticity (E2) was 0.65 x Esus304, the nominal stress (σ2) was 0.35 x σsus304, work hardening coefficient (Eh2 = E2/50, E2/100, E2/150). Material 3 (mat3) has a characteristic modulus of the elasticity (E3) was 0.9 x Esus304, the nominal stress (σ3) was 0.5 x σsus304, work hardening coefficient (Eh3 = E3/50, E3/100, E3/150). Material 1 (mat1), Material 2 (mat2) and Material 3 (mat3) can be clad well with stainless steel in all shapes and sizes [61]. In the next, gasket with a layer of Material 1 (mat1), Material 2 (mat2) and Material 3 (mat3) we called as mat1/SUS304/mat1, mat2/SUS304/mat2, and mat3/SUS304/mat3, respectively.
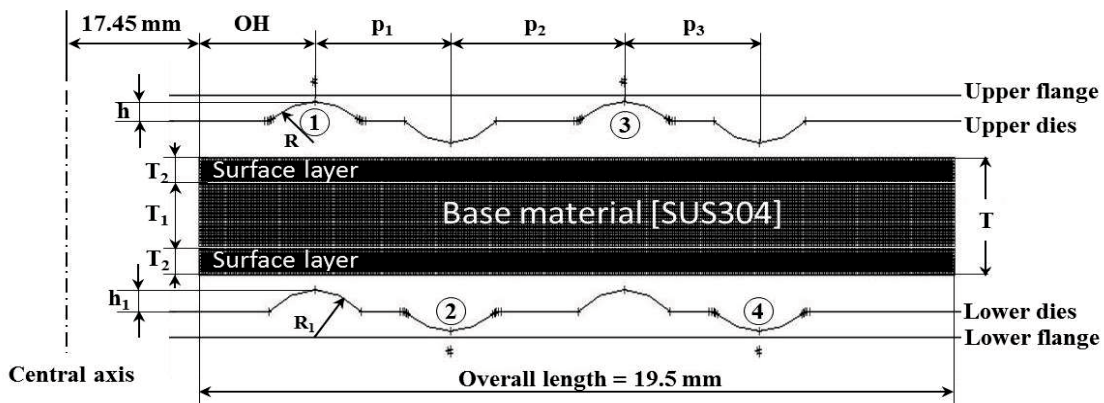

Fig. 3.1 Three layer clad metal sheet design

Table 3.1 Gasket dimension

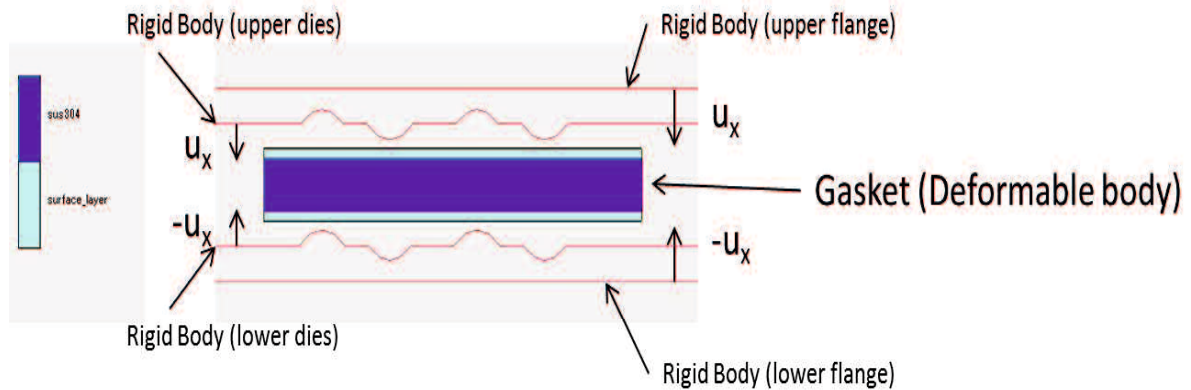| Design Parameter	0-MPa	400-MPa
Over Hang (OH)[mm]	3	3
Pitch 1 (p1) [mm]	4.5	3.5
Pitch 2 (p2) [mm]	4.5	4.5
Pitch 3 (p3) [mm]	4.5	3.5
Lip Height (h)[mm]	0.35	0.3
Lip Height (h1)[mm]	0.39	0.33
Convex Radius (R)[mm]	3.5	2.5
Convex Radius (R1)[mm]	3.2	2.3
Thickness gasket total (T)[mm]	1.2	1.5
Surface layer thickness (T_2) [mm]	0.1	0.1

Fig. 3.2 Three layers Gasket simulation setting up

The elastoplastic behavior of gasket is calculated by using software of FEM, MSC. Marc. Fig. 3.2 shows the loading condition. In our calculation, 2 dimensional axisymmetric solid elements isoparametric quadrilateral type 10 are used to implement compression displacement in the axial direction on the gasket in between the upper and the lower of dies and flange with a constant increasing step of displacement Δu_x.

In our study, the material is assumed to obey isotropic strain hardening, and described by J2-deformation theory of Mises' yield criterion for bilinear stress-strain behavior. The material behavior is initially elastic characterized by a Young's modulus E until yielding commences at the uniaxial yield stress σ_Y. Thereafter the material response is elastic-plastic with the local tangent to the curve continually varying and is termed the elastic-plastic tangent modulus E_T (Fig. 3.3). During our nonlinear analysis with iterative procedure, Newton-Raphson method is used to solve for the equilibrium equations which are composed of finite strain plasticity with multiplicative decomposition of deformation gradient.
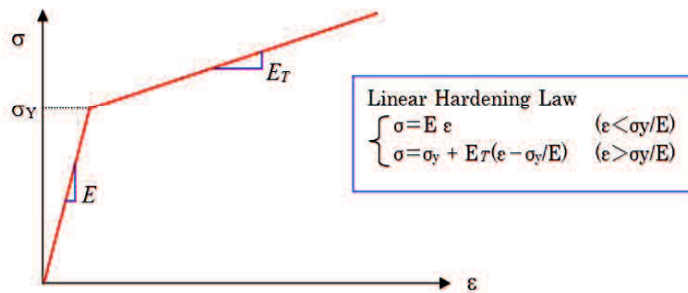
Fig. 3.3 Linear strain hardening model

From MSC Marc result, the contact width is determined based on contact status. Contact status values are1 and 0 which mean contact and no contact, respectively. Only at the beads (convex part) of gasket which is effective for avoiding leak is taken as evaluation part. The top surface and bottom surface of contact width increased step by step due to the increment of the axial force to the gasket.
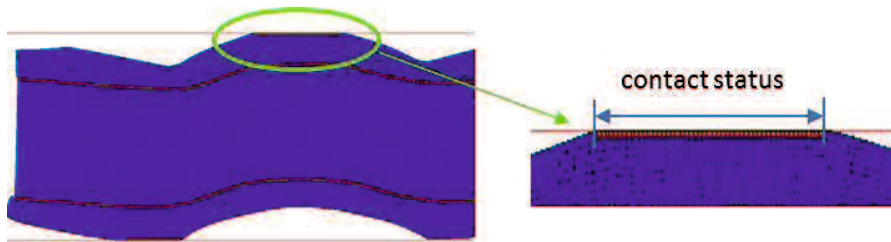

Fig. 3.4 the contact status

The gasket design used based on [20], without considering distribution of contact stress called 0-MPa mode. Otherwise, the gasket design by considering plastic contact stress called 400-MPa mode. In this study, a gasket model is divided into two simulation stages by using forming and tightening simulation. Flowchart of the stage simulation gasket by considering the yield stress of the metal surface, tangent modulus effects is shown in Fig. 3.5.

The deformation mode of the stainless gasket was investigated using an FEM analysis. The stages were modeled using the software MSC. Marc [47]. First, using two-dimensional assumptions, an axis-symmetric model was adopted for the forming process simulation in the axial direction between the upper and lower dies. Second, the gasket

shape produced by mold press then compressed in axial direction between the upper and lower flanges to simulate the relationship between the axial force, average contact stress and contact width curves. Both the upper and lower flanges are assumed to be rigid bodies. Further, the contact stress and contact width evaluation were performed only for the convex portion of the gasket, which is effective at reducing the leakage.
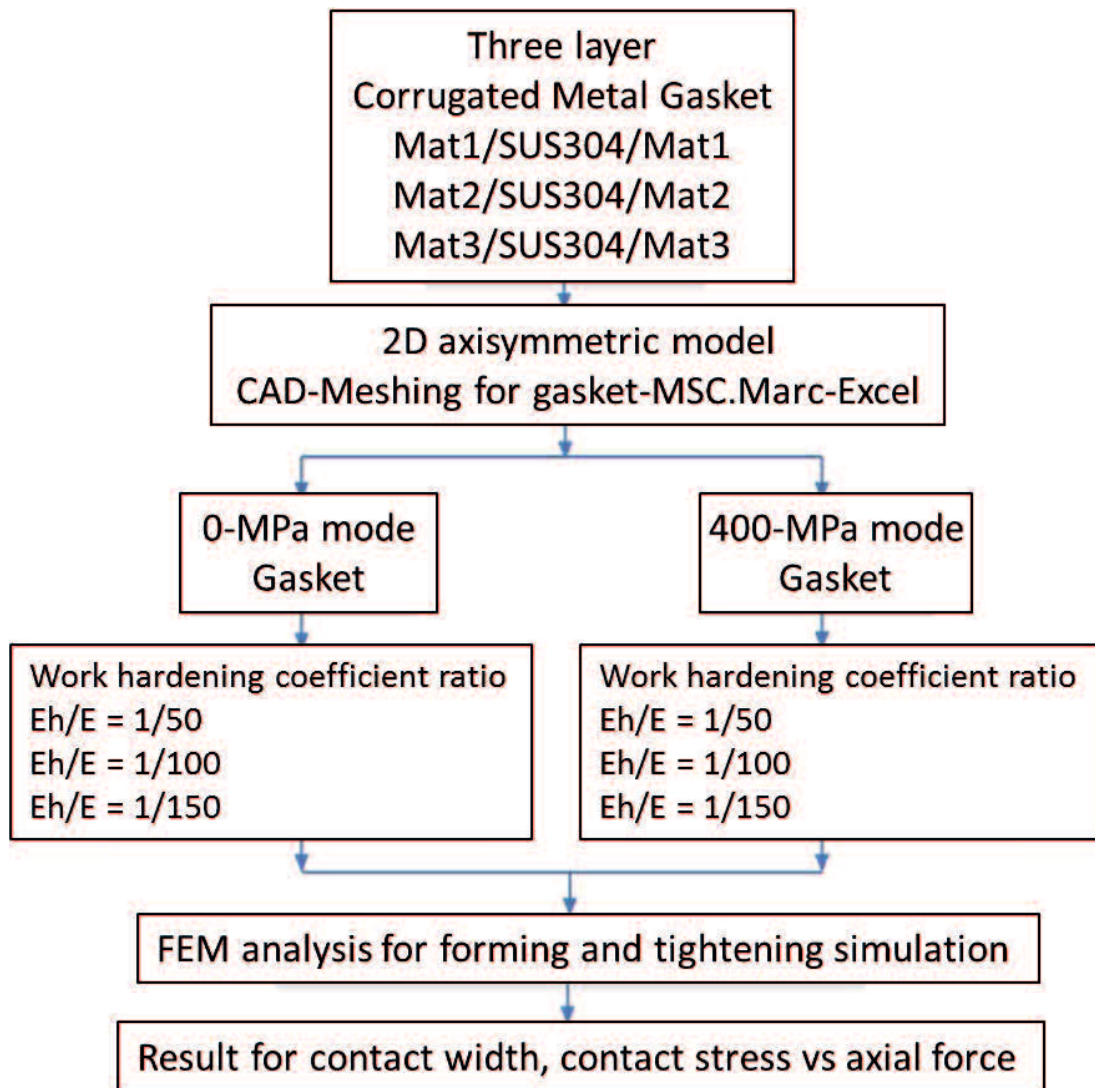
```
                 ┌──────────────────────────────┐
                 │        Three layer           │
                 │  Corrugated Metal Gasket      │
                 │     Mat1/SUS304/Mat1          │
                 │     Mat2/SUS304/Mat2          │
                 │     Mat3/SUS304/Mat3          │
                 └──────────────────────────────┘
            ┌────────────────────────────────────────┐
            │        2D axisymmetric model            │
            │  CAD-Meshing for gasket-MSC.Marc-Excel  │
            └────────────────────────────────────────┘

     ┌──────────────────┐              ┌──────────────────┐
     │   0-MPa mode      │              │   400-MPa mode    │
     │     Gasket        │              │     Gasket        │
     └──────────────────┘              └──────────────────┘

 ┌──────────────────────────────┐  ┌──────────────────────────────┐
 │ Work hardening coefficient    │  │ Work hardening coefficient    │
 │ ratio                         │  │ ratio                         │
 │ Eh/E = 1/50                   │  │ Eh/E = 1/50                   │
 │ Eh/E = 1/100                  │  │ Eh/E = 1/100                  │
 │ Eh/E = 1/150                  │  │ Eh/E = 1/150                  │
 └──────────────────────────────┘  └──────────────────────────────┘

     ┌──────────────────────────────────────────────────────┐
     │  FEM analysis for forming and tightening simulation    │
     └──────────────────────────────────────────────────────┘

     ┌──────────────────────────────────────────────────────┐
     │  Result for contact width, contact stress vs axial force │
     └──────────────────────────────────────────────────────┘
```

Fig. 3.5 Flowchart the stage of the three layer gasket simulation

3.2 Simulation Analysis

Based on [20], [22], peak 2 and peak 3 were higher than peak 1 and peak 4 for contact width and contact stress. Therefore, in this study, the upper contact and lower contact of three layer gasket will be represented by peak 3 and peak 2, respectively.

Fig. 3.6 shows the simulation result for the gasket mat1/SUS304/mat1 in a 0-MPa mode. This figure shows that contact width increases with axial force. The contact width of a gasket mat1/SUS304/mat1 with tangent modulus, Eh1 = E1/150 and Eh1 = E1/50 had the highest and the lowest slope, respectively.

Gasket mat1/SUS304/mat1 has work hardening coefficient Eh1 = E1/50 showed the highest average contact stress propensity than the others. To maintain seal integrity, the effective compressive pressure on gasket must be higher than the internal pressure by some multiple. Usually, the value of internal pressure in the piping system is around 10 MPa. Fig. 3.6 denoted that the contact stress value was around 350 MPa at 100 KN. It is larger enough to reduce the internal pressure effect, which is 35 times internal pressure.

Fig. 3.7 shows the simulation result for the gasket mat2/SUS304/mat2 in a 0-Mpa mode. This figure shows that contact width increases with axial force. The contact width in a gasket mat2/SUS304/mat2 in contact with the flange which has a work hardening coefficient, Eh2 = E2/150 and Eh2 = E2/50 had the highest and the lowest slope, respectively.
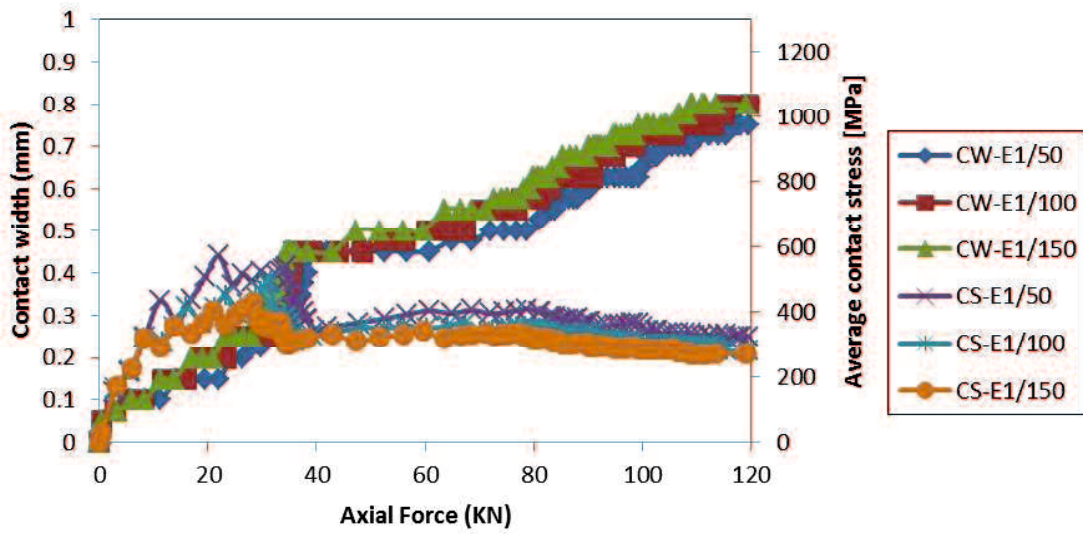
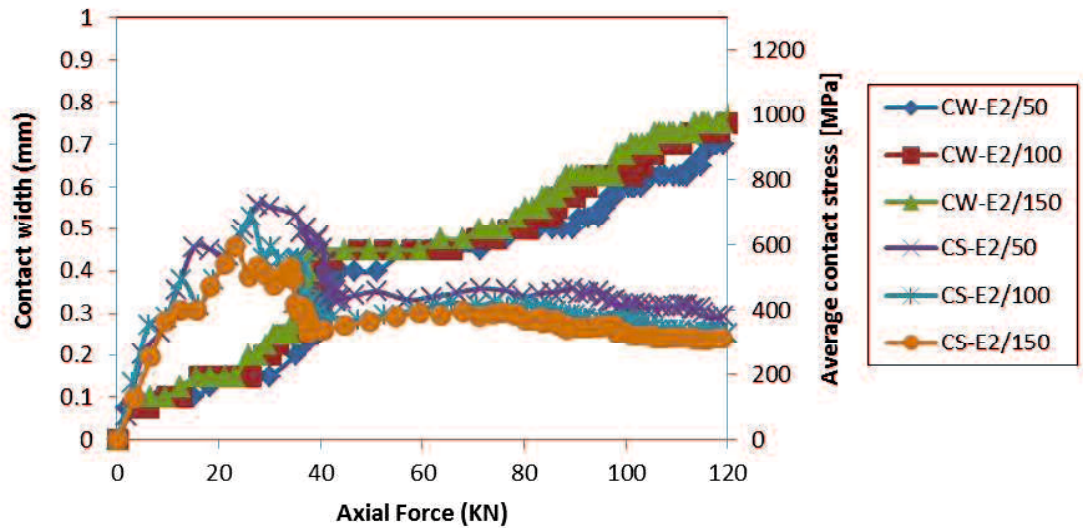Fig. 3.6 Contact width-contact stress for gasket mat1/SUS304/mat1 in 0-MPa mode

Fig. 3.7 Contact width-contact stress for gasket mat2/SUS304/mat2 in 0-MPa mode

The contact stress occurs in the gasket contact with flange all in the upper and lower contact is similar. But, gasket mat2/SUS304/mat2 with work hardening coefficient $Eh2 = E2/50$ showed the highest propensity than the others. The average contact stress for gasket mat2/SUS304/mat2 $Eh2 = E2/150$ was the lowest. Fig. 3.7 denoted that the contact stress value was around 410 MPa at 100 KN. It is larger enough to reduce the internal pressure effect, which is 41 times internal pressure.

Fig. 3.8 shows the simulation result for the gasket mat3/SUS304/mat3 in a 0-MPa mode. This figure shows that contact width increases with axial force. The contact width of a gasket mat3/SUS304/mat3 with work hardening coefficient, $Eh3 = E3/150$ and $Eh3 = E3/50$ had the highest and the lowest slope, respectively. The contact stress gasket mat3/SUS304/mat3 with work hardening coefficient $Eh3 = E3/50$ showed the highest propensity than the others. The average contact stress for gasket mat3/SUS304/mat3 $Eh3 = E3/150$ was the lowest. Fig. 3.8 denoted that the contact stress value was around 500 MPa at 100 KN. It is larger enough to reduce the internal pressure effect, which is 50 times internal pressure.

Fig. 3.9 shows the simulation result for upper and lower contacts of the gasket mat1/SUS304/mat1 in a 400-MPa mode. This figure shows that contact width increases with axial force. The contact width of a gasket mat1/SUS304/mat1 with work hardening coefficient, $Eh1 = E1/150$ and $Eh1 = E1/50$ had the highest and the lowest slope, respectively. Gasket mat1/SUS304/mat1 which work hardening coefficient $Eh1 = E1/50$ showed the highest propensity than the others. The average contact stress for gasket mat1/SUS304/mat1 $Eh1 = E1/150$ was the lowest. Fig. 3.9 denoted that the contact stress value was around 480 MPa at 80 KN. It is larger enough to reduce the internal pressure effect, which is 48 times internal pressure.
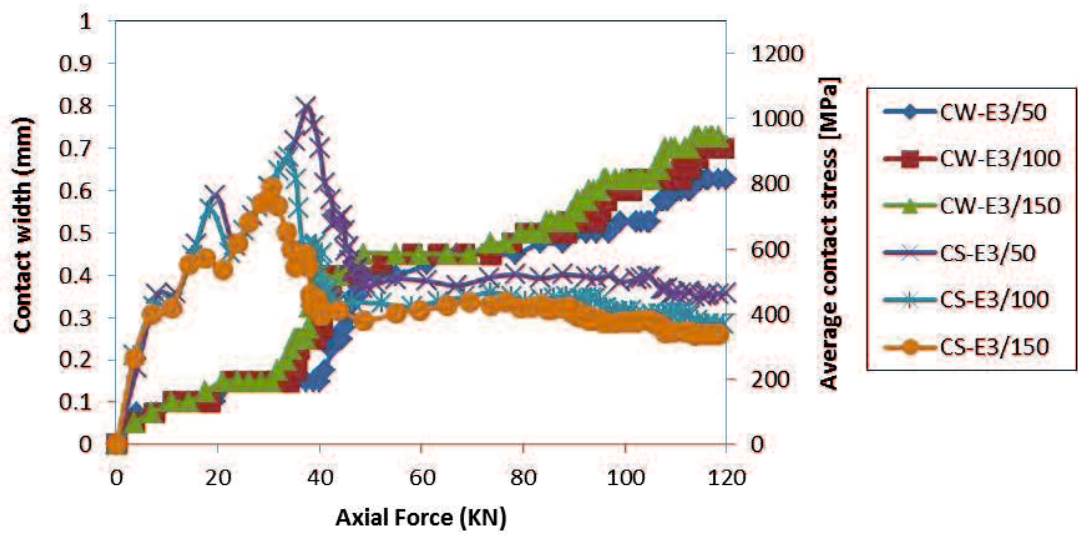
Fig. 3.8 Contact width-contact stress for gasket mat3/SUS304/mat3 in 0-MPa mode
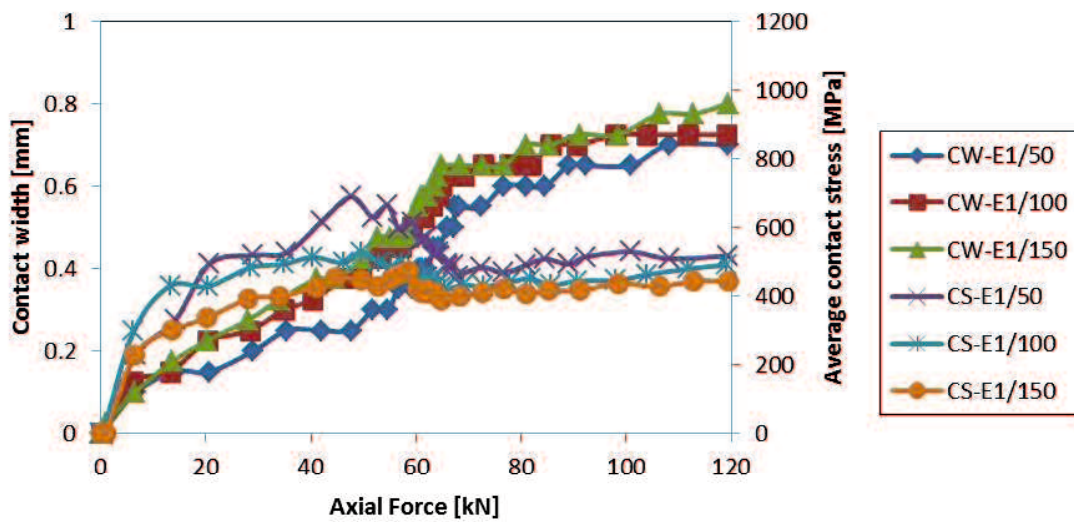

Fig. 3.9 Contact width-contact stress for gasket mat1/SUS304/mat1 in 400-MPa mode
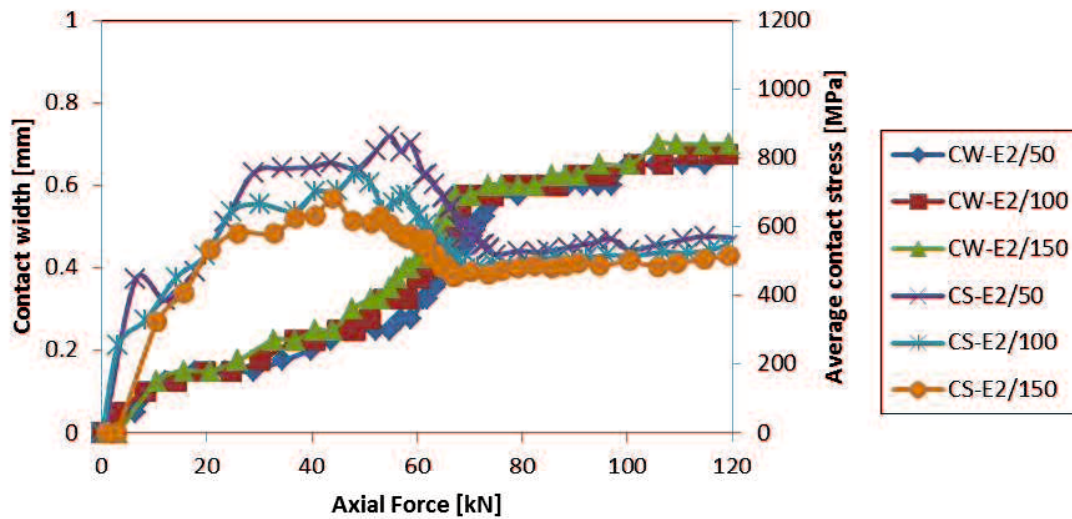
117

Fig. 3.10 Contact width-contact stress for gasket mat2/SUS304/mat2 in 400-MPa mode

Fig. 3.10 shows the simulation result for upper and lower contacts of the gasket mat2/SUS304/mat2 in a 400-MPa mode. This figure shows that contact width increases with axial force. The contact width in a gasket mat2/SUS304/mat2 in contact with the flange which has a work hardening coefficient, $Eh2 = E2/150$ and $Eh2 = E2/50$ had the highest and the lowest slope, respectively. The contact stress gasket mat2/SUS304/mat2 with tangent modulus $Eh2 = E2/50$ showed the highest propensity than the others. The average contact stress for gasket mat2/SUS304/mat2 $Eh2 = E2/150$ was the lowest. Fig. 3.10 denoted that the contact stress value was around 520 MPa at 80 KN. It is larger enough to reduce the internal pressure effect, which is 52 times internal pressure.

Fig. 3.11 shows the simulation result for the gasket mat3/SUS304/mat3 in a 400-MPa mode. This figure shows that contact width increases with axial force. The contact width in a gasket mat3/SUS304/mat3 in contact with the flange with work hardening coefficient, $Eh3 = E3/150$, and $Eh3 = E3/50$ had the highest and the lowest slope, respectively. The average contact stress gasket mat3/SUS304/mat3 with work hardening coefficient $Eh3 = E3/50$ showed the highest propensity than the others. The average contact stress for $Eh3 = E3/150$ was the lowest. Fig. 3.11 denoted that the contact stress value was

around 600MPa at 80 KN. It is larger enough to reduce the internal pressure effect, which is 60 times the internal pressure.

Based on simulation result, the average contact stress for the gasket 0MPa mode was lower than the gasket 400MPa mode.
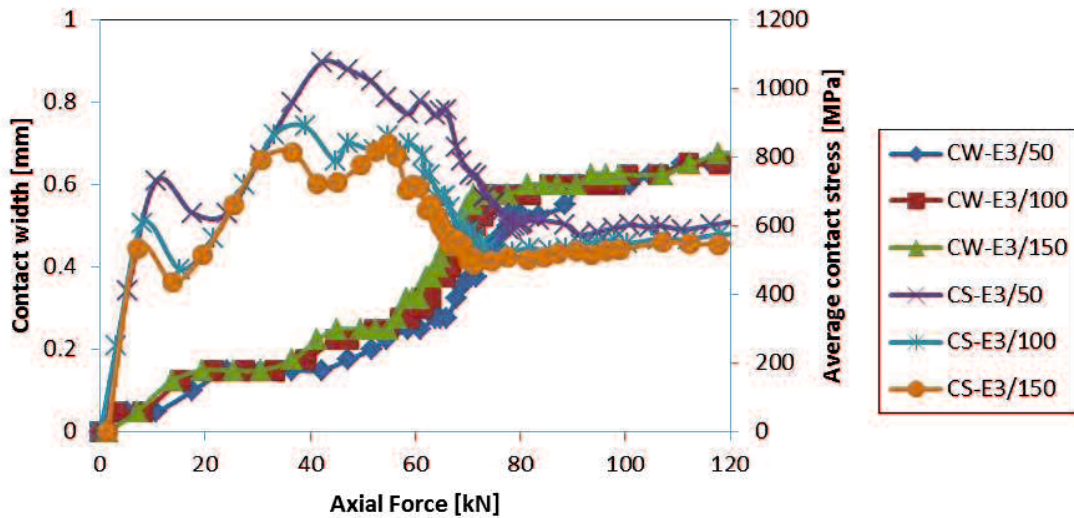

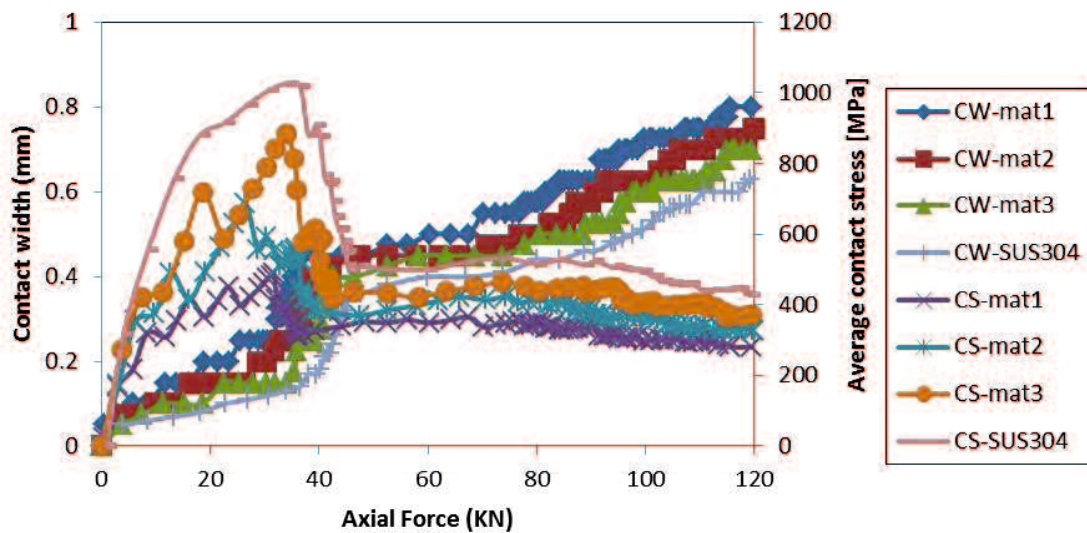Fig. 3.11 Contact width for gasket mat3/SUS304/mat3 in 400-MPa mode
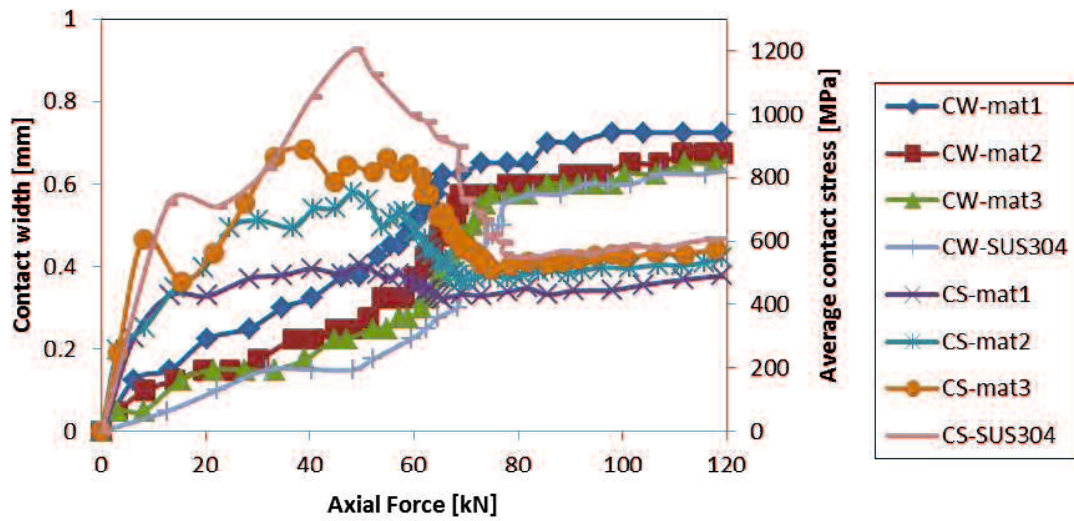


Fig. 3.12 Comparison 0-MPa mode

Fig. 3.13 Comparison 400-MPa mode

If compared with the previous study that only use single material SUS304 [6] for contact width, the three layers gasket with the mat1 layer (Eh=E1/150) 0.1 mm thickness had higher slope for both type of gasket as shown in fig.3.12 and fig.3.13. Fig.3.14a, b, c show that gasket three-layer has larger contact width in plastic contact stress condition than single layer SUS304. Based on simulation result we can state that the three-layer gasket better than gasket single SUS304 and had a good prospect to developed.
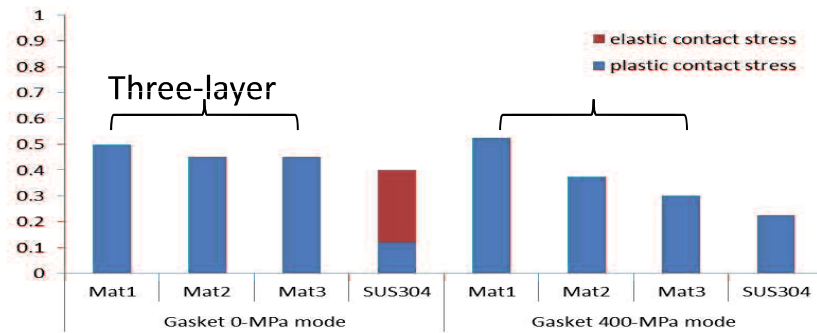
(a) Contact width-contact stress condition at 60kN axial force
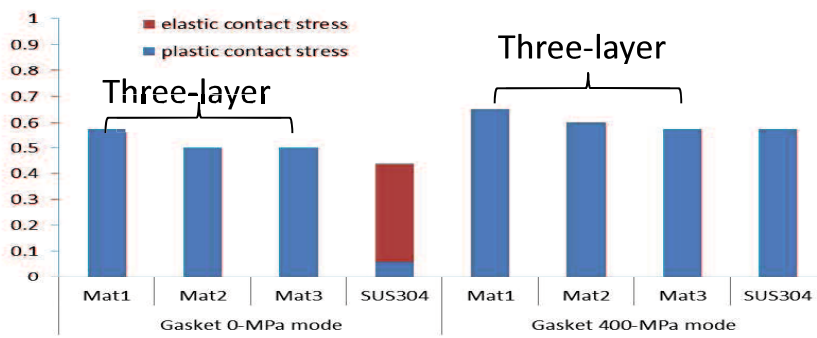
(b) Contact width-contact stress condition at 80kN axial force
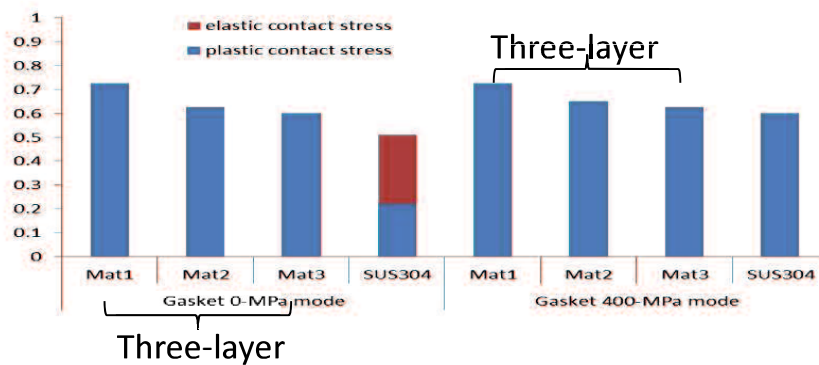
(c) Contact width-contact stress condition at 100kN axial force

Fig.3.14 Contact width-contact stress condition at any axial force (Eh/E=1/100)

3.3 Conclusion

   In this research, from simulation analysis by FEM, we could conclude that:

1) The gasket three-layer 400-Mpa mode has higher average contact stress than the gasket 0-MPa mode. The contact width for the gasket 0-MPa mode was higher than the gasket 400-MPa mode at 60kN. For 80kN and 100kN axial force gasket 400-MPa mode has higher contact width contain larger plastic contact stress condition than 0-MPa mode.

2) The average contact stress for gasket mat3/SUS304/mat3 which $Eh3 = E3/50$ showed the highest propensity than the others. The contact width in a gasket mat1/SUS304/mat1 in contact with the flange with work hardening coefficient, $Eh1 = E1/150$ had the highest slope for both kind of gasket.

CHAPTER IV

ANALYSIS STUDY OF CONTACT WIDTH AND CONTACT STRESS OF THREE-LAYER CORRUGATED METAL GASKET

Study for corrugated metal gasket is still underway to improve its performance. As mentioned [22] in which the performance of the gasket decreases with increasing surface roughness of the flange, even for the gasket type 0-MPa mode leakage still occurs at the time of contact with the flange which has a surface roughness of 3.5 micrometers for a range of axial force up to 120KN. It is considered as a single gasket with SUS304 material when in contact with a flange having a larger surface roughness, contact width decreases and plastically deformed contact surfaces not exhaustive and is unable to fill the gap surface roughness of the flange. The utilization of material softer than the base material as a surface covering material is already widely used to improve performance gaskets. Al, Cu and Ni as the cover layer has also been used on the elastic metal gasket O-ring named "Helicoflex" [62, 63]. Haruyama et.al [65] developed three-layer corrugated metal gasket with SUS304 as base metal and aluminium-, cooper-, nickel- as the surface layer. The surface layer thickness used 0.1 mm and gasket dimension based on [20]. A finite element method employed to determine the effect of a different material layer and tangent modulus material layer on contact width and contact stress of three-layer corrugated metal gasket.

However in Ref. [65] there is no discussion about the effect of modulus elasticity ratio for more materials and effect of surface layer thickness. In this study, therefore effect of modulus elasticity ratio and thickness ratio on contact width and contact stress of each convex a 25A-size three-layer corrugated metal gasket are investigated using Finite Element Analysis (FEA). The modulus of elasticity ratio is the ratio between modulus of elasticity of surface layer material to SUS304 as a base material. Thickness ratio is the ratio of base material thickness to total thickness gasket. The result will give us the mapping of the effects of the layer material selection and thickness on contact width and contact stress. The distribution maps of the three-layer metal gasket plotted in this study are very

123

important in the design process of the three-layer metal gasket and could function as a key reference in the future.

4.1 Material and Method

Fig. 4.1 shows a corrugated metal gasket which is to be inserted between flanges and dimension of three-layer corrugated metal gasket. Gaskets consist of two types: 0-mode MPa and 400 MPa, the detailed information of this gasket describe on table 4.1. Three layers of sheet metal assumed to be fully bound; consequently, delamination interface is beyond the scope of this paper.
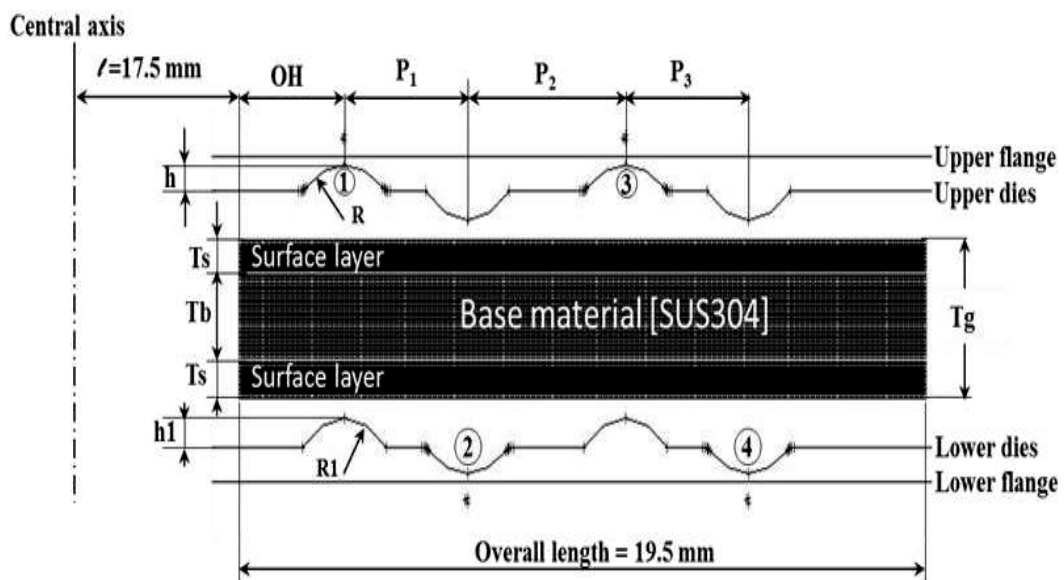
Fig.4.1 2-dimension axisymmetric model of three-layer gasket

Table.4.1 Optimum design of gasket 0-MPa and 400-MPa mode

No	Design Parameter	0MPa	400MPa
A	Over Hang (OH) [mm]	3	3
B	Picth 1 (p1) [mm]	4.5	3.5
C	Pitch 2 (p2) [mm]	4.5	4.5
D	Pitch 3 (p3) [mm]	4.5	3.5
E	Lip Height (h) [mm]	0.35	0.3
	Lip Height (h1) [mm]	0.39	0.33
F	Convex Radius (R) [mm]	3.50	2.5
	Convex Radius (R1) [mm]	3.20	2.30
G	Thickness gasket total (Tg) [mm]	1.2	1.5

Table 4.2.Properties of SUS304 used in simulation

materials	Nominal Stress (σ) [MPa]	Tangent Modulus [MPa]	Modulus of Elasticity (E) [GPa]	Poisson ratio (ν)
SUS304	398.83	1900.53	210	0.3
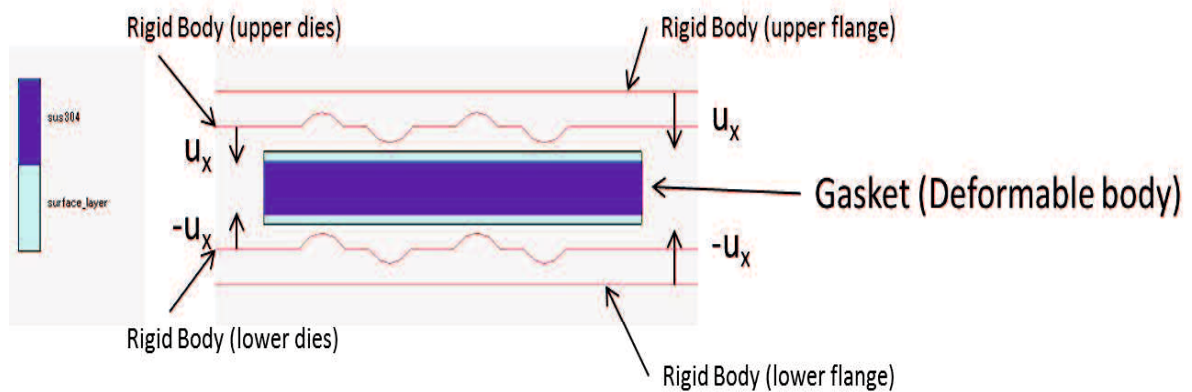
Fig. 4.2 Three layers Gasket simulation setting up

The elastoplastic behavior of gasket is calculated by using software of FEM, MSC. Marc. Fig. 4.2 shows the loading condition. In our calculation, 2 dimensional axisymmetric solid elements isoparametric quadrilateral type 10 are used to implement compression displacement in the axial direction on the gasket in between the upper and the lower of dies and flange with a constant increasing step of displacement Δux.

In our study, the material is assumed to obey isotropic strain hardening, and described by J2-deformation theory of Mises' yield criterion for bilinear stress-strain behavior. The material behavior is initially elastic characterized by a Young's modulus E until yielding commences at the uniaxial yield stress σ_Y. Thereafter the material response is elastic-plastic with the local tangent to the curve continually varying and is termed the elastic-plastic tangent modulus E_T (Fig. 4.3). During our nonlinear analysis with iterative procedure, Newton-Raphson method is used to solve for the equilibrium equations which are composed of finite strain plasticity with multiplicative decomposition of deformation gradient.
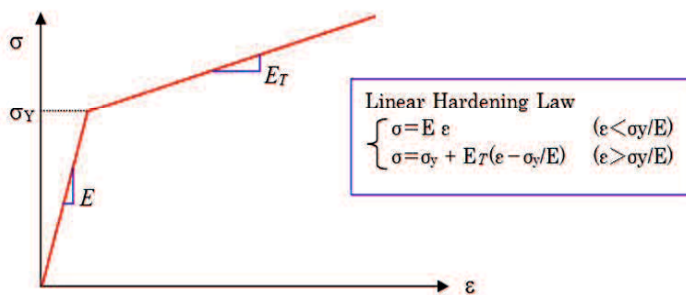

Fig. 4.3 Linear strain hardening model

From MSC Marc result, the contact width is determined based on contact status. Contact status values are1 and 0 which mean contact and no contact, respectively. Only at the beads (convex part) of gasket which is effective for avoiding leak is taken as evaluation part. The top surface and bottom surface of contact width increased step by step due to the increment of the axial force to the gasket.
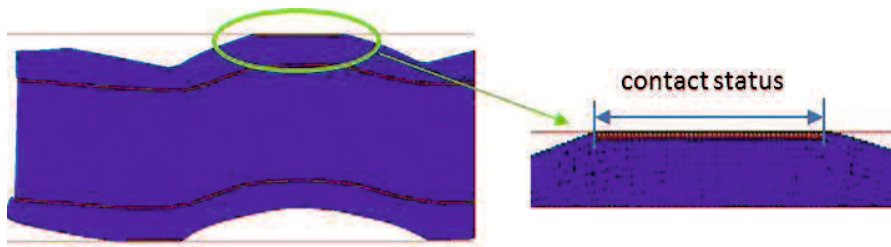
Fig. 4.4 the contact status

In this study, a gasket is divided into two processes by using forming and tightening simulation as shown in Fig. 4.2. First, using two-dimensional assumptions, an axis-symmetric model was adopted for the forming process simulation in the axial direction between the upper and lower dies. Second, the gasket shape produced by mould press then compressed in axial direction between the upper and lower flanges to simulate the relationship between the axial force, average contact stress and contact width. Both the upper and lower dies and flanges are assumed to be rigid bodies. Flowchart of the stage simulation gasket by considering the type of gasket, thickness ratio and modulus of elasticity ratio effects is shown in Fig.4.5.
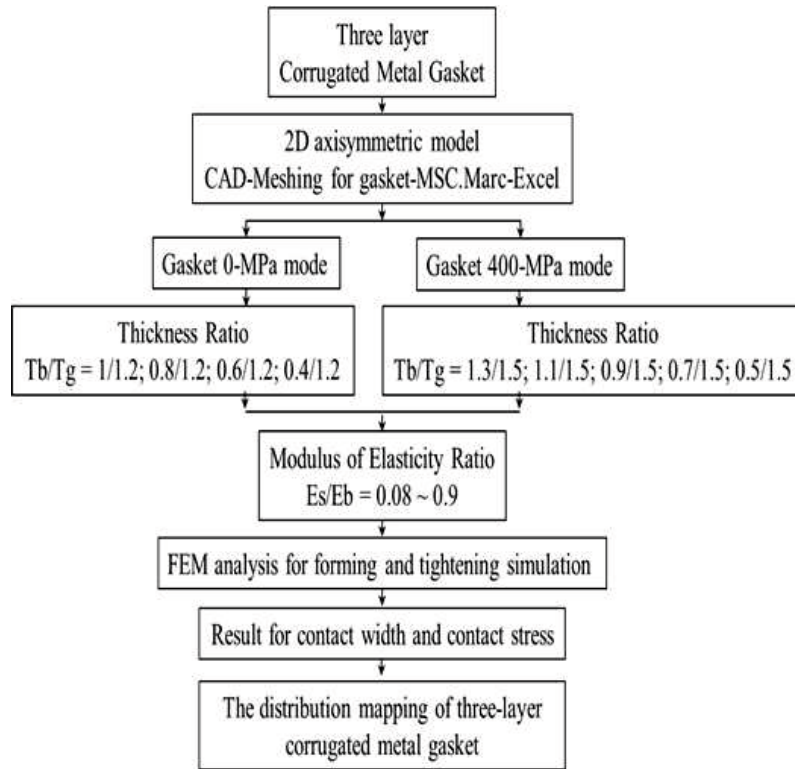
Fig. 4.5 Flowchart the stage of the three layer gasket simulation

Based on [64], the stiffness to weight ratio of a laminate is one of its most attractive properties when considering a need for weight reduction. The stiffness of a laminated sheet is defined as the resistance to elastic deformation in bending, which is equivalent to the bending modulus of the material. The elastic modulus of homogeneous sheet is generally the same in tension and in bending, whereas the bending modulus varies with the volume fraction of base. When the properties of the laminate are symmetrical about its neutral axis, then the tensile and bending moduli of elasticity, ET and EB, can be expressed using the rule of mixtures and simple bending theory from which the specific stiffness can be estimated from known density of face metal and the base:

$$E_T = E_s V_s + E_b (1 - V_s) \tag{4.1}$$

$$V_s = {}^{A_s \, t_s} \big/ {}_{A_{Total} \, t_{Total}} \qquad\qquad (4.2)$$

If $A_s = A_{Total}$

Then

$$V_s = {}^{t_s} \big/ {}_{t_{Total}} \qquad\qquad (4.3)$$

$$E_T = E_s \frac{t_s}{t_{total}} + E_b \left(1 - \frac{t_s}{t_{total}}\right) \qquad\qquad (4.4)$$

$$E_B = E_s \left[1 - (1 - V_s)^3\right] + E_b (1 - V_s)^3 \qquad\qquad (4.5)$$

$$E_B = E_s \left[1 - \left(1 - \frac{t_s}{t_{total}}\right)^3\right] + E_b \left(1 - \frac{t_s}{t_{total}}\right)^3 \qquad\qquad (4.6)$$

Where E and V are the Young's modulus and volume fraction, respectively, of individual component, and subscripts "s" and "b" refer to the surface metal and the base materials, respectively. From equation (4.1 - 4.6), we know the stiffness of the laminate influence by Young's modulus of surface material and base material and thickness ratio. Because that in this research we investigate the effect of Young's modulus elasticity ratio between surface to base and thickness of surface layer on contact width and contact stress of each convex a 25A-size three-layers corrugated metal gasket.

The total thickness of gasket (Tg) is 1.2 mm for gasket 0-MPa mode, 1.5 mm for 400-MPa mode and overall length (L) is 19.5 mm (Fig. 1). The base material (SUS304) has a characteristic as shown table 2. For 0-MPa mode the thickness ratio (Tb/Tg) varies from 1/1.2, 0.8/1.2, 0.6/1.2, 0.4/1.2 and for 400-MPa mode varies from 1.3/1.5, 1.1/1.5, 0.9/1.5, 0.7/1.5, 0.5/1.5. The total thickness of gasket (Tg) is held constant. The thickness ratio (Tb/Tg) 1/1.2 mean the base material thickness is 1 mm, the surface layer thickness for upper and lower side is 0.2 mm and the total thickness of gasket is 1.2 mm. The modulus of elasticity ratio between surface-layer to base material (Es/Eb) varies from 0.1 up to 0.9. The surface layer was considered as elastic perfectly-plastic material with σys/Es of 0.001 and

work hardening coefficient ratio with ETs/Es of 0.01. The poisson's ratio for all surface layer material was 0.3.

4.2 Simulation Analysis

The contact stress and contact width evaluation were performed only for the convex portion of the gasket, which is effective at reducing the leakage.

4.2.1 Effect of modulus of elasticity ratio on contact width and contact stress.

Firstly we plot graphic with vertical axis gives the aspect ratio of modulus of elasticity of the surface layer material to SUS304 while contact width or average contact stress is given along the horizontal axis. To describe the effect of modulus of elasticity ratio on contact width and average contact stress we use thickness ratio (Ts/Tg) 0.1/1.2 as example.
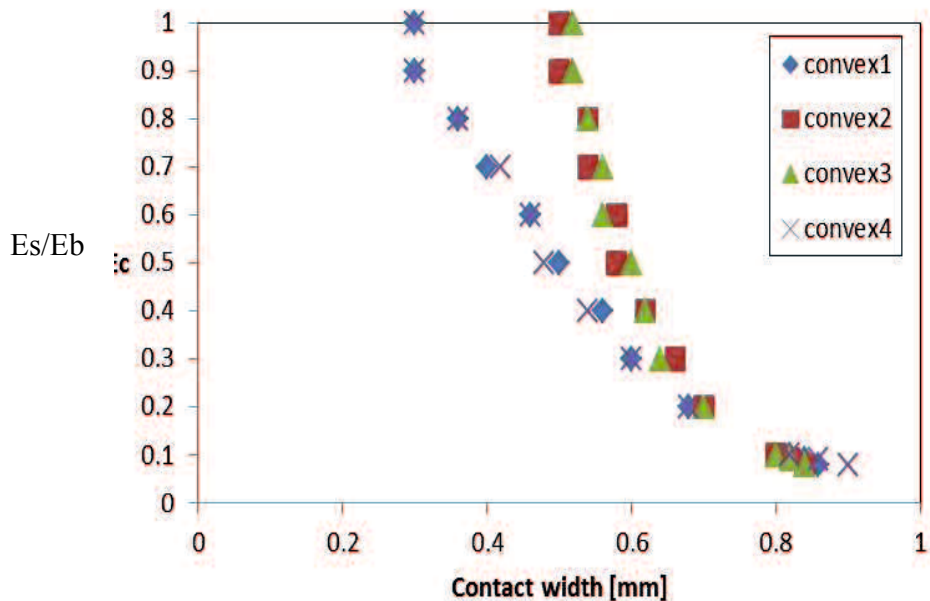
Fig.4.6 The mapping contact width vs. Es/Eb for three-layer corrugated metal gasket (0-MPa mode, Ts/Tg=0.1/1.2, 100KN)
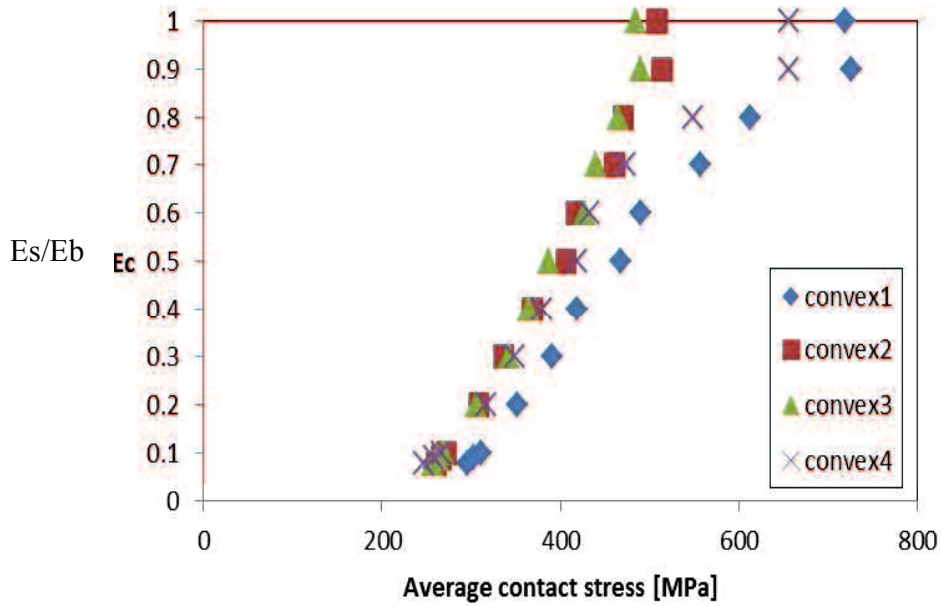
Fig.4.7 The mapping average contact stress vs. Es/Eb for three-layer corrugated metal gasket (0-MPa mode, Ts/Tg= 0.1/1.2, 100KN)

Fig.4.6 shows a distribution map of the contact width with modulus of elasticity ratio from 0.08 up to 1 for gasket 0-MPa mode, Ts = 0.1mm, on 100KN axial force. We choose axial force 100KN because on this axial force gasket 0-MPa single layer SUS304 not leakage based on helium leak rate test [20]. Value Es/Eb = 1 indicated gasket single layer SUS304. From Fig.4.6 for Es/Eb value we got convex 2 and 3 have the higher contact width than convex 1 and 4. We choose Es/Eb lower than 1 because we use the contact width as the evaluation criteria, due to a larger contact width is more beneficial than a larger contact stress because it can cover the roughness of the contact surface as long as the contact stress is greater than the internal pressure based on [13]. When Es/Eb value less than 1 contact width seen increase and the difference for each convex also decrease. Fig.4.6 shows for modulus of elasticity ratio 1 down to 0.1 the contact width on convex 2 and 3 still higher than convex1 and 4. For modulus of elasticity ratio 0.8 down to 0.1, convex 2 and 3 alternated turns to be the highest. In previous study used single layer SUS304,

131

convex 2 and 3 have the highest contact width than convex 1 and 4, therefore the analysis focus only on convex 2 and 3.

Fig.4.7 shows a distribution map of the average contact stress with modulus of elasticity ratio from 0.08 up to 1 for gasket 0-MPa mode, Ts/Tg = 0.1/1.2, on 100KN axial force. The figure shows for modulus of elasticity ratio 1 down to 0.08 the average contact stress on convex 1 and 4 still higher than convex 2 and 3. The lower modulus of elasticity ratio it seems the average contact stress decrease for each convex and the difference for each convex also decrease.

Fig. 4.8 shows the deformation shape for single layer SUS304, gasket single layer SUS304, 0-MPa mode at axial force 100 KN. For gasket single layer at 100 KN there is a small contact between inside and outside flat portion gasket with flange, so when gasket tightening the convex 1 and 4 tend to move to inner and outer radius of gasket, so the deformation concentration focus on convex 2 and 3, therefore contact width on convex 2 and 3 higher than convex 1 and 4. On the other hand, average contact width convex 1 and 4 higher than convex 2 and 3. For gasket three-layer 0-MPa, Es/Eb = 0.1, on 100 KN axial force, because the stiffness of gasket decrease, there is more plastic deformation, therefore there are many contact on flat portion as shown on Fig. 4.9. Because of many contact on flat portion, it held convex 1 and 4 to move out, therefore convex 1 and convex 4 can focus to deformation when tightening and it result contact width increase significantly.
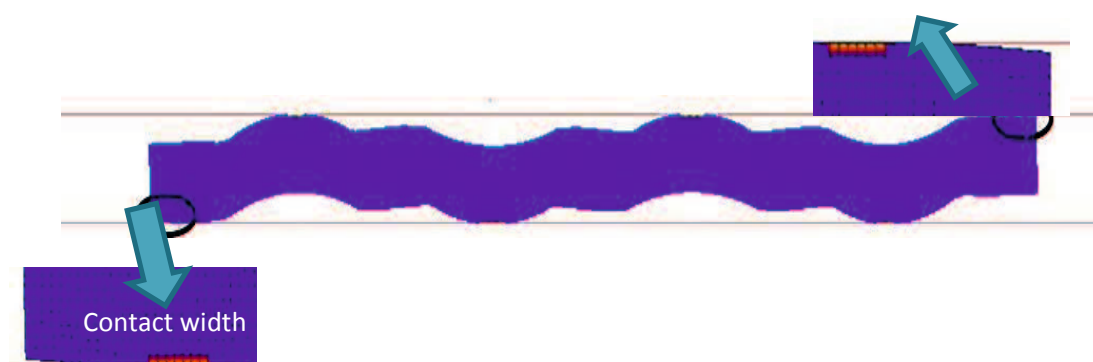

Contact width

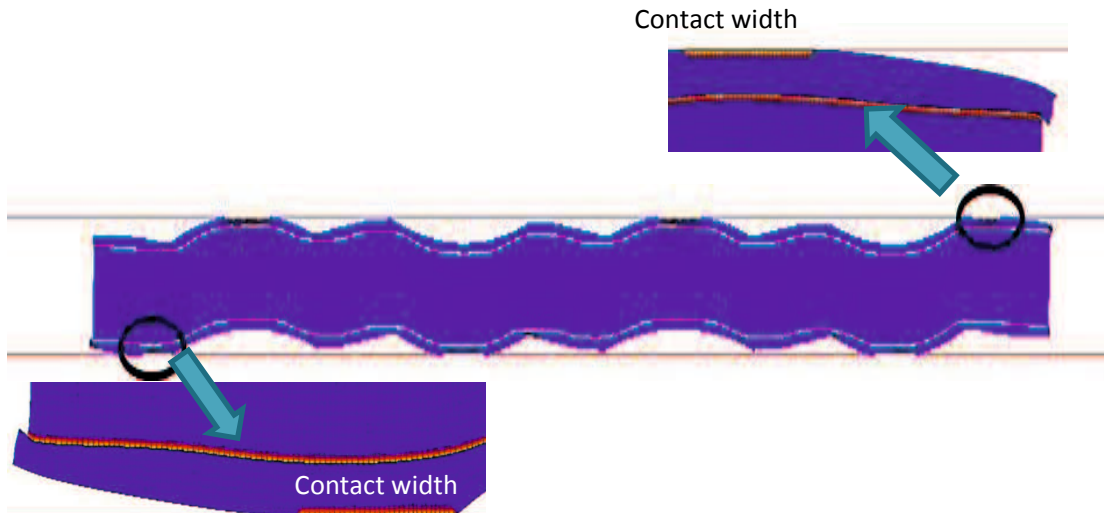Fig.4.8 The deformation shape for single layer SUS304, 0-MPa mode, 100 KN axial force

Fig.4.9 The deformation shape for three-layer metal gasket 0-MPa, Es/Eb = 0.1, 100 KN axial force

The contact width change due to the influence of modulus elasticity ratio is shown in Fig 4.10. If the values of Es/Eb decrease, the percentage contact width changes will increase. This is because the lower the modulus of elasticity of the surface layer, which means that the easier the surface layer to deform plastically when contact with the flange and the more contact on flat portion, therefore give higher contact width on each convex. Thereby giving more uniform deformation of the each convex.

Otherwise the average contact stress change due to the influence modulus of elasticity ratio is shown in Fig 4.11. The minus sign indicated average contact stress decrease. For Es/Eb value 0.9 there is small decrease of average contact stress although the contact width on the convex section is the same with single layer. This is because at that time there is a small contact on flat portion of gasket, so overall there has been an increase in the contact width, therefore the average contact stress decrease. If comparing Fig. 4.10 and Fig. 4.11, the percentage increase in contact width is higher than the percentage decrease in average contact stress.
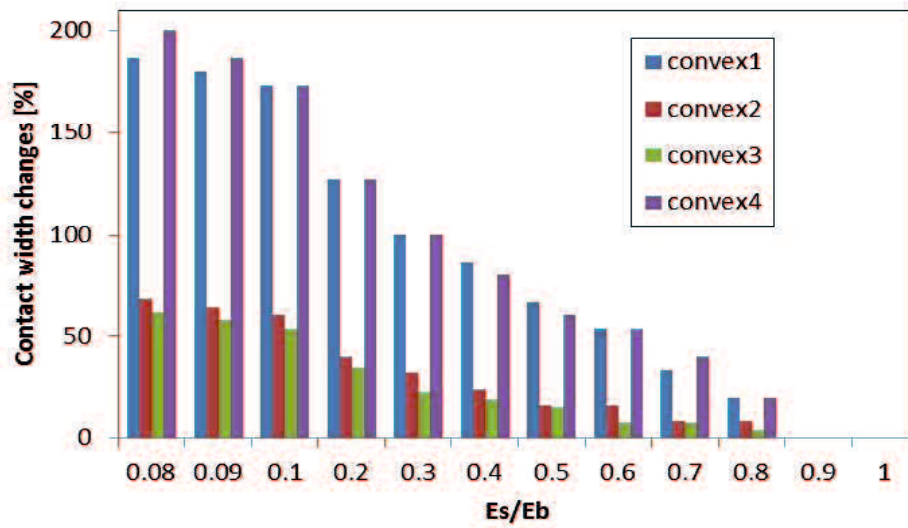
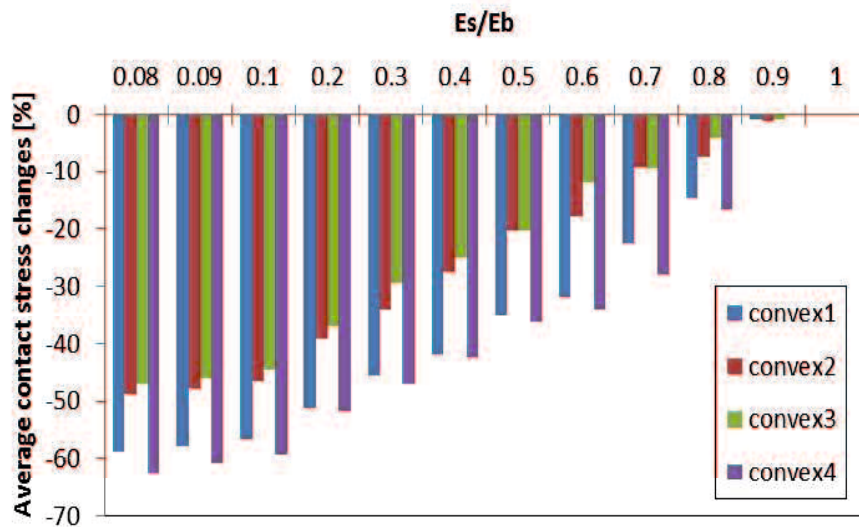Fig.4.10 Percentage contact width, gasket 0-MPa mode, axial force 100KN

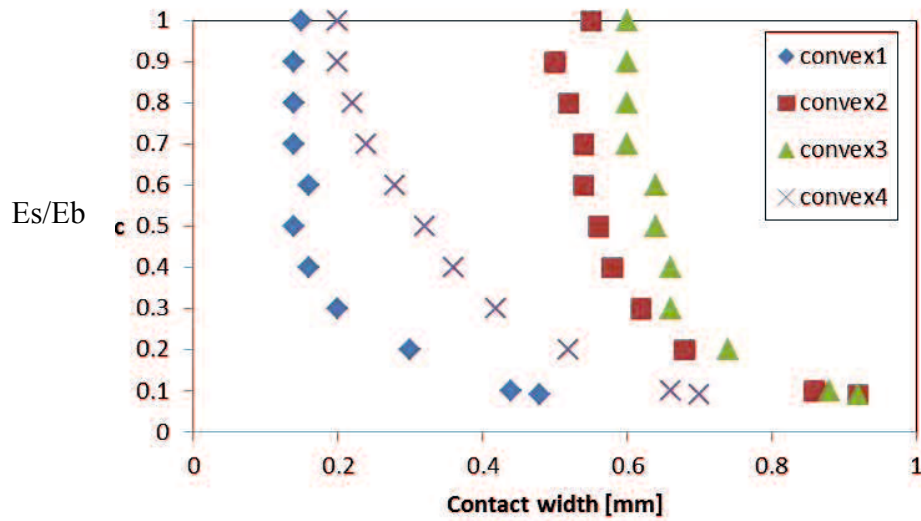Fig.4.11 Percentage average contact stress, gasket 0-MPa mode, axial force 100KN

Fig.4.12 The mapping contact width - modulus of elasticity ratio for three-layer corrugated metal gasket (400-MPa mode, Ts/Tg=0.1/1.5, 100KN)
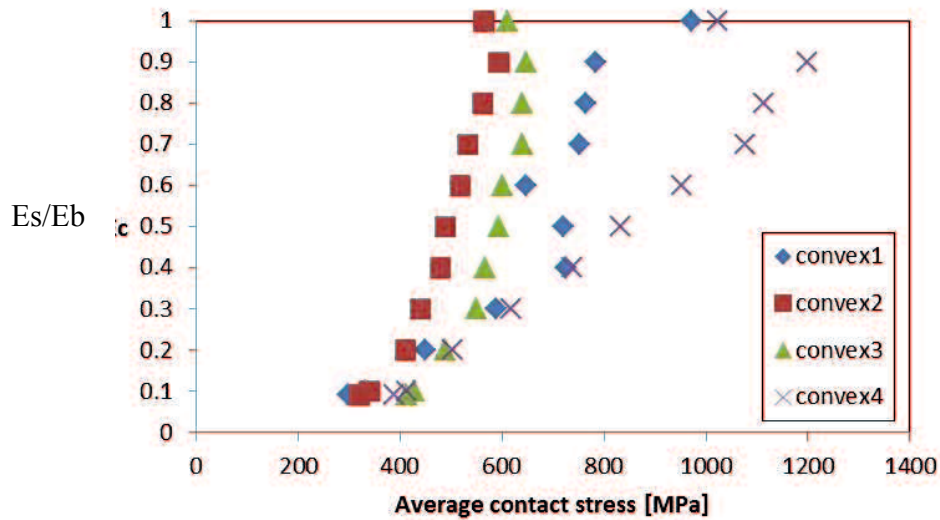

Fig.4.13 The mapping average contact stress - modulus of elasticity ratio for three-layer corrugated metal gasket (400-MPa mode, Ts/Tg=0.1/1.5, 100KN)

Fig.4.12 shows a distribution map of the contact width with modulus of elasticity ratio from 0.09 up to 1 for gasket 400-MPa mode, Ts = 0.1mm, on 100KN axial force. Value 1 indicated gasket single layer SUS304. From Fig.9 for Es/Eb value we got convex 2 and 3 have the higher contact width than convex 1 and 4. When Es/Eb value less than 1, it

seemed there is different behavior for each convex. Here shows for convex 2 and 3 there is no significant changes until Es/Eb 0.2. For convex 1 also shown there is no change until 0.4, under that value contact width increase significant. For convex 3, when Es/Eb decreases, contact width look increase.

Fig.4.13 shows a distribution map of the average contact stress with modulus of elasticity ratio from 0.09 up to 1 for gasket 400-MPa mode, Ts/Tg = 0.1/1.5, on 100KN axial force. The figure shows for modulus of elasticity ratio 1 down to 0.08 the average contact stress on convex 1 and 4 higher than convex 2 and 3. The lower modulus of elasticity ratio it seems the average contact stress decrease for each convex.

The inconsistency trend for this 400-MPa mode can explain by look the deformation shape when forming process on Fig. 4.14 and Fig. 4.15. The figures show the lack of die fills defect happen on all convex as a result of forming simulation. The defect is tending occurred on the radius shape of convex contact, on 400-MPa mode. The lack of die fills tending lower with decreasing modulus of elasticity ratio but there is a dent at the peak of convex. Because of that the result of contact width and average contact stress trend become not consistent.
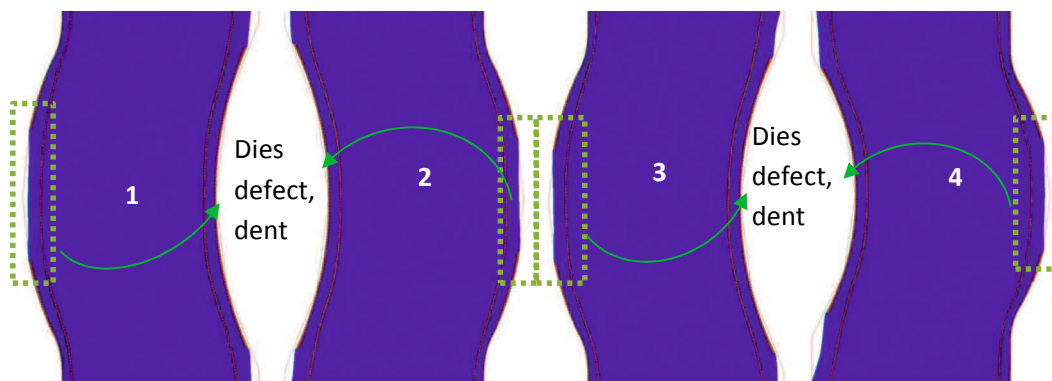

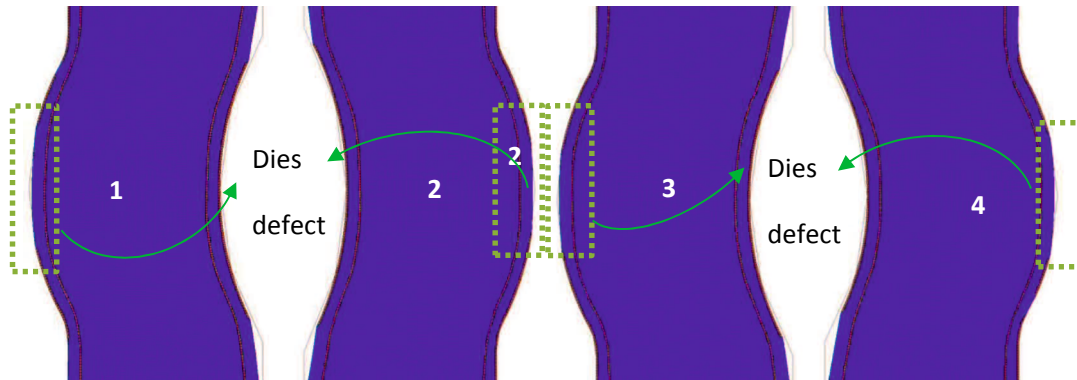Fig.4.14 The deformation shape for three-layer metal gasket 400-MPa, Es/Eb = 0.1, forming process

Fig.4.15 The deformation shape for three-layer metal gasket 400-MPa, Es/Eb = 0.5, forming process.
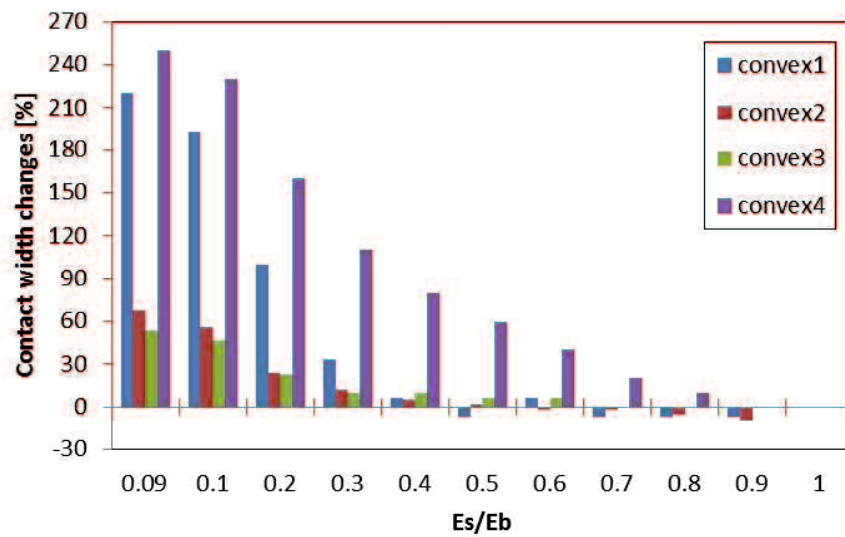

Fig.4.16 Percentage contact width increase, gasket 400-MPa mode, axial force 100KN
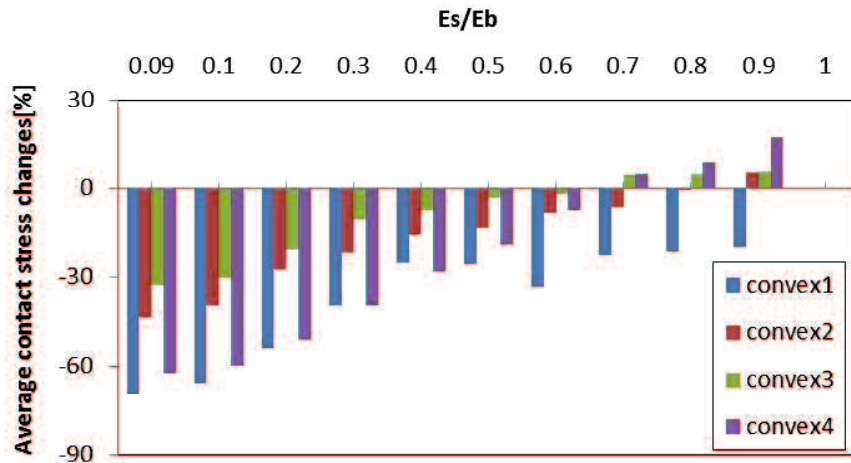
Fig.4.17 Percentage average contact stress, gasket 400-MPa mode, axial force 100KN

The contact width change due to the influence modulus of elasticity ratio is shown in Fig 4.16. If the values of Es/Eb decrease, the percentage contact width changes will increase. This is because the lower the modulus of elasticity of the surface layer, which means that the easier the surface layer to deform plastically when contact with the flange and the more contact on flat portion, therefore give higher contact width on each convex. Thereby giving more uniform deformation of the each convex.

Otherwise the average contact stress change due to the influence modulus of elasticity ratio is shown in Fig 4.17. The minus sign indicated average contact stress decrease. For Es/Eb value 0.9 there is small decrease of average contact stress although the contact width on the convex section is the same with single layer. This is because at that time there is a small contact on flat portion of gasket, so overall there has been an increase in the contact width, therefore the average contact stress decrease. If comparing Fig. 4.16 and Fig. 4.17, the percentage increase in contact width is higher than the percentage decrease in average contact stress.

4.2.2   Effect of thickness ratio on contact width and contact stress.

To describe the effect of surface layer's thickness on contact width and average contact stress we use modulus of elasticity ratio $E_s/E_b = 0.1$ as example.

Fig.4.18 shows the contact width versus surface layer's thickness for 0-MPa mode gasket, axial force 100KN. All model three- layer show higher contact width compared with single layer SUS304. In gasket SUS304 convex 2 and 3 have higher contact width than convex 1 and 4, but with increasing thickness show convex 4 increases significant. For T_s/T_g 0.1/1.2 until 0.3/1.2 shows with increasing thickness then contact width increases significant. For 0.4/1.2 there is no significant effect.

Fig.4.19 shows the average contact stress versus surface layer's thickness for 0-MPa mode gasket, axial force 100KN. This figure shows the increase in surface layer's thickness will cause a decrease in average contact stress. Because the sealing performance of gasket in correlation with contact width, therefore T_s/T_g value 0.1/1.2, 0.2/1.2 and 0.3/1.2 recommend. For T_s/T_g is 0.4/1.2 not recommended because contact width increase not significant but average contact stress decrease.

The percentage of the contact width changes due to the influence of thickness ratio is shown in Fig 4.20. If the thickness of surface layer increase, the percentage of contact width changes will increase. This is because increase surface layer thickness will decrease of gasket stiffness, which means that the easier the surface layer to deform plastically when contact with the flange and the more contact on flat portion, therefore give higher contact width on each convex. Thereby giving more uniform deformation of the each convex.

Otherwise the average contact stress change due to the thickness ratio effect is shown in Fig 4.21. The minus sign indicated average contact stress decrease. This is because at that time there is a small contact on flat portion of gasket as shown at table 4.3, so overall there has been an increase in the contact width, therefore the average contact stress decrease. If comparing Fig. 4.18 and Fig. 4.19, the percentage increase in contact width is higher than the percentage decrease in average contact stress.

Table 4.3 shows the contacts that occur in each flat part of the gasket on the axial force 100KN. Here indicated by the increase in the thickness of the surface causing more

139

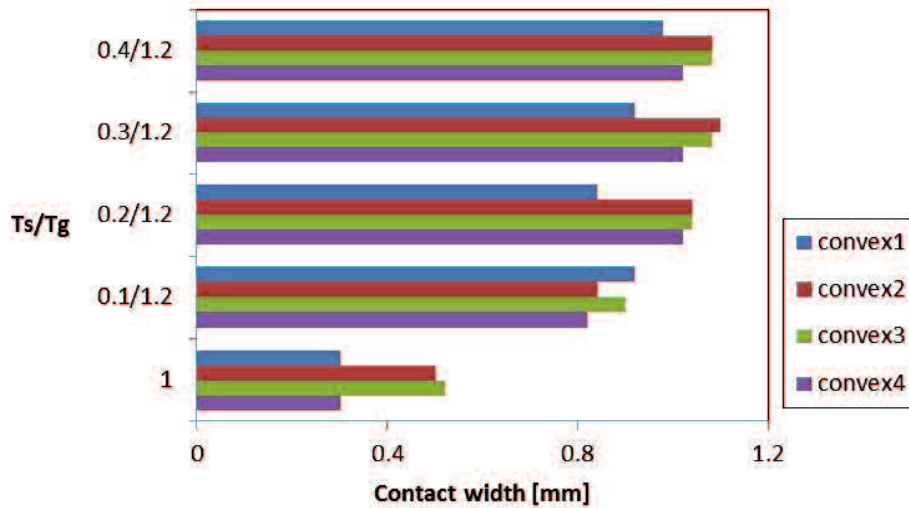flat parts in contact with the flanges. Therefore, the average contact stress on the convex section will decrease.

Fig.4.18 The contact width vs. Tb/Tg for three-layer corrugated metal gasket (0-MPa mode, Es/Eb = 0.1, 100KN)

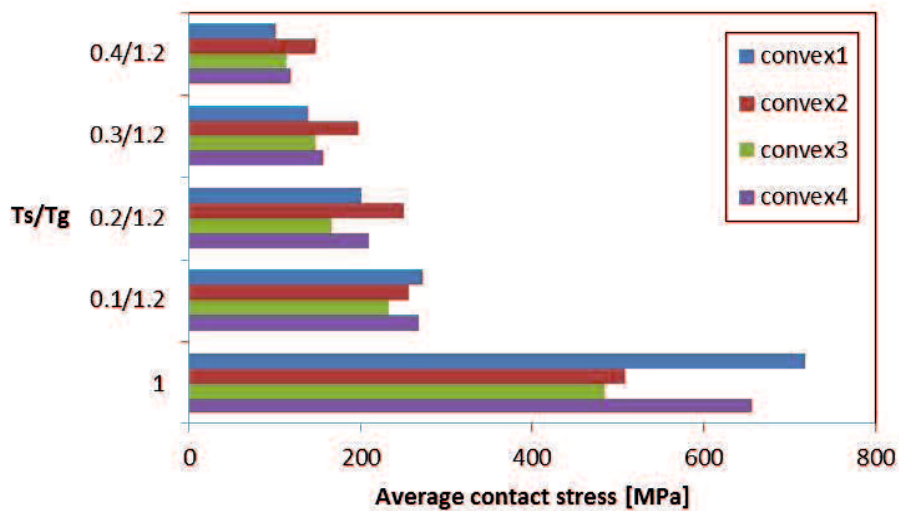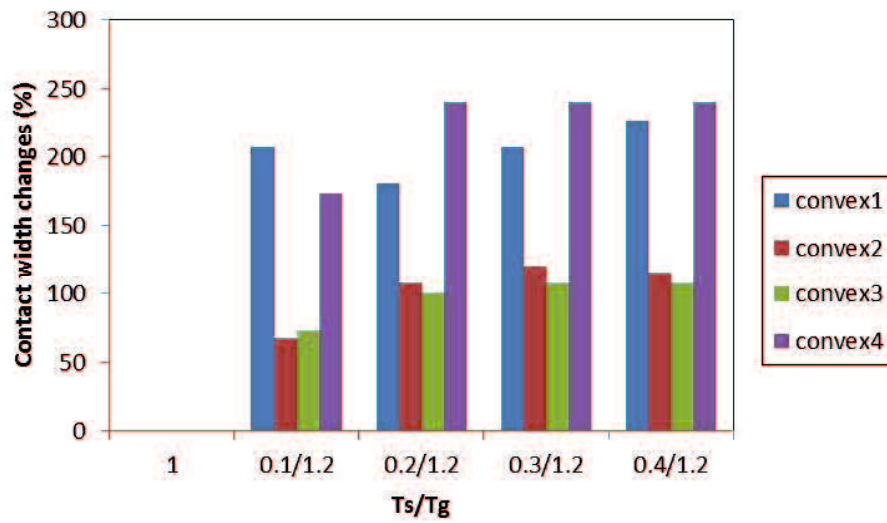Fig.4.19 The average contact stress vs. Tb/Tg for three-layer corrugated metal gasket (0-MPa mode, Es/Eb = 0.1, 100KN)

140

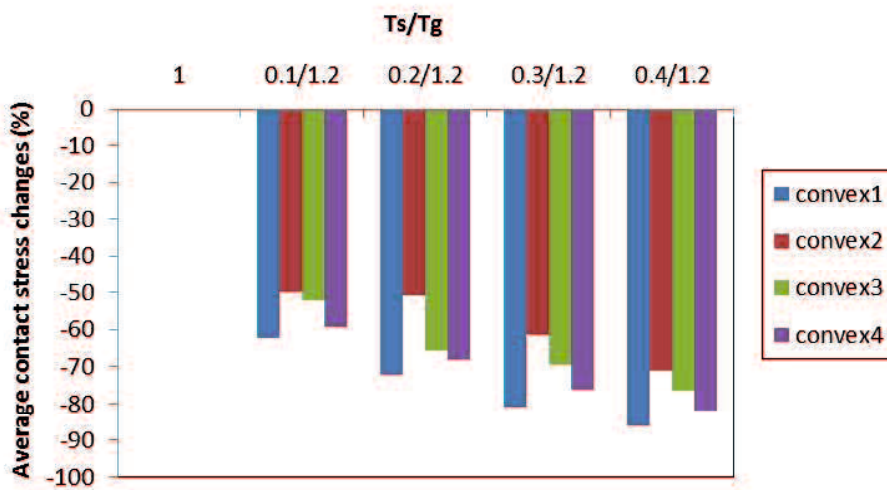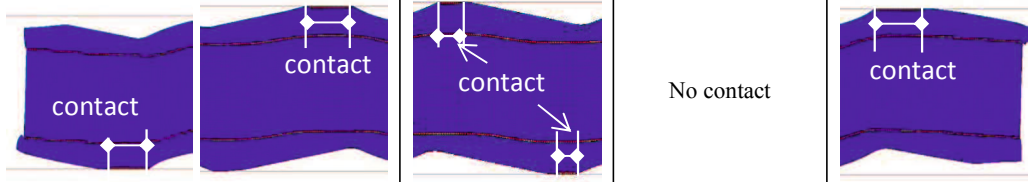Fig.4.20 Percentage contact width increase, gasket 0-MPa mode, axial force 100KN
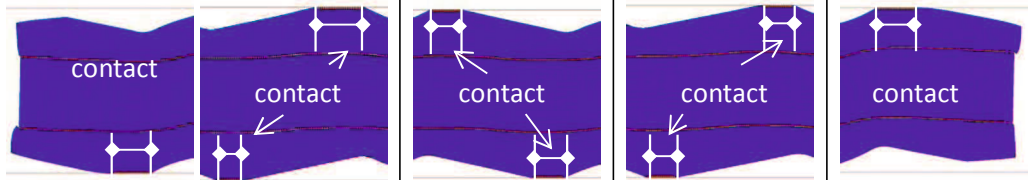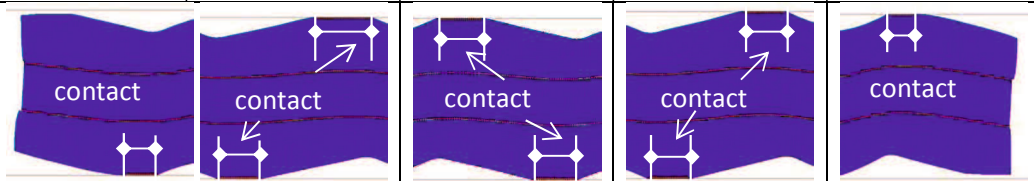

Fig.4.21 Percentage average contact stress, gasket 400-MPa mode, axial force 100KN

Table 4.3. Deformation contact gasket three-layer 0-MPa mode, 100KN

Ts/Tg	Inner	Flat 1-2	Flat 2-3	Flat 3-4	Outer
0.1/1.2	contact	No contact	No contact	No contact	contact
0.2/1.2	contact	contact	contact	No contact	contact
0.3/1.2	contact	contact	contact	contact	contact
0.4/1.2	contact	contact	contact	contact	contact

Note:
Inner means the flat part at the inside radius of gasket.
Outer means the flat part at the outside radius of gasket.
Flat 1-2 means the flat part between convex1 and convex2
Flat 2-3 means the flat part between convex2 and convex3
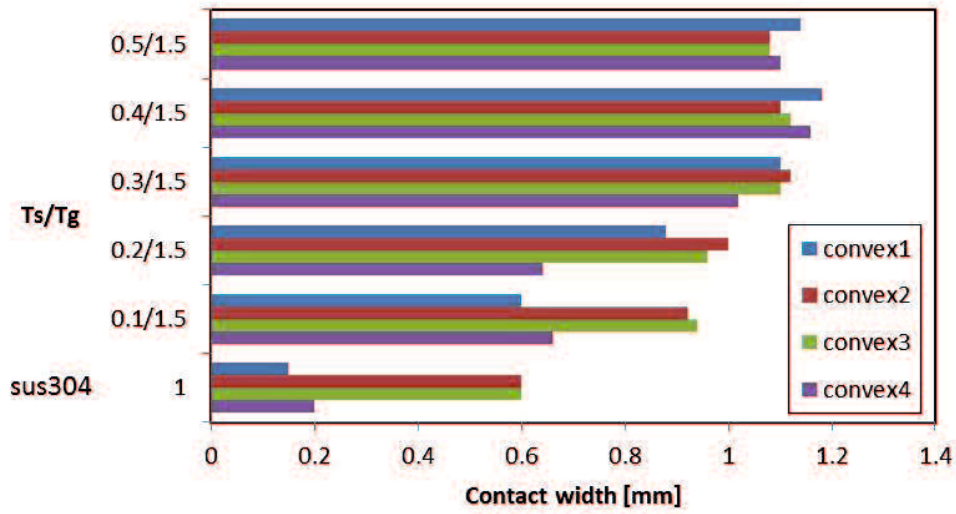Flat 3-4 means the flat part between convex3 and convex4

Fig.4.22 The contact width vs. Ts/Tg for three-layer corrugated metal gasket (400-MPa mode, Es/Eb = 0.1, 100KN)

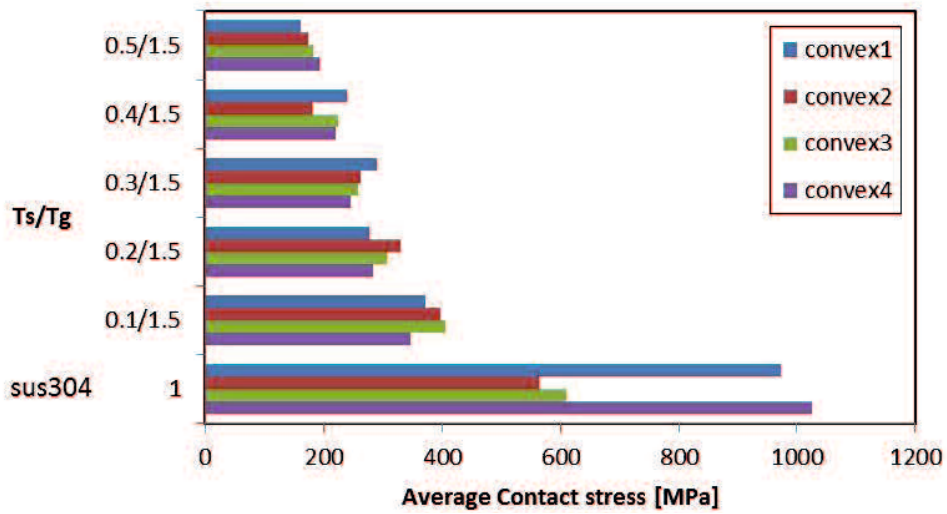Fig.4.23 The average contact stress vs. Ts/Tg for three-layer corrugated metal gasket (400-MPa mode, Es/Eb = 0.1, 100KN)
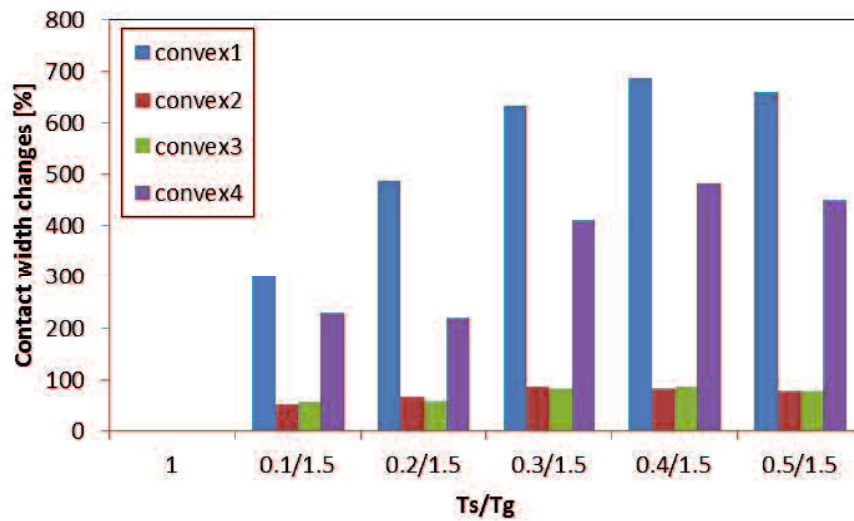
Fig.4.24 Percentage contact width increase, gasket 400-MPa mode, axial force 100KN
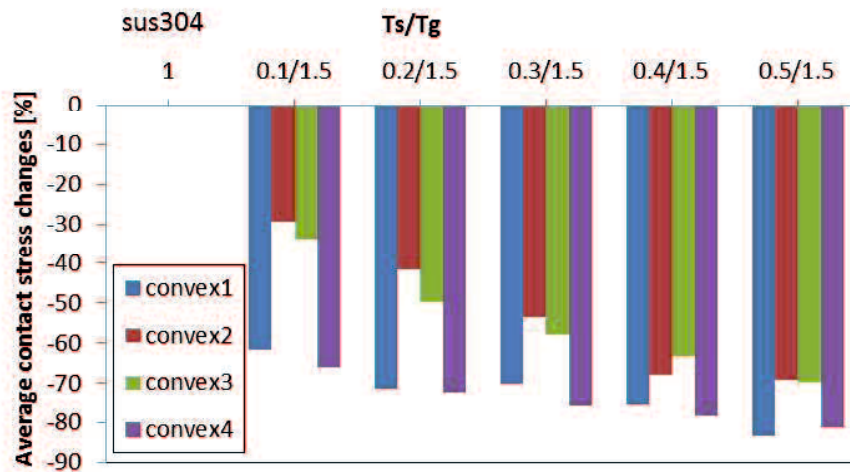

Fig.4.25 Percentage average contact stress, gasket 400-MPa mode, axial force 100KN

Fig.4.22 shows the contact width versus surface layer's thickness for 400-MPa mode gasket, axial force 100KN. All model three- layer show higher contact width compared with single layer SUS304. In gasket SUS304 convex 2 and 3 have higher contact width than convex 1 and 4. For Ts/Tg 0.1/1.5 until 0.3/1.5 shows with increasing thickness

then contact width increases significant. For 0.4/1.5 and 0.5/1.5 there is no significant effect on contact width..

Fig.4.23 shows the average contact stress versus surface layer's thickness for 400-MPa mode gasket, axial force 100KN. This figure shows the increase in surface layer's thickness will cause a decrease in average contact stress. Because the sealing performance of gasket in correlation with contact width, therefore Ts/Tg value 0.1/1.5, 0.2/1.5 and 0.3/1.5 recommended. For Ts/Tg 0.4/1.5 and 0.5/1.5 not recommended because contact width increase not significant but average contact stress decrease

Fig.4.24 shows the contact width change versus surface layer's thickness for gasket 400-MPa mode, axial force 100KN. All model three- layer show higher contact width compared with single layer SUS304. In gasket SUS304 convex 2 and 3 have higher contact width than convex 1 and 4, but with increasing thickness show the contact width difference for each convex is decrease.

Fig.4.25 shows the average contact stress versus surface layer's thickness for 400-MPa mode gasket, axial force 100KN. This figure shows the increase in surface layer's thickness will cause a decrease in average contact stress. If comparing Fig. 4.24 and Fig. 4.25, the percentage increase in contact width is higher than the percentage decrease in average contact stress.

Table 4.4 shows the forming process simulation for gasket three-layer 400-MPa mode. Here indicated there is the lack of die fills defect on forming simulation. The defect decrease by the increase in the thickness of the surface layer. Therefore, the contact width and average contact stress on the each convex section result shows not consistency trend.

Table 4.4. The dies fill defect on forming simulation gasket three-layer 400-MPa mode.

Ts/Tg	
0.1/1.5	
0.2/1.5	
0.3/1.5	
0.4/1.5	

0.5/1.5	
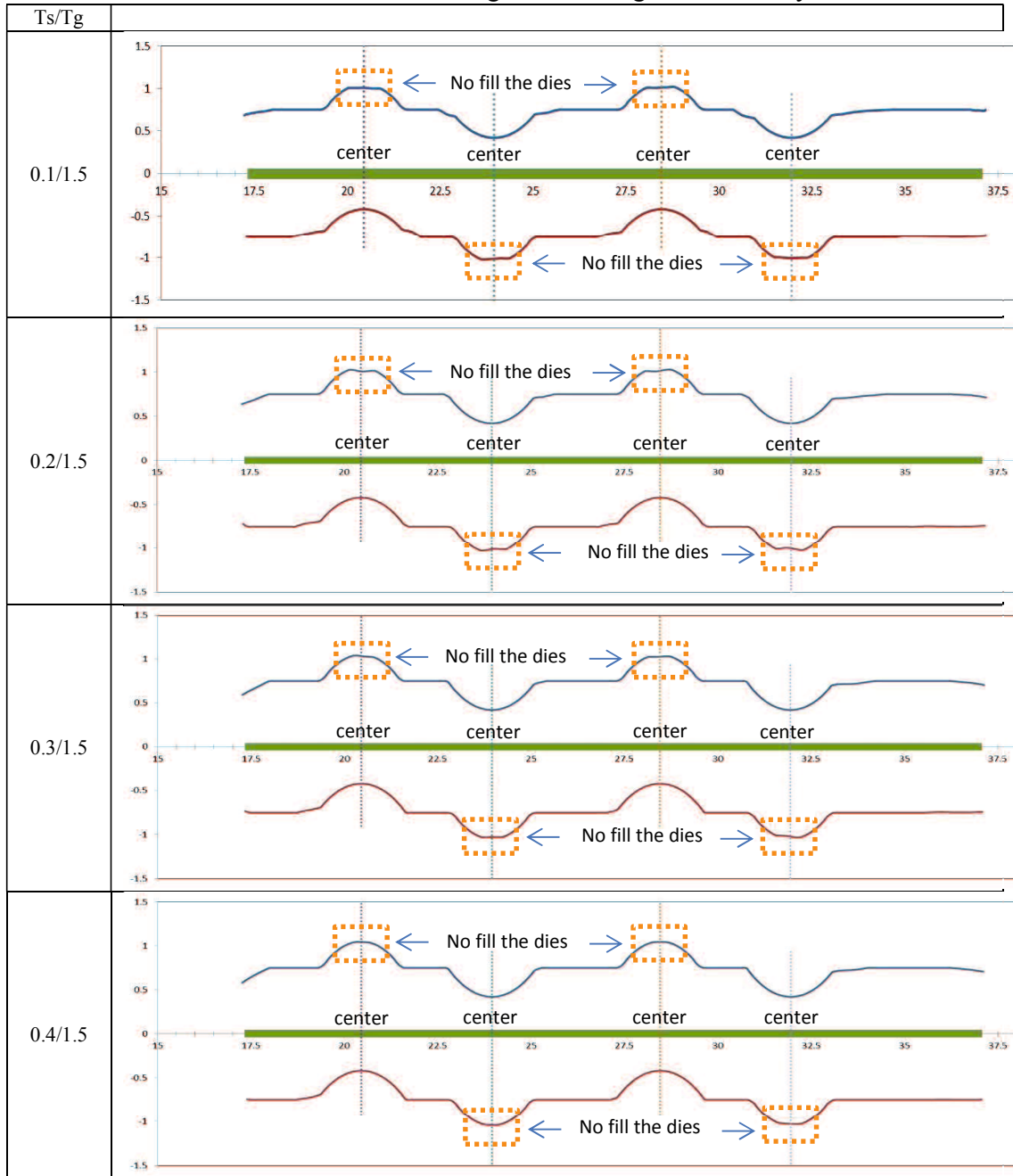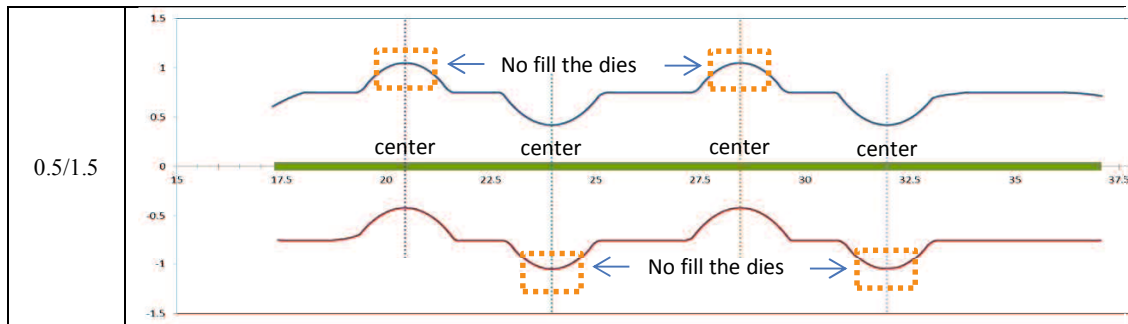
4.3 Conclusion

This paper investigated the surface layer material and thickness of surface layer affecting the contact width and contact stress of the three-layer corrugated metal gasket. The surface layer material needs to be carefully selected to get proper sealing of the flange gasket assembly. Based on FEM analysis thye following results were obtained.

1. The modulus of elasticity ratio decreased generates increased contact width, but instead contact stress decreases. This result shows the same trend for gasket 0-MPa mode and 400-MPa mode.

2. The thickness ratio give different contact width and average contact stress result. If the modulus of elasticity ratio is held constant, decrease thickness ratio produces increase contact width, but the average contact stress has decreases.

3. The inconsistency trend for gasket three-layer 0-MPa because with decrease Es/Eb there is increase contact on flat portion. For 400-MPa the inconsistency trend because the lack of die fill defect on forming process.

4. Based on simulation, for 0-MPa it is recommended Ts/Tg 0.1/1.2, 0.2/1.2 and 0.4/1.2. For 400-MPa mode its recommended Ts/Tg 0.1/1.5, 0.2/1.5 and 0.3/1.5.

5. The finite element analysis predictions provide a helpful reference for design of three-layer corrugated metal gasket, but experimentation to verify them is recommended.

CHAPTER V
THE LEAKAGE PERFORMANCE OF THREE-LAYER CORRUGATED METAL GASKET

The gasket performance is measured from the leakage rate that occurs, however a leak rate of each connection is also influenced by the condition of the contact surfaces in the connection. Therefore, the surface roughness of flange will affect sealing performance.

This paper presents the leakage performance of three layer corrugated metal gasket under different thickness of surface layer and flanges surface roughness. The leakage performance was examined experimentally at room temperature using helium leakage quantity test. The gasket used oxygen free copper (C1020) as surface layer and SUS304 as base material and arranged as three-layer without the use of bonds. Next we call no-fix model. The relation between contact stress, contact width and amount of leakage were analyzed using FEM analysis. Using the obtained result from FEM and experiment, the characteristic of bolted flange connection with three-layer corrugated metal gasket was clarified. The estimated results were fairly good agreement with experiment result.

5.1 Gasket Manufacture

The gasket was manufactured using a mold press. The shape of gasket is realized by using a punch to force the initial material to slide into a die. The gasket used oxygen free copper (C1020) as surface layer and SUS304 as base material and arranged as three-layer without the use of bonds. The dimension of dies based on optimum design single material SUS304 0-MPa mode and 400-MPa mode. The dies used to forming material gasket as shown in Fig.5.1. A UH-1000 KNI universal testing machine was used to perform the forming process. Fig. 5.2 shows the press forming process for manufacturing a gasket. The load for pressing process is shown in Fig. 5.3. The material gasket before forming process and gasket after forming process are shown in Fig. 5.4.

Fig.5.1 The upper and lower dies
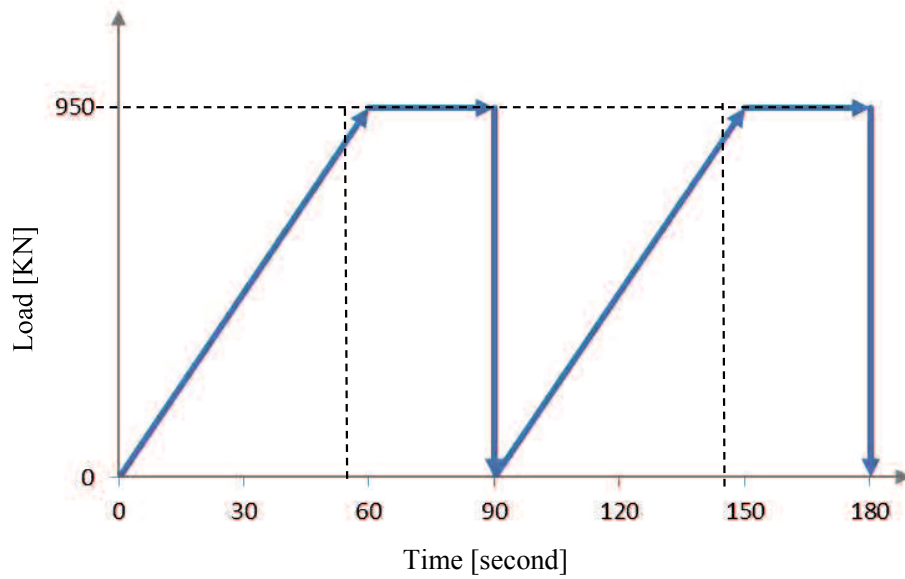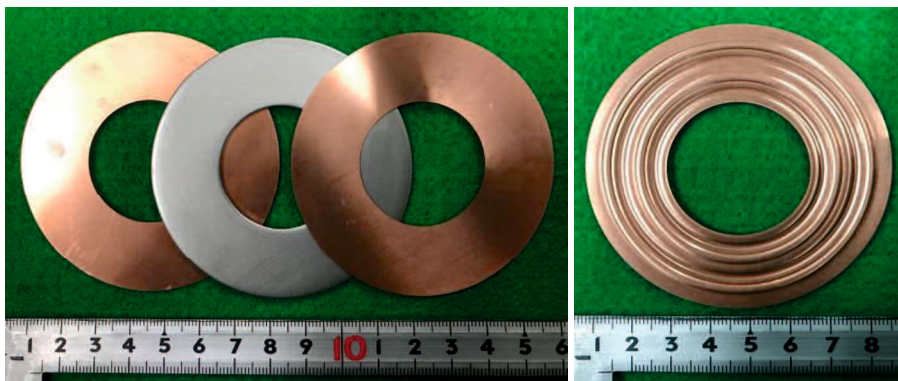

Fig. 5.2 Cold forming process

Fig. 5.3 Load for cold forming

(a)   Material gasket   (b) three-layer gasket

Fig. 5.4 Photographs of 25-A size three-layer metal gasket

5.2 Flange Surface Roughness Measurement

There are no objects that have a perfectly smooth surface; there must be a surface roughness. The actual extent of this roughness varies, depending on the machining processes. This fact causes the contact between two engineering surfaces to be located at only a limited number of asperities although the surfaces apparently have a high degree of surface conformity. A variation in the normal load applied through the contact modifies the deformation of the contact asperities and thus changes the number of asperities in contact.

The surface roughness also affects the sealing performance. The flange surface roughness measurement was based on the JISB0601-2001 standard [60]. Fig.5.5 shows the experimental setup of the surface roughness measurement. A Handysurf E-35B was used to measure the surface roughness. To avoid experimental error due to the surface roughness, the equipment was first calibrated. All function automatically set the ideal values for the measurement range, evaluation length, cut-off value, and recording magnification according to the measurement conditions. This setup allows the measurement conditions, parameter values, and profile curve data to be directly transmitted to a personal computer.
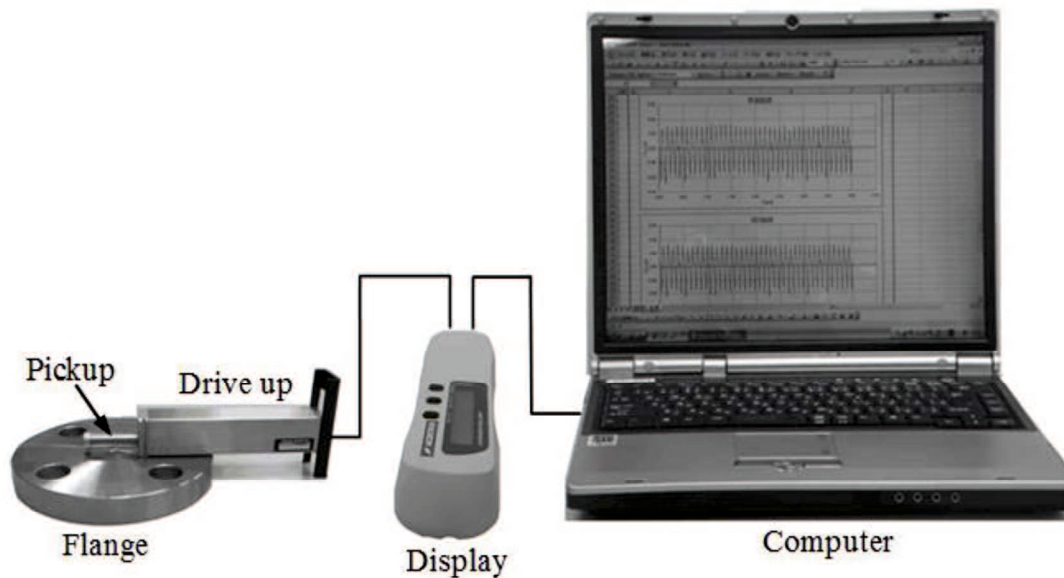

Fig. 5.5 Surface roughness measurement setup

The data processing was transformed to Microsoft Excel. The output result contains the average surface roughness Ra, maximum surface roughness Rz, and another parameter. Furthermore, the output result can be obtained in the form of a roughness curve. Fig. 5.6 shows an example of the surface roughness measurement result. Flanges with two different average surface roughness (Ra) values—2.5, and 3.5μm—were used. This data was used to draw the real flange surface roughness using Solid Work software.
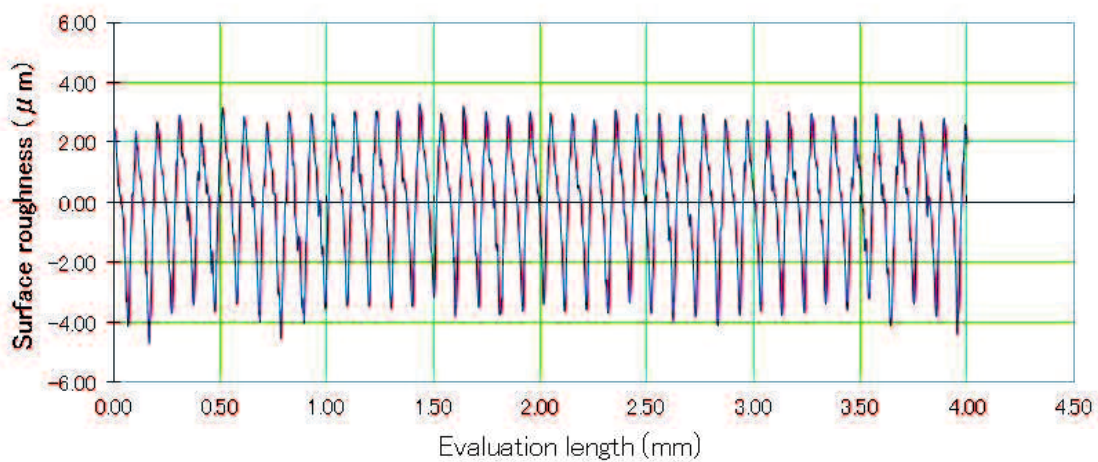

Fig. 5.6 Roughness curve

5.3 Simulation Analysis and Result

A simulation analysis was performed to describe the contact mechanism of the 25A-size metal gasket and the rough flange. By using this approach, the relationship between the surface roughness parameter and the contact stress, contact width were determined. The gasket used in this study was manufactured using a mold press. It had beads along its circumference. When the gasket was tightened to the flange, the beads on both surfaces of gasket created an elastic effect. The flange was assumed to have a rough surface on both sides. The gasket was in contact with both the lower and the upper sides of the flange. The flange pressed the gasket along an axial direction. SUS304 was used as the base gasket material because of its effectiveness in a high-temperature and high-pressure environment. C1020 was used as the surface material and the flange material was SS400. Detail material properties as shown in table 5.1.

Table 5.1 material properties data used in simulation analysis.

Materials	Nominal Stress (σ) [MPa]	Tangent Modulus [MPa]	Modulus of Elasticity (E) [GPa]	Poisson ratio (ν)
SUS304	398.83	1900.53	210	0.3
SS400	240	1000	206	0.3
C1020	195	1360	136	0.31

In this study, we analyze a flange having two different surface roughness values: 2.5, and 3.5μm. According to the explanation above, the surface roughness was modeled as a real rough surface. The real surface roughness of the flange was measured using a Handysurf E-35B. Through the surface roughness measurements, we obtained the average roughness (Ra), maximum surface roughness Rz, the mean spacing of profile irregularities (RSM) and another parameter. Then, both Ra and RSM were used to model the surface roughness of the flange. The average roughness describes height asperities and RSM describes the wavelength of the surface roughness.
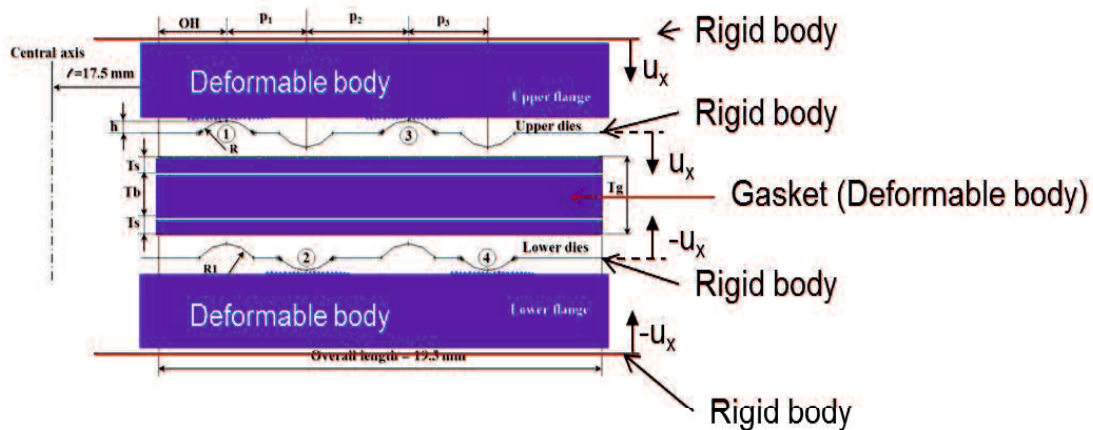

Fig. 5.7 Analysis model

The elastoplastic behavior of gasket is calculated by using software of FEM, MSC. Marc. Fig. 5.7 shows the loading condition. In our calculation, 2 dimensional axisymmetric

solid elements isoparametric quadrilateral type 10 are used to implement compression displacement in the axial direction on the gasket in between the upper and the lower of dies and flange with a constant increasing step of displacement Δux.

In our study, the material is assumed to obey isotropic strain hardening, and described by J2-deformation theory of Mises' yield criterion for bilinear stress-strain behavior. The material behavior is initially elastic characterized by a Young's modulus E until yielding commences at the uniaxial yield stress σ_Y. Thereafter the material response is elastic-plastic with the local tangent to the curve continually varying and is termed the elastic-plastic tangent modulus E_T (Fig. 5.8). During our nonlinear analysis with iterative procedure, Newton-Raphson method is used to solve for the equilibrium equations which are composed of finite strain plasticity with multiplicative decomposition of deformation gradient.
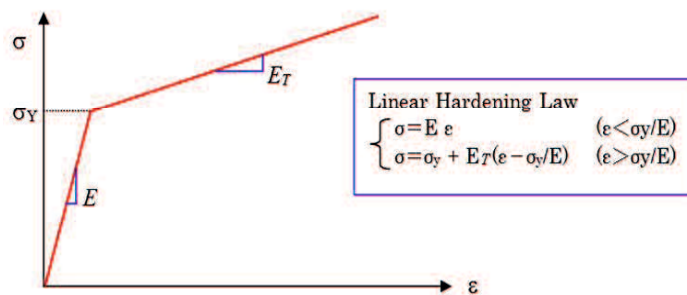

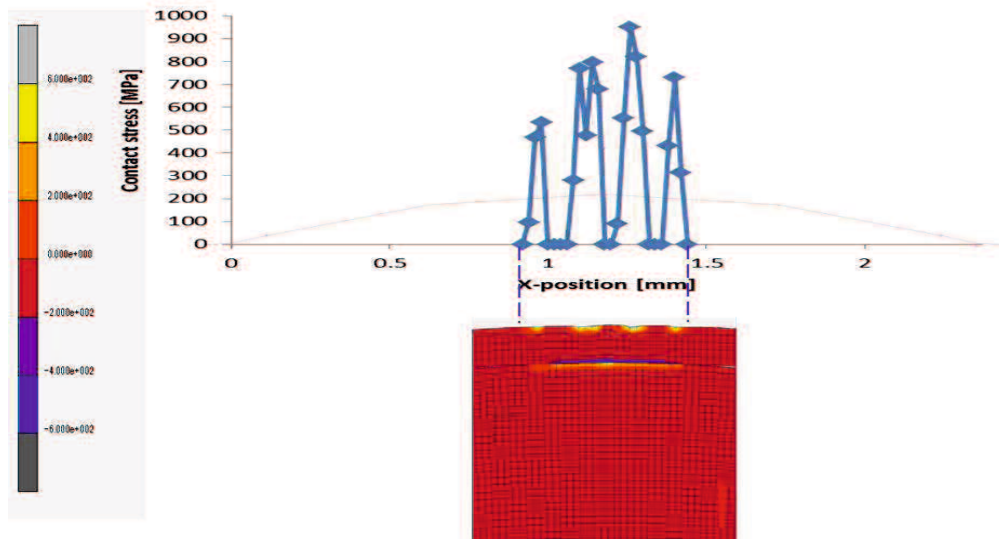Fig. 5.8 Linear strain hardening model

Fig. 5.9 Contact width

The contact width can be modeled using contact stress value in horizontal position. The contact stress value 0MPa is no contact condition, the contact stress value between 0-195MPa is elastic contact condition and, the contact stress value up to 195MPa is plastic contact stress. The real contact width is number of nodes which plastic contact stress times element width.

A virtual gasket model with various designs was generated through four basic steps. Tightening analysis was conducted to obtain the contact stress, and contact width. First, 2-D parameter models of the flange and the gasket were built using Solidwork software. To connect the drawing data obtained from Solidwork (IGES file) and the automatic meshing performed using Hypermesh, a batch command file was developed, using which a NAS file was generated. We used a quadrilateral mesh for the gasket and flange material because it has a rectangular section. The procedure file was configured to perform the pre-processing and run the model on MARC. A graphic user interface (GUI) does not appear; instead, the program runs commands in the background. After the FEM analysis is completed, an output file including the analysis results can be generated in TXT file that can be converted to a Microsoft Excel file. The output result contains the contact status, contact width, and contact stress force at each time at every peak position. The calculation of the contact width

versus the axial force at peak position 1 — 4 are performed using a multi-step MACRO command.

Fig. 5.10 shows three-layer sheet metal with Ts is thickness of surface layer, Tb is thickness of base metal and Tg is total thickness gasket. Fig. 5.11 shows the setting for gasket material, flange, and curve. The gasket shape produced by mold press was compressed along the axial direction to tighten the gasket and the flanges, see Fig. 5.12. The base metal (SUS304) and surface layer (C1020) contact is no fix (without bonding). Both the gasket and the flange were assumed as deformable bodies on both sides.

In this simulation, two types of gaskets—0-MPa mode and 400-MPa mode design [20] used. Thickness ratio varies [Ts/Tg] 0.1/1.2; 0.2/1.2; 0.4/1.2 for 0-MPa mode 0.1/1.5; 0.2/1.5; 0.4/1.5; 0.5/1.5 for 400-MPa mode—and two flange surface roughness levels— 2.5, and 3.5μm—were investigated.
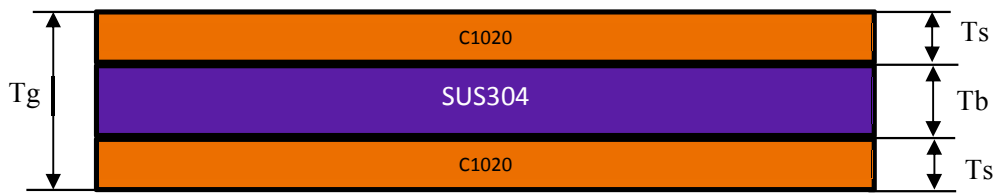
Total thickness three-layer gasket (Tg) = 2Ts + Tb

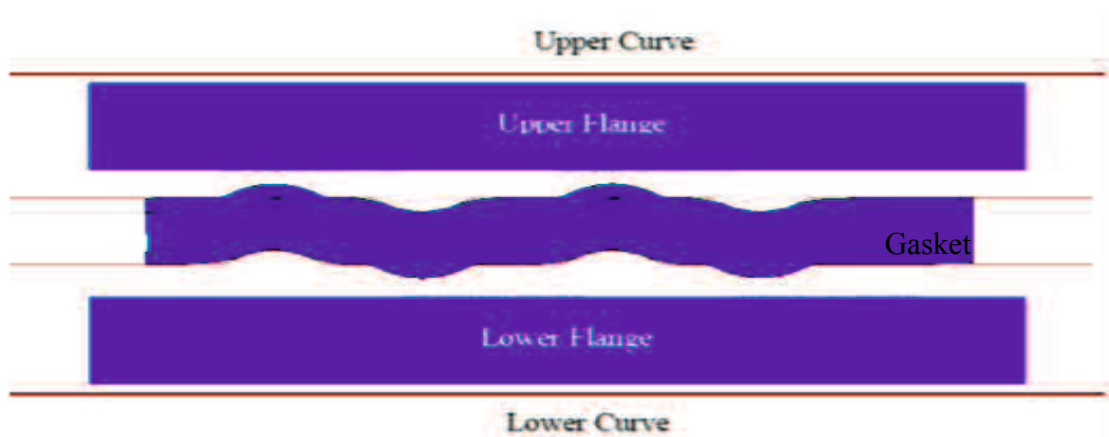Fig. 5.10 Three-layer sheet metal
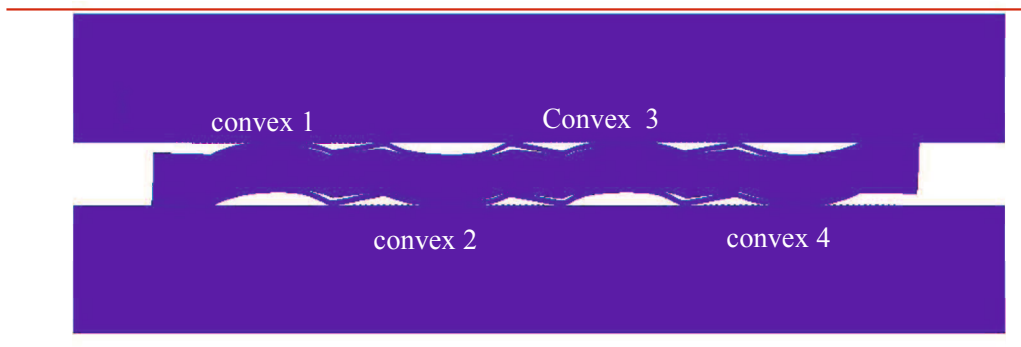

Fig. 5.11 Forming simulation

Fig. 5.12 tightening simulation

The Fig. 5.13 shows the contact width and average contact stress of three-layer metal gasket for convex 1, 2, 3, and 4 in any axial force. The figure shows that average contact stress and contact width for convex 2 and 3 were higher than those convex 1 and 4. Therefore, we focused our analysis on convex 2 and 3, which respectively called as the lower and upper contacts.
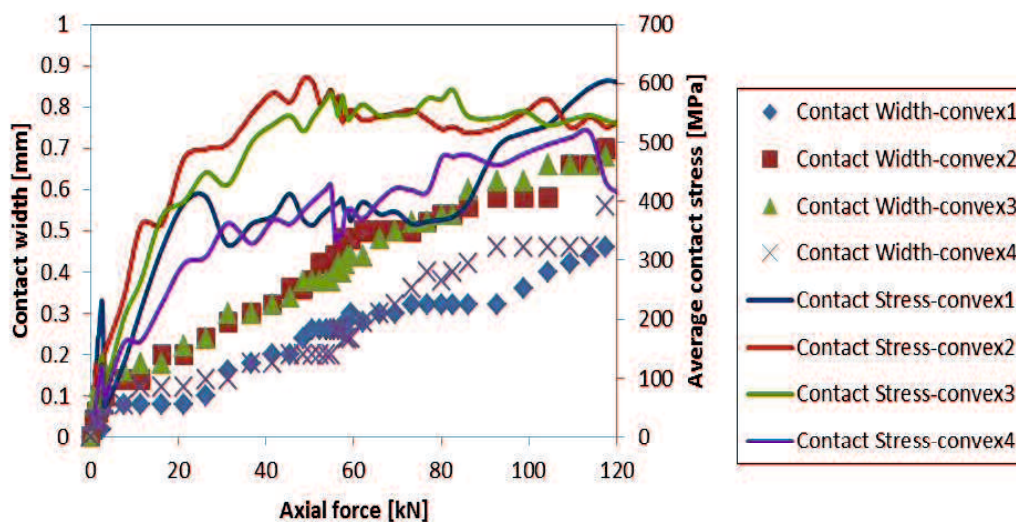

Fig.5.13 Contact width - Average contact stress in any axial force

Fig. 5.14 shows the simulation result for the upper and lower contact of a gasket in the 400-MPa mode in contact with flanges having surface roughness values of 3.5µm for average contact stress. The contact stress for a gasket for various thickness ratios was similar for both the upper and the lower contacts. But, a gasket with thickness ratio 0.1/1.5 showed the highest propensity than the others. The figure shows that average contact stress increases significantly with the axial force.

Fig. 5.15 shows the simulation result for contacts width of a gasket in the 400-MPa mode for contact width. This figure shows that the contact width increases with the axial force. The contact width in a gasket with thickness ratio 0.1/1.5 and 0.4/1.5 had the highest and the lowest slope, respectively.

As seen from the figure, the contact width increased due to an increase in axial force. For the value of axial force 0kN to 50kN, it can be shown that the contact width increased significantly. In this range, the contact stress of surface convex is large plastic contact stress condition. The value of the contact stress of flat portion between convex is elastic distribution and the phenomena still fulfill the elastic stress condition produce the spring back effect of metal gasket. However, the value of axial force from 50kN to 120kN, the contact width still increases. In this range, the distribution of stress of flat portion between convex is mixing the elastic and plastic region. The plastic contact stress distribution in the region between convex contact reduce the spring back effect, therefore reduce the value of contact stress, then the graph of the contact stress tend to go down. With increase axial force the plastic area higher and the contact stress tend to constant.
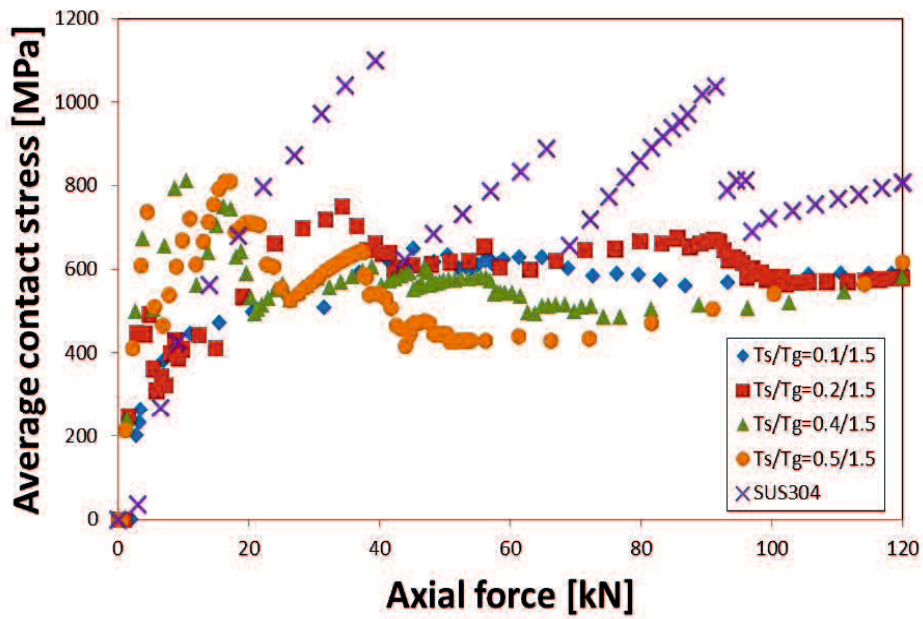
Fig.5.14 Average contact stress for gasket in 400-MPa mode [3.5μm]

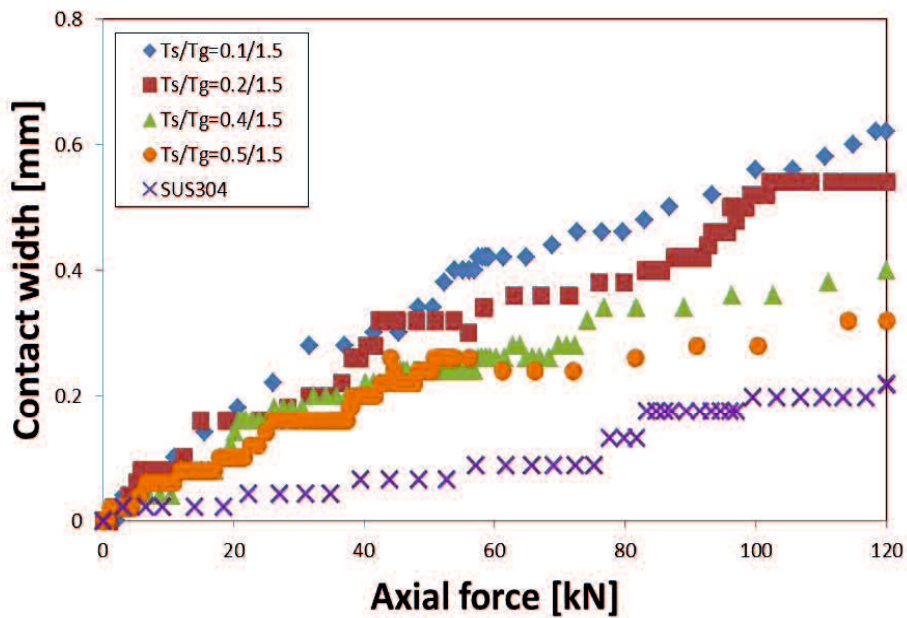Fig.5.15 Contact width for gasket in 400-MPa mode [3.5μm]

159
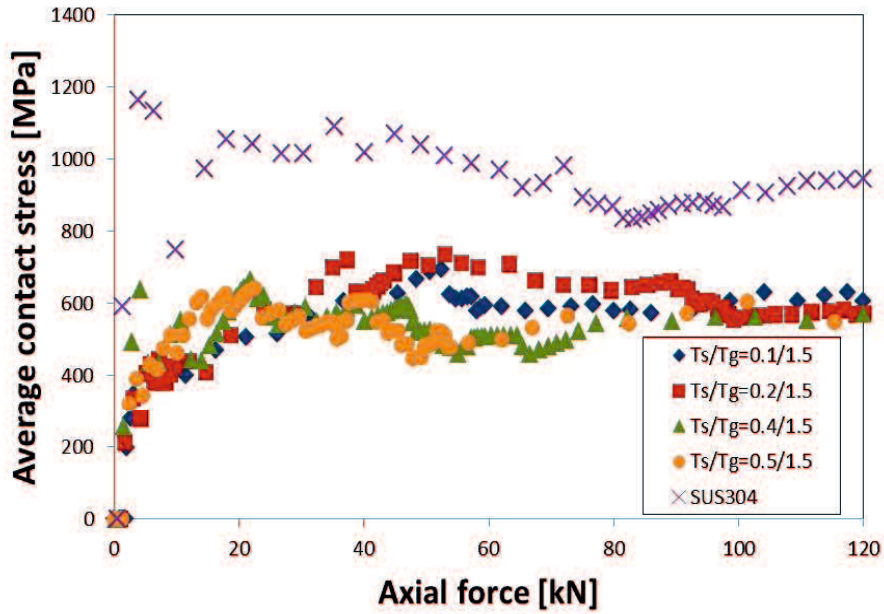
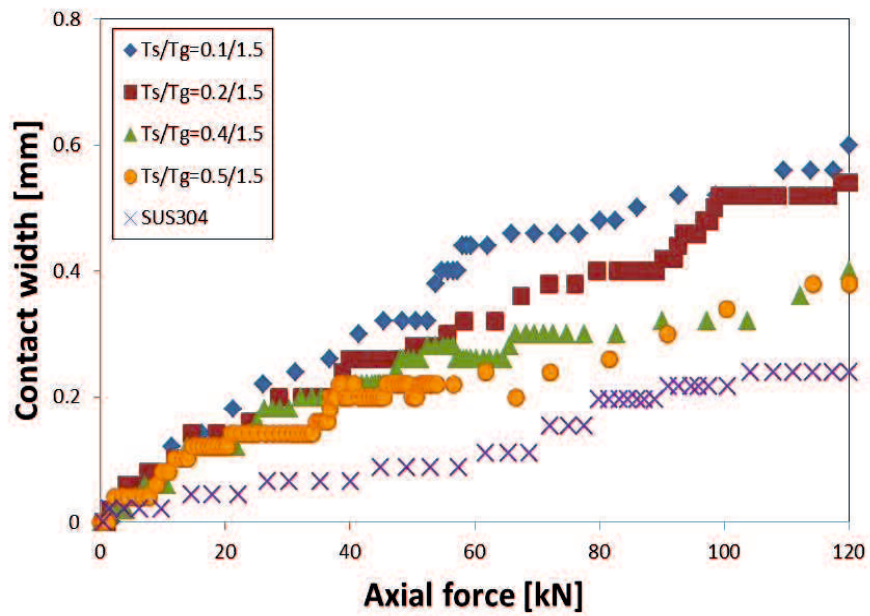Fig.5.16 average contact sress for gasket in 400-MPa mode [2.5μm]

Fig.5.17 Contact width for gasket in 400-MPa mode [2.5μm]

Fig. 5.16 shows the simulation result for the average contact stress of a gasket in the 400-MPa mode in contact with flanges having surface roughness values of 2.5µm. The contact stress for a gasket for various thickness ratios was similar for both the upper and the lower contacts. But, a gasket with thickness ratio 0.1/1.5 showed the highest propensity than the others. The figure shows that average contact stress increases significantly with the axial force.

Fig. 5.17 shows the simulation result for contacts width of a gasket in the 400-MPa mode for contact width. This figure shows that the contact width increases with the axial force. The contact width in a gasket with thickness ratio 0.1/1.5 and 0.4/1.5 had the highest and the lowest slope, respectively.

Fig. 5.18 shows the simulation result for the upper and lower contact of a gasket in the 0-MPa mode in contact with flanges having surface roughness values of 3.5µm for average contact stress. The contact stress for a gasket for various thickness ratios was similar for both the upper and the lower contacts. But, a gasket with thickness ratio 0.4/1.2 showed the highest propensity than the others. The figure shows that average contact stress increases significantly with the axial force.
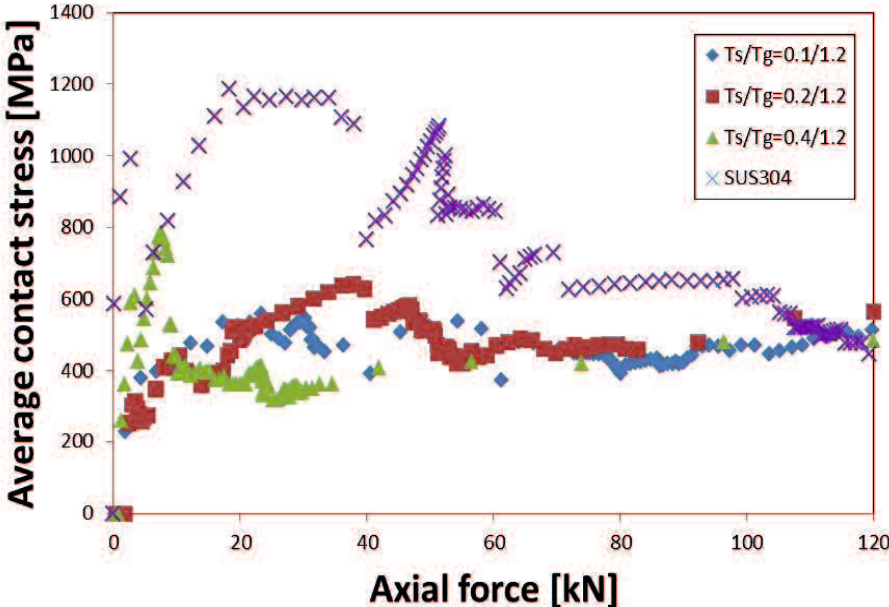

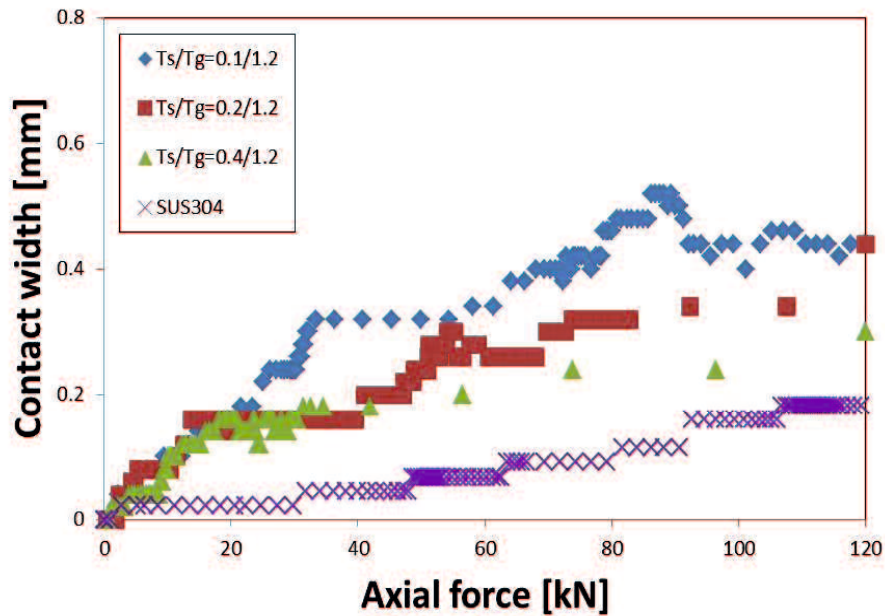Fig.5.18 average contact sress for gasket in 0-MPa mode [3.5µm]

Fig.5.19 Contact width for gasket in 0-MPa mode [3.5μm]

Fig. 5.19 shows the simulation result for upper and lower contacts width of a gasket in the 0-MPa mode for contact width. This figure shows that the contact width increases with the axial force. The contact width in a gasket with thickness ratio 0.1/1.2 and 0.4/1.2 had the highest and the lowest slope, respectively.

Fig. 5.20 shows the simulation result for the upper and lower contact of a gasket in the 0-MPa mode in contact with flanges having surface roughness values of 2.5μm for average contact stress. The contact stress for a gasket for various thickness ratios was similar for both the upper and the lower contacts. But, a gasket with thickness ratio 0.4/1.2 showed the highest propensity than the others. The figure shows that average contact stress increases significantly with the axial force.

Fig. 5.21 shows the simulation result for upper and lower contacts width of a gasket in the 0-MPa mode for contact width. This figure shows that the contact width increases with the axial force. The contact width in a gasket with thickness ratio 0.1/1.2 and 0.4/1.2 had the highest and the lowest slope, respectively.
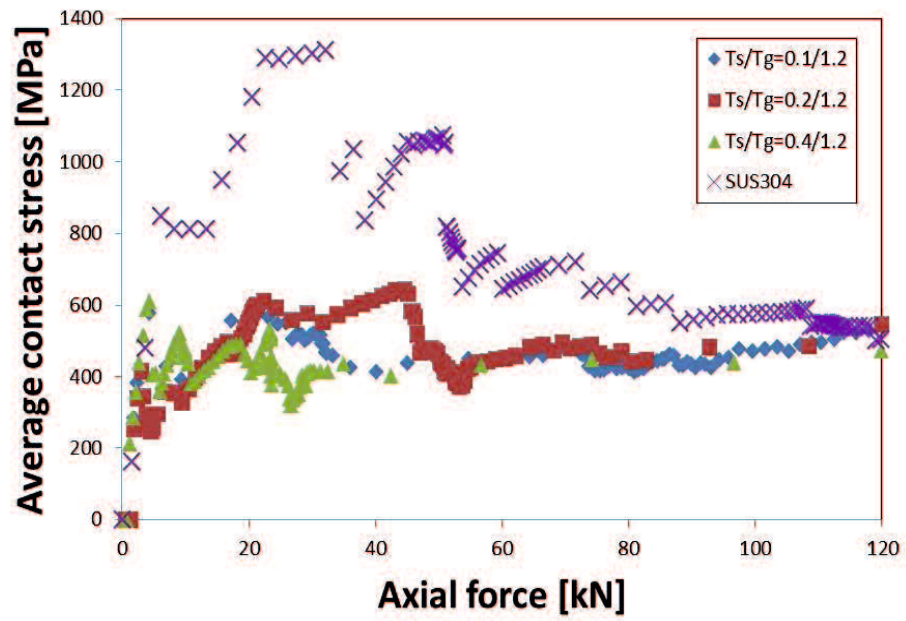
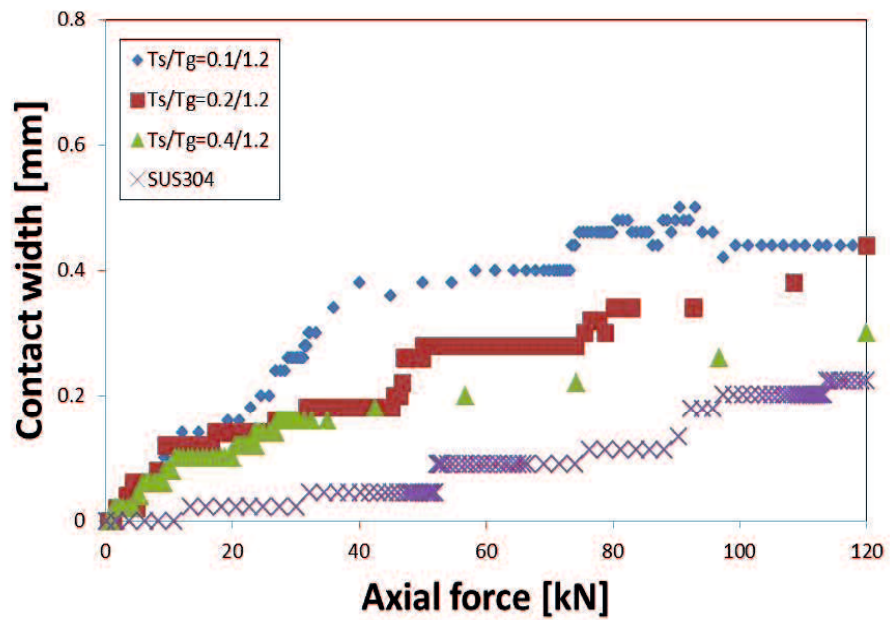Fig.5.20 average contact sress for gasket in 0-MPa mode [2.5µm]

Fig.5.21 Contact width for gasket in 0-MPa mode [2.5µm]

163

5.4 Leak Quantity Measurement

Fig. 5.21(a) and (b) shows a general-purpose flange based on JIS B2220 [57] with 10 K pressure and 25A diameter used in this test. The upper flange and the joint were welded carefully to avoid distortions. To avoid the experiment error due to the leakage from the joint of the flange and pipe, the leakage flow quantity of joint part was also calibrated. The axial force will produced by the bolt as shown in Fig.5.21.

(a)   Lower flange   (b) Upper flange

Fig. 5.22 General-purpose 25A flange

There are a wide variety of flange styles and configuration, as shown in Fig. 5.23, but only four types of facing are widely used, which are raised face, flat face, ring-joint facing and lap-joint flange. In this study, flat face flange is used due to same flange with Nurhadiyanto study. Flat faced flanges are used with a gasket whose outer diameter equals

that of flange. In this case, the gasket is relatively easy to install and remove. It becomes challenge for other research to explore another type of flange.
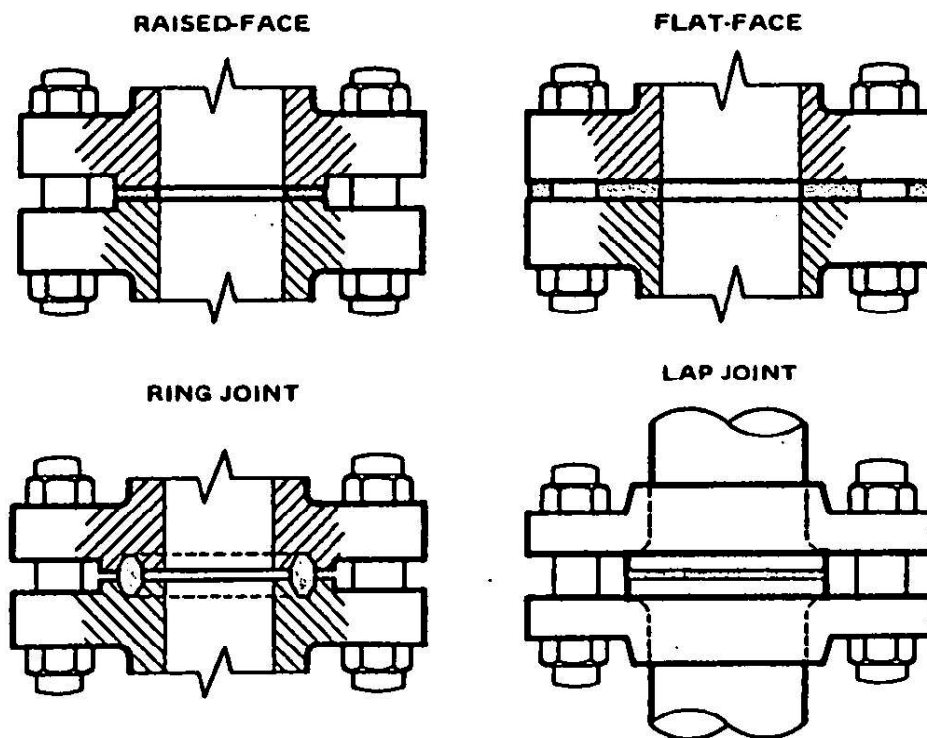

Fig. 5.23 Four type of flange face configurations for gasket joints

To evaluate the axial force and leakage quantity, the leakage quantity was measured based on the measurement of that of a helium flow. Fig. 5.24 shows a schematic diagram of the helium leakage measurement device that was developed for the leakage quantity evaluation test. The helium flow leakage quantity was quantitatively. The highest detection ability in the helium leakage measurement was chosen based on the JIS Z2330 [58] and JIS Z2331 standard [59]. The measurement method employed is called the vacuum method. First, gas from the test tube and the internal part of the chamber was evaluated using vacuum pumps. The helium gas was injected into the outer part of the gasket in the chamber and the

residual air was measured by using an oxygen density sensor. The helium density could be calculated in the outer part of the gasket.
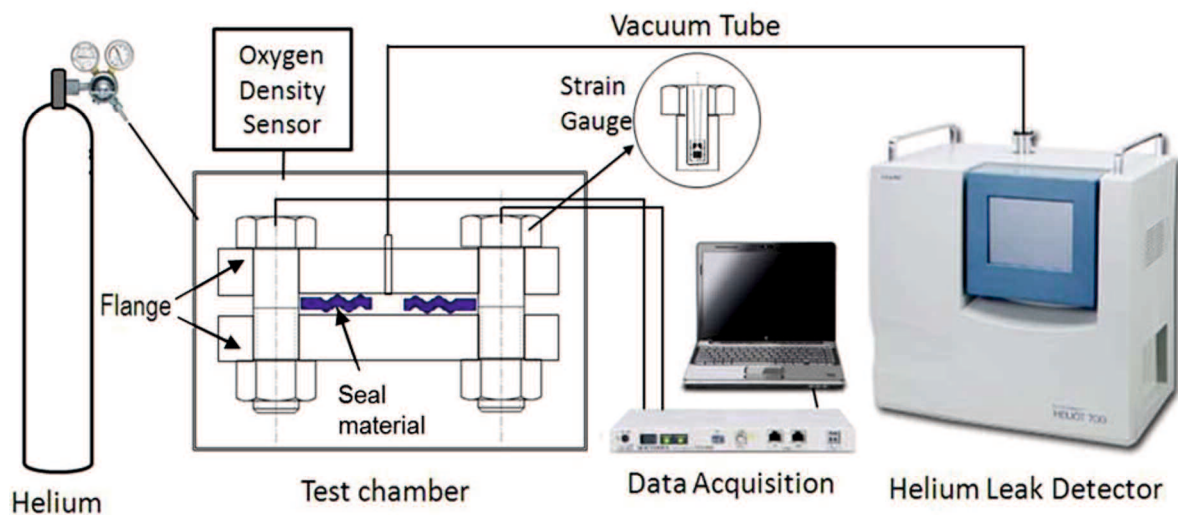

Fig. 5.24 Schematic diagram of helium leakage measument device

During the experiment, helium gas was substituted in the test chamber and the residual air was measured by an oxygen density sensor. The helium density was measured when the oxygen density was below 0.2 % and the helium density was above 99 % under atmospheric condition. The helium density at the outer part of the gasket was calculated by using a helium leakage detector (HELIOT 702D1, ULVAC); in particular, the minimum leakage quantity could be detected. The helium leakage measurement system is built to measure approximately 1.0×10^{-09} Pa m^3/s. The minimum and maximum leakage quantity detectable using this device was $1.0E^{-11}$ Pa m^3/s and approximately $1.0E^{-0.3}$ Pa m^3/s, respectively. To avoid the influence of leakage flow fluctuation at stages, measurement was performed between 300 to 500 s. The leakage flow quantity of joint part was calibrated to avoid experimental errors due to the leakage from the joint of the flange and the pipe.

Gasket performance is evaluated by using the relationship between axial force and helium leak rate. An axial force was produced on the flange by the tightening of the flange using bolts. To approximate the axial force, the tightening torque of the bolt is commonly

converted into an axial load. Nevertheless, the axial force could not be predicted accurately owing to the different friction coefficients of each bolt and nut used in the clamping as well as the variation of the axial force due to the clamping order of the bolt. To overcome these problems, in this study, the axial force was directly measured by embedding a strain gage into the bolts, as shown in Fig. 5.25. The leakage quantity was measured based on the measurement of the helium flow leakage quantity. Axial force levels of 10, 15, 20, 25, and 30 KN were measured for every bolt. The axial force of every bolt was monitored in order to adjust the axial force error to below 3%. Four bolts were used to clamp the flange, and therefore, we also tested axial force of 40, 60, 80, 100, and 120 KN.

In the previous study [16], the qualitative explanation produced by water pressured test was transformed into quantitative value using helium leak test. Therefore, quantitative decision criterion to prevent the leak is determined under the condition of helium leak quantity below the 1.0×10^{-6} Pa.m^3/s and it is observed that the leak by water pressure test did not occur.
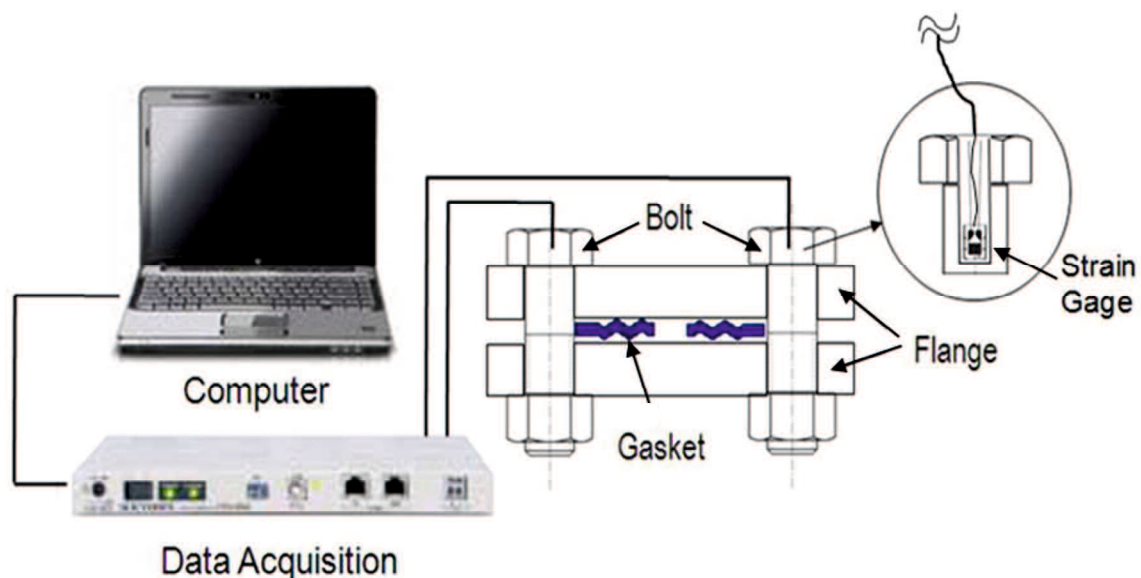

Fig. 5.25 Measurement of axial force

In this study, two types of gaskets—elastic (0-MPa mode) and plastic (400-MPa mode) design [20] with thickness ratio varies [Ts/Tg] 0.1/1.2; 0.2/1.2; 0.4/1.2 for 0-MPa mode 0.1/1.5; 0.2/1.5; 0.4/1.5; 0.5/1.5 for 400-MPa mode—and two flange surface roughness levels— 2.5, and 3.5µm—were investigated.

Fig. 5.26 shows the result of the helium leakage test for a gasket in 0-MPa mode in contact with flange having surface roughness Ra 2.5µm. A three-layer gasket with thickness ratio 0.1/1.2 and 0.2/1.2 in contact with a flange having a surface roughness of 2.5µm showed not leakage at 120 axial force. Gasket with thickness ratio 0.4/1.2 shows leakage at all axial force, making this roughness level unsuitable choice for this gasket.

Fig. 5.27 shows the result of the helium leakage test for a gasket in 0-MPa mode in contact with flange having surface roughness Ra 3.5µm. A three-layer gasket with thickness ratio 0.1/1.2 and 0.2/1.2 showed not leakage at 120 axial Force. Gasket with thickness ratio 0.4/1.2 and single material SUS304 show leakage at all axial force, making this roughness level unsuitable choice for this gasket.
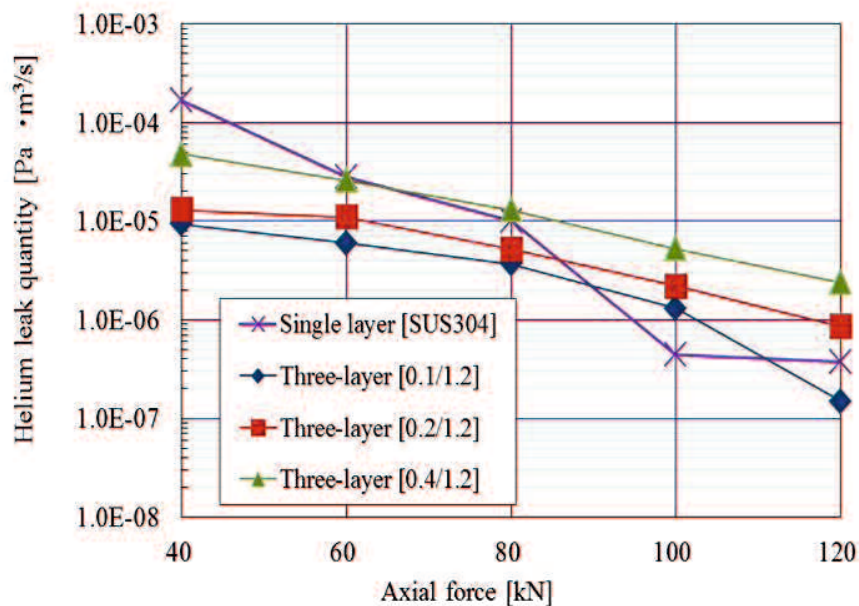

Fig. 5.26 Leakage measurement test result for Gasket 0-MPa mode Ra 2.5µm
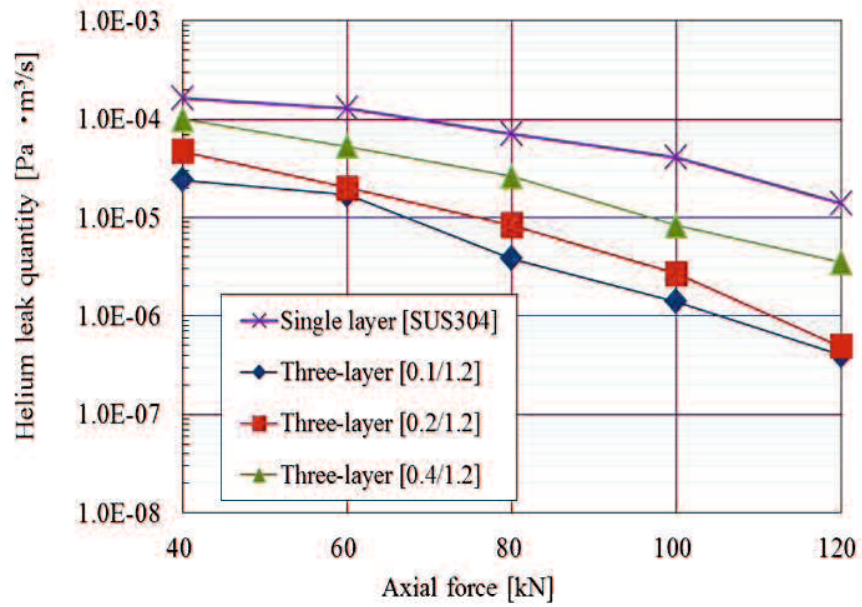
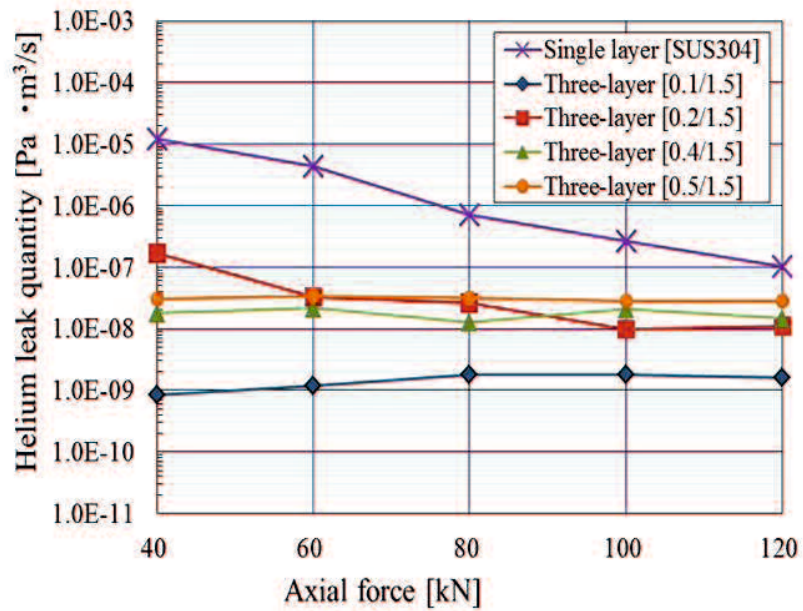Fig. 5.27 Leakage measurement test result for Gasket 0-MPa mode Ra 3.5µm

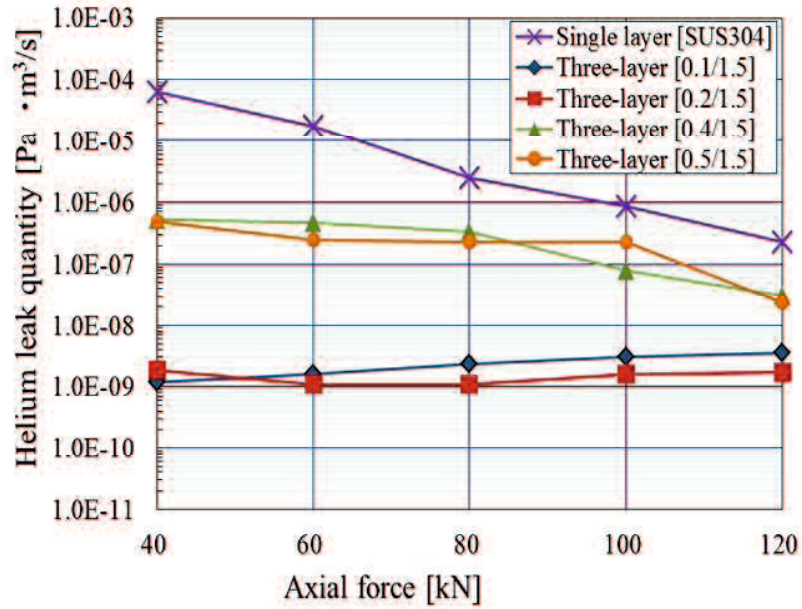Fig. 5.28 Leakage measurement test result for Gasket 400-MPa mode Ra 2.5µm

Fig. 5.29 Leakage measurement test result for Gasket 400-MPa mode Ra 3.5µm

Fig. 5.28 shows the result of the helium leakage test for a gasket in 400-MPa mode in contact with flange having surface roughness Ra 2.5µm. All three-layer gasket showed not leakage at 40 axial force. Gasket single material SUS304 shows not leakage at 80 axial force. Gasket three-layer show better sealing performance than gasket SUS304.

Fig. 5.29 shows the result of the helium leakage test for a gasket in 400-MPa mode in contact with flange having surface roughness Ra 3.5µm. All three-layer gasket showed not leakage at 40 axial force. Gasket single material SUS304 shows not leakage at 100 axial force. Gasket three-layer show better sealing performance than gasket SUS304.
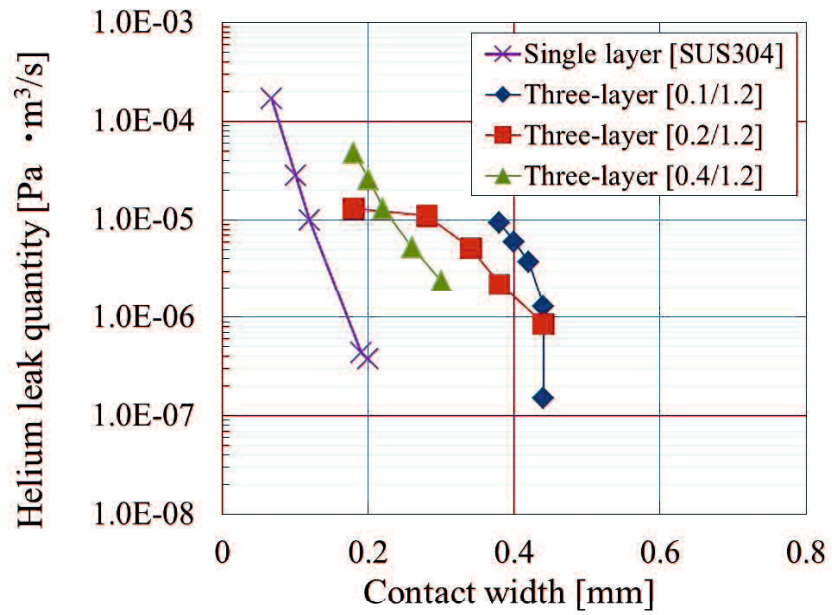
(a)
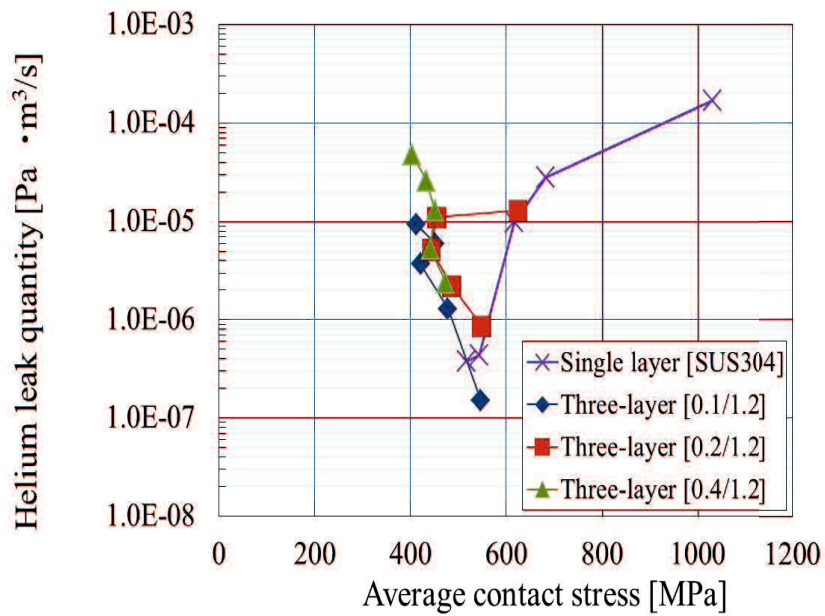
(b)

(c)

Fig. 5.30 Helium leak measurement related to (a) contact width (b) average contact stress (c) stress ratio for gasket 0-MPa mode [Ra 2.5μm]

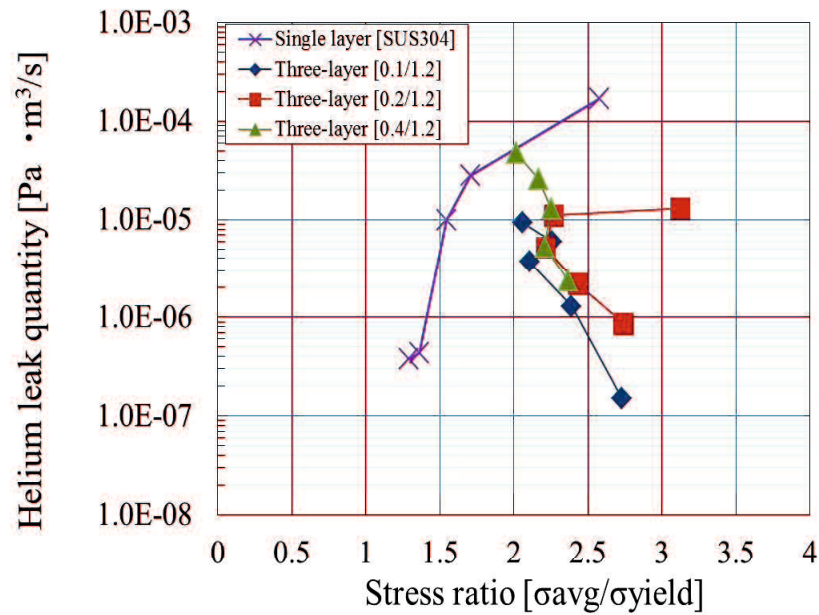Figure 5.30 shows the helium leak measurement related to contact width, average contact stress and stress ratio for gasket 0-MPa mode in contact with flange having surface roughness 2.5μm. Gasket single layer SUS304 the leakage did not occur when axial force 100kN. In that time the real contact width for simulation result is 0.2mm and average contact stress is 576.3339MPa. Gasket with thickness ratio 0.1/1.2 the leakage did not occur when axial force 120kN. In that time the real contact width for simulation result is 0.44 mm and average contact stress is 546.2342MPa. Gasket with thickness ratio 0.2/1.2 the leakage did not occur when axial force 120kN. In that time the real contact width for simulation result is 0.44 mm and average contact stress is 548.3219MPa. Gasket with thickness ratio 0.4/1.2 is still leak when axial force 120kN. In that time the real contact width for simulation result is 0.3 mm and average contact stress is 473.001MPa.
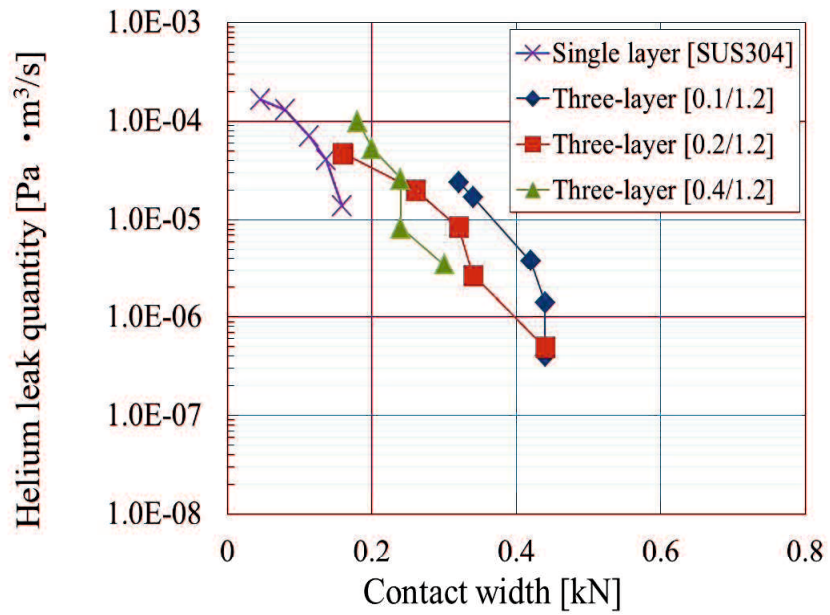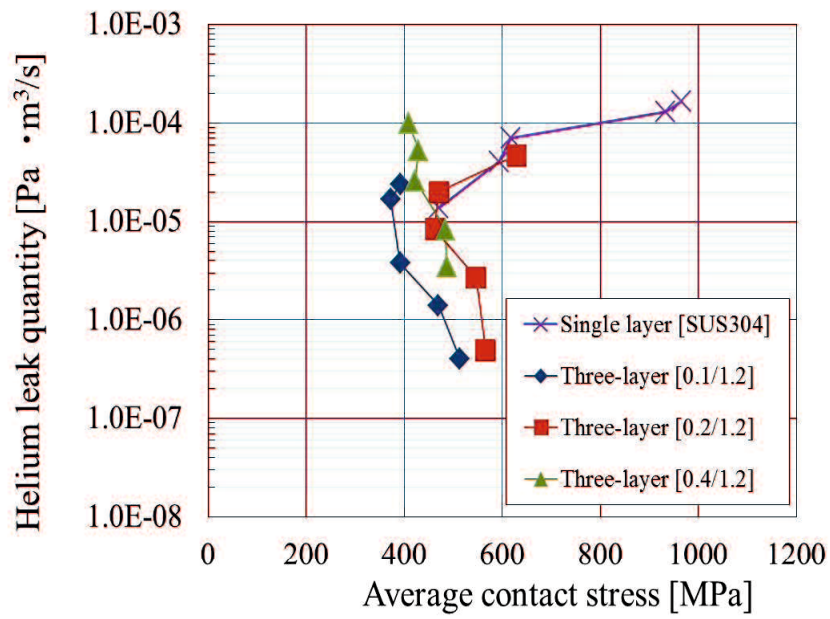
(a)

(b)

(c)

Fig. 5.31 Helium leak measurement related to (a) contact width (b) average contact stress (c) stress ratio for gasket 0-MPa mode [Ra 3.5μm]

Figure 5.31 shows the helium leak measurement related to contact width for gasket 0-MPa mode in contact with flange having surface roughness 3.5μm. Gasket single layer SUS304 showed leakage when axial force 120kN. In that time the real contact width for simulation result is 0.18mm and average contact stress is 448.05378MPa. Gasket with thickness ratio 0.1/1.2 the leakage did not occur when axial force 120kN. In that time the real contact width for simulation result is 0.44 mm and average contact stress is 513.732MPa. Gasket with thickness ratio 0.2/1.2 the leakage did not occur when axial force 120kN. In that time the real contact width for simulation result is 0.44 mm and average contact stress is 566.0269MPa. Gasket with thickness ratio 0.4/1.2 is still leak when axial force 120kN. In that time the real contact width for simulation result is 0.3 mm and average contact stress is 486.7347MPa

174

(a)

(b)

175

(c)

Fig. 5.32 Helium leak measurement related to (a) contact width (b) average contact stress
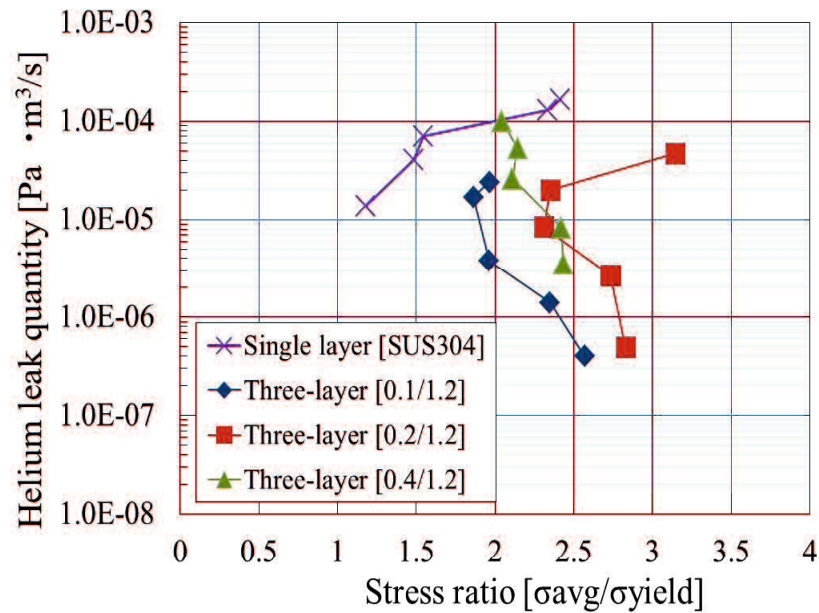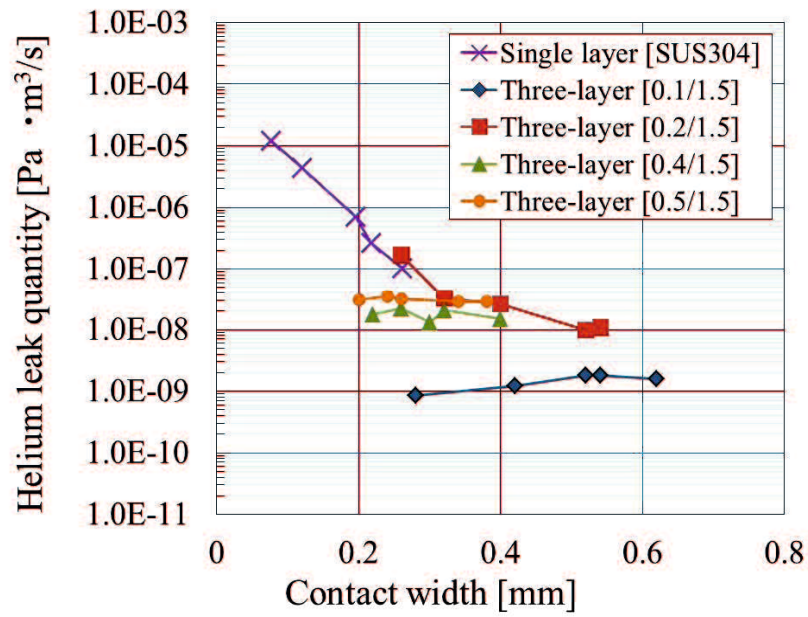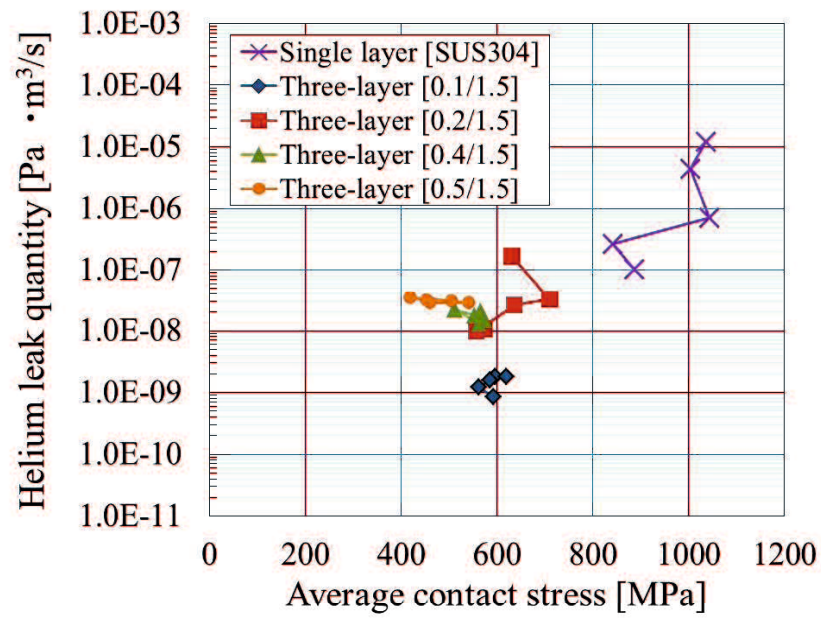(c) stress ratio for gasket 400-MPa mode [Ra 2.5μm]

Figure 5.32 shows the helium leak measurement related to contact width for gasket 400-MPa mode in contact with flange having surface roughness 2.5μm. Gasket single layer SUS304 show the leakage did not occur when axial force 80kN. In that time the real contact width for simulation result is 0.195mm and average contact stress is 837.3109MPa. All Gasket three-layer show the leakage did not occur when axial force 40kN. In that time the contact width for gasket 0.1/1.5 from simulation result is 0.28mm and average contact stress is 611.24MPa. Gasket with thickness ratio 0.2/1.5 the contact width for simulation result is 0.26mm and average contact stress is 630.976MPa. Gasket with thickness ratio 0.4/1.5 the contact width for simulation result is 0.22mm and average contact stress is 553.496MPa. Gasket with thickness ratio 0.5/1.5 the contact width for simulation result is 0.2mm and average contact stress is 504.342MPa.
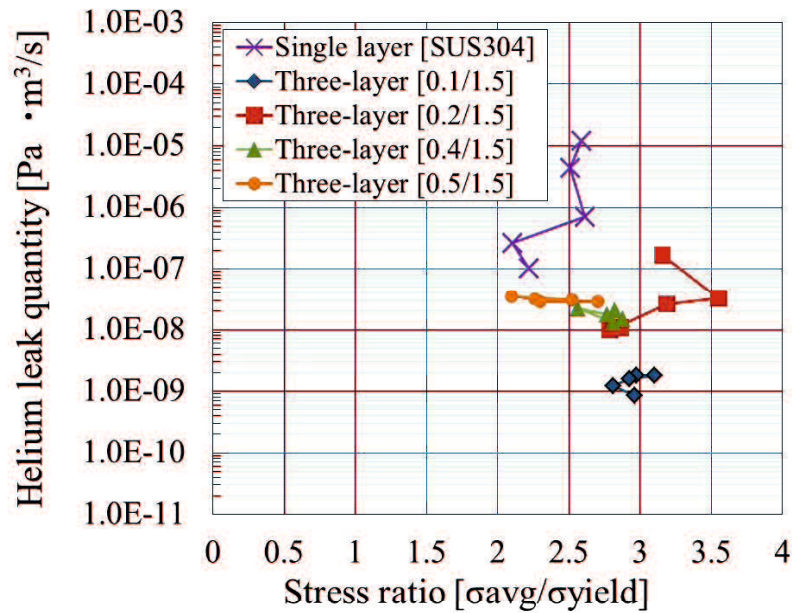
Figure 5.33 shows the helium leak measurement related to contact width for gasket 400-MPa mode in contact with flange having surface roughness 3.5μm. Gasket single layer

176

SUS304 show leakage did not occur when axial force 100kN. In that time the real contact width for simulation result is 0.195mm and average contact stress is 721.5MPa. All Gasket three-layer show the leakage did not occur when axial force 40kN. In that time the contact width for gasket 0.1/1.5 from simulation result is 0.3 mm and average contact stress is 616.261MPa. Gasket with thickness ratio 0.2/1.5 the contact width for simulation result is 0.28 mm and average contact stress is 638.947MPa. Gasket with thickness ratio 0.4/1.5 the contact width for simulation result is 0.22 mm and average contact stress is 563.194MPa. Gasket with thickness ratio 0.5/1.5 the contact width for simulation result is 0.2 mm and average contact stress is 539.597MPa.

(a)

(b)
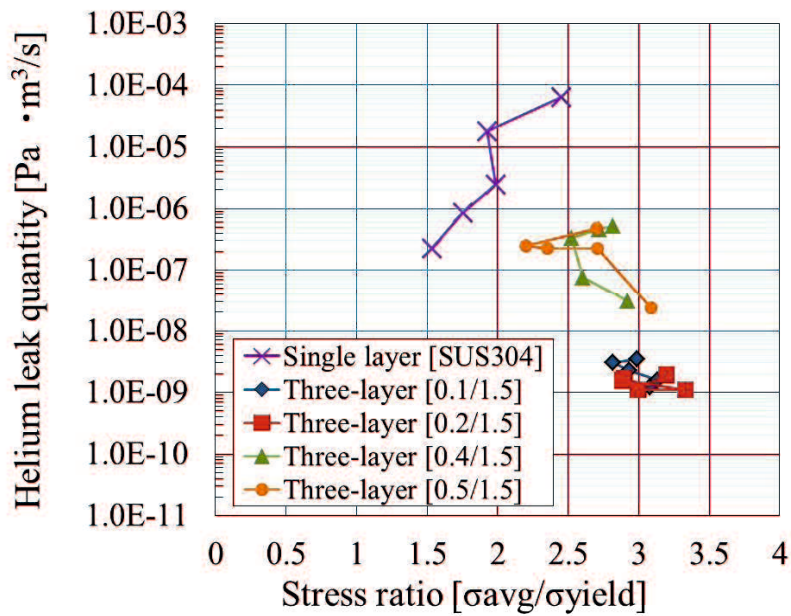
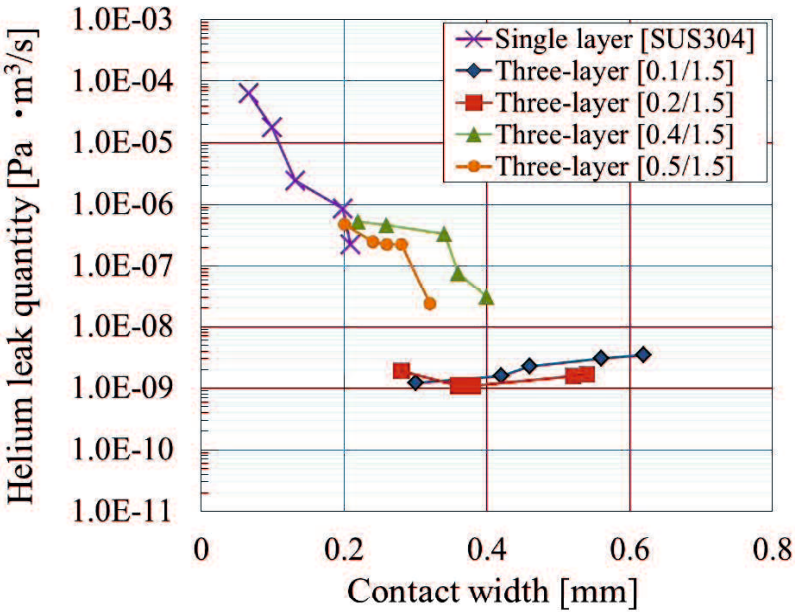(c)

Fig. 5.33 Helium leak measurement related to (a) contact width (b) average contact stress
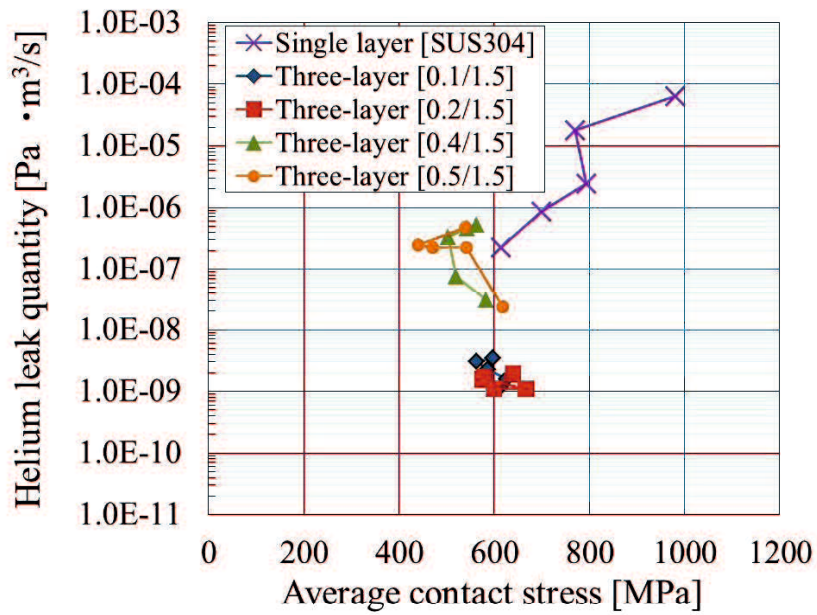(c) stress ratio for gasket 400-MPa mode [Ra 3.5μm]

A comparison of simulation results and experimental data showed good agreement. In theory, helium leakage will decrease with an increase in the contact width and contact stress. Previous research [ ] clarified that the leakage did not occur when real contact width is 0.195 mm but the minimum average contact stress did not clarified yet. In the present study, it was found that the three-layer metal gasket 0-MPa mode in the 120kN axial force is still leaking and the contact width is 0.3mm has exceeded the minimum requirement. This is because the average contact stress that occurs at that time has not reached the minimum contact stress. While the three-layer gasket 400-Mpa mode Ts/Tg = 0.5/1.5 does not leak in axial force 40kN with real contact width 0.2mm and average contact stress is 504.342MPa. Based on this result we can clarify that the leakage did not occur if the average contact stress is 504.342MPa. Furthermore, the helium leakage test result suggests that gasket three-layer 400-MPa mode superior to that in 0-MPa mode and better sealing performance than gasket single layer SUS304.

5.5 Real Contact Width Experiment

Surface gaskets after leak test with helium leak test were observed to obtain real contact width that occurred. Because of the surface roughness of the flange, in the tightening process where the flanges contact with the surface of the gasket will be formed groove pad convex part as shown figure 5.34. Real contact width measurement using digital microscope VH-Z250 series with magnification used 150X as shown figure 5.35. The total number of groove widths is the real contact width occurring between the gasket with the flange, see equation 5.1.

$$CW = \sum_{i=1}^{n} h_i \qquad\qquad\qquad (5.1)$$
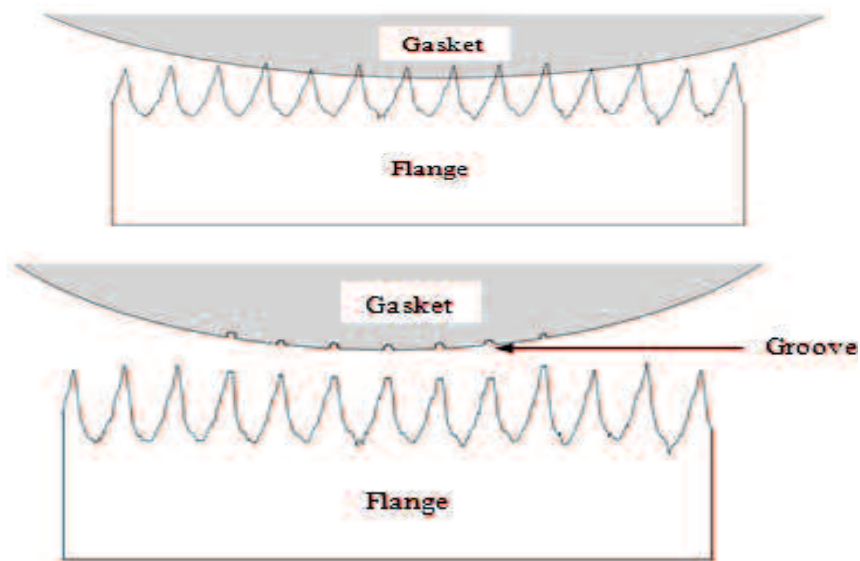
Fig. 5.34 Gasket and flange in contact and after contact condition

Fig. 5.35 Digital microscope VH-Z250

Figure 5.36 shows contact width simulation results for 0-MPa mode gaskets that are in contact with flange for surface roughness 2.5µm and 3.5µm at 120kN axial force. Figure 5.37 shows contact width simulation results for 400-MPa mode gaskets that are in contact with flange for surface roughness 2.5µm and 3.5µm at 120kN axial force.
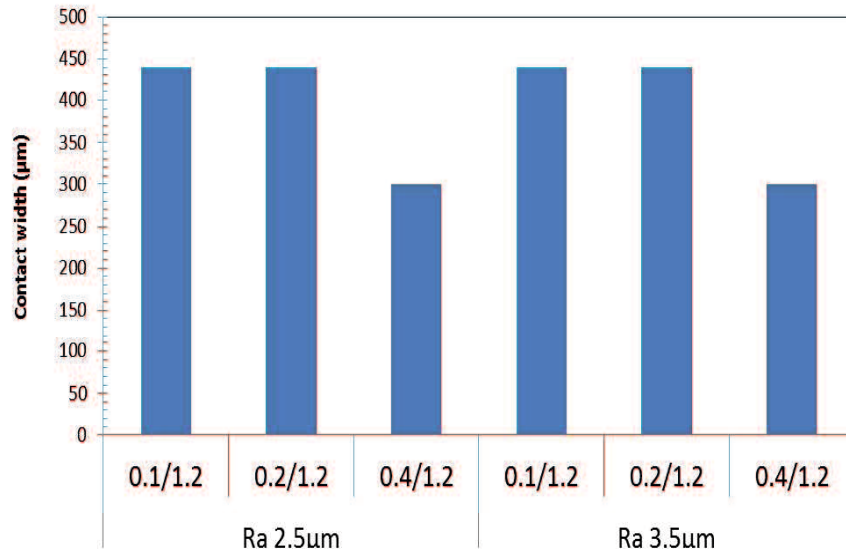
Figure 5.36 Contact width simulation result for real surface roughness model of flange and all thickness ratio when axial force 120kN [0MPa-mode].

Figure 5.37 Contact width simulation result for all level real surface roughness model of flange and all thickness ratio when axial force 120kN [400MPa mode]

Based on previous study, we measured two places of surface layer gasket, which were convex potion 2 and convex portion 3, because both convex were similar character

and very influence for leakage process. Both of these convex have higher contact stress and longer contact width compare with convex portion 1 and convex portion 4 [23].

(a) 0.1/1.2

(b) 0.2/1.2
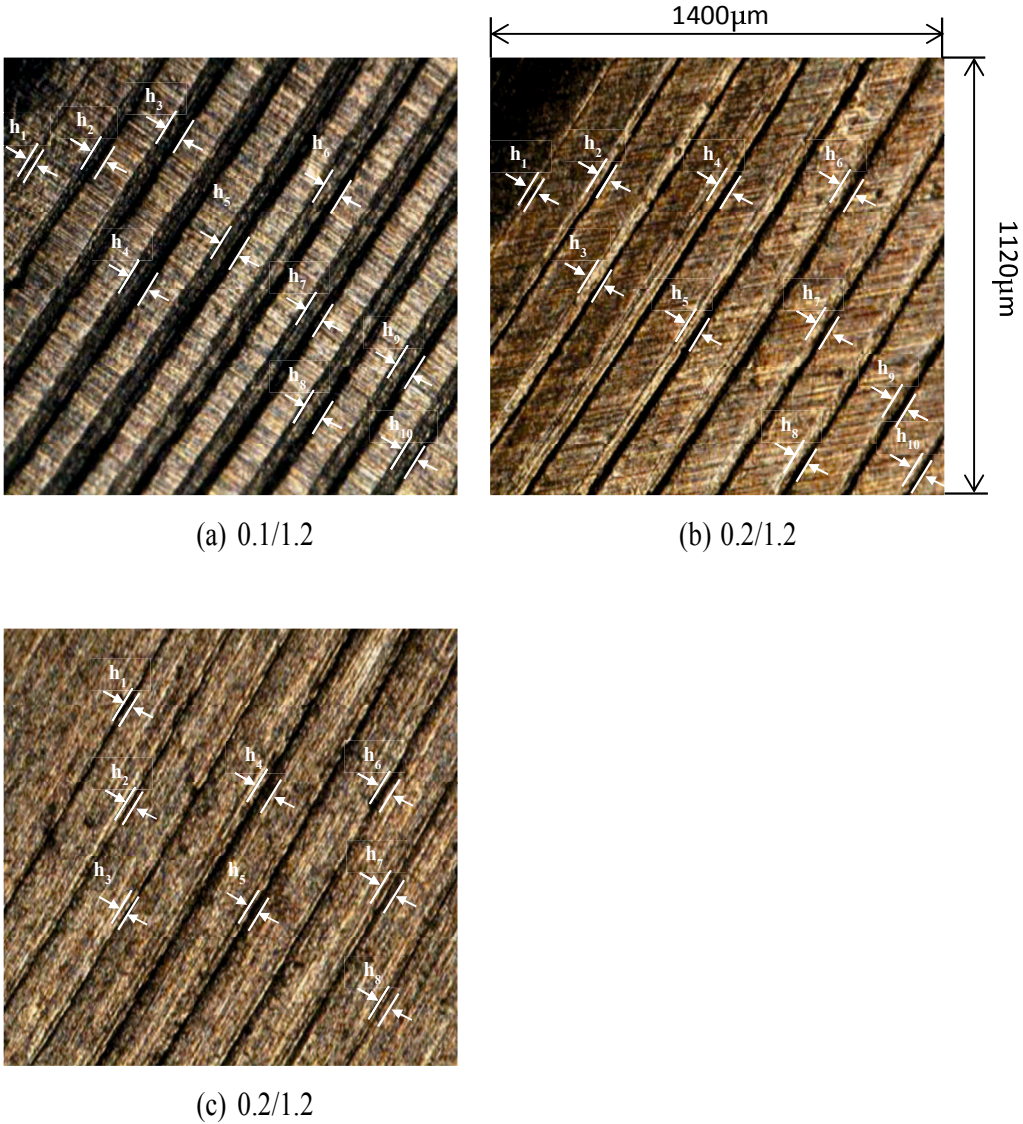
(c) 0.2/1.2
Fig. 5.38 Gasket surface roughness for gasket 0-MPa after contact for Ra 2.5μm

(a) 0.1 /1.2   (b) 0.2/1.2

(c) 0.4/1.2
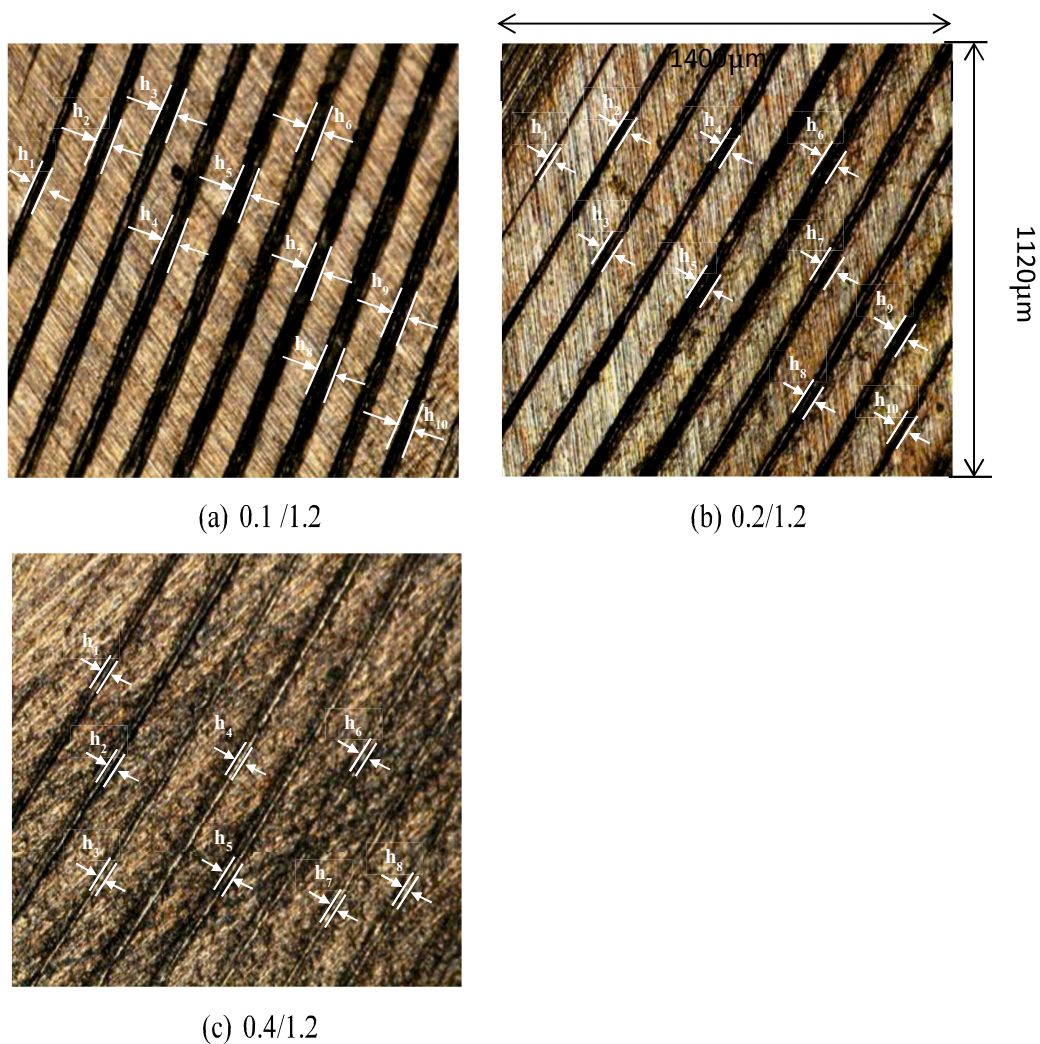
Fig. 5.39 Gasket surface roughness for gasket 0-MPa after contact for Ra 3.5 µm

Fig. 5.38 and Fig. 5.39 show the surface roughness condition of gasket 0-MPa mode after contact with flange having surface roughness Ra 2.5µm and Ra 3.5µm. Fig. 5.40 and Fig. 5.41 show the surface roughness condition of gasket 400-MPa mode after contact with flange having surface roughness Ra 2.5µm and Ra 3.5µm. When tightening process between upper and lower rough flanges, there were grooves formed in gasket surface. Based on these figures with use equation 5.1, we got the real contact width of surface layer gasket.

(a) 0.1/1.2

(b) 0.2/1.2

(c) 0.2/1.2
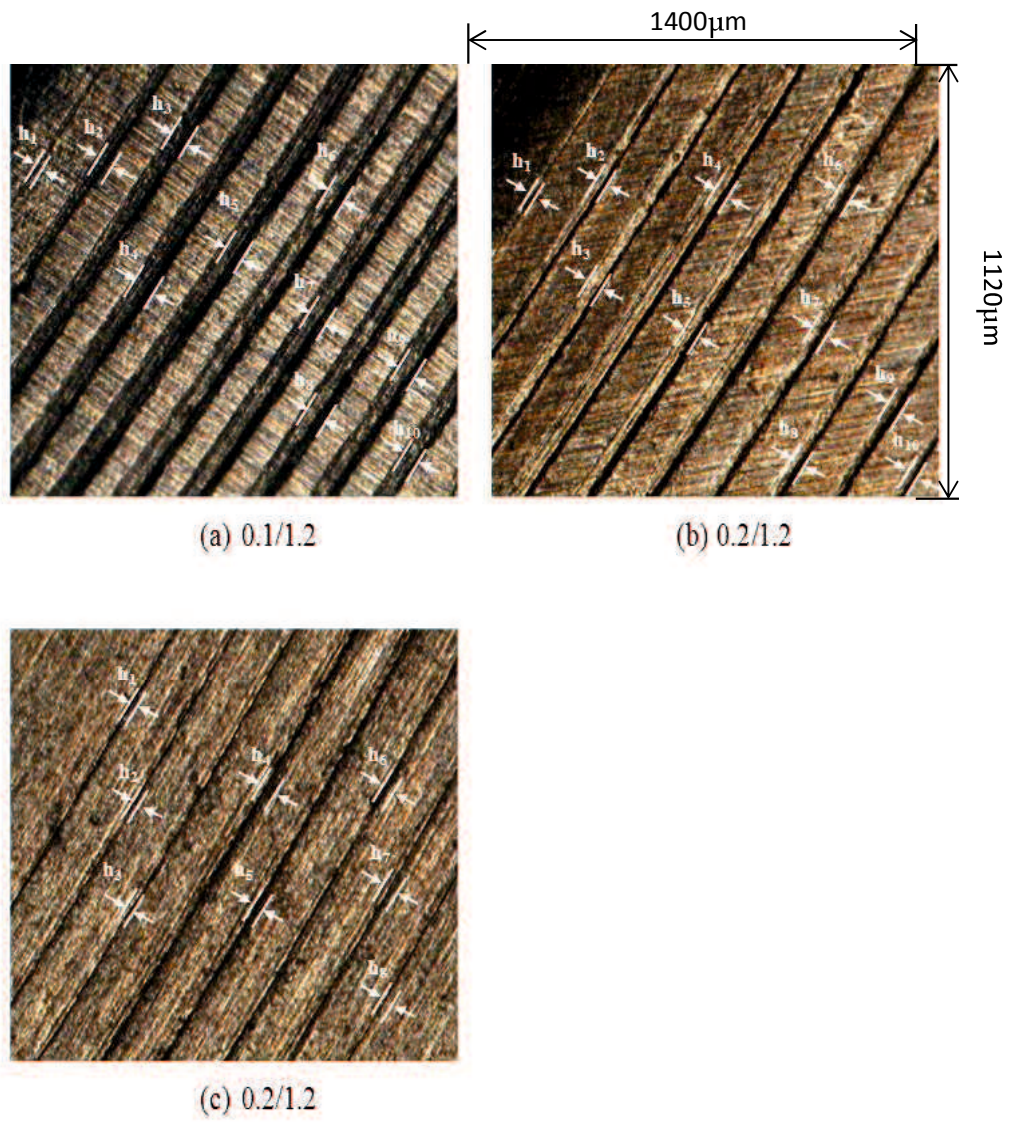
Fig. 5.40 Gasket surface roughness for gasket 400-MPa after contact for Ra 2.5

(a) 0.1 /1.2

(b) 0.2/1.2

(c) 0.4/1.2
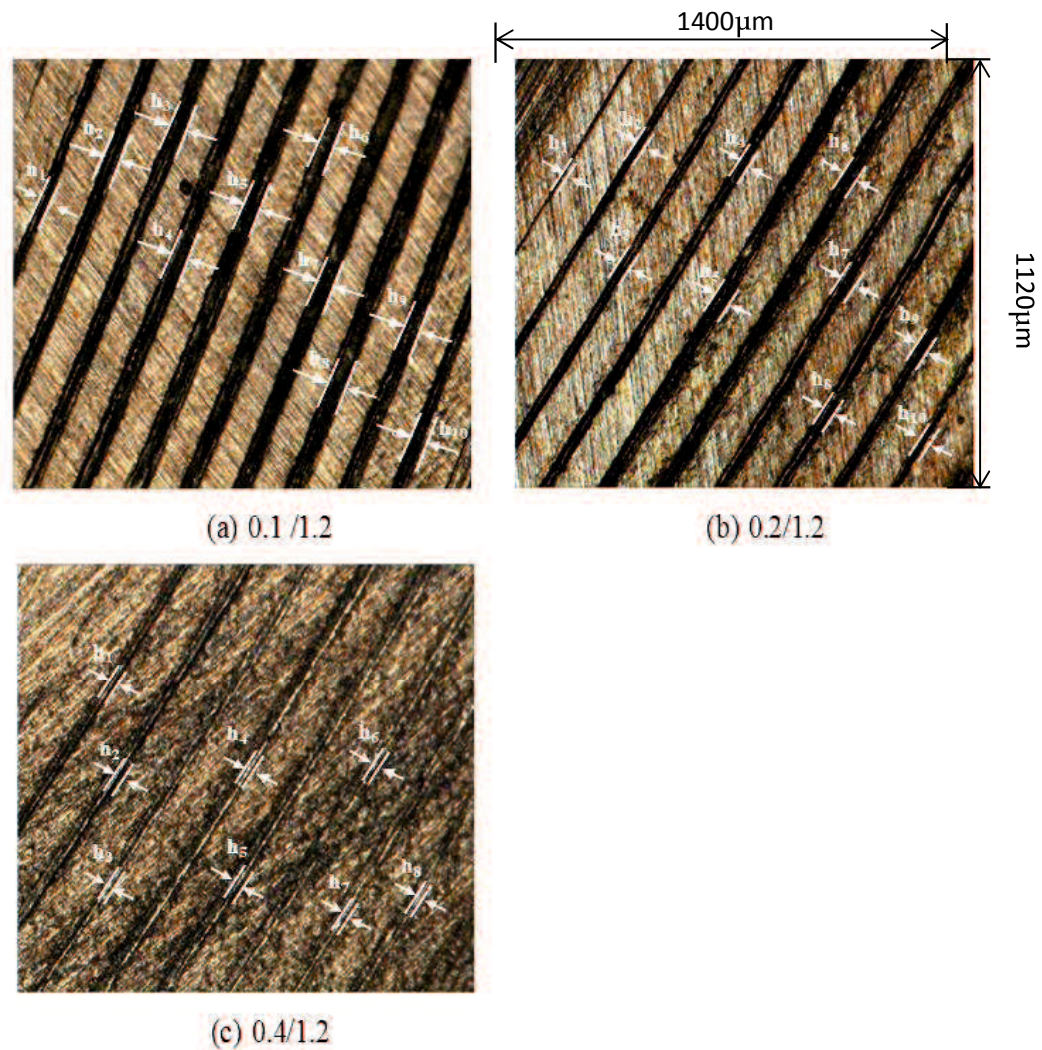
Fig. 5.41 Gasket surface roughness for gasket 400-MPa after contact for Ra 3.5

Fig. 5.42 shows the real contact width of gasket 0-MPa mode for all level thickness ratios. For gasket three-layer no bond model, increase thickness ratio result decrease contact width. Gasket with thickness ratio 0.1/1.2 shows longest real contact width than the other. There is small different value of contact width between surface roughness Ra 2.5µm and Ra 3.5µm. It denotes that effect surface roughness not significant for gasket three-layer.

Fig. 5.43 shows the real contact width of gasket 0-MPa mode for all level thickness ratios. For gasket three-layer no bond model, increase thickness ratio result decrease contact width. Gasket with thickness ratio 0.1/1.5 shows longest real contact width than the other. There is small different value of contact width between surface roughness Ra 2.5µm and Ra 3.5µm. It denotes that effect surface roughness not significant for gasket three-layer.
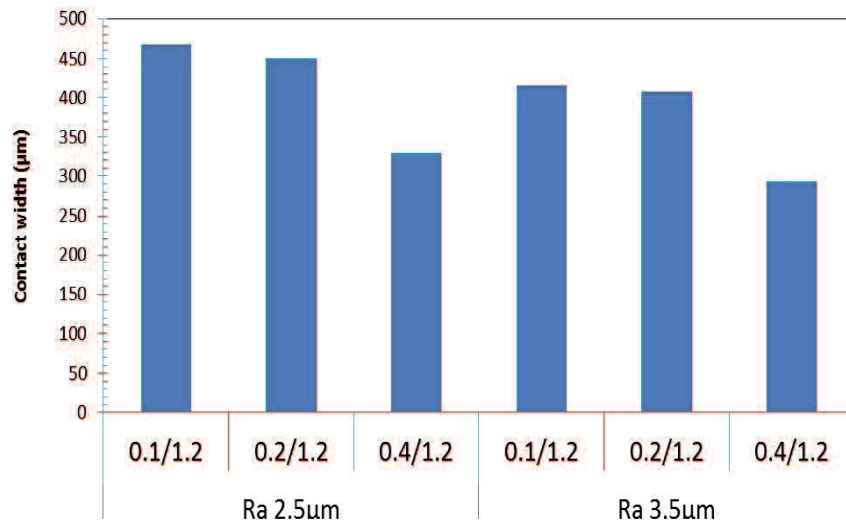
Fig. 5.42 Real contact width experiment result all level real surface roughness model of flange and all thickness ratios [0MPa-mode]

Fig. 5.43 Real contact width experiment result all level real surface roughness model of flange and all thickness ratios [400MPa-mode]
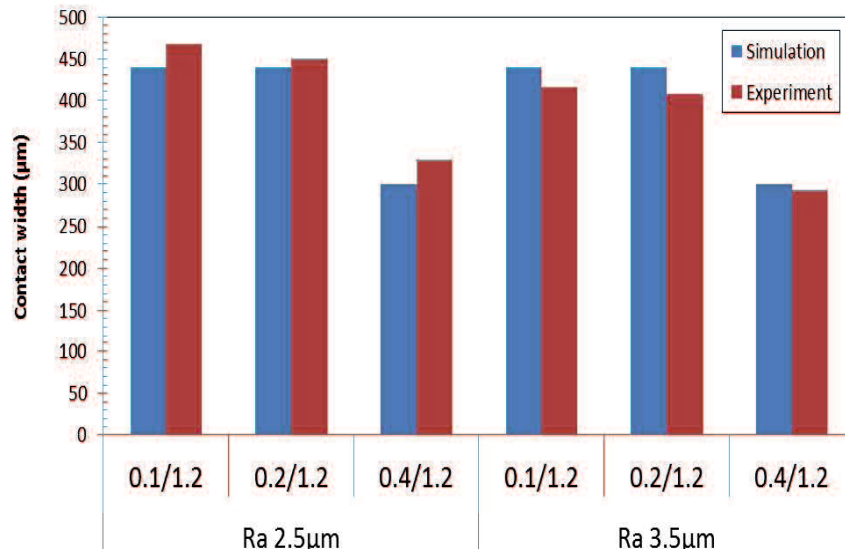
Fig. 5.44 Differences of contact width between simulation result and experiment for gasket
0-MPa mode
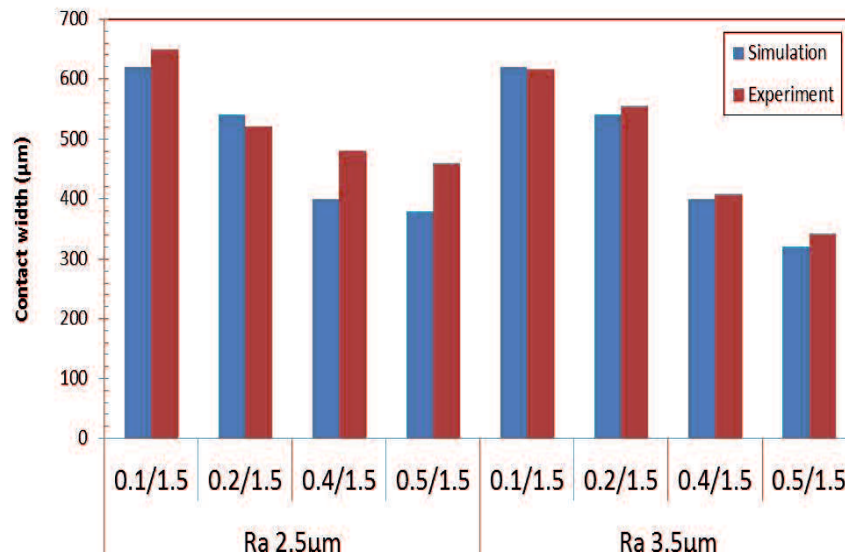
Fig 5.45 Differences of contact width between simulation result and experiment for gasket
400-MPa mode

Fig. 5.44 and 5.45 show the comparison of contact width between simulation and experiment for gasket three-layer 0-MPa mode and 400-Mpa mode. The figure show the contact width trend is similar. The real contact width for the gasket 400-MPa mode was longer than the gasket 0-MPa mode. Surface roughness effect shows not significant.

The total differences of real contact width measurement between experiment result and simulation result for gasket 0-MPa mode is 5.62%. The total differences of real contact width measurement between experiment result and simulation result for gasket 400-MPa mode is 6.86%. Table 5.2 and Table 5.3 show the differences of measurement between experiment result and simulation result.

Table 5.2 Differences of contact width between simulation result and experiment for gasket 0-MPa mode

	Ra 2.5			Ra 3.5		
	0.1/1.2	0.2/1.2	0.4/1.2	0.1/1.2	0.2/1.2	0.4/1.2
Simulation result (μm)	440	440	300	440	440	300
Experimental result (μm)	467.8375	450.19125	330.5225	414.8475	407.89875	293.1
Differences (%)	5.95	2.26	9.23	6.06	7.87	2.35
	5.82			5.43		
	5.62					

Table 5.3 Differences of contact width between simulation result and experiment for gasket 400-MPa mode

	Ra 2.5				Ra 3.5			
	0.1/1.5	0.2/1.5	0.4/1.5	0.5/1.5	0.1/1.5	0.2/1.5	0.4/1.5	0.5/1.5
Simulation result (μm)	620	540	400	380	620	540	400	320
Experimental result (μm)	649.13	521.01542	479.54	460.53	615.5	555.56	409.36	343.57
Differences (%)	4.49	3.64	16.59	17.49	0.73	2.80	2.29	6.86
	10.55				3.17			
	6.86							

5.6 Conclusion

This study investigates the helium leakage quantity for a flange with different surface roughness value through a simulation analysis using FEM, leakage test and real contact width measurement. The following conclusions are derived from this study:

1. Simulation results show that gasket three-layer in 400-MPa mode has longer contact width than 0-MPa mode.

2. The helium leakage test shows that the gasket three-layer in 400-MPa mode shows better sealing performance than gasket single layer SUS304.

3. For a gasket in 400-MPa mode in contact with flange, leakage did not occur for all surface roughness for low axial force 40kN.

4. The contact width which has no leak in gasket three-layer for no bond model was clarified. The leakage did not occur when real contact width is 0.2mm and minimum average contact stress is 504.342MPa (2.52 x σ_{yield}).

5. Gasket three-layer with small thickness ratio shows better sealing performance.

6. Flange surface roughness shows not significant effect in gasket three-layer.

7. The total differences of measurement between simulation result and real model of surface roughness and experimental result is small, so we can state that our simulation model approach real model.

CHAPTER VI

OPTIMIZATION OF THREE-LAYER METAL GASKET USING TAGUCHI

A metal gasket SUS304 performance decrease when contact with flange having high surface roughness. This is because when gasket SUS304 contact with a flange that has high surface roughness, contact width containing plastic contact stress condition is also reduced so that the sealing performance of the gasket also decreased. Based on this reason, improvement of metal gasket performance continues researched therefore not leakage when contact with flange having high surface roughness.

In this research we inserted the soft metal as surface layer at the top and bottom of the SUS304 gasket therefore when contact with the flange having high surface roughness the soft metal will be deformed plastically and fill the gap of the imperfect flange surface. Thereby increase the contact width and reduced the axial force when tightening.

6.1 Gasket Optimization by Using Taguchi Method

The three-layer metal gasket composed of SUS304 as base metal (hard material) and C1020 as surface layer, respectively. SUS304 was used as the gasket material because of its effectiveness in a high-temperature and high-pressure environment. Its material properties were first determined through a tensile test carried out based on JIS Z2241 [50] —the nominal stress, modulus of elasticity (E), and tangent modulus were respectively found to be 398.83MPa, 210GPa, and 1900.53MPa. The materials were considered as elastic-plastic materials. For C1020 the nominal stress, modulus of elasticity (E), and tangent modulus were respectively found to be 200MPa, 136GPa, and 1360MPa
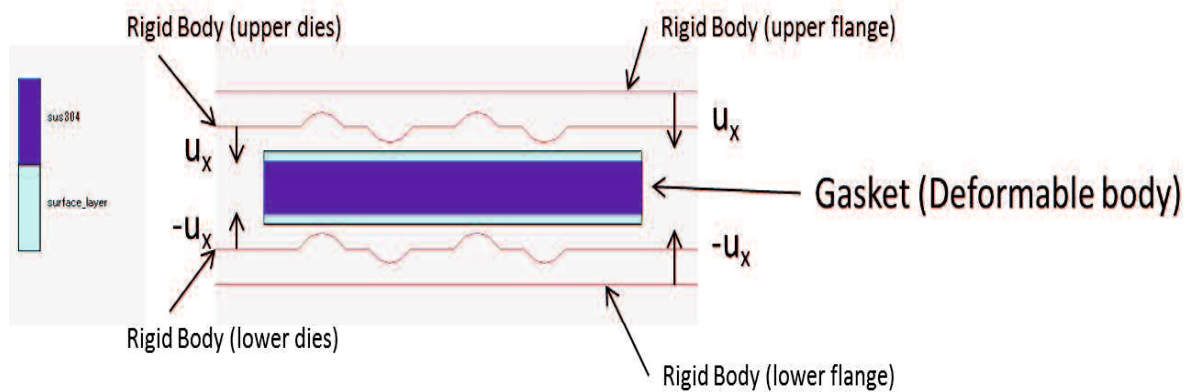
Fig. 6.1 Three layers Gasket simulation setting up

The elastoplastic behavior of gasket is calculated by using software of FEM, MSC. Marc. Fig. 6.1 shows the loading condition. In our calculation, 2 dimensional axisymmetric solid elements isoparametric quadrilateral type 10 are used to implement compression displacement in the axial direction on the gasket in between the upper and the lower of dies and flange with a constant increasing step of displacement Δux.

In our study, the material is assumed to obey isotropic strain hardening, and described by J2-deformation theory of Mises' yield criterion for bilinear stress-strain behavior. The material behavior is initially elastic characterized by a Young's modulus E until yielding commences at the uniaxial yield stress σ_Y. Thereafter the material response is elastic-plastic with the local tangent to the curve continually varying and is termed the elastic-plastic tangent modulus E_T (Fig. 6.2). During our nonlinear analysis with iterative procedure, Newton-Raphson method is used to solve for the equilibrium equations which are composed of finite strain plasticity with multiplicative decomposition of deformation gradient.
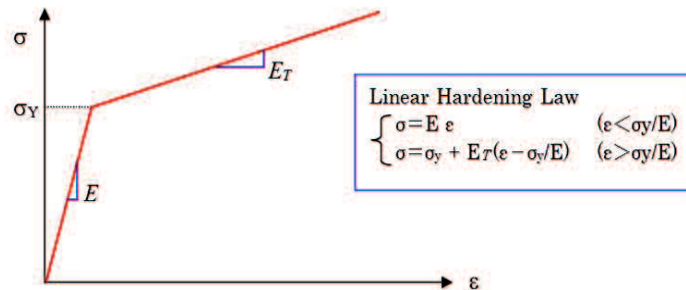
Fig. 6.2 Linear strain hardening model

From MSC Marc result, the contact width is determined based on contact status. Contact status values are1 and 0 which mean contact and no contact, respectively. Only at the beads (convex part) of gasket which is effective for avoiding leak is taken as evaluation part. The top surface and bottom surface of contact width increased step by step due to the increment of the axial force to the gasket.
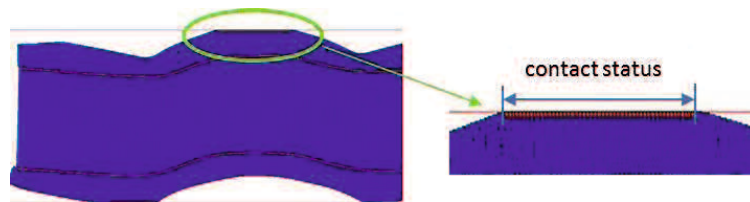
Fig. 6.3 the contact status

Previous research clarified that gasket in plastic contact stress condition will give better sealing performance. In this study the optimization based on the gasket plastic design by deleting the contact stress value below of surface layer yields stress.
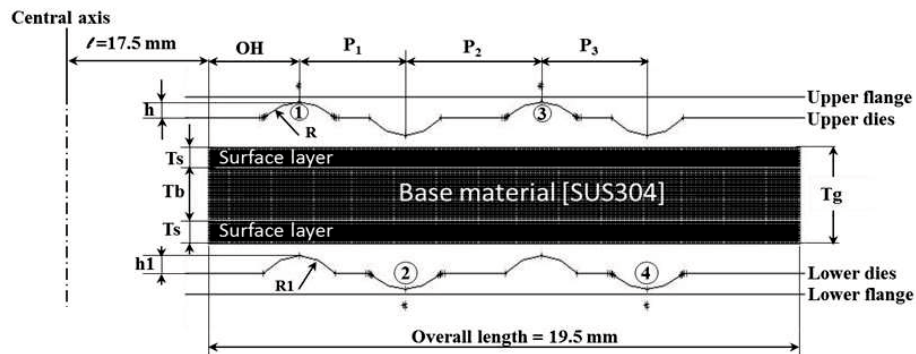
Fig. 6.4 Dimension of gasket

This study investigated the optimization design of gasket based on contact between surface layer and base material No-fix model. The contact between surface layer and base material is touching namely no-fix model. The dimension of gasket will be optimization is shown in Fig. 6.4.

6.1.1 Gasket no-fix model

A gasket model is divided into two simulation stages by using two pressing model which is forming and tightening simulation. Both stages were modeled using finite element method analysis software MSC. Marc [48]. The virtual gasket model with various designs was generated by using four basic steps. They were the parameterization the models, automatic meshing, computation of preprocessing and post-processing in batch mode and optimization. Firstly, 2-D parameter model is built by utilizing the Solidwork software. To connect drawing data from Solidwork (IGES file) and automatic meshing by using Hypermesh, batch command file was built and a NAS file was produced with this procedure. Then the procedure file was configured to obtain preprocessing and running the model on MSC.Marc software. The graphic user interface (GUI) was not appear and the program run command in the background. After the FEM analysis was complete, an output file including analysis results could be generated in TXT file. The TXT result file was transformed to Microsoft excel by using MACRO command. The output result contains the contact status, stress value, and body force at each time at every convex position.

193

Calculation of the contact width versus axial force on convex position number 1 until 4 is produced with several step of MACRO command.

Figure 6.5 shows the simulation setting up before forming and tightening simulation. Material gasket in this study was circumference and deformable. The dies and flanges were assumed as rigid body in both sides. In the first stage, using two-dimensional assumptions, the axis symmetric model was adopting a forming process simulation in axial direction on gasket material between the top and the bottom of the dies, see Fig. 6.6. Forming simulation will produce the circumference beads gasket. The second stage was the gasket shape produced by mold press was continuity compressed in axial direction to adopt tightening of the gasket on the flanges, see Fig. 6.7. When the gasket was tightened by the flanges, each of beads of both surfaces of gasket created elastic effect and produced high local contact stress for preventing leakage. This circumstance made the range of conventional axial force could be possible to use.
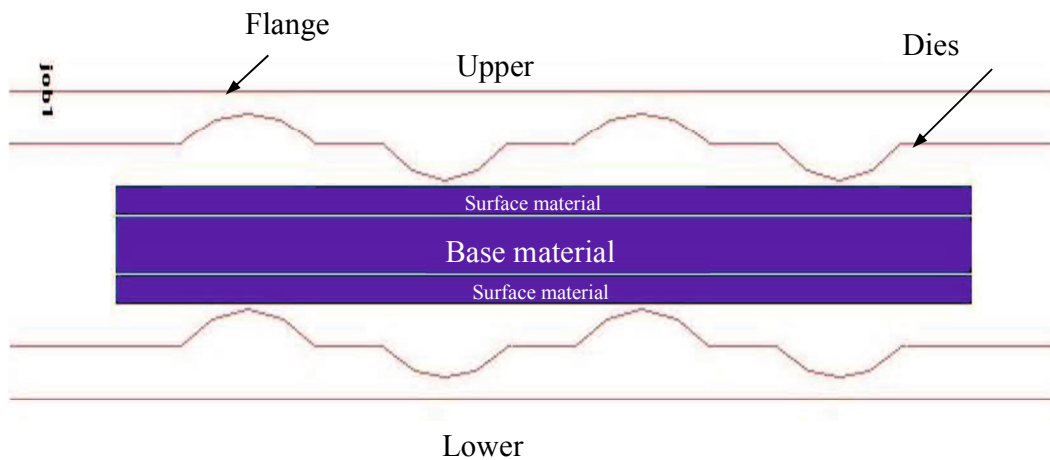
Fig. 6.5 Setting-up of gasket material, dies and flange before forming and tightening
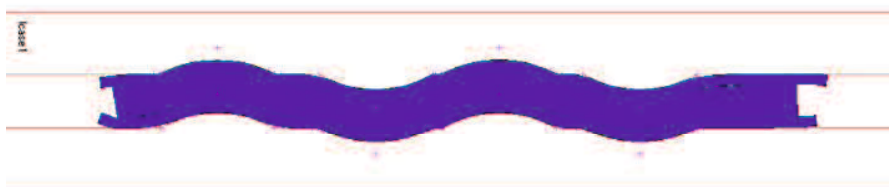
Fig. 6.6 Forming simulation no-fix model
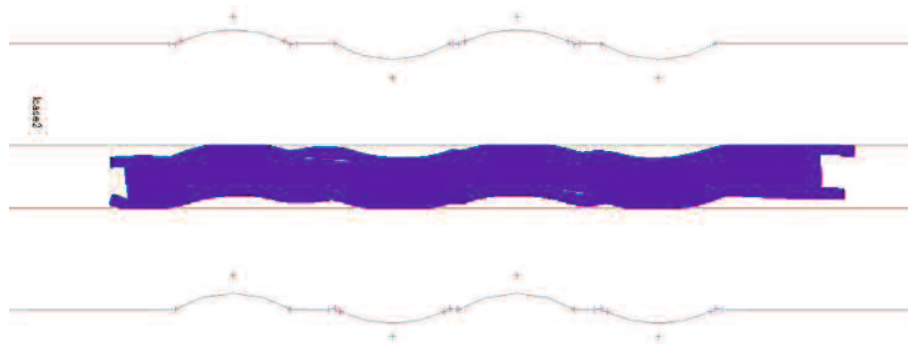
Fig.6.7 Tightening simulation no-fix model

The Taguchi method was used to evaluate the effect of each parameter design and predict optimal design of 25A-size three-layer metal gasket. Taguchi method uses a special set of arrays called orthogonal arrays. These standard arrays stipulate the way of conducting the minimal number of experiments, which could give the full information of all the factors that affect the performance parameters. The Taguchi method can be applied on simulation experiment, is becoming as a popular as actual experiments. Simulation result yields no error in repeatability but has problem on error modeling. The optimum design was determined based on reducing the axial force. It could be denote by using the slope or gradient of the curve of relationship between contact width and axial force, see Fig.6.8. The upper and lower contact width was the value of convex contact position number 1 plus 3 and 2 plus 4, respectively. The slope of curve is increased; it will be reduce the axial force. Due to the optimization design based on increasing contact width is combined with considering contact stress. The gasket design with higher slope is choose as optimum design.
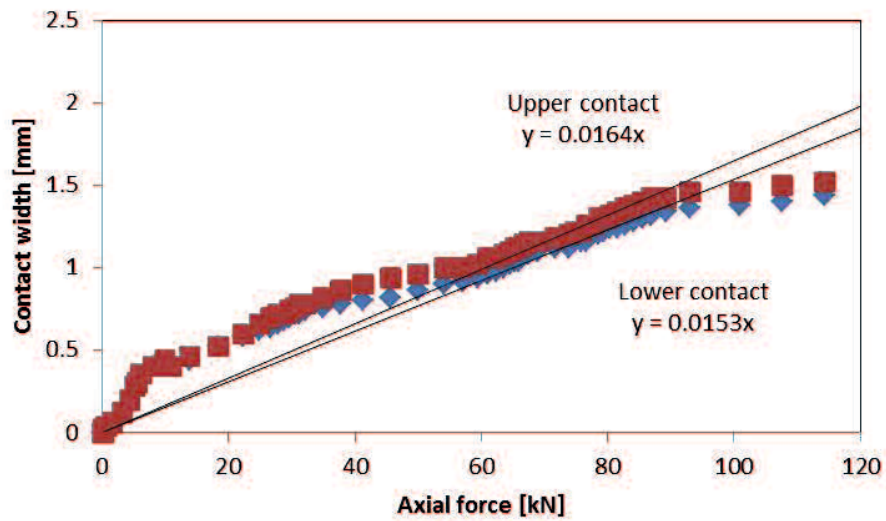
Fig.6.8 Slope of curve of relationship between contact width and axial force.

The slope of curve was increased; it would be reduce the axial force. The slope of curve was built manually by using trend line command in Microsoft Excel software. The process of optimization using L18 Taguchi was illustrated as a circulating loop. Due to the optimization design based on increasing contact width was combined with considering contact stress, and the optimized design was divided as two modes which are all in Plastic modes. The next circulating loop was generated to fulfill the forming effect by adding forming simulation before the tightening simulation. Finally the optimized design considering forming effect could be achieved.

To design experimental matrix for seven factors with three levels, the L18 orthogonal array was most applicable. The following Table 6.1 and Table 6.2 show the factor and levels description and Taguchi test matrix.

Table 6.1 Factors and levels description

Factor	Factor Description	Level 1	Level 2	Level 3
A	Pitch 1(p_1)	3.5	4	4.5
B	Pitch 2 (p_2)	3.5	4	4.5
C	Pitch 3 (p_3)	3.5	4	4.5
D	Thickness (Tg)	1.2	1.5	1.8
E	Radius (R)	1.5	2.5	3.5
F	Height (h)	0.3	0.35	0.4
G	Thickness surface material (T_s)	0.1	0.2	0.3

Table 6.2 L18 test matrix

Trial	Factor						
	A	B	C	D	E	F	G
1	1	1	1	1	1	1	1
2	1	2	2	2	2	2	2
3	1	3	3	3	3	3	3
4	2	1	1	2	2	3	3
5	2	2	2	3	3	1	1
6	2	3	3	1	1	2	2
7	3	1	2	1	3	2	3
8	3	2	3	2	1	3	1
9	3	3	1	3	2	1	2
10	1	1	3	3	2	2	1
11	1	2	1	1	3	3	2
12	1	3	2	2	1	1	3
13	2	1	2	3	1	3	2
14	2	2	3	1	2	1	3
15	2	3	1	2	3	2	1
16	3	1	3	2	3	1	2
17	3	2	1	3	1	2	3
18	3	3	2	1	2	3	1

The L18 matrix was conducted and the slope of the curve of relationship between contact width and axial force as observed values (Y) was calculated for Plastic mode as shown in the Table 6.3. The slope of curve has been obtained by the slope average of upper and lower contact.

Table 6.3 Result of L18 Taguchi method for no-fix model

Run#	Factor	Slope of curve
		Plastic mode
1	$A_1B_1C_1D_1E_1F_1G_1$	0.0152
2	$A_1B_2C_2D_2E_2F_2G_2$	0.0148
3	$A_1B_3C_3D_3E_3F_3G_3$	0.0119
4	$A_2B_1C_1D_2E_2F_3G_3$	0.0126
5	$A_2B_2C_2D_3E_3F_1G_1$	0.0133
6	$A_2B_3C_3D_1E_1F_2G_2$	0.0167
7	$A_3B_1C_2D_1E_3F_2G_3$	0.0158
8	$A_3B_2C_3D_2E_1F_3G_1$	0.0132
9	$A_3B_3C_1D_3E_2F_1G_2$	0.0127
10	$A_1B_1C_3D_3E_2F_2G_1$	0.0139
11	$A_1B_2C_1D_1E_3F_3G_2$	0.0121
12	$A_1B_3C_2D_2E_1F_1G_3$	0.0144
13	$A_2B_1C_2D_3E_1F_3G_2$	0.0127
14	$A_2B_2C_3D_1E_2F_1G_3$	0.0096
15	$A_2B_3C_1D_2E_3F_2G_1$	0.0145
16	$A_3B_1C_3D_2E_3F_1G_2$	0.016
17	$A_3B_2C_1D_3E_1F_2G_3$	0.0152
18	$A_3B_3C_2D_1E_2F_3G_1$	0.0157

To calculate the main effect of each factor, the result for trials of the factor is added and then divides by the number of such trials [52]. The main effect is plotted for a visual inspection of each factor for various level conditions at plastic mode is shown in Fig. 6.9. The highest value for slope of curve is supposed as the axial force reducing. The main

factor of the design is providing the larger contact width and reducing the axial force. For Fig. 6.9 the higher value is p_1 is 4.5mm, p_2 is 3.5mm, p_3 is 4mm, Tg is 1.5mm, R is 1.5mm, h is 0.35mm and Ts is 0.1mm.

For Plastic gasket no-fix mode:

$A_1 = (0.0152+0.0148+0.0119+0.0139+0.0121+0.0144)/6 = 0.013717$

$A_2 = (0.0126+0.0133+0.0167+0.0127+0.0096+0.0145)/6 = 0.013233$

$A_3 = (0.0158+0.0132+0.0127+0.016+0.0152+0.0157)/6 = 0.014767$

$B_1 = (0.0152+0.0126+0.0158+0.0139+0.0127+0.016)/6 = 0.014367$

$B_2 = (0.0148+0.0133+0.0132+0.0121+0.0096+0.0152)/6 = 0.013033$

$B_3 = (0.0119+0.0167+0.0127+0.0144+0.0145+0.0157)/6 = 0.014317$

$C_1 = (0.0152+0.0126+0.0127+0.0121+0.0145+0.0152)/6 = 0.013717$

$C_2 = (0.0148+0.0133+0.0158+0.0144+0.0127+0.0157)/6 = 0.01445$

$C_3 = (0.0119+0.0167+0.0132+0.0139+0.0096+0.016)/6 = 0.01355$

$D_1 = (0.0152+0.0167+0.0158+0.0121+0.0096+0.0157)/6 = 0.014$

$D_2 = (0.0148+0.0126+0.0132+0.0144+0.0145+0.016)/6 = 0.0143$

$D_3 = (0.0119+0.0133+0.0127+0.0139+0.0127+0.0152)/6 = 0.013283$

$E_1 = (0.0152+0.0167+0.0132+0.0144+0.0127+0.0152)/6 = 0.014567$

$E_2 = (0.0148+0.0126+0.0127+0.0139+0.0096+0.0157)/6 = 0.013217$

$E_3 = (0.0119+0.0133+0.0158+0.0121+0.0145+0.016)/6 = 0.013933$

$F_1 = (0.0152+0.0133+0.0127+0.0144+0.0096+0.016)/6 = 0.013533$

$F_2 = (0.0148+0.0167+0.0158+0.0139+0.0145+0.0152)/6 = 0.01515$

$F_3 = (0.0119+0.0126+0.0132+0.0121+0.0127+0.0157)/6 = 0.013033$

$G_1 = (0.0152+0.0133+0.0132+0.0139+0.0145+0.0157)/6 = 0.0143$

$G_2 = (0.0148+0.0167+0.0127+0.0121+0.0127+0.016)/6 = 0.014167$

$G_3 = (0.0119+0.0126+0.0158+0.0144+0.0096+0.0152)/6 = 0.01325$
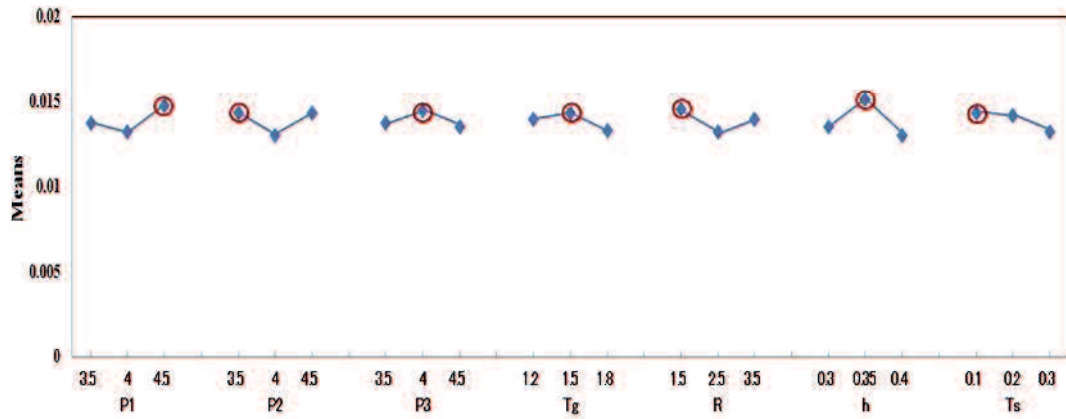
Fig. 6.9 Main effects of each factor for various levels at slope of curve

Finally, this study suggests the optimum gasket design based on results of each models is shown in Table 6.4 and Fig.6.10.

Table 6.4 Optimum design of gasket no-fix model

Factor	Forming model
	Plastic mode
p_1	4.5 mm
p_2	3.5 mm
p_3	4 mm
Tg	1.5 mm
R	1.5 mm
h	0.35 mm
T_s	0.1 mm
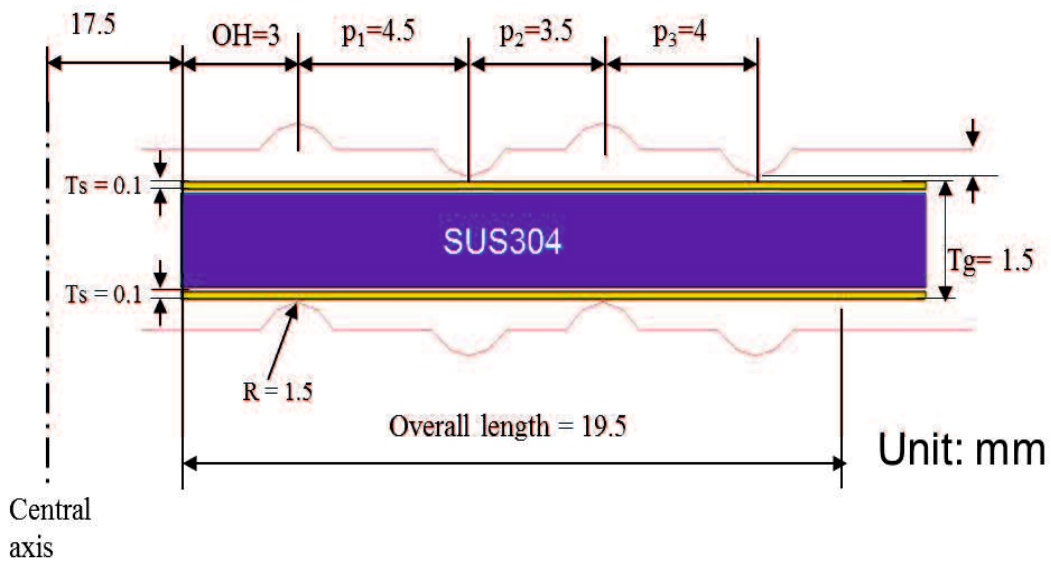
Fig. 6.10 Optimum three-layer metal gasket in no-fix model
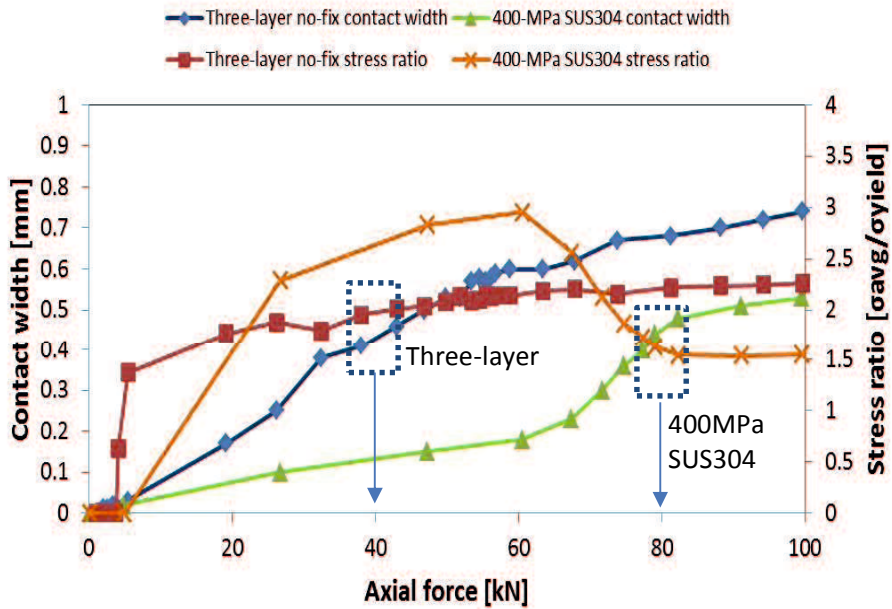
Fig. 6.11 Comparison for gasket in plastic mode

Fig. 6.11 shows the comparison simulation result for contact width and stress ratio of gasket in plastic mode, based on optimum design gasket new model no-fix compared to previous research (400-MPa mode single SUS304). Based on previous research gasket 400-MPa mode not leakage in 80kN axial force has contact width around 0.44mm and stress ratio 1.5. A new three –layer gasket has contact width 0.46mm and stress ratio 2 in 40kN axial force. Based on this we can assume that the gasket three-layer will be started not leakage in low axial force.
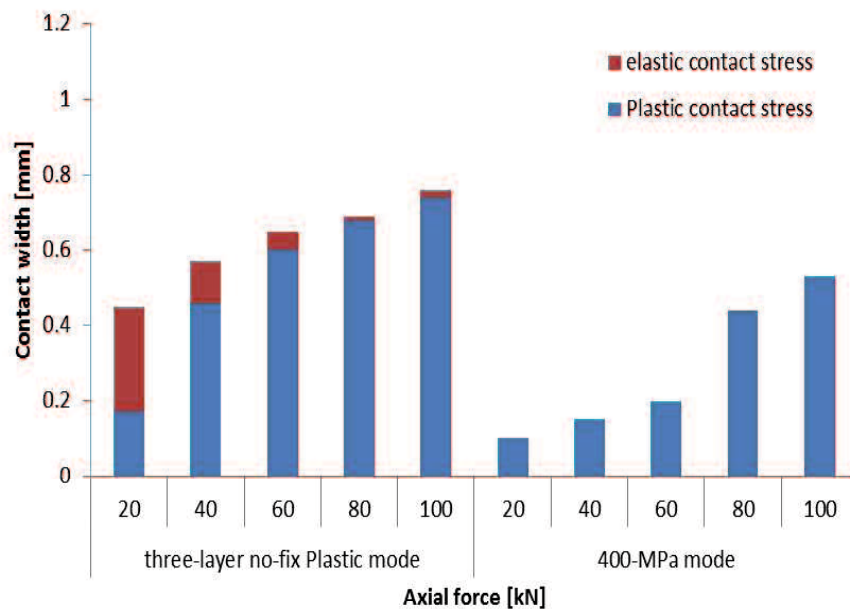
Fig. 6.12 The distribution of contact stress gasket in no-fix model

For other description about distribution of contact stress on both optimum design, it can be used a composition of contact stress distribution bar curve as shown in the Fig.6.12. It shows composition of contact stress distribution at 20, 40, 60, 80, 100 kN axial force. The blue colour bar show the contact stress distribution in plastic contact stress and red colour bar show the contact stress distribution in elastic contact stress. It denotes that contact stress distribution in plastic condition on gasket three-layer fix plastic mode larger than 400MPa mode. Therefore, the optimum design gasket three-layer fix plastic mode has

better sealing performance.

For further study, the optimum design of three-layer corrugated metal gaskets require an experimental confirmation test for final step in verifying the result drawn based on Taguchi's design approach.

6.2 Conclusion

This study investigates the optimum design of gasket by a simulation using FEM and a leakage test. The following conclusions are derived from this study:

1. Based on plastic contact stress consideration on contact width, by using the slope of curve relationship between contact width and axial force, the optimum design was found. The result shows that thickness of surface layer has a stronger influence on increasing the slope of curve of relationship between contact width and axial force and the three-layer metal gasket has larger contact width than gasket single material (SUS304). The optimum design of three-layer metal no-fix model based on simulation result is a gasket with core metal SUS304, Plastic mode p1 = 4.5 mm, p2 = 3.5 mm, p3 = 4 mm, T g= 1.5 mm, R = 1.5 mm, h = 0.35 mm and Ts = 0.1 mm.

2. Numerical analysis of the optimum shape under non-fixed model condition by contact stress condition showed has higher contact width in plastic contact stress condition and high stress ratio, based on this we can state that the optimum design three-layer gasket has better sealing performance than single layer.

CHAPTER VII
CONCLUSION

7.1 Summary of Result

The current work is dedicated to finding out the evaluation method of new metal gasket as asbestos substitution which uses a new approach of leak test results and the results of the FEM analysis concerning leakage performance. In this chapter, conclusions from the study are drawn and recommendations are presented for future research.

The three stage work is done to provide the result as follows:

1. From the study by numerical analysis, It shows the lower Yield stress of surface layer the slope contact width-axial force increase but the average contact stress decrease. When the work hardening coefficient increase, the slope contact width-axial force decrease as average contact stress increase.

2. From the study by numerical analysis with fixed model, clarify using the material with low modulus elasticity showed a decrease in the contact stress as contact width increase, and it was shown that the average contact stress decreased as the contact width increased, when the thickness ratio was further increased.

3. The analysis of the non-fixed model as the boundary condition between the laminated members in the three-layer metal gasket revealed the influence of flange surface roughness on contact stress and contact area. The evaluation by the leakage test, it was revealed that the three-layer metal gasket in 400-MPa mode, which is surface layer mainly the plastic region, is less affected by the surface roughness of the flange than the single layer metal gasket and has high sealing performance. It also shows a good agreement between simulation and experimental (digital microscope) result.

4. Numerical analysis of the optimum shape under non-fixed and fixed model condition by contact stress condition showed has higher contact width in plastic contact stress condition and high stress ratio, based on this we can state that the optimum design three-layer gasket has better sealing performance than single layer.

7.2 Future Consideration

Suggestions for future studies are:

1. Under high temperatures, the leak tightness of bolted joints is compromised due to the loss of the bolt load as a result of creep is not only on the gasket and bolt materials but also the flange material. Therefore the effect of creep-relaxation can be continued to maintain the performance of this gasket in the next project.

2. Development of three-layer corrugated gasket considering vibration effect.

REFERENCES

[1] Asbestos is hard to replace as Japan heads for ban, *Sealing Technology* 1 (2006) 1.

[2] Estrada, H., Parsons, I.D., Strength and Leakage Finite Element Analysis of GFRP Flange Joint, *International Journal of Pressure Vessel and Piping* 76 (1999) pp. 543-550.

[3] Krishna, M.M., Shunmugam, M.S., Prasad, N.S., A Study on the Sealing Performance of Bolted Flange Joints with Gaskets using Finite Element Analysis, *International Journal of Pressure Vessel and Piping* 84 (2007) pp. 349-357.

[4] Ross, E., Kockelmann, H., Hann, R., Gasket Characteristics for Design of Bolt Flange Connections of Metal-to-metal Contact Type, *International Journal of Pressure Vessel and Piping* 79 (2002) pp. 45-52.

[5] Huang, J., Lee, W., Sealing and Mechanical Behaviors of Expanded PTFE Gasket Sheet Characteristic by PVRC Room Temperature Tightness Tests, *Materials Chemistry and Physics* 68 (2001) pp. 180-196.

[6] Persson B.N.J., Albohr, O., Tartaglino, U., Volokitin, A.I., and Tosatti, E., On the Nature of Surface Roughness with Application to Contact Mechanics, Sealing, Rubber Friction and Adhesion, *Journal of Physics: Condensed Matter* 17 (2005) pp. 1–62.

[7] Persson B.N.J., Bucher F., and Chiaia B., Elastic Contact between Randomly Rough Surfaces: Comparison of Theory with Numerical Results, *Physical Review Letter* Vol. 65.184106 (2002).

[8] Persson, B.N.J. and Yang, C., Theory of the Leak-Rate of Seals, *Journal of Physics Condensed Matter*, 20 (2008) pp. 1-11.

[9] Lorenz B. and Persson B.N.J., Leak-rate of Seal: Comparison of Theory with experiment, *Journal of Euro Physics Letter* 86: 4 (2009).

[10] Person, B.N.J., Elastoplastic Contact between Randomly Rough Surfaces, *Physical review letters*, vol. 87, Number 11, (2001).

[11] http://www.valqua.co.jp/products/download/catalog/zy03_1103.pdf, Nippon Valqua Industries Co., Ltd. (ASME data).

[12] Bouzid A., Chaaban A., Bazergui, The Effect of Gasket Creep-Relaxation on the Leakage Tightness of Bolted Flanged Joints, *Journal of Pressure Vessel Technology* 117 (1995) pp. 71 – 78.

[13] Saeed, H.A, Izumi, S., Sakai, S., Haruyama, S., Nagawa, M., Noda, H., Development of New Metallic Gasket and its Optimum Design for Leakage Performance, *Journal of Solid Mechanics and Material Engineering* 2: 1 (2008) pp. 105-114.

[14] Haruyama S., Choiron M.A, Kaminishi K., *A Study of Design Standard and Performance Evaluation on New Metallic Gasket*, Proceeding of the 2nd International Symposium on Digital Manufacturing, Wuhan China, (2009) pp. 107-113.

[15] Choiron M.A, Haruyama S., Kaminishi K., *Simulation and Experimentation on the Contact Width of New Metal Gasket for Asbestos Substitution*, World Academy of Science, Engineering and Technology, vol. 5, (2011) pp. 1182-1186.

[16] Choiron M.A, Haruyama S., Kaminishi K., *Optimum Design of New 25A-size Metal Gasket Considering Plastic Contact Stress*, International Journal of Modeling and Optimization, vol. 1, no. 2 (2011) pp. 146-150.

[17] Schafer B.W., Pekoz T., "Computational modeling of cold-formed steel: characterizing geometric imperfections and residual stresses", Journal of Constructional Steel Research 47 (1998) pp. 193–210.

[18] Santos Abel D., et.all, The Use of the Finite Element Simulation for Optimization of metal Forming and Tool design", Journal of Material Processing Energy 119 (2001) pp. 152-157.

[19] Widder, E., Gaskets: Surface Finish Effects in Static Sealing, *ASME B46 Seminar* (2004).

[20] Nurhadiyanto D., Choiron M.A., Haruyama S., Kaminishi K., Optimization of New 25A-size Metal Gasket Design Based on Contact Width Considering Forming and Contact Stress Effect, *World Academy of Science, Engineering and Technology* Vol.6 (2012) pp. 661-665.

[21] Haruyama, S., Nurhadiyanto, D., Choiron, M.A., Kaminishi, K., Surface Roughness of flange Contact to the 25A-size Metal Gasket by Using FEM Simulation, *World Academy of Science, Engineering and Technology*, Vol. 7 (2013) pp. 565-569.

[22] Haruyama, S., Nurhadiyanto, D., Choiron, M.A., and Kaminishi, K., Influence of Surface Roughness on Leakage of New Metal Gasket, *International Journal of Pressure Vessels and Piping*, 111-112 (2013) pp. 146-154.

[23] Haruyama, S., Nurhadiyanto, D., and Kaminishi, K., Contact Width Analysis of Corrugated Metal Gasket based on Surface Roughness, *Advanced Material Research*, Vol. 856 (2014) pp. 92-97.

[24] Nurhadiyanto, D., Haruyama, S., Kaminishi, K., Karohika, IM.G., and Mujiyono, Contact Stress and Contact Width Analysis of Corrugated Metal Gasket, *Applied Mechanics and Materials*, Vol. 799-800 (2015) pp. 765-769.

[25] Toxicological Profile for Asbestos, *US Department of Health and Human Services, Public health Service Agency for Toxic Substances and diseases Registry* (2001).

[26] Kenji Morinaga, Asbestos in Japan, *European Asbestos Conference* (2003).

[27] ASME. *Boiler and Pressure Vesseal Code Section VIII Division I.* New York:

American Society of Mechanical Engineers (1995).

[28]   The Gasket Company, ISO-9002 Certified. *Gasket Handbook*. Web: www.lamonsgasket.com.

[29]   Rao, S. S., *The Finite Element Method in Engineering*, Elsevier Science & Technology Books (2004).

[30]   Madenci, E. and Guven, I., *The Finite Element Method and Applications in Engineering Using Ansys*, Springer Science-Business Media, LLC (2006).

[31]   Cook, R.D., *Finite Element Modeling for Stress Analysis*, John Wiley & Sons, Inc. (1995).

[32]   Taguchi, G. and Konish, S. *Orthogonal arrays and linear Graphs*. ASI Press, Dearborn, Michigan (1987).

[33]   H. Hertz, J. Reine *Angew. Math*. 92 (1882) pp. 156.

[34]   Stauffer, D. and Aharony, A., An Introduction to Percolation Theory, *Boca Raton, FL: CRC Press*, (1991).

[35]   Person, B.N.J., Contact Mechanics for Randomly Rough Surfaces, *Surface Science Reports* 61 (2006) pp. 201-227.

[36]   Bottiglione, F., Carbone, G., Mantriota, G., Fluid Leakage in Seals: An Approach Based on Percolation theory*, Tribology International* 42 (2009) pp. 731–737.

[37]   Gao, Y.F., Bower, A.F., Kim, K.S., Lev, L., Cheng, Y.T., The Behavior of an Elastic-Perfectly Plastic Sinusoidal Surface Under Contact Loading, *Wear* (2006) pp. 145-154.

[38]   Valloire, F.R., Paffoni, B., Progi, R. Load Transmission by Elastic, Elasto-plastic, or Fully Plastic Deformation of Rough Interface Asperities. *Mechanics of Materials* Vol. 33 (2001) pp. 617-633.

[39]   Kadin, Y., Kligerman, Y., Etsion, I., Unloading an Elastic-plastic Contact of Rough Surfaces, *Journal of The Mechanics and Physics of Solid* Vol. 54 (2006) pp. 2652-2674.

[40]   Francis, H.A., Application of Spherical Indentation Mechanics to Reversible and Irreversible Contact between Rough Surfaces. *Wear* 45 (1977) pp. 221-269.

[41]   O`Callagham, M., Cameron, M.A., Static Contact under Load between Nominally Flat Surfaces in which Deformation is Purely Elastic, *Wear* 36 (1976) pp. 79-97.

[42]   Toshimichi F., Tomohiro T., Finite Element Simulation of Bolt-Up Process of Pipe Flange Connections, *Journal Pressure Vessel Technology 123 Issue 3* (2001) pp. 282-287.

[43]   Zhou, H.Q., and GU, B.Q., Investigation into Leakage Behavior of Bolted Flange Connection with Octagonal Gasket, *Advanced Materials Research* 44-46 (2008) pp. 165-171.

[44]   Lee, C.Y., Lin, C.S., Jian, R.Q., Wen, C.Y., Simulation and Experimentation on the Contact Width and Pressure Distribution of Lip Seals, *Tribology International* 39 (2006) pp. 915–920.

[45]   Stakenborg, M.J.L., On the Sealing Mechanism of Radial Lip Seals, *Tribology International* 21: 6 (1988) pp. 335-340.

[46]   Weber, D., Haas, W., Wear Behaviour of PTFE Lip Seals with Different Sealing Edge Designs, Experiments and Simulation, *Sealing Technology* 2 (2007) pp. 7-12.

[47]   Pressure measuring film-FUJI prescale film instruction manual.

[48]   MSC Marc. *User manual* (2014).

[49]   Noda, NA., Nagawa, M., Shiraishi, F., and Inoue, A., Sealing Performance of New Gasket Flange, *Journal of Pressure Vessel Technology*, vol. 124 (2002) pp.239-246.

[50]   Fowlkes, W.Y., Creveling, C.M., *Engineering Methods for Robust Product Design*, Massachusetts, MA: Addison Wesley Longman, Inc., (1995).

[51]   JIS B2404, *Dimensions of Gaskets for Use with the Pipe Flanges*, Japanese Standards Association (2006).

[52]   JIS Z2241, *Method of Tensile Test for Metallic Materials*, Japanese Standards Association (1998).

[53]   Tickel, B., Getting It Right the First Time, *ANSYS Advantage* 1: 3 (2007) pp. 10-12.

[54]   Roy, Ranjit, *A Primer on the Taguchi Method*, Van Nostrand Reinhold (1990).

[55]   Liu, H., Yuan, J.L., Jin, J., Visualization Simulations for a Cold Press Die, *Journal of Materials Processing Technology*, vol. 129, (2002) pp. 321 − 325.

[56]   Nurhadiyanto, D., Choiron, M.A., Haruyama, S., and Kaminishi, K., Contact width evaluation of New 25A-size Metal gasket Considering Forming Effect, *Proceeding of the 8th International Conference on Innovation & Management*, (2011) pp. 296-301.

[57]   JIS B2220, *Steel Pipe Flanges*, Japanese Standards Association, (2004).

[58]   JIS Z2330, *Standard Recommended Guide for the Selection of Helium Leak Testing*, Japanese Standards Association (1992).

[59]   JIS Z2331, *Method of Helium Leak Testing*, Japanese Standards Association (2006) .

[60]   Handysurf E-35A/B User Manual, (2010).

[61]   Choiron, M.A., Haruyama, S., Kaminishi, K., Optimization of New Metal Gasket Shape by using Simulation Experiment, *International Journal of Academic Research*, Vol 3 No. 3 (2011).

[62]   Serror MH., Analytical study for deformability of laminated sheet metal, *Journal of Advanced Research*, 4 (2013) 83-92

[63]   I. Sakai, H. Ishimaru, , G. Horikoshi, 1982, Sealing Concept of Elastic Metal Gasket 'Helicoflex', *Vacuum*, Vol. 32, No. 1, pp. 33-37

[64]   H. Ishimaru, H. Yoshiki, 1991, Sealing performance of gaskets and flanges against superfluid helium, *Cryogenics*, Vol. 31, June,pp.456-458

[65]   J.K. Kim, T.X. Yu,1997, Forming and failure behavior of coated, laminated and sandwiched sheet metal: a review, Journal of Materials Processing Technology 63,pp.33-42

[66]   Haruyama, S., Karohika, IM.G., Sato, A., Nurhadiyanto, D., Kaminishi, K., Development of 25A-Size Three-Layer Metal Gasket by Using FEM Simulation, *International Journal of Mechanical, Aerospace, Industrial, Mechatronic and Manufacturing Engineering*, vol. 10 No. 3 (2016) pp. 577-583.

[67]   Karohika, IM.G., Haruyama, S., Kaminishi, K., Nurhadiyanto, D., Analysis of Contact Width and Contact Stress of Three-Layer Corrugated Metal Gasket, *International Journal of Mechanicals and Mechatronics Engineering*, Vol.4 No.3 (2017)

[68]   Karohika, IM.G., Haruyama, S., Kaminishi, K., Optimization of Three-Layer Corrugated Metal Gasket by Using Finite Element Method, *Proceeding of 19th International Conference on Mechanical Engineering and Mechatronics* (2017) pp. 2842-2846.